2021

Coexistence of directional and non-directional technologies in 6G wireless dense networks

BOSTON UNIVERSITY

COLLEGE OF ENGINEERING

Dissertation

COEXISTENCE OF DIRECTIONAL AND NON-DIRECTIONAL TECHNOLOGIES IN 6G WIRELESS DENSE NETWORKS

by

IMAN ABDALLA

B.Sc., Alexandria University, 2010
M.Sc., Nile University, 2014

Submitted in partial fulfillment of the

requirements for the degree of

Doctor of Philosophy

2021

Approved by

First Reader

Thomas D.C. Little, PhD
Associate Dean of Educational Initiatives
Professor of Electrical and Computer Engineering
Professor of Systems Engineering

Second Reader

Bobak Nazer, PhD
Associate Professor of Electrical and Computer Engineering
Associate Professor of Systems Engineering

Third Reader

Michael B. Rahaim, PhD
Assistant Professor of Engineering
University of Massachusetts - Boston

Fourth Reader

Jeffrey B. Carruthers, PhD
Associate Professor of Electrical and Computer Engineering

"*Can Imagination picture what the future of this invention is to be!*
We may talk by light to any visible distance without any conduction wire
In general science, discoveries will be make by the Photophone that are undreamed of just now." -Alexander Graham Bell

Acknowledgments

Looking back over my Ph.D. journey, I find myself immersed in so much support from friends and family that it is quite hard to concisely give everyone the acknowledgment they deserve but this is my trial.

In a culture where Engineering is mainly for men, I met people who convinced me otherwise and motivated me to go for a career I am passionate about. This started with my high school Mathematics teacher Mr Khalid Khamis all the way to last year of my Bachelors where I met professor Ahmed Sultan. Their confidence in me gave me the strength to pursue this career and head on all the way to a Ph.D. They will always remain special to me. I also appreciate the support of professors Tamer ElBatt, Mohammed Nafie and Fadel Digham, my M.Sc advisors who guided me and helped push me a step closer to the Ph.D.

I was blessed to work with Professor Thomas Little and Dr Michael Rahaim. Professor Little allowed me to grow as an independent researcher and pursue the ideas I was most excited for. That is a unique experience for which I am grateful. As for Dr Rahaim, his support was extremely valuable to my progress. He taught me a lot and I hope one day I can mentor students the way he mentored me. I appreciate all the wonderful conversations with Professors Bobak Nazer, Prakash Ishwar, Janusz Konrad, Hamid Nawab, Anna Swan and Daniel Weiner, they will always stay with me. I cherish them deeply.

I thank my distinguished thesis committee for their guidance and technical insight. Professor Jeffrey Carruthers' work provided a lot of the basics I needed in my journey and Professor Nazer helped me redevelop my appreciation for wireless communications in EC508 as well as in teaching Probability theory with him. I enjoyed that time and learned a lot from it.

Christine Ritzkowski, Allison Kleber and Kim Gayoon at the ECE department have always been wonderful in all the times I needed help. In the CISE department, Maureen Stanton and Christina Polyzos have also supported me immensely during my PhD and always found a way to put a smile on my face.

I would like to thank my friends in photonics Kubra Cilingir, Furkan Eris, Mohammed Usman, Waleed Tahir, John Bruce Murray, Mustafa Ozan, Parisa Babaheidarian, Annie Rabie, Prachi Shukla, Zeynep Kahraman and Nozomi Ito for all the wonderful memories and times we spent together.

Special thanks goes to my childhood friends Maysara Ahyad, Reham El Samadisy, Eman Hossam and Doaa Allam. Maysara Sabry, Aya Khalil and Ghada Hatem for their continued support. Thanks to them once I needed more computing power, I immediately got access to all their devices. An extra shout out goes to Ghada for her emotional support and for being a remedy to my mental health during rough times. I also appreciate Corina Ionita's support throughout the Ph.D., specially for leaving me sticky notes everywhere in the office to provide encouragement. My MCL family Jessica Morrison, Michael Rahaim, Emily Lam and Nataša Trkulja. I will miss our mischievous pranks and banter. I also thank Constantinos Gerontis for helping build the latest version of PATT.

I am and will forever be indebted to my mom and dad who raised me to always push my limits and motivated me to seek knowledge anywhere it is offered even if that means thousands of miles away from home. When I count my blessings I count you twice. My amazing sisters Gihan, Abir and Heba, a unique support system although we are all scattered in different countries. I love and appreciate you all so much. I also have to thank my kids Zain and Talya. I used to think that having kids meant the end of career life but because of them I managed my time better than usual just so I can make more time for them. To Islam El Bakoury, my dear husband and best friend, you are our rock. I most certainly would not have pursued a Ph.D. without your support. Writing how much I appreciate you would turn this acknowledgement into a tiny thesis so I will stop here.

Most importantly, I thank God for bringing all these wonderful people in my life and giving me strength everyday to work on my career and myself. Alhamdulelah.

Iman Abdalla

ECE Department

Boston University

COEXISTENCE OF DIRECTIONAL AND NON-DIRECTIONAL TECHNOLOGIES IN 6G WIRELESS DENSE NETWORKS

IMAN ABDALLA

Boston University, College of Engineering, 2021

Major Professor: Thomas D.C. Little, PhD
Associate Dean of Educational Initiatives
Professor of Electrical and Computer Engineering
Professor of Systems Engineering

ABSTRACT

Dense networks are characterized by the prevalence of wireless access points (APs) in close proximity to a population of user devices on a similar scale. By increasing AP density, the aggregate data consumption of a system can be dramatically increased.

In this dissertation we consider dense deployment of directional visible light APs. Firstly, we analyze the performance of a visible light communication (VLC) link and propose algorithmic methods as well as novel receiver structures to enhance its quality. Secondly, we study handover algorithms and investigate an AP placement strategy that ties to the system outage probability. Thirdly, we use a geometric model for an indoor space and a reference optical channel model to formulate an optimization problem that proposes a dynamic field of view (FOV) receiver with a goal of optimizing receiver FOV for maximum signal to noise ratio (SNR). From the promising results we get, we then propose the dynamic FOV technique with receiver tracking capability. Its results show an average SNR increase of up to 40% when compared to a fixed FOV receiver. These results motivate the adoption of dynamic pointing and adaptive FOV at the receiver in order to realize improved performance for mobile devices in an optical wireless dense network. This opts us to study

interference in VLC systems and how to mitigate it using our proposed receivers.

In the context of multi-user networks, we formulate two main novel optimization problems i) a joint optimization of transmit emission pattern and transmit power while satisfying illumination requirements and ii) an optimization to allocate users, balance the network load and optimize device FOV for best performance. We then evaluate the effect of self-blockage as well as random human blockers on our proposed receivers. Finally, we propose to deploy the VLC system in a hybrid setting of other technologies to evaluate the overall system performance for future 6G networks.

Contents

List of Tables

List of Figures

List of Abbreviations

5G	....	Fifth Generation Cellular Network
6G	....	Sixth Generation Cellular Network
AA	....	Anticipatory Association
ACM	....	Attocell Minimization
ADR	....	Angle Diversity Receiver
AP	....	Access Point
APC	....	Access Point Controller
APD	....	Avalanche Photodiode
ASE	....	Area Spectral Efficiency
AUM	....	Attocell User Maximization
BB	....	Busy Bursts
BD	....	Block Diagonalization
BER	....	Bit Error Rate
BFM	....	Backward Forward Marking
BIA	....	Blind Interference Alignment
CB	....	Coordinated Beamforming
CCI	....	Co-Channel Interference
CDF	....	Cumulative Density Function
CDMA	....	Code Division Multiple Access
CSI	....	Channel State Information
CT	....	Combined Transmission
DA	....	Distance Association
DC	....	Direct Current
DFOV	....	Dynamic Field of View
DL	....	Downlink
DMT	....	Discrete Multi-tone Modulation
EVM	....	Error Vector Magnitude
FA	....	Fairness Association
FBMC	....	Filter Bank Based Multiple Carrier

FCC	. . . .	Federal Communications Committee
FDMA	. . . .	Frequency Division Multiple Access
FFOV	. . . .	Fixed Field of View
FFR	. . . .	Fractional Frequency Reuse
FOV	. . . .	Field of View
GHz	. . . .	Gigahertz
GRPA	. . . .	Gain Ratio Power Allocation
GUI	. . . .	Graphical User Interface
HHO	. . . .	Horizontal Handover
HO	. . . .	Handover
ICI	. . . .	Inter-Cell Interference
IMDD	. . . .	Intensity Modulation with Direct Detection
IL	. . . .	Interference Level
IoT	. . . .	Internet of Things
IP	. . . .	Internet Protocol
IR	. . . .	Infrared
ISI	. . . .	Inter Symbol Interference
ISO	. . . .	International Standard Organization
JD	. . . .	Joint Detection
JT	. . . .	Joint Transmission
JTC	. . . .	Joint Technical Committee
kHz	. . . .	Kilo Hertz
KPI	. . . .	Key Performance Indicator
LED	. . . .	Light Emitting Diode
LiFi	. . . .	Light Fidelity
LOS	. . . .	Line of Sight
MA	. . . .	Multiple Access
MA-PHY	. . . .	Multiple Access - Physical Isolation
MA-SP	. . . .	Multiple Access - Signal Processing
MATT	. . . .	Motion Aperture Tilt Turret
MIMO	. . . .	Multiple Input Multiple Output
MISO	. . . .	Multiple Input Single Output
MMSE	. . . .	Minimum Mean Square Error
mmWave	. . . .	Millimeter Wave
MP2P	. . . .	Multi-Point to Point
MP2MP	. . . .	Multi-Point to Multi-Point
MRC	. . . .	Maximum Ratio Combining
MU-MISO	. . . .	Multiple User Multiple Input Single Output
NLOS	. . . .	Non Line of Sight
NOMA	. . . .	Non Orthogonal Multiple Access

OFDM	....	Orthogonal Frequency Division Multiplexing
OFDMA	....	Orthogonal Frequency Division Multiple Access
OMA	....	Orthogonal Multiple Access
OOC	....	Optical Orthogonal Codes
OOK	....	ON Off Keying
OPC	....	Optimal Combining
OWC	....	Optical Wireless Communications
P2P	....	Point-to-Point
P2MP	....	Point to Multi-Point
PAJO	....	Power Allocation Joint Optimization
PAM	....	Pulse Amplitude Modulation
PATT	....	Pan Aperture Tilt turret
PC	....	Personal Computer
PD	....	Photodiode
PDF	....	Probability Density Function
PHY	....	Physical
PN	....	Pseudo Noise
PPM	....	Pulse Position Modulation
PPP	....	Poisson Point Process
PWM	....	Pulse Width Modulation
RA	....	Responsive Association
RF	....	Radio Frequency
RGB	....	Red, Green and Blue
RSS	....	Received Signal Strength
RMS	....	Root Mean Square
Rx	....	Receiver
SDFOV	....	Steerable Dynamic Field of View
SDR	....	Software Defined Radio
SFR	....	Soft Frequency Reuse
SIC	....	Successive Interference Cancellation
SIMO	....	Single Input Mulitple Output
SINR	....	Signal to Interference plus Noise Ratio
SIR	....	Signal to Interference Ratio
SISO	....	Single Input Single Output
SLM	....	Spatial Light Modulator
SNR	....	Signal to Noise Ratio
SP	....	Signal Processing
SS	....	Signal Strength
STBC	....	Space Time Block Code

TDD	....	Time Division Duplexing
TDM	....	Time Division Multiplexing
TDMA	....	Time Division Multiple Access
THO	....	Total Number of Handovers
THz	....	Terahertz
TOA	....	Time of Arrival
Tx	....	Transmitter
UD	....	User Device
UL	....	Uplink
USRP	....	Universal Software Radio Peripheral
VHO	....	Vertical Handover
VLC	....	Visible Light Communications
VoIP	....	Voice Over Internet Protocol
VOV-FOV	....	Velocity Orientation Variable Field of View
VT	....	Vectored Transmission
WDM	....	Wave Division Multiplexing
WH	....	Walsh-Hadamard
WiFi	....	Wireless Fidelity
WLAN	....	Wireless Local Area Network
ZF	....	Zero Forcing
ZF-DPC	....	Zero Forcing Dirty Paper Coding

Chapter 1

Introduction

Since the onset of wireless communications in the late 19^{th} century, scientists and engineers have been working on ways to increase range, capacity, and versatility. This dissertation is no exception. Today the global penetration of the mobile smartphone is 76% in advanced countries and 45% in emerging economies (Pew Research Center, 2019) with unit shipments of 1.56 billion (S. O'Dea, 2020) supporting annual traffic with a compound annual growth rate of 26% between 2016-2021 (Cisco, 2021). The need for continued growth in capacity is necessary to meet the diverse needs of human interaction through modern communication innovations.

This work focuses on the potential for the optical spectrum to be used to increase capacity when used in collaboration with the prevailing radio frequency (RF) technologies used today. Ironically, it was Bell's optical solution that provided the communication medium for the first wireless phone conversation (Bell, 1880), but the many uses that followed were based on radio frequencies. We now have the benefit of more than a century of research on communications technology. But what is fundamentally different today is the increased density and close proximity of wireless devices that requires rethinking connectivity when interference is expected and prevalent.

Specifically, this dissertation considers the unique properties of the optical spectrum and how they can be used in short range indoor communications applications especially when coupled to providing light emitting diode (LED) lighting. This has been called a "dual-use" paradigm, leveraging the location of lighting for providing communications infrastructure.

We dive into optical wireless communications (OWC) and study how to utilize the optical medium through its unique characteristics to realize higher rates and better communication quality. The work explores system-level optimizations beginning with single links and then moving to multiple transmitters and receivers competing for shared resources. Ultimately the goal is to understand and provide a design methodology for exploiting the optical medium in the indoor wireless access scenario applied as a compliment to existing and emerging RF solutions.

This chapter provides our motivation for studying an alternative spectrum band suitable for indoor environments. It also contains a brief discussion on the difference between directional and non-directional media followed by an overview and background on Visible Light Communications (VLC) which is the focus technology in this work. Finally, this chapter outlines the remainder of the dissertation as well as its research accomplishments.

1.1 Motivation

Not only are the number of devices expected to grow but also the nature of the applications used on the Internet. First the transition was from talk and text to voice over internet protocol (VoIP) and web surfing, now we are speculated to move from video streaming and virtual/augmented reality to holographic communications, remote surgeries, holographic texting, smart cities and flying cars, to name a few. Fig. 1·1 illustrates some of the present changes in indoor spaces which are expected to grow in the coming years. All these applications will move current data requirements to a new realm where ultra low latency and Gigabit rates per user will become a requirement. Work on 6G (Calvanese Strinati et al., 2019; Tariq et al., 2020; Saad et al., 2020) predicts that the key performance indicators (KPIs) would be around the numbers presented in Table 1.1. In the current 5G map, the focus is on millimeter wave (mmWave) deployments which have been known to reach much

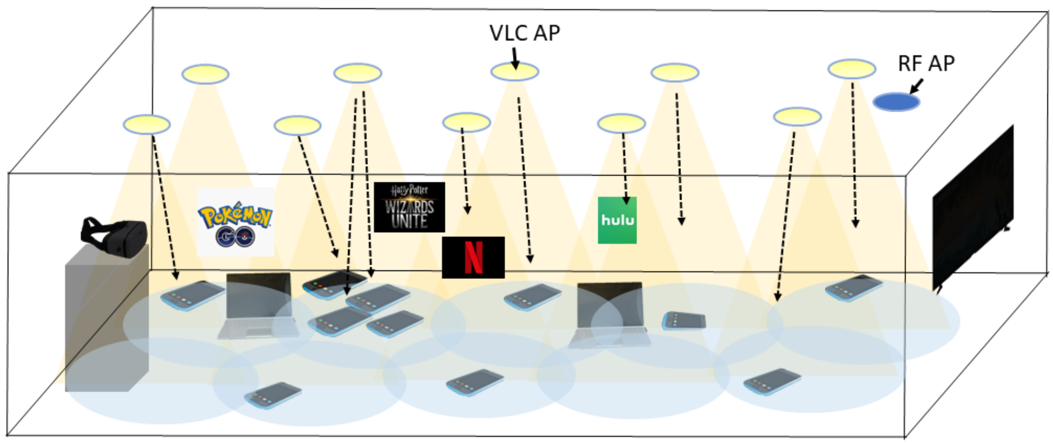

Figure 1·1: General Coexistence Setup Highlighting The Different Present Forms of Data Traffic.

Table 1.1: 5G and 6G KPIs

KPI	**5G**	**6G**
Downlink Data Rate:	20 Gb/s	1 Tb/s
Individual Data Rate	1 Gb/s	100 Gb/s - 1 Tb/s
Uniform User Experience	50 MB/s, 2D everywhere	10 Gb/s, 3D everywhere
Latency	1 ms	0.1 ms
Mobility	Up to 500 km/hr	Up to 1000 km/hr

higher rates than 4G. However, these rates are still not in the ranges required for the applications anticipated for 6G. This in turn will trigger more usage of different parts of the spectrum such as Terahertz (THz) and Visible Light. In (Strinati et al., 2019) the authors discuss that the required rates can be achieved through massive parallelization of micro-LEDs. VLC at this point in time is hardware limited but with the production of efficient micro-LEDs, which is imminent, it is considered a front runner for providing Gigabyte rates. Researchers that are moving from the analysis of traditional RF communications, sub-6 gigahertz (GHz), to studying VLC need to discern the differences in the properties of these two unique media to fully benefit from their union. We discuss these next.

1.2 Directional and Non Directional Technologies

Directional Communications require pointing the receiver at the transmitter whereas non-directional (omni-directional) do not. The directionality property comes from the transmitter beam width as well as the receiver which needs to find the signal within its field of view (FOV) to detect it. This property is the cause of signal variability with different receiver FOV and orientation which we discuss in detail throughout this dissertation. Meanwhile sub-6 GHz RF is modeled as omni-directional. This part of the spectrum has advantages that are not found in its directional counterparts, such as handling blockage effects and bad weather. However, some of the disadvantages associated with omni-directional technologies are less security and scarcity on the spectrum band. Here arises the usage of the non-RF bands which can provide larger free unutilized bandwidths that have high probability of reuse due to their containment within a specific space (e.g., walls).

This discussion is also highlighted in (Marzetta et al., 2016) where the authors mention: "There are three timeless truths in the field of wireless communications: 1) Demand for wireless throughput, both mobile and fixed, will always increase. 2) The quantity of available electromagnetic spectrum will never increase, and the most desirable frequency bands that can propagate into buildings and around obstacles and that are unaffected by weather constitute only a small fraction of the entire spectrum. 3) Communication theorists and engineers will always be pressured to invent or to discover breakthrough technologies that provide higher spectral efficiency."

This statement is in line with our world today and the way with which we approach our analysis in a hybrid RF/VLC setup.

1.3 Introduction to Visible Light Communications

Visible Light Communications (VLC) is an attractive technology to be used complementary to RF. Visible Light is the part of the electromagnetic spectrum in which frequencies

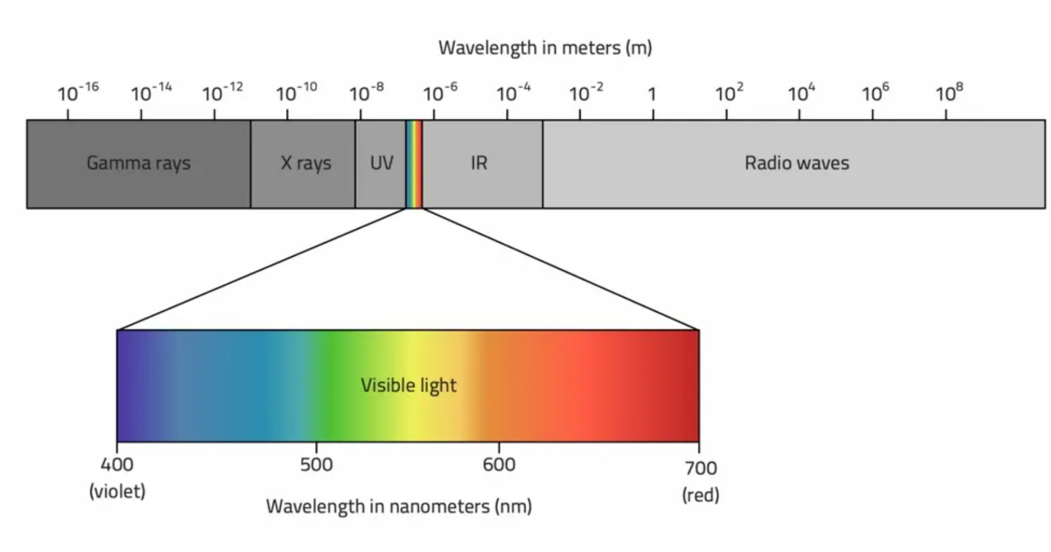

Figure 1·2: Components of The Electromagnetic Spectrum. Image from *radiotospace.com*.

are between 405 - 790 THz, or 380 to 740 nanometers in terms of wave lengths, depicted in Fig.1·2 . One must note that using visible light for communications is not a novel endeavor. The first known scholar to go down this path is, former Boston University professor, Alexander Graham Bell. His 1880 invention, namely the Photophone, with his assistant Charles Tainter is considered a precursor in optical wireless communications (OWC) (Bell, 1880). The Photophone is able to transmit speech through a modulated light beam. Bell considered it his greatest achievement that he had intended to name his second daughter after it. Later on, research on the Photophone concept continued into the 1950s, mostly by army research and development labs. Recent revivals of this technology are mainly in Europe by private companies such as PureLiFi and Oledcomm.

The attractiveness of VLC lies in its 1) Dual-use; where it can be used for both lighting and communication. 2) Relatively inexpensive infrastructure; digging underground to place cables is not necessary. The main changes come from replacing regular bulbs with modulated LEDs. 3) Non-Interfering property; it does not interfere with RF which makes it a perfect candidate for coexistence with RF cells. 4) Security; while nothing is totally

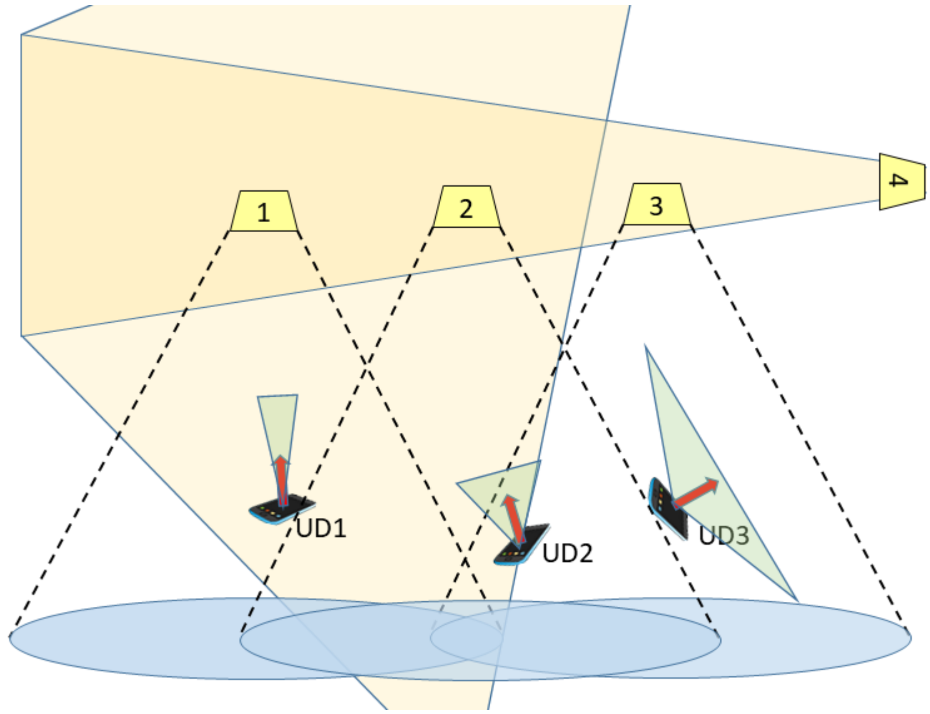

Figure 1·3: Light-Based Sources Exhibit Directionality, Divergence, and Reflections. Receivers and Transmitters Can Have Different Orientations and Fields of View.

secure, VLC has the added advantage of not allowing its waves to pass through walls. Thereby adding an extra layer of protection to the data conveyed. 5) Ideal for places where RF signals need to be minimized such as elevators, planes, hospitals, . . . etc., and most importantly its 6) Directivity; which is ripe with potential for spatial reuse.

The reason VLC is suggested as a complementary technology to RF (not be used solely) is because there does not exist a practical uplink design to date. It would not be ideal for users to have light shining out of their devices which is why most literature relies on either RF or infrared (IR) technologies for the uplink. Another reason one might prefer RF is due to the ability to have a non-directional communication in the control plane to help in case of blockages.

Next we discuss some characteristics relating to VLC specifically, and OWC generally (Abdalla et al., 2020b).

- Directionality of the medium which we discussed in Section 1.2. Fig. 1·3 illustrates this property through various receivers pointed in different directions, rotations and FOVs with respect to a transmitter.

- Channel Characteristics: Optical signal power consists of LOS and reflected multipath (NLOS) signals (e.g., Fig. 1·3, access point (AP) number 4). However, most research, with a few exceptions, considers reflections to have negligible impact when a LOS path exists. For example, the work in (Komine and Nakagawa, 2004) shows results that conclude that for most environments the total average power in reflections can be ignored.

- Modulation scheme: The modulation used is intensity modulation with direct detection (IM/DD) where the current amplitude is modulated by the signal then received by a photodetector (PD). Optical signals transmitted are real-valued and non-negative (Kahn and Barry, 1997). This property leads to many modulation techniques such as pulse amplitude modulation (PAM), pulse position modulation (PPM), and asymmetrically clipped orthogonal frequency division multiplexing (AC-OFDM) for reconciling light as a carrier.

- Optical power constraints:

  1). The optical carrier is expected to provide illumination that is why the optical signal must conform to lighting conventions and the nature of human perception including intensity, glare, flicker, and color quality.

  2). IM/DD signals have a different relationship between the constraint (average optical power vs. electrical power) and the signal current or voltage. For an electrical signal X(t), Average optical power in IM/DD relates to a constraint on E[X] whereas average electrical power sets a constraint on the variance of X, or E[X^2] assuming

X(t) is a 0 mean signal (Rahaim and Little, 2016).

- Noise: Ambient lighting (i.e., sunlight) produces shot noise in OWC systems. Direct current (DC) optical power from ambient light sources can also result in saturation at the receiver, potentially clipping transmitted modulated signals.
- Occlusions: Light signals are blocked by opaque objects whereas RF typically can propagate with some degree of attenuation. This can be a security enhancement for limiting eavesdropping on VLC, or it can be a nuisance when moving objects pass between a transmitter and receiver obstructing the LOS path. RF adopts this characteristic in the millimeter wavelengths.

1.4 Related Work

The advancement in LED technology and the ability to digitally modulate an LED spurred the excitement towards using visible light for communications (Komine and Nakagawa, 2004). VLC provides a dual-use advantage which means system designers need to take into consideration not only the communication aspects of the system but also the illumination constraints (Elgala et al., 2011; Karunatilaka et al., 2015; Bao et al., 2015) all for the advantage of higher aggregate rates.

Another method to increase aggregate rates and remedy the increase in traffic demands indoors (Cisco, 2020) is to add more VLC APs indoors (Rahaim and Little, 2015). An advantage of VLC is that this can be done locally and does not need provider supervision as in RF. Dense indoor networks allow support for much higher rates which is a speculated need for 6G applications. However adding more cells can be tricky. In a dense network, if the cell beam emission pattern is too narrow, interference would be mitigated but handovers would increase causing overall throughput reduction and disrupting the communication experience. Wide beams would cause high interference. The deployment of VLC APs should be designed smartly to not cause high inter-cell interference as well as ensure seamless connectivity.

This generated two streams of research; 1) VLC AP deployment and its effects on coverage and communications such as the work in (Vavoulas et al., 2015) which studies network coverage and communication aspects. Meanwhile cellular coverage optimization is studied in (Jian-Hui Liu and Zhang, 2014) and dynamic emission patterns are investigated by (Rahaim et al., 2017); and 2) Interference mitigation methods and techniques. Work on mitigating interference should encompass the inherent differences between RF and OWC links (Rahaim and Little, 2017). There is a plethora of work in this area, part of it employs a spatial diversity methodology for interference management (Ntogari et al., 2009; Lian and Brandt-Pearce, 2017; Chen et al., 2014a; Ryoo et al., 2016) and the other is concerned with investigating forms of multiple access whether through signal processing techniques (Marsh and Kahn, 1997; Jung et al., 2016; Chen et al., 2013b; In Hwan Park et al., 2012; Yu et al., 2013; Marshoud et al., 2018) or through exploiting the physical characteristics of the channel (Wang et al., 2012; Vegni and Biagi, 2019; Shashikant et al., 2017; Rahaim and Little, 2013; O'Brien, 2019; Rahaim et al., 2017).

Previous work in the literature was not concerned with the orientation of the receiver and its FOV with a few exceptions such as (Bas et al., 2015). Most analyses considered the receiver orientation fixed with a wide FOV. This is mainly owing to the lack of a realistic model to mimic the user device rotation and how humans actually move and hold their devices in indoor spaces. This model would also change with the type of device used, whether it is a tablet, a phone, a virtual reality headset . . . etc. However, receiver parameters have to be taken into account to help model the actual performance of VLC systems.

Due to the impracticality of having the receiver shine a light at the user in an uplink connection, most works migrated towards IR or RF for the uplink. In our work we assume an RF uplink which creates an overall asymmetrical RF/VLC link which has been tested

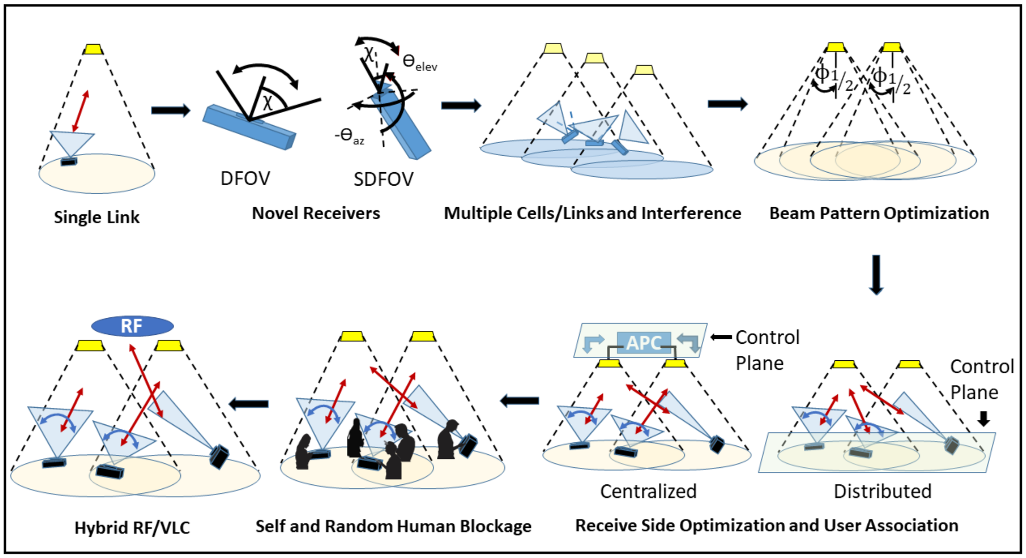

Figure 1·4: Thesis Flow and Overview.

experimentally as well (Shao et al., 2014; Li et al., 2018). The hybrid RF/VLC setup has been discussed in the literature (Rahaim et al., 2019; Ayyash et al., 2016; Li et al., 2018) as a successful method to achieve higher aggregate rates. Hybrid settings allow VLC to offload the crowded RF and also allow VLC to be aided by a non-directional medium to serve the devices that might not have LOS links, which is advantageous. The fact that they do not interfere with each other made this very appealing which triggered a lot of work on RF/VLC hybrid systems (Rahaim et al., 2011; Li et al., 2016; Obeed et al., 2018; Kashef et al., 2016).

1.5 Thesis Overview and Accomplishments

The remainder of the dissertation can be summarized as follows (a visual summary is illustrated in Fig. 1·4). Chapters 2, 3 focus on the characterization of the directional VLC link. In Chapter 2 we characterize the VLC channel model used in our work, clarifying how it varies in empirical studies. We also discuss the RF models used within this dissertation. Chapter 3 characterizes the VLC link in dense networks as a step towards integrating it into multiple links. This becomes the goal we aim for in Chapters 4 through 6. We focus, in particular, on exploiting the directionality property of light which allows manipulations at the transmitter or the receiver to mitigate interference and improve performance. Chapter 3 emphasizes the importance of receiver FOV and orientation. Here we discuss two novel receivers we propose detailing their structures, the optimization problems involved in each one and show their performance when compared to a baseline single photo-detector with fixed field of view. In Chapter 4 we discern the differences between studying interference in VLC systems specifically (OWC generally) and RF traditional systems. We also discuss the techniques implemented in the literature to manage interference and show preliminary results for the receivers we propose in interference scenarios. Chapter 5 prepares our system on the transmit side (access points) for satisfying an illumination constraint and achieving a communication goal (dual-use) by optimizing the transmitter beam emission and transmit power. This is met by more involved work on the receive side studied in Chapter 6 where we propose a user association and FOV optimization problem that aims at load balancing in a coordinated VLC-only system. We also compare the results with those of a distributed system. Finally we evaluate how self- and random-human blockages affect the system performance.

Chapter 7 is dedicated to studying outage probability through two different approaches, to allow for system design while considering system parameters. One of our approaches aims for seamless connectivity without sacrificing quality of service. Analysis is done for single/multi-user scenarios. Next in Chapter 8, we evaluate a hybrid RF/VLC system. We study two load balancing techniques one aiming for enhancing the minimum user throughput while the other enhances the total sum throughput. We then derive a hybrid system outage for users employing steerable dynamic FOV receivers also aimed at balancing the load between the two systems.

In Chapter 9 we end our analysis with a discussion of our lab setup and experiments as well as results that confirm our analytical findings from the previous chapters. We also reconcile the theoretical model and the data measured in the lab showing the error between simulated and measured optical received power and confirming the accuracy of our models. Chapter 10 concludes the dissertation and discusses future work and promising directions for the future.

The contributions of this dissertation are:

- Validating our proposed VLC model through testbed measurements.
- Establishing the effects of varying the receiver parameters on the VLC link signal quality as well as seamless connectivity analytically and experimentally.
- Enhancing the signal to noise ratio (SNR) of the VLC link by proposing a dynamic field of view (DFOV) receiver to mitigate noise and interference effects and providing experimental proof of concept.
- Formulating a dynamic algorithm for DFOV to change its field of view (FOV) based on the receiver location, orientation and velocity. The proposed algorithm improves SNR simulated results for our lab setting almost three times (3x) better than the baseline fixed field of view (FFOV) receiver.
- Proposing a steerable dynamic field of view (SDFOV) receiver that is able to reject interference signals. The proposed receiver shows an average SNR increase of up to 40% compared to the FFOV receiver.
- Analyzing the reuse vs. scope trade-off generated by dynamic FOV. This establishes a range of applications for DFOV receivers in dense OWC networks and confirms the possibility of making full use of spatial diversity while mitigating interference effects on user devices.

- Proposing a novel generalized optimization to jointly optimize transmitter emission pattern and transmit power which allows the evaluation of both the communication and illumination aspects of VLC systems in practical deployments.

- Proposing FOV optimization to enhance user association in a novel joint formulation for a multi-user indoor VLC system with non-point-source transmitters under the proposed dynamic FOV receivers. In the evaluated configuration, SDFOV and DFOV outperform FFOV by up to 5.6x and 2.2x in average minimum throughput gain respectively.

- Proposing two heuristics, for a multi-user coordinated system, that require less information at the controller to achieve enhanced fairness and throughput performance respectively for SDFOV receivers. Heuristics show near-optimal performance in lower order Lambertians and overall better performance than distributed systems.

- Proposing a novel orientation based association method for DFOV max-min fairness performance in a coordinated system. The heuristic we propose reduces the optimal search space while achieving $97-99\%$ of the optimal performance in our setup.

- Evaluating the effect of self-blockage as well as random human blockers on VLC links at different transmit beam widths in both active and passive systems. Results show a high blockage impact on SDFOV receivers yet their overall performance is superior to DFOV and FFOV receivers.

- Proposing a novel AP placement strategy that is tied to outage probability, handover time and user velocity to promote seamless connectivity. We also provide an upper bound on outage probability that proves to be effective in evaluating the effect of system parameters on the outage.

- Deriving the exact closed form user outage probability when employing the SDFOV receiver in a practical symmetric VLC deployment.

- Proposing a hybrid RF/VLC indoor deployment and deriving an approximation to the hybrid system user outage probability.

Chapter 2

Preliminary Mathematical Models

In this chapter we present the channel modeling used for each medium. We start with the VLC channel model and the variations in this model to incorporate the empirical analysis. Finally, we move on to discussing the WiFi indoor model used in our simulations as well as the Nakagmi fading model used in our hybrid system analysis.

2.1 VLC Model

We introduce the VLC model used to characterize the physical medium necessary to establish performance of VLC systems.

2.1.1 Channel Model

For any given room setup, we assume that each transmitter j is rectangular and consisting of a grid of $w \times l$ point sources (elements). The LOS DC channel model gain of an element i within transmitter j, illustrated in Fig. 2·1a, is defined as:

$$H_{DC,e}^{(ji)}(\phi_{ji}, \psi_{ji}, d_{ji}) = \frac{P_{r,e}^{(ji)}}{P_{t,e}^{(ji)}} = \frac{G_T(\phi_{ji})G_R(\psi_{ji})}{d_{ji}^2} \tag{2.1}$$

where $P_{t,e}^{(ji)}$ and $P_{r,e}^{(ji)}$ are the optical power transmitted and received from the i-th element within transmitter j, respectively. ϕ_{ji} is the emission angle, ψ_{ji} is the acceptance angle, and d_{ji} is the distance between the receiver and the element. All the parameters defined with subscript/superscript ji describe the point source element i within transmitter j. The subscript e indicates element models. The transmitter gain or radiant intensity (i.e., G_T) and the receiver gain (i.e., G_R) are defined as:

$$G_T(\phi) = \frac{m+1}{2\pi}\cos^m(\phi)$$

and

$$G_R(\psi) = A\cos(\psi)1\{\psi < \chi\}$$

respectively. We consider a Lambertian emission with order m and model a photodetector with area A and no filter or optical lens. χ is the receiver's FOV and $1\{.\}$ represents the indicator function. We define the receiver's FOV, χ as the half angle of the receiver's view. For an untilted receiver, the FOV can be calculated as $\chi = \tan^{-1}\frac{r_v}{V}$, where r_v is the radius of the circle covered by the receiver's view and V is its vertical height away from the light sources' plane.

We consider signal transmission via Intensity Modulation with Direct Detection (IM/DD). Substituting in eq. (2.1), the optical power received from element i is evaluated as:

$$P_{r,e}^{(ji)} = \frac{P_{t,e}^{(ji)}(m+1)A\cos^m\phi_{ji}cos\psi_{ji}}{2\pi d_{ji}^2}1\{\psi_{ji} < \chi\} \tag{2.2}$$

where $P_{t,e}^{(ji)} = P_t^{(j)}\alpha_{ji}$. We define $P_t^{(j)}$ as the optical power transmitted from transmitter j; therefore, $\sum_i \alpha_{ji} = 1$. We consider $\alpha_{ji} = \frac{1}{wl}\forall i$ to normalize the transmitter's power over all the elements that it contains. The transmitter LOS channel gain which sums over all the elements i within the transmitter j is

$$H_{DC}^{(j)} = \sum_{i=1}^{wl}\alpha_{ji}H_{DC,e}^{(ji)}$$

The total received optical power from the j-th transmitter can be evaluated using

$$P_r^{(j)} = \sum_{i=1}^{wl}P_{r,e}^{(ji)} \tag{2.3}$$

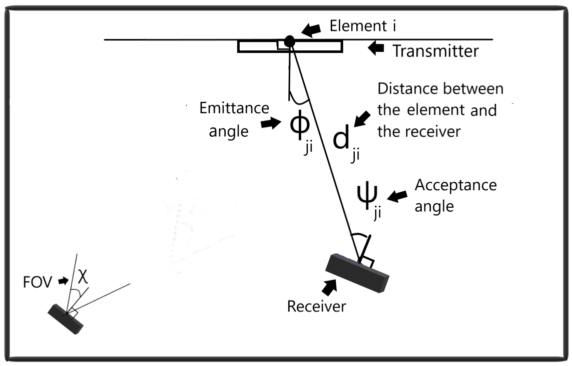

(a)

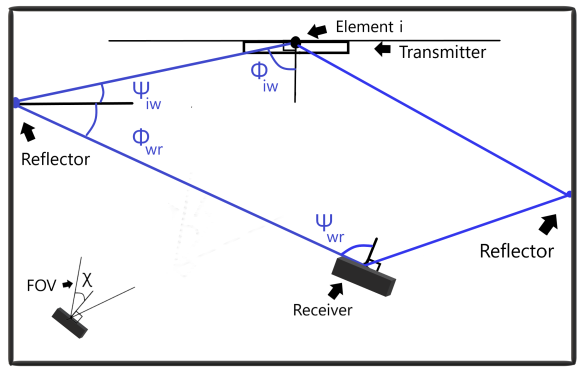

(b)

Figure 2·1: General Receiver Location and Orientation Geometry: (a) Line of Sight; (b) Non Line of Sight.

The signal to noise ratio (SNR) is defined as:

$$SNR^{(j)} = \frac{\sigma_j^2}{\sigma_a^2} = \frac{(R_r P_r^{(j)})^2}{\sigma_a^2} \tag{2.4}$$

σ_j^2 is the variance of the desired signal from transmitter j, σ_a^2 is the noise current variance and R_r is the receiver responsivity [A/W]. The second equality is accurate for On-Off-keying (OOK) modulation[1]. For multi-user environments we define the signal to interference plus noise ratio (SINR) of user u connected to the j-th transmitter as:

$$SINR_u^{(j)}(\chi) = \frac{\sigma_j^2}{\sum_{q,q\neq j}\sigma_q^2 + \sigma_a^2} \tag{2.5}$$

σ_q^2 is the interfering signal variance and we sum over q depending on the number of interference signals.

For a shot-noise-dominated system, the noise current variance σ_a^2 is modeled as follows

[1] As opposed to RF, the average optical received power in OWC varies according to the specified modulation (Rahaim and Little, 2016).

(Ramirez-Iniguez et al., 2008; Kahn and Barry, 1997):

$$\sigma_a^2 = \overline{i_q^2} + \overline{i_d^2} \tag{2.6}$$

where $\overline{i_d^2}$ is the dark current noise, which is caused by the current flowing in the photodiode independent of the optical signal, and $\overline{i_q^2}$ is the quantum noise, which is due to the discrete nature of the photodetection process. $\overline{i_q^2} = 2qR_rP_nB$, q is the electron charge, B is the receiver bandwidth and P_n is the average optical power incident on the photodiode. Meanwhile, $\overline{i_d^2} = 2qI_dB$ where I_d is the dark current.

$$P_n(\chi) = \sum_j P_{txDC} H_{DC}^{(j)} \tag{2.7}$$

We define P_{txDC} as the transmitted DC power that contributes to noise. Note that both P_n and P_{txDC} are defined in the optical domain. Eq. (2.7) assumes that all optical power comes from local sources (i.e., does not include power from non-transmitters / external sources).

2.1.2 Empirical Model Variations

In case of using our model to compare to data measured in our lab at Boston University, which we describe in length in Chapter 9, we have a few variations to introduce to the model used above.

Is is worth noting that we may analyze the relation between the amplitudes of the received and transmitted electrical signals using eq. (2.2) as well. As R_rP_r is proportional to the received electrical amplitude, A_r, in the optical medium. We show this analysis for completeness but it follows along straightforwardly as the one modeled above.

The relation between the amplitude of the received electrical signal to the transmitted one by:

$$\frac{A_{r,e}^{(ji)}}{A_{t,e}^{(ji)}} = C_T C_R H_{DC,e}^{ji} \tag{2.8}$$

where $A_{t,e}^{(ji)}$ and $A_{r,e}^{(ji)}$ are the electrical amplitudes transmitted and received from the i-th element within transmitter j, respectively. C_T and C_R are conversion factors (i.e., the transmitter and receiver conversions between the electrical and optical domains) measured in the lab. $C_T C_R$ encapsulate the effect of receiver responsivity and receiver area. Substituting in eq. (2.1), the electrical current amplitude received from element i is evaluated as:

$$A_{r,e}^{(ji)} = \frac{A_{t,e}^{(ji)}(m+1)C_T C_R \cos^m \phi_{ji} cos\psi_{ji}}{2\pi d_{ji}^2} 1\{\psi_{ji} < \chi\} \tag{2.9}$$

where $A_{t,e}^{(ji)} = A_t^{(j)}\alpha_{ji}$. We define $A_t^{(j)}$ as the electrical amplitude transmitted from source j. The j-th transmitter received electrical amplitude is $A_r^{(j)} = \sum_{i=1}^{wl} A_{r,e}^{(ji)}$.

We assume On-Off-keying (OOK) modulation in our empirical setup, and so define the Signal to Noise Ratio (SNR) from transmitter j as:

$$SNR^{(j)}(\chi) = \frac{(\sum_i^{wl} A_{r,e}^{ji})^2}{\sigma_a^2} \tag{2.10}$$

In this analysis, we sum the square of the amplitudes of the OOK signals for different elements ignoring the difference in propagation delay, considering it negligible.

SINR follows along to be defined as:

$$SINR^{(j)}(\chi) = \frac{\sigma_s^2}{\sum_{q,q\neq s}\sigma_q^2 + \sigma_a^2} = \frac{(A_r^{(j)})^2}{\sum_{q,q\neq s}(A_r^{(q)})^2 + \sigma_a^2} \tag{2.11}$$

Empirically, we get the signal power by measuring the observed voltage. To compare it with the theoretical model, we need to convert it back to current. To relate σ_a^2 to noise voltage variance σ_n^2 we use (ThorLabs Inc, 2013):

$$V_{out} = P_{opt} RMG \tag{2.12}$$

where V_{out} is the output voltage from the photodiode, P_{opt} [W] is the optical power incident on the photodiode, M is a multiplication factor and G is the transimpedance gain of the receiver [V/A]. Finally, to get σ_n^2, we get the variance of both sides and so $\sigma_n^2 = \sigma_a^2 M^2 G^2$.

As for P_n we use eqn. (2.7). It is normalized as we divide it by the number of elements in the luminaire grid wl. In this calculation we do not need to consider $C_T C_R$ because P_{txDC} is a number evaluated empirically and encompasses this factor. Note that, the receiver area A is substituted back into the equation to factor the receiver area because $C_T C_R$ is no longer used.

2.1.3 Reflections

Optical signal power consists of LOS and reflected multipath signals Fig. 2·1. Most research, with a few exceptions, considers reflections to have negligible impact when a LOS path exists. For example, the work in (Komine and Nakagawa, 2004) shows results that conclude that for most environments the total average power in reflections can be ignored. However, part of our work has environments where the first bounce ($k = 1$) reflection is necessary to model, we use (Wu and Haas, 2019, eqn. (3)) defined below to do so.

$$H_{NLOS}^{(j)} = \int_{A_w} \frac{(m+1)A\rho\cos^m(\phi_{j,w})\cos(\psi_{j,w})\cos(\phi_{w,r})\cos(\psi_{w,r})}{2\pi^2 d_{j,w}^2 d_{w,r}^2} dA_w \tag{2.13}$$

Define ρ as the wall element reflectivity, a number between 0 and 1 indicating the increase of the wall reflectivity. To study the effect of wall reflections, by discretizing eq. (2.13), the areas of the walls (A_w) are divided into grids of reflectors to be summed over, dA_w is a small area on the reflective walls. The angles are illustrated in Fig. 2·1b, where $\phi_{j,w}$ is the emittance angle from transmitter j to the reflector and $\psi_{j,w}$ is the acceptance angle. Then the second emittance angle from the reflector to the receiver is $\phi_{w,r}$, finally met with an acceptance angle $\psi_{w,r}$ at the receiver. The total channel gain from a transmitter j can be expressed as $H^{(j)} = H_{LOS}^{(j)} + H_{NLOS}^{(j)}$.

2.2 RF Models

In this section we introduce two popular RF models: 1) Joint Technical Committee (JTC) which has some traits from the Okumura-Hata model and the log distance path loss model and 2) Nakagami-m fading model.

2.2.1 Joint Technical Committee Path Loss Model

The JTC indoor path loss model is known to be very accurate in modeling the 2.4 GHz IEEE 802.11 wireless local area network (WLAN) in indoor office environments (Cebula III et al., 2011). It is presented by the International Standard Organization (ISO) and is defined as below:

$$L_{Total} = A + B_e log10(d_{RF}) + L_f(n) + X_\sigma \tag{2.14}$$

where A is an environment dependent fixed loss factor in decibels, B_e is the distance dependent loss coefficient and d_{RF} is the distance between the RF transmitter and the receiver. Meanwhile $L_f(n)$ is a floor/wall penetration loss factor in decibels and n represents the number of walls/floors between the transmitter and the receiver. Finally, X_σ is a Gaussian random variable with zero mean and σ standard deviation in decibels. Table 2.1 lists the corresponding variables along with the environment type.

Table 2.1: JTC Indoor Model Path Loss Variables

Environment	Residential	Office	Commercial
A(dB)	38	38	38
B_e	28	30	22
$L_f(n)$ (dB)	4n	15+4(n-1)	6+3(n-1)
Log normal shadowing standard deviation (dB)	8	10	10

2.2.2 Nakagami Fading

The Nakagami-m fading is very versatile in the sense that through manipulating the fading parameter[2] m_{Nak}, which can take any value between 0.5 and ∞, one can model different forms of fading. For instance, at: $m_{Nak} = 1$ it reduces to Rayleigh fading, $m_{Nak} = 0.5$ it represents a one sided Gaussian, and for $m_{Nak} > 1$ there is a one to one mapping to Nakagami-n which closely approximates Ricean K Fading (Simon and Alouini, 2005). This mapping is useful because in indoor communications, the presence of a strong LOS component aligns well with the Ricean model as well.

Let the RF channel gain be $|h_{RF}|^2$. It can be modeled by a Nakagami-m distribution and so its probability density function (PDF) can be expressed as:

$$f_{|h_{RF}|^2(x)} = \frac{m_{Nak}^{m_{Nak}} x^{m_{Nak}-1}}{\Omega^{m_{Nak}} \Gamma(m_{Nak})} \exp(-\frac{m_{Nak} x}{\Omega}), \quad x \geq 0 \tag{2.15}$$

and its cumulative density function (CDF) as:

$$F_{|h_{RF}|^2(x)} = \frac{1}{\Gamma(m_{Nak})} \gamma(m_{Nak}, \frac{m_{Nak} x}{\Omega}), \quad x \geq 0 \tag{2.16}$$

where $\gamma(.,.)$ is the lower incomplete gamma function and $\Omega = E[|h_{RF}|^2]$ is the Nakagami distribution spread.

The relation between the m_{nak} parameter and the Ricean K parameter can be formulated as (Simon and Alouini, 2005):

$$m_{nak} = \frac{(1+K)^2}{1+2K} \tag{2.17}$$

---

[2]Due to the fact that Lambertian order in VLC is defined as m, to resolve this we specifiy the Nakagami fading parameter here as m_{Nak}.

Chapter 3

Standalone VLC: Single User

In this chapter we discuss the single VLC link and ways to improve its quality by using the directivity property to enhance the received SNR. First we discuss the effect of receiver parameters such as device FOV and orientation on the signal quality and investigate how these parameters can affect user mobility. Second we propose novel receivers that adapt these parameters to allow for better received signal strength through channel isolation while providing comparisons to a baseline receiver with fixed parameters. Finally, we look into this analysis in terms of system resource reuse vs. receiver scope (analogous to transmitter coverage).

3.1 Impact of FOV and Orientation on Signal Quality and Mobility

When this work was initiated no direct work was available to address device orientation effects except for (Bas et al., 2015). This pushed us to study both receiver orientation and FOV effects theoretically and experimentally in our lab, resulting in numerous observations and results. Since we conducted our research recent studies, involving receiver orientation impact, followed (Eroğlu et al., 2019; Dehghani Soltani et al., 2019). There has been no experimental work on both FOV and orientation effects other than ours to date.

We start this discussion by showing the impacts on signal strength and discussing a few handover algorithms and their results when orientation and FOV are considered. In Chapter 9 we show extensive measured data from our lab setup that confirm the effects we show here as well.

In this chapter, we assume OOK modulated signals and accordingly the BER is evaluated as:

$$BER = Q(\sqrt{SNR}) \tag{3.1}$$

where SNR is modeled as discussed in Section 2.1. Generally, the achievable rate is considered as[1]:

$$R = B\log(1 + SNR) \tag{3.2}$$

For clarity we use the definition of **receiver scope** as analogous to the transmitter coverage but on the receive side. It describes what the receiver sees within its FOV (Abdalla et al., 2020d).

3.1.1 Signal Strength

In this section we use the empirical model described earlier in Section 2.1.2 using the simulation parameters in Table 3.1. It is worth noting that our model is general and can accommodate any layout. We choose our lab setup as an operating point to compare our results with our measured data later on in Chapter 9. Our transmitter layout is illustrated in Fig. 3·1b. This figure shows the rectangular transmitter grid which is mapped to our BU lab grid. The grid dimensions are 427 cm $\times$ 162 cm (x$\times$y): The luminaires are positioned from the center with increments of 0.7 m in the x-axis and 0.5 m in the y-axis at a height of 2.1 m from the floor. The red circle shows an example of the receiver scope at FOV$=20^\circ$. If it is assumed that the desired signal comes from transmitter 8 (Tx8) then everything else in the scope is either a source of noise or both noise and interference. The black square shows an area of data collection utilized later in Chapter 9.

[1]The Shannon representation of throughput serves as a tractable model, that is not concerned with specific modulation, for a good approximation of VLC link performance (Kashef et al., 2016; Guo et al., 2013)

Table 3.1: Impact of FOV and Orientation Simulation Parameters

BER threshold	10^{-3}
B	5×10^{7}
N_o without lens tube	1.25×10^{-11}
$C_T C_R$	1.4
N_o with lens tube	3.75×10^{-12}
Frequency	100 kHz

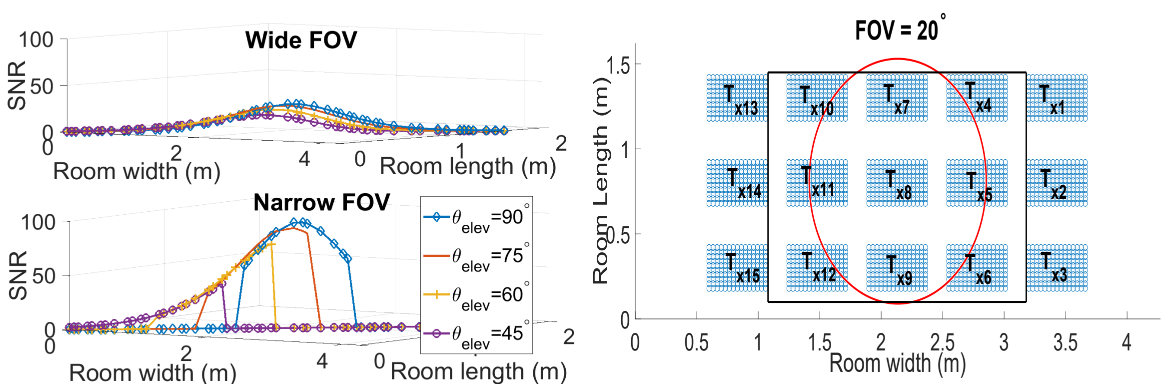

(a) (b)

Figure 3·1: (a) SNR Profile Under Central Transmitter for Different Tilts and FOVs; (b) Transmitter Plan View.

Table 3.2: Advantages and Disadvantages of Wide vs Narrow FOV

Narrow FOV	**Wide FOV**
Less noise.	Higher noise.
Less interference.	More interfering sources.
Higher received SNR/SINR.	Lower SNR/SINR.
Causes multiple regions with no signal reception (Coverage holes).	Minimal coverage holes therefore allows more reliable communications.
Smaller scope.	High scope.
Higher susceptibility to orientation and blockages as well as Tx-Rx misalignment. As it is observed in Fig. 3·1a that the highest SNR is directly underneath the light then it sharply drops off.	Regular susceptibility to orientation and occlusions. Enhances the ability to find alternative signals (faster than Narrow FOV) in case of occurrence of blockages.
High system resource reuse and thus spectral efficiency.	Low reuse and spectral efficiency.

In Fig. 3·1a we plot the signal received from the central transmitter (Tx8) when different tilts, $\theta_{elev} = \{90°, 75°, 60°, 45°\}$, and FOVs are assumed. The top subfigure shows the results at a wide FOV (90°) to be compared with the narrow FOV (20.89°) case in the bottom subfigure. The implications associated with the results are populated in Table 3.2.

Within each subfigure we plot different tilts to see the effect of orientation and it can be observed that flat receivers (with elevation angle, $\theta_{elev} = 90°$) get the best signal then the signal level gets worse with different tilts. Tilt also causes signals to disappear from scope.

In Fig. 3·1a, if we were to plot all the received signal strength (RSS) from all of the 15 transmitters, we will get many combinations of possible handovers based on all the possible curves due to tilt, FOV and location. This highlights the impact of orientation and FOV and how strongly they affect the seamlessness of the user connectivity and play a key role in analyzing handover schemes.

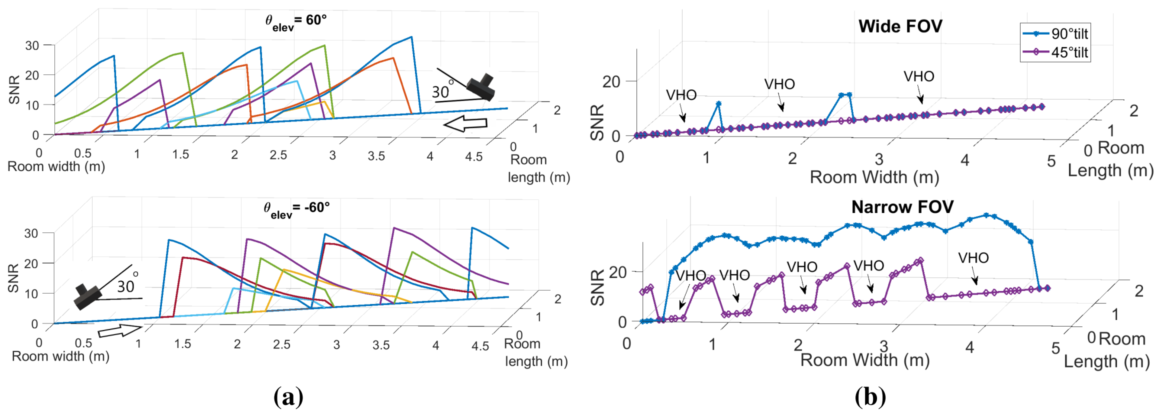

Figure 3·2: Impact of FOV and Orientation on Signal Strength and Handovers: (a) Orientation Effects when Using a Narrow FOV and Walking a Diagonal; (b) Possible Handover Scenarios when Traversing the room with Different Tilts and FOVs.

3.1.2 Mobility: Handover Analysis

In studying handover our objective is to have seamless connectivity without sacrificing rate or throughput performance. We focus on maintaining a lower bound on bit error rate (BER) and reducing the number of handovers experienced. Imagine the following scenario, for a person walking through an AP dense room. What is the nature of RSS for a user carried device? What if the device is tilted, and how does the FOV of the device impact performance? It is favorable to minimize number of handovers in a system while ensuring a required quality of service, as handovers usually introduce delays, can cause toggling effects and affect the overall system performance.

The metrics we analyze are: 1) Vertical handover (VHO) which happens when the VLC system cannot provide the minimum SNR needed to attain the desired BER and so the user is switched to the RF system; 2) Horizontal handover (HHO) is triggered between VLC APs based on device location/orientation; and 3) Total number of Handovers (THO) which is the sum of VHOs and HHOs. We also calculate the average rate for the user to monitor how each handover algorithm's reduction of THO affects it and what tradeoffs occur. For

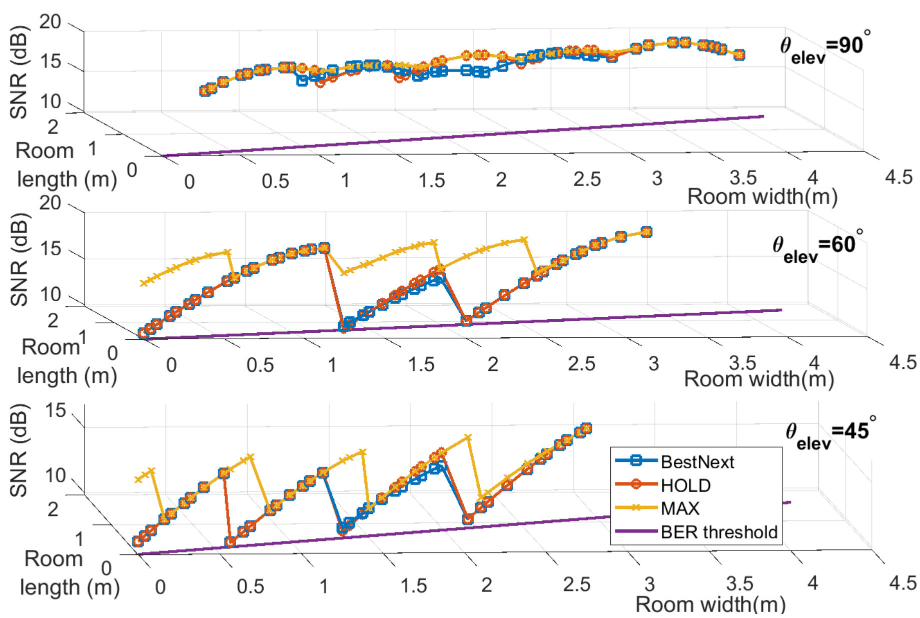

Figure 3·3: Handover Algorithm Results when Entering the Room from the Right Corner and Walking a Diagonal at a Narrow FOV.

average rate, we discretize the path that the user takes, get the instantaneous rate through eq. (3.2) and then get the average of all the points evaluated.

Fig. 3·2a illustrates a diagonal transit of the room. It shows the SNR profile for mobility with a tilted device, with narrow FOV, entering the room from different sides and walking diagonally across the room. The resultant handover output for the two scenarios are quite different due to direction of transit and the opposing orientations of the receiver. Meanwhile, Fig. 3·2b enhances the effect of how the narrow FOV allowed higher SNR but then the 45° elevation caused a lot of coverage holes which translate to handovers while the 90° elevation did not suffer as much.

Angular changes as well as FOV changes can trigger handovers depending on their severity. While conventional omni-directional systems have VHOs and HHOs due to translational motion, orientation in directional systems can cause an angular handover. Also, orientation combined with narrow receiver FOV can trigger higher VHOs and HHOs depending on the surrounding SNR values and the SNR threshold required.

This motivates us to study a few handover algorithms and later on in Section 7.1 propose an AP placement strategy.

Handover Algorithms

- Max Algorithm: is an RSS based algorithm where the receiver is always trying to connect to the strongest signal it can detect. We use it as our baseline scheme.

- Hold Algorithm: is an RSS based thresholding algorithm where the receiver tries to keep connected to its current access point (AP) as long as the received signal is greater than the threshold constraint. Otherwise, it connects to the highest signal detected and holds on to it in the manner mentioned above.

- Best Next Algorithm: is a predictive algorithm we propose in which the receiver compares the past SNR value with the present, predicting the slope of measured SNR changes (Abdalla et al., 2018). The handover occurs when the receiver finds an increasing slope.

Tables 3.3 and 3.4 show how each algorithm performs, in terms of the metrics we study, for different tilts and FOV for the scenarios of Fig. 3·3 and 3·4 respectively. Table 3.5 shows the results for a random walk case where we simulate a receiver moving in a random walk pattern for 1,000 steps within the lab.

Our simulations show that BestNext outperforms the other two policies in terms of lowest number of handovers when the receiver elevation angle is 90° while maintaining a reasonable average rate for the user. BestNext is based on following the highest slope when connectivity is about to be lost. For narrow FOVs the curve is no longer the full Lambertian and so there are no guarantees that it will outperform Hold. In the narrow FOV scenario, BestNext gives an almost equal performance to Hold while both are still better

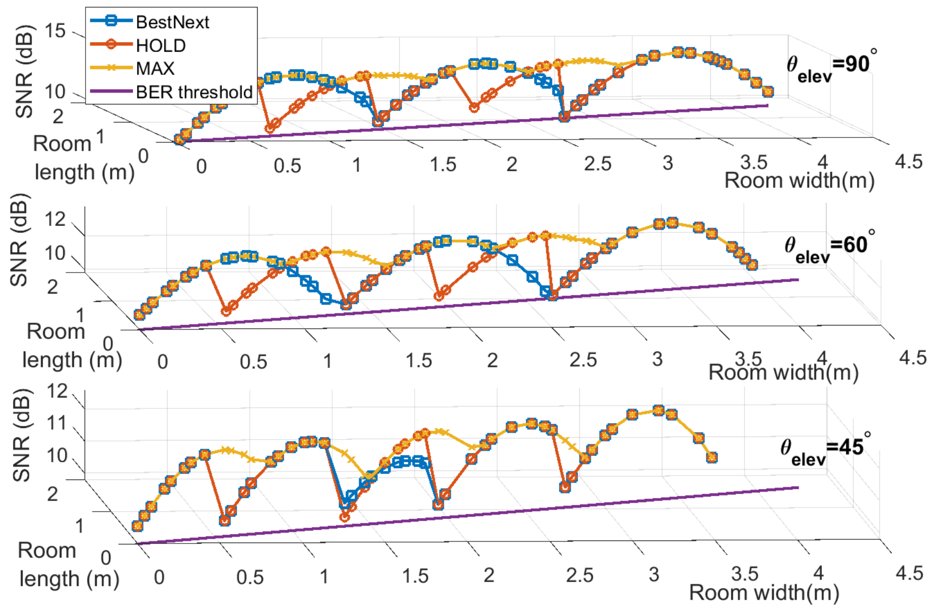

Figure 3·4: Handover Algorithm Results when Entering the Room from the Right Corner and Walking a Diagonal at a Wide FOV.

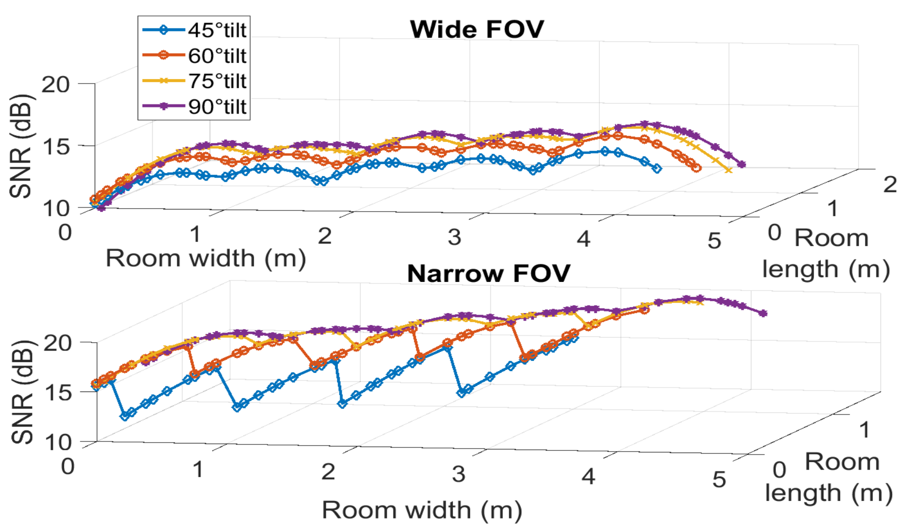

Figure 3·5: MAX Algorithm Results

Table 3.3: Diagonal Scenario at FOV = 20.89°

	Tilt (°)	Average rate (Mbps)	THO	VHO
Max	90	193.87	8	2
Hold	90	192.04	6	2
BestNext	90	190.1	6	2
Max	60	164.81	7	1
Hold	60	139.86	3	1
BestNext	60	139.19	3	1
Max	45	125.94	7	1
Hold	45	114.71	4	1
BestNext	45	114.04	4	1

than Max. In terms of average SNR, Max outperforms the other two policies marginally and is mostly worst in terms of number of handovers. The superior performance of Hold and BestNext depends on the FOV and the tilt of the receiver. However, when the receiver is directly underneath the luminaires, they tend to give almost the same performance. It is also worth noting that Hold's performance results in terms of handover will depend on the BER threshold desired. Fig. 3·5 also shows the effect of different tilts on the output of the Max algorithm and shows how the receiver FOV impacts the user device SNR. Our results highlight the impact of orientation and FOV and how strongly they affect the seamlessness of connectivity as well as the average user rate. Next we introduce two proposed variable FOV receivers and define a baseline fixed FOV receiver.

3.2 Baseline Fixed FOV Receivers

The fixed field of view (FFOV) receiver is our baseline receiver to which we compare the two dynamic FOV receivers that follow. Assume the FFOV receiver has a fixed FOV

Table 3.4: For the Diagonal Scenario at FOV $= 90^\circ$

	Tilt ($^\circ$)	Average rate (Mbps)	THO	VHO
Max	90	157.35	7	1
Hold	90	146.35	5	1
BestNext	90	149.69	3	1
Max	60	143.5	7	1
Hold	60	135.56	5	1
BestNext	60	136.85	3	1
Max	45	122.75	7	1
Hold	45	119.41	5	1
BestNext	45	119.04	5	1

Table 3.5: For a Random Walk Scenario at FOV $= 90^\circ$

	Tilt ($^\circ$)	Average rate (Mbps)	THO	VHO
Max	90	155.32	100	7
Hold	90	147.94	14	7
BestNext	90	148.68	12	7
Max	60	130.6	122	24
Hold	60	126.08	36	24
BestNext	60	124.72	41	24
Max	45	106.89	98	10
Hold	45	104.5	19	10
BestNext	45	104.5	19	10

χ_{FFOV}. Unless otherwise stated, χ_{FFOV} is set at 90° so that the receiver scope may capture all transmitters in any room and at any orientation. In a few cases we set the fixed FOV to χ_{max}, calculated based on room geometry, which covers all transmitters if the receiver were flat-oriented and centered in the space for performance comparison. The FFOV receiver does not provide channel isolation, however it is the least complex receiver of the three.

3.3 Novel Dynamic FOV Receivers

In Table 3.2 we discuss the benefits of wide versus narrow FOV which we observed from our study and analysis done in this dissertation. The two extremes have different advantages and disadvantages which can make one of them desirable in a scenario and less desirable in another. This trade-off can be resolved through employing a dynamic FOV functionality which would give the receiver the best of both worlds (Abdalla et al., 2020d) at the price of higher receiver complexity and practical considerations in the design phase. Here we describe the optimization problem and algorithms that go into designing the receiver. Later in Chapter 9 we discuss the lab measured data.

With the use of DFOV, a receiver can adjust to changing conditions, finding the optimal configuration. For example, by using a wide FOV to search for and acquire a link and then a narrow FOV to isolate a transmitter to improve link performance. We propose the DFOV receiver to enhance the VLC link SNR at the receiver.

Using the system model in Section 2.1.2, and utilizing the channel model eq. (2.9) we note that the important optimization parameter for this receiver is the FOV χ. Accordingly, we formulate the following optimization problem:

$$\begin{aligned} \max_{j=1,\ldots,S} \quad & \max_{\chi} \mathsf{SNR}^{(j)}(\chi) \\ \text{s.t.} \quad & \chi_{\min} \leq \chi \leq \chi_{\max} \end{aligned}$$

where S is the total number of transmitters in the room. We define χ_{min} as the minimum FOV to pick only one transmitter within the FOV and χ_{max} as the maximum FOV that can cover all the transmitters in the room when the receiver is flat, centered under the central transmitter and facing the lights.

The problem is non-convex and thus we solve the two following problems in their respective order, which together are equivalent to the previous problem, to obtain the best possible FOV for the best SNR that the receiver can achieve within a general room setting.

$$\text{(a)} \qquad \chi_j^* = \arg\max_{\chi} \mathsf{SNR}^{(\mathrm{j})}(\chi), \; j = 1, \ldots, S$$
$$\text{s.t.} \quad \chi_{\text{min}} \le \chi \le \chi_{\text{max}}$$

$$\text{(b)} \qquad \chi^* = \arg\max_{j=1,\ldots,S} \mathsf{SNR}^{(\mathrm{j})}(\chi_j^*)$$

Problem (a) finds the best FOV for the receiver per transmitter then Problem (b) picks the highest SNR amongst all the transmitters and identifies the FOV χ^* that yielded this highest SNR.

We show a simplified scenario (Fig. 3·6a) where we fix the location of the receiver in this simulation, underneath the middle transmitter in our layout (from Fig.3·1b). Then rotate it around its elevation angle θ_{elev} from 0 to 180. Fig. 3·6b shows the results of this scenario where for each θ_{elev} the optimization problem gives the best (Tx-FOV) pair that achieves the highest SNR. The curves plotted are the maximum SNR achieved, the FOV that was required for it and the colored regions show the transmitter to connect to. For example, at $\theta_{elev} = 20°$ the transmitter that gives the highest SNR (23.5 dB) is Tx5 at FOV $\chi = 58°$. When receiver motion is considered, the optimal FOV will be time varying. In this case, there is a need for repeated calculation of the FOV for each change sensed in location or orientation; however, depending on the device speed and the recomputation granularity, it can become impractical to use this approach. For the sake of practicality we design an

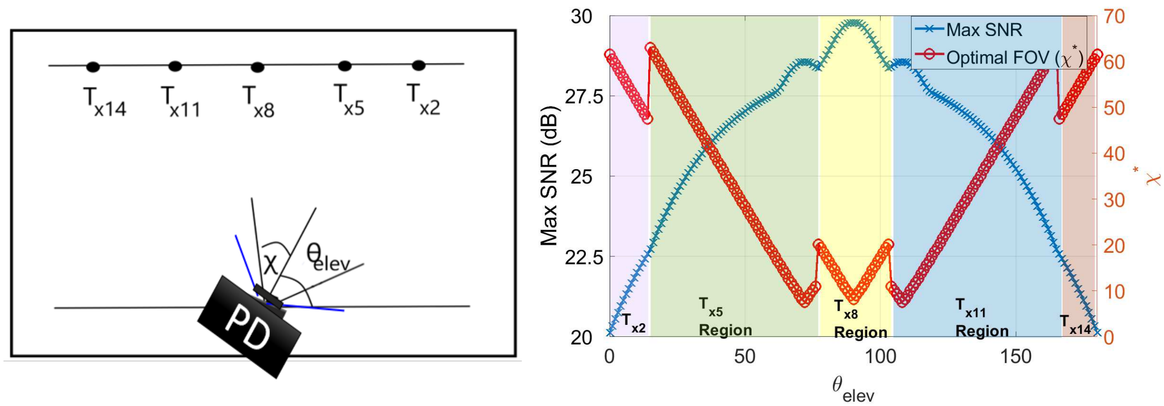

(a) **(b)**

Figure 3·6: Optimization Problem Setup and Results: (a) Example Receiver Centered in the Room with Variable Elevation; (b) Handover Algorithm Results of Setup in (a).

algorithm, namely velocity orientation variable FOV (VOV-FOV), to account for the user's velocity indoors. This algorithm is based on the optimization problem but tunes the FOV differently based on 3 possible user velocity states: quasi-static, slow and fast (since our discussion is mainly concerned with indoor VLC networks) that help in speeding up the receiver reaction based on the device velocity.

To study the impact of device velocity, we model device motion as a random walk with N steps and model velocity in a block-fading model fashion, where velocity is fixed over a number of blocks N_b. The device's elevation angle is uniformly variable between an interval of 90° and 75° and its azimuth angle is fixed at 0°. There exists two thresholds between the three intervals V_{T1} and V_{T2}. The states' description follows;

- **Quasi-Static Interval:** If a user velocity is below the first threshold V_{T1}, it is considered quasi-static and in this case based on device orientation changes, the receiver FOV is reduced/increased gradually in steps ,χ_{step}, until the best SNR is reached.

- **Slow Interval:** In this case, the user velocity is between the two thresholds V_{T1} and V_{T2}. The user is considered moving slowly in which case having a variable FOV still

Algorithm 1 VOV-FOV Algorithm

Input: Number of steps N, Block length N_b, $\{V_1, \ldots, V_N\}$
Initialization: Set Room dimensions, number of sources and their positions, receiver info.
for n=1:N **do**
  Calculate Fixed FOV SNR: $\max_j \mathsf{SNR}_\mathsf{j}(90)$ from eqn. (2.10)
  if $V_n > V_{T2}$ (Fast State) **then**
    $\chi = \chi_{\max}$
    Calculate $\mathsf{SNR}_\mathsf{j}(\chi)$ from eqn. (2.10)
  else if $V_n < V_{T1}$ (Quasi-Static State) **then**
    Calculate $\mathsf{SNR}_j(\chi), \forall j$ from eqn. (2.10)
    if $\max_j \mathsf{SNR}_j(\chi) = 0$ **then**
      while $\max_j \mathsf{SNR}_j(\chi) = 0$ and $\chi < \chi_{\max}$ **do**
        $\chi = \chi + \chi_{\text{step}}$
        Calculate $\mathsf{SNR}_{j,+}(\chi) \triangleq \mathsf{SNR}_j(\chi + \chi_{\text{step}})$
        if $\max_j \mathsf{SNR}_{j,+}(\chi) < \max_j \mathsf{SNR}_j(\chi)$ **then**
          break;
        end if
      end while
    else
      Calculate $\mathsf{SNR}_{j,-}(\chi) \triangleq \mathsf{SNR}_j(\chi - \chi_{\text{step}}),\ \forall j$ and $\mathsf{SNR}_{j,+}(\chi)\ \forall j$
      if $\max_j \mathsf{SNR}_{j,+}(\chi) > \max_j \mathsf{SNR}_{j,-}(\chi)$ **then**
        Keep Increasing χ till $\chi_{\max}$ or $\max_j \mathsf{SNR}_{j,+}(\chi) < \max_j \mathsf{SNR}_{j,-}(\chi)$.
      else
        Keep Decreasing χ till $\chi_{\min}$ or $\max_j \mathsf{SNR}_{j,+}(\chi) > \max_j \mathsf{SNR}_{j,-}(\chi)$.
      end if
    end if
  else(Slow State)
    $\chi = \chi_{\text{med}}$
    Calculate $\mathsf{SNR}_j(\chi), \forall j$
    if $\max_j \mathsf{SNR}_j(\chi) = 0$ **then**
      Increase χ until $\exists j$ s.t. $\mathsf{SNR}_j(\chi) \neq 0$ while $\chi < \chi_{\max}$
    end if
  end if
end for
Calculate Average max Variable FOV SNR Vs. Average max Fixed FOV SNR

allows for improvement in SNR but still needs a faster response from the receiver because the device is already on the move. This is why in this velocity range, the algorithm sets the FOV to a medium FOV, χ_{med}, a design parameter that depends on the room geometry. The algorithm then checks to see if the receiver is trapped in a coverage hole due to χ_{med}. If so, it gradually increases the FOV to get any available signal and avoid a disconnection. The algorithm re-evaluates when location, velocity or orientation change.

- **Fast Interval:** This is when the user velocity is above a threshold V_{T2}. In this case, a wide FOV that covers all the transmitters and thus prevents dropouts is preferred so we fix the FOV at χ_{max}. Note that, χ_{max} does not necessarily need to be a maximal value (e.g., 90°). In this specific state (Fast), we show the effects of fixing the FOV to be less than χ_{max} and how this can introduce coverage holes but give a higher average maximum SNR. This trade-off is represented in Fig. 3·7.

  Note: Maintaining the best coverage in the quasi-static and slow cases by dynamically changing the FOV to tune it to the best SNR makes sense but when it comes to the fast scenario, FOV needs to be fixed, mainly because the user's speed will not allow for useful optimization in the limited time available to traverse the room. During the transit time the optimal FOV may have changed before a new computation is complete. The sensitivity of the receiver to orientation increases with the decrease in FOV.

The different operating procedures per velocity interval allow the algorithm to be flexible so that the receiver does not suffer from coverage holes or low signal quality especially when mobile.

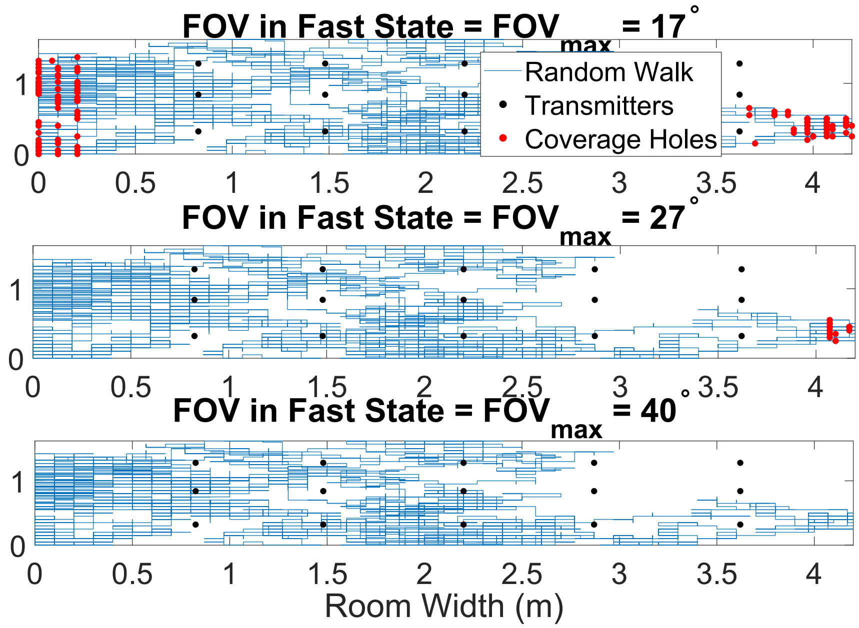

Figure 3·7: Coverage Holes for a Receiver with Variable θ_{elev} at Different Fixed FOVs in the Fast State: For FOV = 17°, Average Max SNR = 22.33 dB. While for FOV = 27°, Average Max SNR = 20.7 dB and for FOV = 40°, Average Max SNR = 20.33 dB.

FOV Step Size The FOV step size of the algorithm impacts the instantaneous difference between the FOV and the optimal value. Different step sizes are interesting because the circular view area is quadratic in FOV step size, as illustrated in Fig. 3·8. The figure shows how the number of transmitter elements found in range is linked to FOV step size expansion for a fixed room size and receiver height. It also shows the growth of FOV when the receiver is centered in the room. Once all elements are in the FOV (χ_{max} is reached), the cumulative effect of the visible APs reaches its limit. There is also an inherent tradeoff between step size and the convergence time for the algorithm; i.e., the smaller the step size, the longer it takes to converge to the solution, yet the closer the result is to the optimal. Thus step size should be tuned according to room design and the accuracy expected from the receiver. While the algorithm in the quasi-static interval resembles the gradient descent method (Bertsimas and Tsitsiklis, 1997), it differs in that it moves in the direction opposite to the gradient but not taking into account the actual gradient value within the step. This is

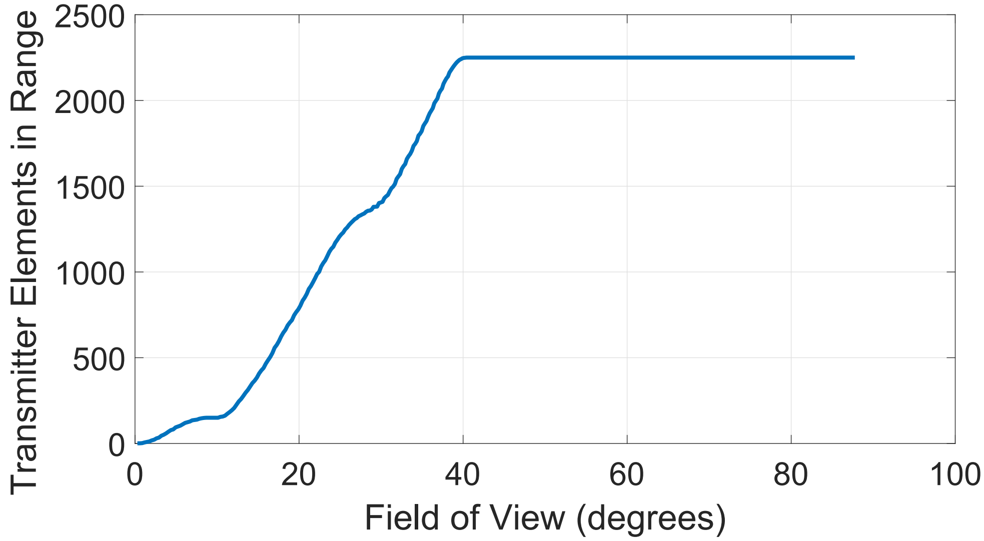

Figure 3·8: Number of Transmitter Elements Seen by the Receiver in Expanding FOV.

mainly because we choose to fix the step to produce faster results to the receiver.

We evaluated three different fixed FOVs for the same random walk pattern for the fast case as shown in Fig. 3·7. This includes 1) $\chi_{max} = 40°$, which yields full coverage but the least average maximum SNR, 20.33 dB, 2) $\chi_{med} = 27°$ which ensures that a flat receiver is always covered by 2 transmitters when we simulate between the possible number of sources (for a less dense network). The latter achieves 99.24% coverage in the shown scenario but allows for a higher maximum SNR on average than χ_{max}, with coverage holes only in the room corners that are tolerable in most cases. Finally 3) $\chi_{med} = 17°$ ensures being covered by 4 transmitters (useful in more dense optical networks) and gives the best SNR performance on average but produces more coverage holes at 96.18% coverage of the random walk. Note that these results are from the variable FOV algorithm and we only fix the FOV in the Fast case. This same scenario gives full coverage in the fixed FOV baseline and an average maximum SNR of 15.44 dB. Figs. 3·9a and 3·9b show the tradeoffs discussed but for different number of sources vs. the baseline fixed FOV of 90° adopted by most works. Our results are based on the study of different sets of APs including cases for 3,

Table 3.6: DFOV Scenario Simulation Parameters

Parameter	Parameter Description	Value
m	Lambertian order	0.88
B	Bandwidth	5×10^7 Hz
A	Receiver area	785×10^{-9} m^2
V_{T1}	Velocity threshold 1	0.1 m/s
V_{T2}	Velocity threshold 2	0.5 m/s
χ_{min}	Minimum FOV	$7°$
χ_{med1}	Medium FOV 1	$17°$
χ_{med2}	Medium FOV 2	$27°$
χ_{step}	FOV step	$7°$
χ_{max}	Maximum FOV	$40°$
$C_T C_R$	Constants @$100kHz$	1.4
N_b	Blocks	5
N	Random walk steps	$5,000$
A_{tx}	Transmitted amplitude	1.4 pk-pk
S	Number of sources	3,6,9,15
w	T_x Element grid width	15
n	T_x Element grid length	10
R	Responsivity	28
M	Multiplication factor	57
G	Transimpedance gain	10^5 V/A
i_d^2	Dark current noise	68×10^{-20} A^2
P_{txDC}	Noise DC power	0.0022 V

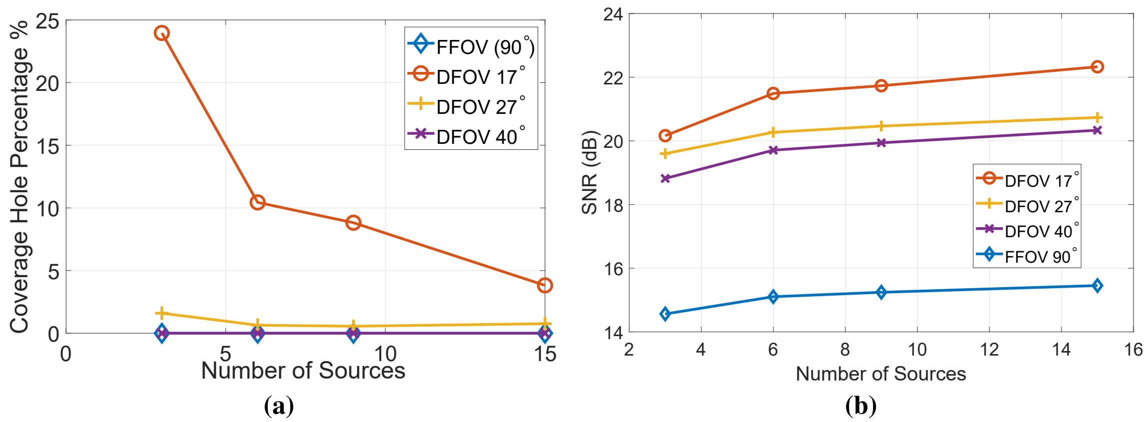

Figure 3·9: VOV-FOV results: (a) Coverage Hole Percentage versus Number of Sources; (b) SNR versus Number of Sources.

6, 9, and 15 APs. Both our baseline and novel algorithms consider orientation and location with the added advantage of including velocity as a parameter. This addition specifically improves results in our lab setting almost three times (3x) better than the baseline fixed FOV case. We argue that the higher the noise in an environment the better our algorithm will perform because it will be able to mask more noise than the case of lower noise setting.

Fig. 3·9b shows the improvement in average max SNR in the 3 cases of fixed fast FOV mentioned above versus the baseline fixed FOV meanwhile Fig. 3·9a shows how the improvement between the 3 variable FOV cases arises and shows the coverage loss percentage for each of these cases versus number of sources. The scenario at 15 sources in both of these figures is shown in detail in Fig. 3·7. Each of Figs. 3·9a and 3·9b shows how having a dense network improves coverage and average maximum SNR. Note however, a dense network providing multiple access must also reconcile frequency assignment or other means to mitigate inter-cell SINR when studying the multi-user case.

The results in Fig. 3·9 confirm the benefits of dynamically changing the FOV to achieve higher SNR. The results also highlight the need to balance the number of sources within a room, how they are spaced, and the inherent trade-off between coverage and SNR. Through optimization it is possible to find the FOV that provides satisfactory performance in both connectivity and SNR.

The optimization problem, VOV-FOV and the lab data (in Chapter 9) all show promise in using a DFOV receiver, where in some cases the DFOV receiver showed around 40% gain when compared to a basic fixed FOV receiver.

3.4 Novel Steerable Dynamic FOV Receivers

As confirmed in the previous section, allowing the receiver to adapt its FOV enhances the link quality and provides higher SNR gains. In this section we allow the receiver to adapt its orientation (elevation and azimuth angles of the receiving component, Fig.3·10) to help improve more on these gains (Abdalla et al., 2019a). For this receiver the parameters of interest are the FOV χ, the elevation angle θ_{elev} and the azimuth angle θ_{az}, optimizing the last two allows the receiving component to steer towards the center of a desired transmitter. Tracking receivers have multiple benefits; such as 1) Reducing the number of handovers, 2) Reducing overhead on the transmit side. Mobile Assisted Handover (where the mobile users manage the tracking of the APs) frees up the APs from the responsibility of tracking mobile users, and 3) Avoiding blockages.

The receiver experiences two phases, illustrated in Fig. 3·10b:

- Pointing Phase: From eq. (2.2), we deduce that a receiver can maintain best signal quality if $\psi = 0$, based on the cosine function for which a peak of 1 is achieved at angle $0°$. We assume the receiver knows the fixed location of the APs and knows its position relative to the APs. We then use our mathematical model to identify the best elevation and azimuth angles that allow the receiving component to always position with $\psi = 0$ with respect to the center of the tracked source. These angles, represented in Fig. 6·5, are geometrically deduced as follows:

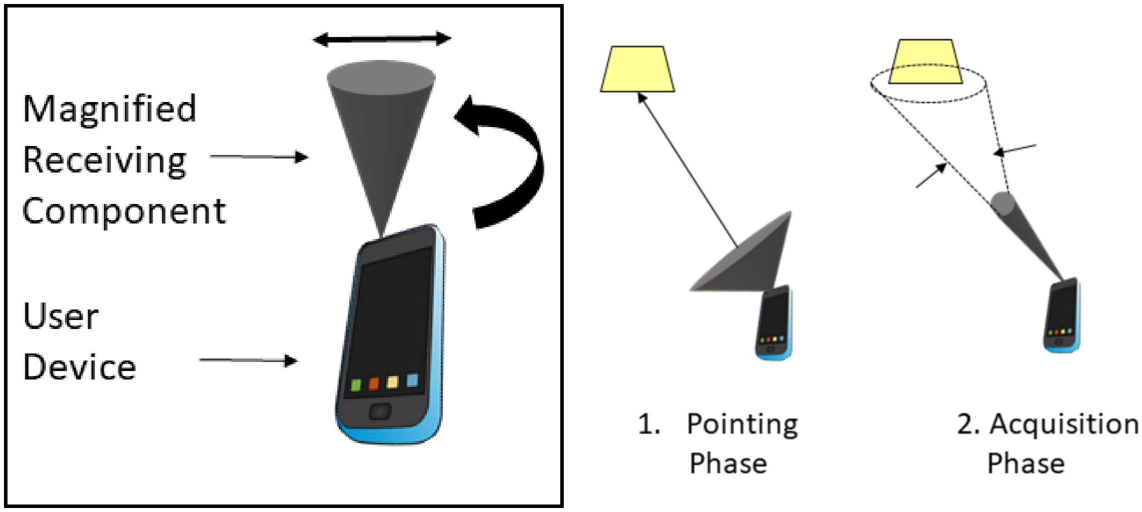

(a) **(b)**

Figure 3·10: SDFOV Receiver: (a) Structure; (b) Phases of Operation.

$$\theta_{elev} = \tan^{-1}\left(\frac{V}{\sqrt{(x_r - x_t)^2 + (y_r - y_t)^2}}\right)$$
$$\theta_{az} = \tan^{-1}\left(\frac{y_t - y_r}{x_t - x_r}\right)$$

where V is the vertical height between the transmitter and the receiver. (x_t, y_t) and (x_r, y_r) are the x, y coordinates of the transmitter's center and the receiver, respectively.

- Acquisition Phase: Once the pointing phase decides on the best transmitter to track and the angles θ_{elev} and θ_{az}, one can either dynamically search for the FOV that achieves the highest SNR from the tracked transmitter using the following optimization problem:

$$\max_{\chi} \quad \mathsf{SNR}^{(\mathrm{j})}(\chi)$$
$$\text{s.t.} \quad 0 \leq \chi \leq \chi_{\max} \tag{3.3}$$

χ_{max} can be 90° for an unknown space or it can be deduced geometrically for any known room setting depending on the physical constraints of the receiver FOV.

The optimal FOV can be scanned for, however, if the receiver knows full information about the transmitter's four corner element locations, as well as its own location, the optimal FOV can be evaluated as follows:

$$\chi = \cos^{-1}\left(\frac{u_c.u_e}{||u_c||||u_e||}\right) \tag{3.4}$$

where u_c is the vector from the receiver to the midpoint of the transmitter and u_e is the vector from the receiver to any element within the transmitter. The equation is evaluated for 3D lines so we need to transfer their intersection point to the origin. This can be done by subtracting the receiver location from both known points on the lines. This only needs to be evaluated for the four corner elements. The largest χ from this calculation is the optimal FOV. The geometry behind this is that due to the random orientation of the receiving element, the FOV cone's intersection with the transmitter plane generally forms an ellipse. By testing the edge elements of the transmitter we find the best intersection of this ellipse so that all elements are included.

This receiver can achieve full channel isolation as long as the transmitters are not touching or overlapping which is a logical assumption. In terms of hardware complexity, it has the highest complexity of the three receivers.

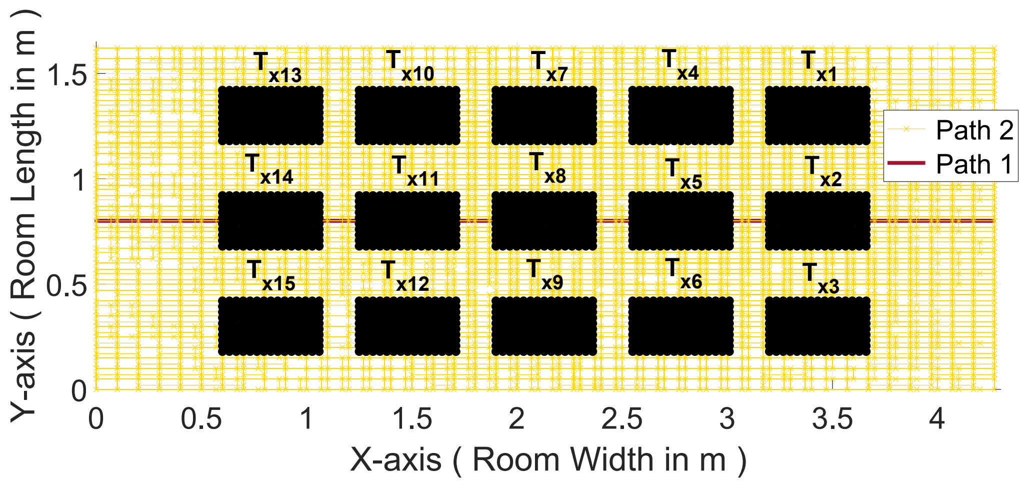

Figure 3·11: Simulation Paths Taken by the SDFOV Receiver.

Single User Simulation Setup and Results: We show simulation results for mobility cases where 1) the receiver is traversing the room in a horizontal path underneath the lights grid and 2) a random walk path throughout the space. Both paths are highlighted in Fig. 3·11. The receiver finds the closest transmitter to its position within its range of motion (in our simulation it is assumed that the receiver has full range of motion) and locks on to it. The condition for which the receiver decides to stop tracking one transmitter and lock on to another depends on the configuration of the overall system (room size, AP placement, handover protocol, receiver range of motion, etc.). We choose to use the SNR threshold β as the transition criterion. Once the receiver meets this condition, it initiates pointing and tracking of a new transmitter and subsequent optimization of FOV for the new source.

We show results that compare the SDFOV receiver and show its superior performance in comparison to :1) the non-tracking DFOV, 2) non-tracking FFOV with the FOV set to either $\{7.8°, 40°, 90°\}$ where $7.8°$ is the largest angle output from the optimization problem in eq. (3.3), $40°$ is χ_{max} and $90°$ is the baseline receiver FOV. The simulation parameters can be found in Table 3.7.

Table 3.7: SDFOV Single User Simulation Parameters

Parameter	Parameter Description	Value
m	Lambertian order	0.88
B	Bandwidth	5×10^7 Hz
A	Receiver area	785×10^{-9} m^2
χ_{min}	Minimum FOV	7.54°
χ_{max}	Maximum FOV	40°
P_t	Transmitted power	1.4 W
w	T_x Element grid width	15
n	T_x Element grid length	10
R	Responsivity	28
h	Vertical height between Tx and Rx	1.96 m
i_d^2	Dark current noise	68×10^{-20} A^2
P_{txDC}	Noise DC power	0.0022 V

We employ the Max and Hold handover policies explained in detail in Section 3.1.2 to show the different receivers' performance under these two policies, at two different thresholds β and two paths.

In Fig. 3·12a we show the performance when the receiver traverses horizontally throughout the room (at a fixed y on the y-axis) under Max Policy at $\beta = 26$ dB. The superior performance of the SDFOV receiver in terms of SNR is evident as it follows the highest signal envelope without running into coverage holes (dead zones). It is closely followed in performance by the DFOV receiver which suffers when it is not exactly aligned under a transmitter due to its inability to change its orientation. However, both dynamic field of view receivers show better SNR performance than the remaining fixed FOV receivers. The FFOV non steerable receivers show different performances. When set to 1) 7.8° the performance is best when the receiver is exactly under the transmitter otherwise it goes through

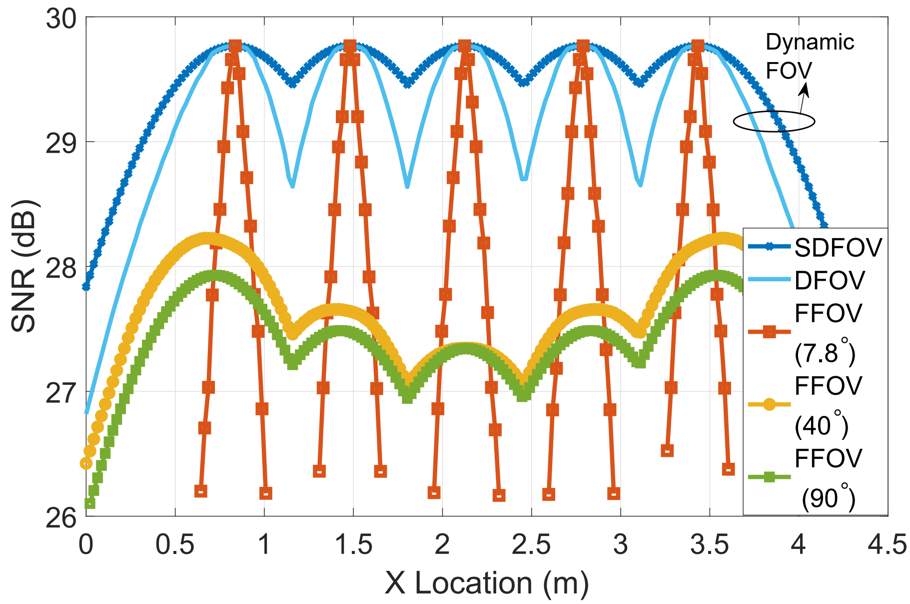

(a)

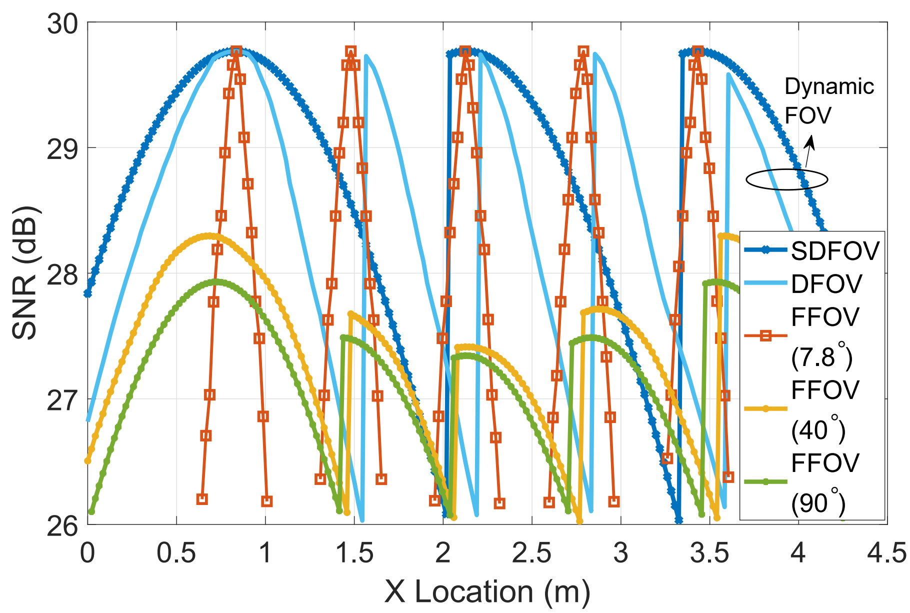

(b)

Figure 3·12: Scenario Performance Comparison of Fixed and Variable FOV, Tracking and Non-Tracking Receivers at $\beta = 26$ dB : (a) Comparison Under Max Policy; (b) Comparison Under Hold Policy.

Table 3.8: Path 1 Performance Statistics

HO policy	Tracking Status	Average max SNR (dB) $\beta = 26$ dB	$\beta = 28.5$ dB	HOs $\beta = 26$ dB	$\beta = 28.5$ dB	FOV (°)
Hold	Tracking	28.86	28.97	3	5	dynamic
Hold	Non-tracking	28.39	28.62	5	5	dynamic
Hold	Non-tracking	24.74	22.42	5	5	7.84°
Hold	Non-tracking	27.41	NA	5	NA	40°
Hold	Non-tracking	27.15	NA	5	NA	90°
Hold	Tracking	28.86	28.97	3	5	7.84°
Max	Tracking	29.46	29.46	5	5	dynamic
Max	Non-tracking	29.15	29.15	5	5	dynamic
Max	Non-tracking	25.82	25.82	5	5	7.84°
Max	Non-tracking	27.68	27.68	5	5	40°
Max	Non-tracking	27.38	27.38	5	5	90°

abrupt signal changes and loss, 2) 40° shows reduced performance than the previous fixed FOV setup but an overall stable signal performance and 3) 90° shows similar performance to the previous receiver but sees worse noise at the edges of the transmitter grids due to its wider scope. All receivers show the same performance in terms of handovers simply due to the Max policy which prefers higher signal level over reduced number of handovers. The simulation results are specified in details in Table 3.8.

In Fig. 3·12b we plot the results for the Hold policy, interestingly, the results show that only the SDFOV is able to reduce the number of handovers in this scenario while all the others have the same performance in terms of handovers. Still the dynamic FOV receivers outperform the fixed FOV receivers and the trends seen in the previous figure are the same. More results are populated in Table 3.8.

One can note that the receivers attain the same performance under Max policy and the performance does not change with different thresholds. This is evident in the results in Table 3.8. β affects the Hold policy performance. We show this in Fig. 3·13a where we plot the performance at a higher threshold $\beta = 28.5$ dB. The SDFOV receiver in this case exhibits higher handover usage to attain the higher SNR threshold and the FFOV receivers fixed at 40° and 90° could not keep up under the higher threshold. All performance results for this figure are available in Table 3.8. Fig. 3·13b shows the result of optimizing the three angles that SDFOV receivers are able to tune; azimuth, elevation and FOV. The elevation angle moves in direction of tracking the source, the azimuth moves between either 0° or 180° because the receiver is under the lights and the FOV χ gets smaller when aligned under the lights. (Note that the dip in the FOV underneath the lights is due to the optimization seeking the minimum FOV that achieves highest SNR even if the surrounding neighborhood of this FOV, slightly larger FOVs, may also achieve the same SNR).

Fig.3·14 shows the CDF of SNR of the different receiver types when the devices move in a random walk consisting of 1 million steps in our lab layout (Path 2). The performance order is still in favor of the dynamic FOV receivers with an edge to the steerable one. The FFOV receivers have poorer performance but within them the order of superiority is 40° which sees less noise than 90°, followed by 90° then finally 7.8° which obviously runs through a lot of coverage holes. Results of Max and Hold policies for Path 2 are all listed in Table 3.9 which also shows the handover reduction performance results of using SDFOV receivers as well as the higher SNR average.

Angle Sensitivity Analysis Fig. 3·15 shows results for the minimum FOV reached by the optimization including the maximum and the mean. Table 3.10 shows the average maximum SNR for each FOV. From the table we can see that within less than 2° difference,

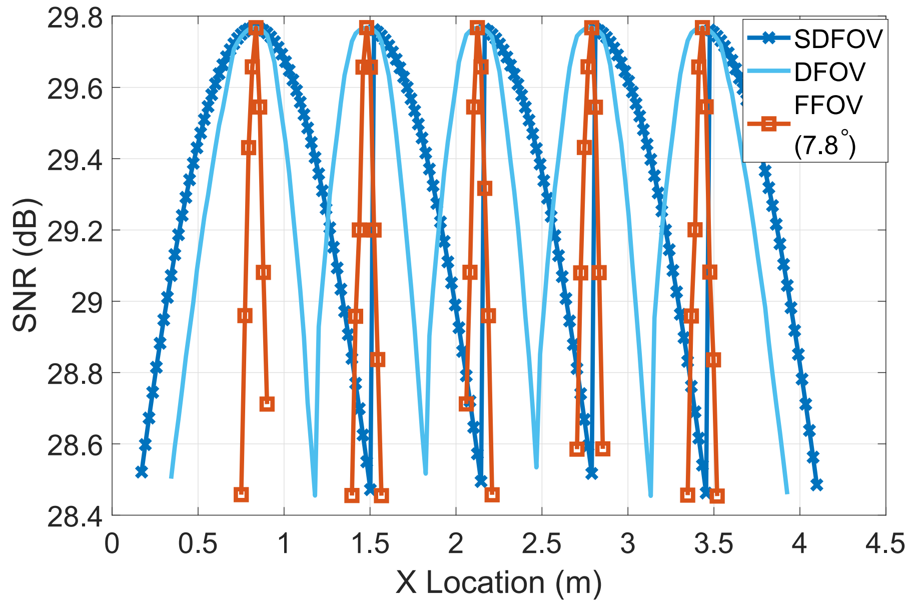

(a)

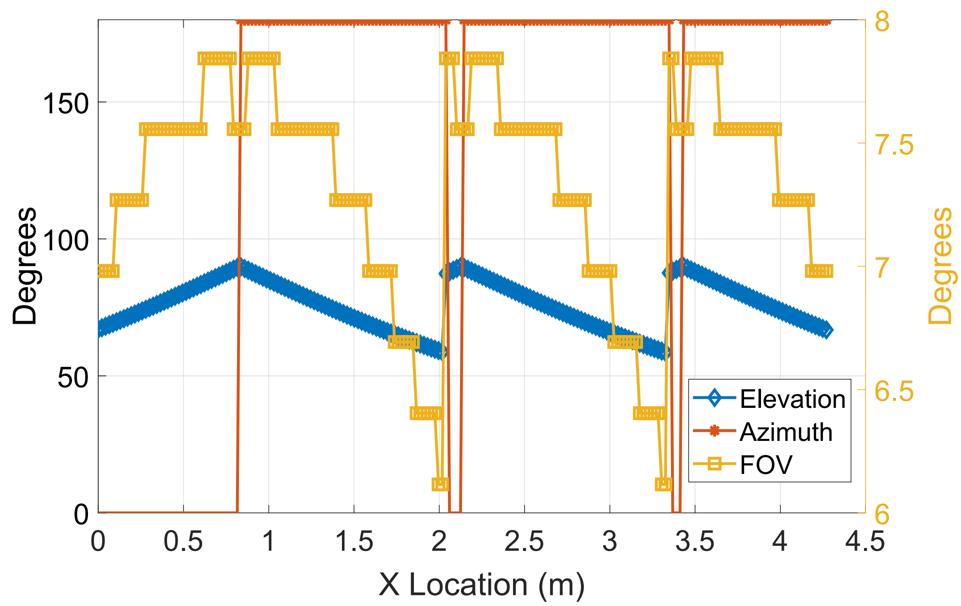

(b)

Figure 3·13: Scenario Performance Comparison of Fixed and Variable FOV, Tracking and Non-Tracking Receivers (Path 1) : (a) Comparison Under HOLD Policy at $\beta = 28.5$ dB; (b) Optimized Angles Results.

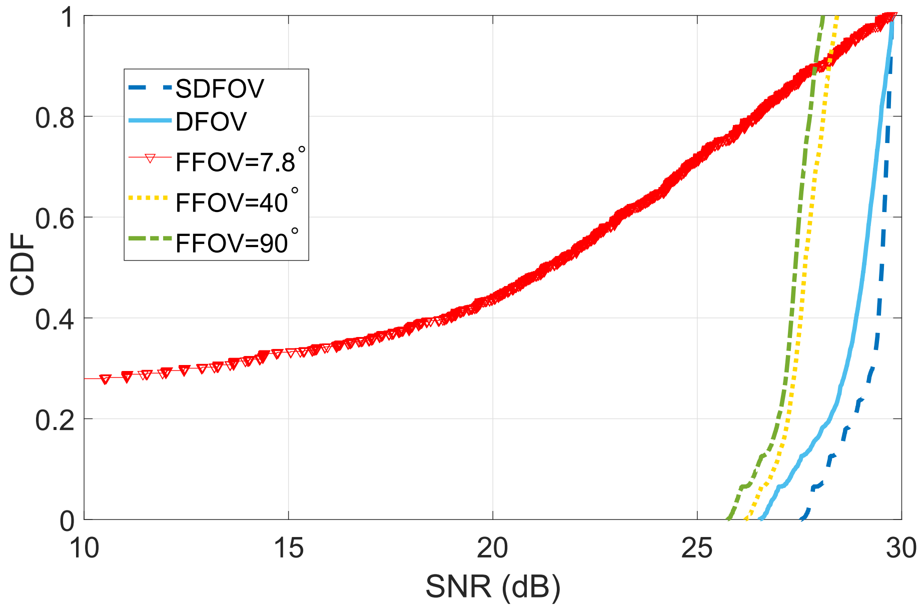

Figure 3·14: SDFOV Receiver SNR Statistics Under Path 2.

Table 3.9: Path 2 Performance Statistics at $\beta = 26$ dB

HO policy	Tracking Status	Average max SNR (dB)	HOs	FOV (°)
Hold	Tracking	28.73	110	dynamic
Hold	Non-tracking	28.48	300	dynamic
Hold	Non-tracking	21.45	5477	7.84°
Hold	Non-tracking	27.45	422	40°
Hold	Non-tracking	27.04	1773	90°
Hold	Tracking	28.73	110	7.84°
Max	Tracking	29.35	3626	dynamic
Max	Non-tracking	28.89	4019	dynamic
Max	Non-tracking	21.45	4732	7.84°
Max	Non-tracking	27.63	4019	40°
Max	Non-tracking	27.18	4019	90°

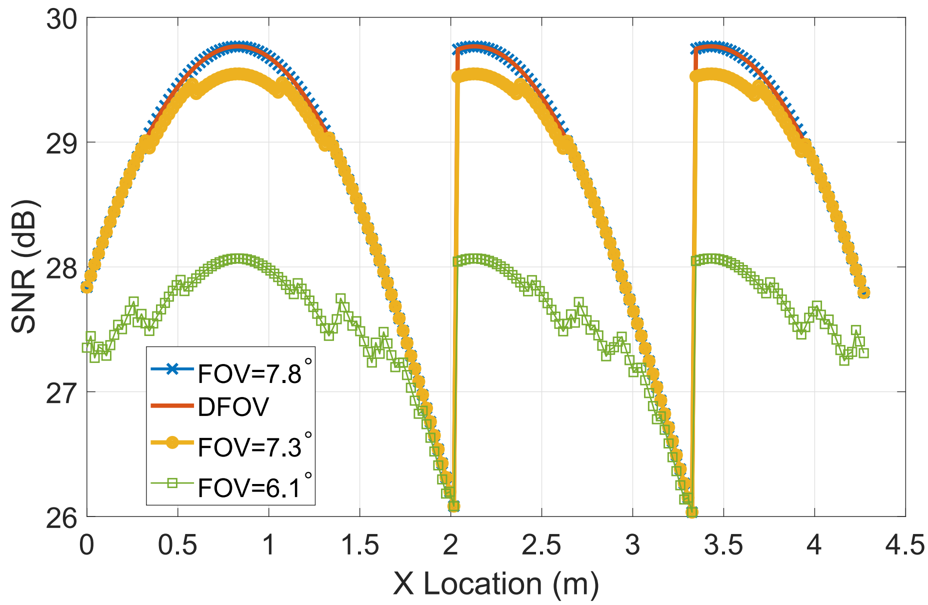

Figure 3·15: Effects of Angle Sensitivity on SDFOV Performance.

Table 3.10: Average Max SNR for Tracking with Fixed FOVs

Average max SNR (dB)	FOV (°)
28.86	7.84°
28.84	χ_{min}
28.76	7.34°
27.58	6.12°
28.86	dynamic

the average max SNR dropped by approximately 1.3 dB. This confirms how sensitive SNR is to the FOV.

The results in Tables 3.8, 3.9 and 3.10 confirm that for the tracking receiver, if the FOV is fixed at the maximum from the optimization result (7.84° in this scenario, not to be confused with χ_{max}), we realize identical performance, mainly because the noise pattern does not change significantly at that FOV level. As the FOV increases more than 7.84°, the SNR decreases. To be able to get the required FOV, the receiver can either keep solving the optimization problem until it goes underneath a light and then use the maximum FOV reached or if it knows the light source size, it can use eq. (3.4) directly, however this is a sensitive number as the FOV does not change substantially; but the SNR can differ drastically as shown in Fig. 3·15. Note that for a rectangular source as in our model, setting the FOV fixed at χ_{min}, yields a lower average max SNR, see Table 3.10.

SDFOV Receiver Designs and Complexities

- While it makes sense to use the SDFOV receiver based on its performance results, it is important to keep in mind that it is the most complex of the other receivers, as it needs to optimize χ, θ_{az} and θ_{elev}. A good compromise is the tracking receiver with fixed FOV which is a variation of the previous receiver. Once the best FOV from the optimization is applied, we realize the same performance but without the need to recalculate χ, for a fixed receiver height. Next in terms of complexity is the DFOV receiver without tracking which optimizes χ to give high SNR.

- The lowest-performing receiver is the one with fixed χ_{FFOV} and fixed orientation because while it is the least complex one, based on the fixed FOV, it sacrifices coverage or SNR. The smaller the FOV, the higher SNR per location and the more coverage holes occur, and vice versa.

- Practically speaking if the receiver FOV is not dynamic then it will likely be set at 90° to adapt to any environment because otherwise the communication might suffer in coverage specially when devices are tilted.

3.5 Receiver Height Effect

Fig. 3·16 shows the relationship between FOV and SNR and the importance of controlling the device FOV to attain the required communication quality. It also shows that the relation

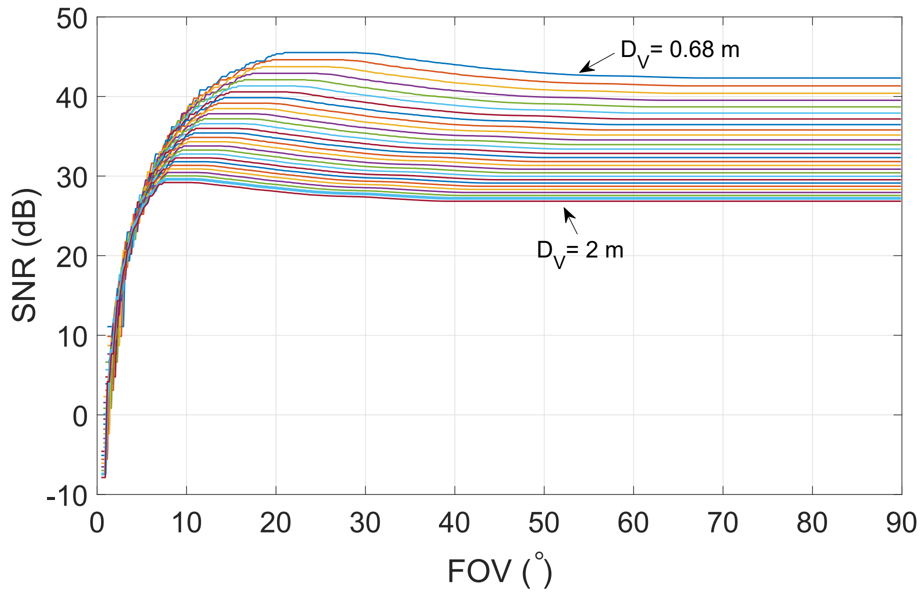

Figure 3·16: SNR-FOV Relation at Different Heights.

between SNR and FOV is not strictly increasing. As it goes through two phases, scanning for more signal until the best FOV is reached (SNR increases) then with admittance of more transmitter elements the SNR decreases due to the introduction of noise. The figure also shows the dependency of the vertical height V (between the transmitter and the receiver) on the received SNR and thus optimal FOV. It is also noticed that with decreasing V the optimal FOV grows.

3.6 Reuse vs Scope Trade-off

In this section we discuss a different aspect impacted by receiver FOV and orientation. We focus our analysis on the trade-off that involves system resource reuse and receiver scope (how many APs a receiver can see). We define **system resource reuse** as the number of possible instantaneous non-interfering transmissions in a system.

Our approach is to evaluate the receiver scope in a room based on static or dynamic FOV while assuming fixed orientation and height of the device. We also assume that once

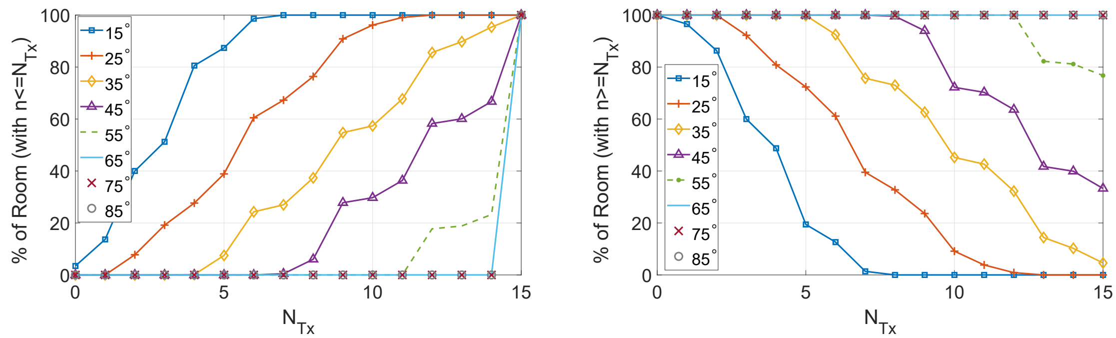

(a) **(b)**

Figure 3·17: Impact of FOV and Orientation on System Resource Reuse and Scope at $V = 1.96$ m : (a) Reuse Percentage Statistics Shown Through the Scope For Different FOVs; (b) Receiver Scope Percentage Statistics.

a receiver sees one or more elements of an AP, the AP is considered within receiver scope. We then consider implications of single vs. multiple transmitters on limiting spatial reuse.

We discuss the results of simulating a receiver moving within the space illustrated in Fig. 3·1b (the 15 AP layout). We define n as the number of APs seen by the receiver, where n is a variable that takes an integer value between 0 and 15, and N_{Tx} to be the maximum number of APs seen.

In Fig. 3·17a we show results for resource reuse percentage for each location in a 500×500 uniform span of the room. Results are obtained by iterating over the FOV to determine n and form the percentage of transmitter occurrence within the room. For reuse we evaluate the percentages where $n <= N_{Tx}$. Each curve represents a different FOV. When the number of transmitters seen by the receiver is low, the system reuse factor grows because the receiver is able to isolate channels therefore more transmitters can transmit simultaneously without causing interference to neighbors. On the other hand when FOV increases, so does the receiver scope, resulting in less resource reuse due to additional transmitters in the FOV. In Fig. 3·17a, we see that smaller FOVs yield higher resource reuse. This is due to the ability to control the presence of fewer interfering signals within the received signal. Wide FOVs do not allow for such selectivity. Extremely small FOVs on

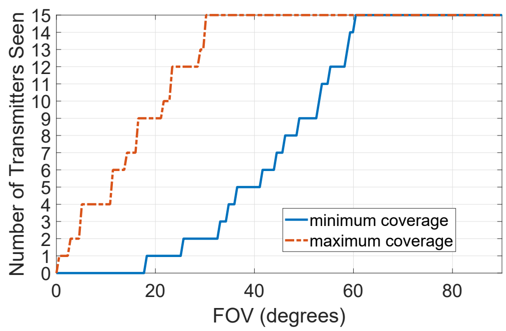

(a)

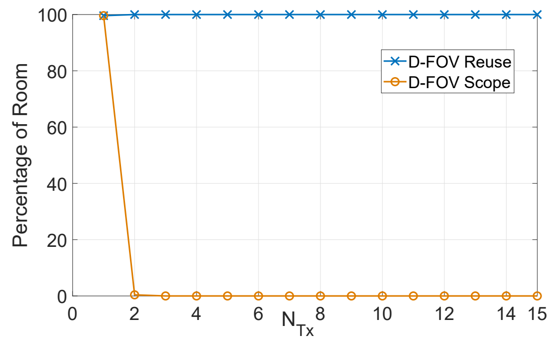

(b)

Figure 3·18: (a) Scope vs. FOV; (b) DFOV Scope and Reuse.

the other hand end up having a percentage of the room with $N_{Tx} = 0$, which is a guaranteed outage condition.

Fig. 3·17b, shows the receiver scope aspect of this tradeoff. Here we evaluate $n >= N_{Tx}$, where N_{Tx} in this case is the minimum number of APs seen. Wider FOV supports seeing all transmitters, allowing more reliability and faster connections as well as possible cell merging techniques. Generally, the lower the FOV, the worse the receiver scope but the better the SNR performance because of the isolation from extra noise.

We simulate a receiver moving in the same uniform 500×500 grid that covers the room, record the maximum and minimum number of transmitters seen for each FOV and plot the results in Fig. 3·18a which shows the role of FOV in the scope/reuse trade-off. For example, a fixed 20° FOV can range in redundancy from 1 transmitter to 9 throughout the environment whereas a 40° fixed FOV can range from 5 transmitters in view up to 15 depending on the location. This example confirms that some FOVs are limited in terms of scope because they cannot see more than a certain number of transmitters while other FOVs are reuse limited and cannot see fewer than a fixed number of transmitters. The usage of the DFOV receiver fits in the discussion here to break this rigidity and allow for more flexibility in both aspects depending on the needs of a user device.

This is why we simulate the performance of a DFOV receiver, with the goal of maximizing SNR at different locations as the device moves throughout the specified room. We use the optimized FOVs from the receiver's motion in the uniform 500×500 grid and iterate to find n. Fig. 3·18b shows the reuse statistics as well as the scope percentage but for the dynamic optimized FOVs resultant from the DFOV receiver. The results of this simulation show that optimizing SNR yields high reuse. The DFOV receiver achieves both high SNR and high reuse while its scope ≤ 2.

Multi-User Reuse/Scope Case Study We discuss a case study for a multiple user scenario to motivate our work later in Chapter 6. In a multiple user scenario, mobility will introduce random placement of user devices within the transmitter grid, revealing the limitations of a deterministic analysis. In this case, the optimal FOV will depend on the density of the users as the system reuse depends on where devices are located relative to each other. Subsequently, resource reuse impacts system capacity and so overall system performance. To this end, we compute an empirical resource reuse upper bound on the average across all locations for a multi-user scenario. This is achieved by evaluating the best possible reuse factor (number of links that can transmit simultaneously such that receivers do not experience interference from neighboring APs) per FOV and average the results over 10, 000 possible random locations in the room for four receivers and four transmitters. We assume that seeing a single element of an AP or more causes interference to a receiver.

The four transmitters we use are illustrated in the form of grids within the overall setup we use, Fig. 3·19a. Fig. 3·19b shows three cases corresponding to three different grid sizes shown. The transmitters we use in our simulations per grid are the ones at the edge of the specified grid. For Grid 1 we use transmitters $\{1,2,4,5\}$, Grid 2 has transmitters $\{7,9,13,15\}$ and for Grid 3 we use $\{1,3,13,15\}$. These grids also correspond to decreasing density. From Fig. 3·19b, we see that resource reuse depends on FOV, density of the transmitters, and the location of the receivers. In the Grid 2 and Grid 3 cases the reuse fluctuates between a high and low number depending on where the devices are located. For

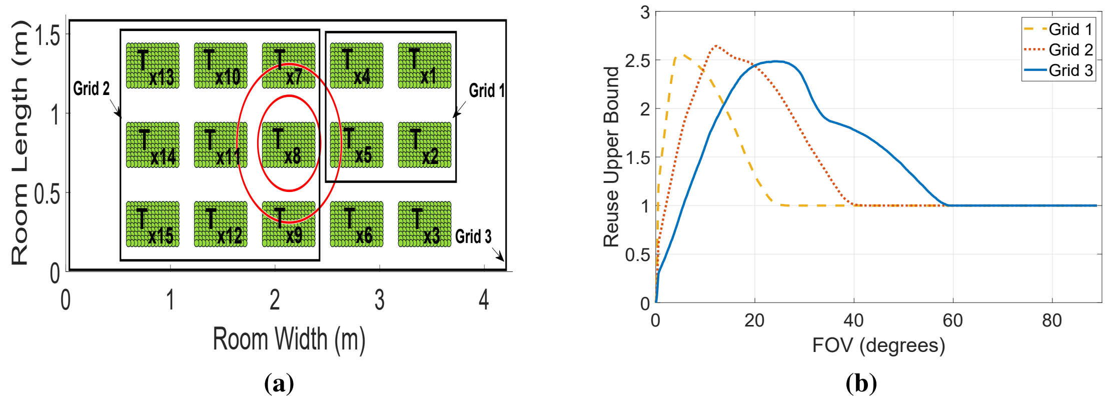

Figure 3·19: (a) Transmitter Layout; (b) Different Grid Reuse Upper Bound with Variable Device FOV.

a device in a corner of the room, higher FOVs enable higher receiver scope, more possible transmitter/receiver connections and more possibilities for higher reuse. Meanwhile, in the cases where the devices are underneath the APs, narrow FOVs achieve better reuse. These results also support the case for using a dynamic approach to controlling FOV.

3.7 Chapter Conclusions

In this chapter we focus on enhancing the importance of receiver FOV and orientation in realistic VLC systems. We start by enlisting the impacts observed in our analysis as well as the advantages and disadvantages of narrow vs. wide FOV on several communication aspects; 1) Handovers, 2) SNR, 3) Average rate, 4) Scope, 5) System Resource Reuse. All while varying several receiver parameters such as receiver location, height, velocity and orientation. This is why we propose two dynamic FOV receivers; non-steerable and steerable. The former remedies the FOV effects and the latter remedies both FOV and orientation to allow more receiver control for a better overall communication performance. We compare our proposed receivers to a baseline FFOV receiver.

Our simulations show superiority of the SDFOV specifically and the dynamic FOV receivers generally. The proposed SDFOV technique shows an average SNR increase of up to 40% compared to the baseline receiver associated with a user device with dynamic translational/rotational motion (We discuss the experimental gains in Chapter 9).

We also propose the VOV-FOV algorithm which is a strong candidate for dynamic systems that take user orientation, location and velocity into account. VOV-FOV improved SNR simulated results for our lab setting almost three times (3x) better than the baseline fixed FOV case. In terms of the reuse vs. scope trade-off for a single user (as well as a multi-user case study), our simulations show performance gains in overall system performance, and user SNR/SINR.

This establishes a range of applications for DFOV receivers in dense OWC networks. The performance results also hint at the possibility of adjusting the receiver FOV so that a system can have gains in the range of whole system reusability, making full use of spatial diversity while mitigating interference effects on user devices. These results motivate us to study the possible usages for these receivers in multi-user settings to manage interference.

Chapter 4

Directional OWC Interference Distinction, Categorization and Management

This chapter focuses on interference in OWC systems, the differences between RF interference and optical medium interference, and interference management techniques used in the literature. Firstly, we overview the unique characteristics of OWC interference. Secondly, we introduce interference management techniques for static systems. Thirdly, we discuss strategies to dynamically adapt the techniques to the characteristics of the environment. Finally we show a case study of employing dynamic FOV receivers in a multi-user case study compared to the baseline FFOV receiver.

VLC as an emerging technology has areas that have not been fully explored by the research community; some of which (most importantly) are the impact of large scale VLC installations and the impact of increasing densities of APs to serve the growing number of devices supported by the network.

Early research in VLC mainly focuses on single link implementations to ensure successful point-to-point communication. The focus in that line of research is improving link performance through signal processing and proposing novel modulation techniques. More recent works delve into the system level by deploying cells of multi-point-to-point or multi-point-to-multi-point communication. These multi-AP systems introduce neighboring cells which naturally induce interference. While interference can also occur from multiple user transmissions, little work has analyzed interference in the context of VLC uplinks. This is primarily because many systems consider asymmetric links by using an alternative medium

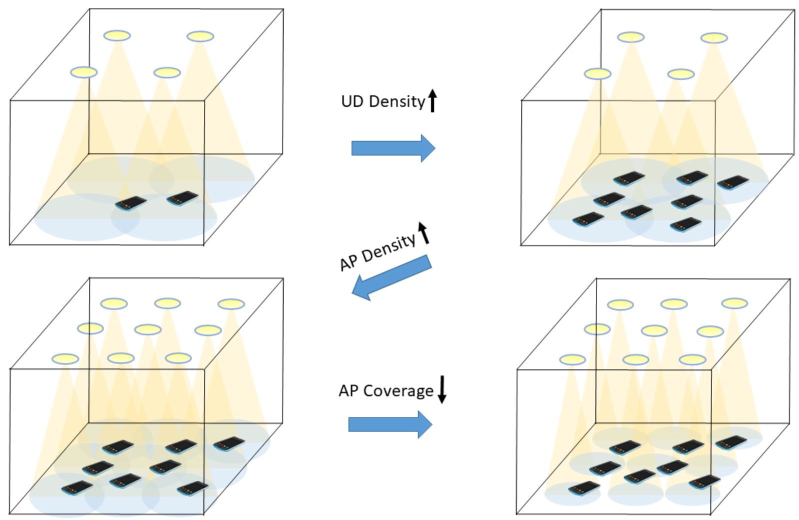

Figure 4·1: Parameters Impacting Interference in Multiple Cell VLC Systems.

for uplink. For this reason, this chapter focuses on downlink interference, leaving the uplink interference analysis as an open research opportunity.

Fig. 4·1 depicts most of the parameters that affect the interference analysis of VLC AP densification. These parameters include:

- Number of user devices.
- Receiver density.
- AP coverage.
- AP distribution.
- AP density.
- Coverage overlap.
- Transmitter Emission Pattern
- Receiver acceptance pattern (FOV)

By increasing AP density, it is assumed that the additional capacity provided will automatically support the aggregate demands of growing device density. However, higher AP density also implies either smaller AP coverage or increased coverage overlap as well as interference. This is where system design and toggling some of these parameters can help determine and control interference.

While wireless capacity can be added to indoor spaces by increasing AP density, doing so can also increase interference. The plus side of using light, with its directional property, offers performance gains with respect to interference. In this chapter we use the term OWC rather than VLC or LiFi (Light Fidelity, its trade name) to imply the use of the visible spectrum. Other optical spectra such as ultraviolet (UV) or IR are applicable as well as covered by the more general OWC label.

4.1 Interference in Optical Wireless Networks

Interference is a vital parameter when deploying systems where multiple links are simultaneously active and close to each other. Although interference is thoroughly studied in the RF domain, there are differences exhibited due to the properties of the media at different operating points in the electromagnetic spectrum which renders the RF interference models insufficient for characterizing light-based models (Rahaim and Little, 2015; Rahaim and Little, 2017; Kahn and Barry, 1997). We discuss the reasons why OWC interference analysis is distinguished from the traditional RF interference analysis techniques next.

- **Interference sources**: The well-known intra-cell interference, which exists between users that reside within the same cell, and inter-cell interference, which is caused by neighboring cells exist in OWC systems, however, opaque walls as well as directionality can sequester the inter-cell interference and thus limit its scope (with added benefits of security and privacy). On the other hand, OWC has new sources of interference such as conventional lighting and different OWC technologies (e.g.,

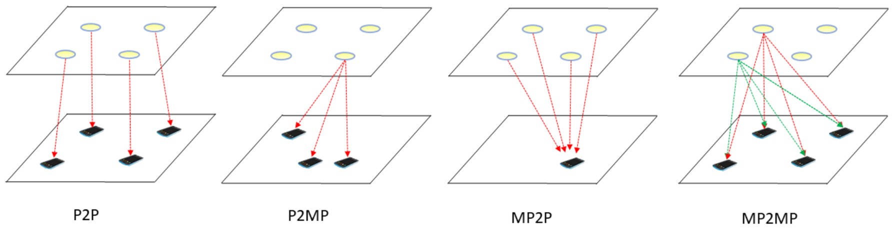

Figure 4·2: System Models for Multiple AP-based OWC Systems: 1) P2P, 2) P2MP, 3) MP2P, and 4) MP2MP.

sensors, cameras, or differing OWC products) (Kahn and Barry, 1997; noi, ; Adiono and Fuada, 2017).

- **Impact of scale**: The containment of LOS light signals means that the physical deployment will impact the nature of interference and will not necessarily be scale-invariant, as opposed to interference in RF systems which is invariant to scale (Similar challenges exist across many scales i.e, macro-cells to small cells).

- **Gaussian interference model accuracy**: Due to the directionality of light and receiver FOV, only a subset of the transmitted signal may be received. When only a small number of interfering signals fall within the receiver FOV, the central limit theorem does not hold and interference may not be modeled accurately as a Gaussian distribution since it follows the distribution of the dominant interference source (Rahaim and Little, 2017).

- **Signal variance**: In IM/DD OWC systems, in contrast to RF ones, the relationship between the optical power constraint and signal variance is modulation-specific. The variance is directly related to the electrical power constraint (i.e., $E[X^2]$) in most RF systems; however the relationship between the variance and the average optical power constraint (i.e., $E[X]$) depends on the modulation used.

System Models for Interference Mitigation A wireless network with multiple simultaneous transmissions may be modeled as a single coordinated AP or as multiple coordinated APs. Due to the directionality of light, it is expected for OWC that the coverage of interfering devices would be more constrained which is in contrast to RF-based APs which have much larger spatial coverage. Fig. 4·2 shows different system models for downlinks in multiple AP OWC systems. These include: 1) Point-to-point (P2P), in which each connected transmitter and receiver have a dedicated connection throughout the transmission; 2) Point-to-multipoint (P2MP), where an AP can transmit to many devices and maintain several connections according to a specific multiple access technique; 3) Multipoint-to-point (MP2P), in this case APs synchronize their transmissions to a device, adding overhead but allowing higher user throughput and/or connection reliability; and 4) Multipoint-to-multipoint (MP2MP), where devices can receive from several APs and the APs are allowed to transmit to many devices. Usually signal processing is employed to sort out desired signals per user.

We point out the distinction from single-input-single-output (SISO), single-input-multiple-output (SIMO), multiple-input-single-output (MISO) and multiple-input-multiple-output (MIMO) which focus on the elements from specific devices like sensors, pixels and photodetectors (PDs). In this context a "point" refers to either an AP or a user device.

The different types of interference that the above systems are prone to face include: *inter-cell interference*: User devices (UDs) share the same resources but are in different cells; *intra-cell interference*: UDs consume different resources but are within the same cell; *cross-cell interference*: UDs are in different cells and have different resources (ex., non-ideal filters within the system or frequency leakage).

Interference Metrics The impact of interference can be characterized by direct and indirect metrics. Table 4.1 summarizes the critical metrics that are used in the literature to

Table 4.1: Summary of Performance Metrics for Evaluating Interference

Metric	Definition
SINR	Signal to interference plus noise ratio, usually evaluated at the physical layer level to describe the signal quality.
SIR	Signal to interference ratio for evaluation of scenarios that are interference dominant.
ASE	Area spectral efficiency defined in (Alouini and Goldsmith, 1997) as the sum of the maximum average data rates per unit bandwidth per unit area.
BER	Bit error rate; shows the reliability of the network.
Complexity	Can represent hardware or software.
Robustness	Sensitivity to changes in model assumptions or use case.
Outage Probability	The probability that packets are lost and/or users are not able to access a network or stay connected.
Max Users	Maximum number of users allowed to access the system.
System Throughput	Aggregate throughput (vs. user throughput).
Fairness	Equal access for all users to the capacity.
EVM	Error Vector Magnitude. An error vector is the difference between the transmitted signal and the received signal. EVM can be defined as the ratio between the error vector mean and the original signal's mean.

characterize interference in OWC systems (Abdalla et al., 2020b).

Interference Management Terms Many terms are used to describe managing interference we reconcile and define these terms:

- *Rejection*: is the strictest term used to describe completely removing interference from a system. Usually employed in physically isolated techniques that can effectively separate resources or channels.

- *Coordination*: is done in systems that attempt to either use interfering signals to their advantage or arrange transmissions in a way to cause the least possible interference.

Coordination is normally done in networked or synchronized systems.

- *Alignment*: is a technique performed in systems that can achieve diversity in the signal space. This scheme, developed for RF (Cadambe and Jafar, 2008), increases the degrees of freedom (DoF) of the interference channel by the alignment of signal spaces (in time, frequency, space, and codes) such that signals arrive relative to the receiver to yield interference-free or near-interference-free reception.

- *Avoidance, Mitigation, Cancellation and Suppression*: are ways to minimize interference. Although cancellation sounds as strong as rejection, most of the literature uses it to describe minimizing interference where some interference effect remains. These techniques are mostly adopted in systems with fixed resources that deploy resource allocation or load balancing.

- *Management*: is a term that is usually used broadly to describe each of the previous systems that aim to combat interference effects in any manner. This is why we choose it to describe all the other terms as it encapsulates them.

4.2 Interference Management Techniques Categorized

A review of the state-of-the-art related to OWC interference studies motivated us to classify interference management techniques into two main categories: multiple access and spatial diversity, see Fig. 4·3. Next we consider the state-of-the-art for interference management in each of these classes and corresponding to the different system models (Fig. 4·2). For each class we summarize important results from representative papers to convey the main achievements reached by the research community.

- **Multiple Access (MA)**: This class consists of the techniques that allow an AP or set of APs to distribute defined resources across a set of users. It is divided into two further categories:

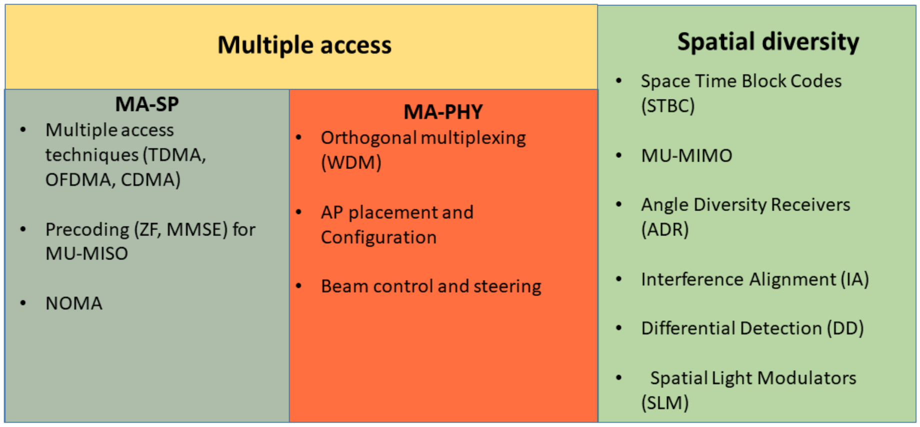

Figure 4·3: Interference Management Techniques Categorization

- **MA-Signal Processing (MA-SP):** This class of techniques applies pre-processing at a transmitter to enable distinction of signals at the receiver, such as employing orthogonal multiple access. The received signal is the superposition of the intended signal and some number of interfering signals.
- **MA-Physical Isolation (MA-PHY):** This class of techniques isolates signals by using the physical characteristics of the channel such as using orthogonality of physical resources, (e.g., wavelength division multiplexing) or by leveraging the properties that are distinct to optical wireless communication, such as directionality or receiver FOV).

- **Spatial Diversity**: This class encompasses both of the PHY and SP cases and is concerned with receiving data by many spatially unique channels or multiple PDs then performing signal processing to have them de-correlated.

Delving into the details of each category, subcategory and providing example research. We start with the multiple access category.

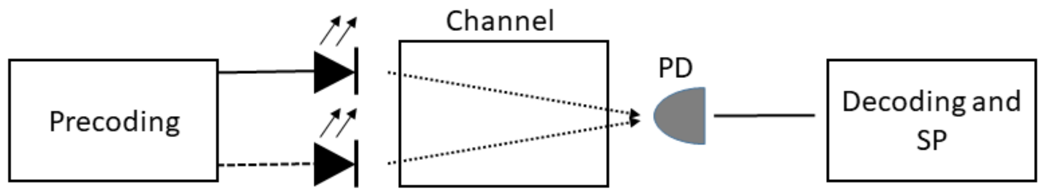

Figure 4·4: MA-SP Configuration

4.2.1 Multiple Access - Signal Processing (MA-SP)

Under MA-SP (illustrated in Fig. 4·4) we have three sub-cases: (i) multiple access, (ii) precoding for multiuser-MISO (MU-MISO) and (iii) Non-orthogonal multiple access (NOMA). These are described below.

(i) Access Techniques

Multiple access refers to how a set of resources can be distributed to serve multiple user devices. The techniques applied for sharing the channel reflect the medium characteristics. In one case, resource distribution provides fairness from a single AP to multiple users, in another a receiver detects multiple sources. Here the resolution can include more complex coordination among APs or more advanced coding techniques.

(Marsh and Kahn, 1997) provide an early study, assuming IR channels, of the effects of the classical fixed (static) channel reuse techniques including time-division multiple access (TDMA), frequency-division multiple access (FDMA) and code division multiple access (CDMA), comparing them with cell radii as an important parameter. The authors conclude through simulations that in a small cell (3 m) and the use of Optical Orthogonal Codes (OOC), performance is dominated by co-channel interference with an irreducible BER performance for smaller cells (< 1.5 m). The exception is the use of CDMA with m-sequences.

(Kim et al., 2012) study frequency carrier allocation in VLC systems. Channel performance is analyzed through EVM and they perform experiments to confirm their results for mitigating inter-cell interference. Static channel reuse is the focus of both works (Marsh and Kahn, 1997; Kim et al., 2012). It helps in increasing SINR values and decreasing error vectors but unfortunately degrades overall spectral efficiency and subsequent system throughput.

For the visible spectrum, (Jung et al., 2016) analyze reducing inter-cell interference in multi-cellular VLC cells by using OFDMA (multiple access) cell partitioning. This work seeks to improve spectral efficiency using a reduction in the guard band in the frequency partitioning by using a filter bank-based multi-carrier (FBMC) to suppress the effect of OFDM sub-carrier sidelobes. Their work reports improvements of 1.5x capacity and spectral efficiency compared to OFDMA.

(ii) Precoding Schemes for MU-MISO

The techniques mentioned here use *Cooperative transmission or Joint Transmission* (JT) which allows transmission from multiple transmitters to a single VLC receiver, similar to MP2P systems as shown in Fig.4·2. MU-MISO combines multiple distributed APs to act as a single cell or AP.

(Prince and Little, 2010) introduce an approach using synchronized time of arrival (TOA) from multiple sources. This method was designed to source identical data to improve signal strength at a targeted receiver in the lighting field. The work shows that cooperative transmissions reduce inter-symbol-interference (ISI), at the price of adding a significant overhead and transmission delay affecting delay-intolerant systems drastically. Unfortunately, it would not scale with many or highly mobile users.

(Chen et al., 2013b) adapt JT to the downlink transmission in an optical atto-cell network to mitigate co-channel interference (CCI) improving overall cell-edge user throughput and SINR. Communication between the light emitting diodes (LEDs) and the user devices is assumed to establish who the best transmitter is, calculate SINR based on the highest signal received and then the devices form a look-up table based on the possible transmitters.

This introduces system overhead specially for mobile users. Frequency allocation is employed in the JT scheme. This inherently means reduced spectral efficiency and throughput. The authors however show an improvement over static frequency reuse cases.

(In Hwan Park et al., 2012) study an interference mitigation scheme for VLC systems deployed in aircraft employing a minimum mean square error (MMSE) and zero forcing (ZF) algorithm for canceling interference signals. They then use successive interference cancellation (SIC) with optimal ordering. The performance of their scheme is evaluated using BER, comparing ZF, ZF with SIC, MMSE and MMSE with SIC, with the latter giving the lowest BER performance. However, they do not report a quantification of the latency introduced by their technique.

(Yu et al., 2013) tackle MU-MISO in indoor broadcast VLC systems by applying two precoding techniques, linear ZF and ZF-dirty-paper-coding (ZF-DPC) to eliminate interference between users under the illumination constraints with ZF-DPC outperforming ZF specifically when two users are close to each other. The authors assume perfect channel state information (CSI) which is not practical. (Ma et al., 2013) study robust MMSE linear precoding for MU-MISO VLC broadcast systems assuming imperfect CSI to create a more robust precoder. This system requires a powerline backbone communication systems controller to allow data sharing and synchronization for successful communications. (Pham et al., 2017) explore ZF to suppress multiple user interference and propose a generalized inverse based ZF scheme to maximize the system sum rate. The authors report through numerical simulations that their scheme outperforms pseudo-inverse design.

(Li et al., 2015a) design two transceivers in an indoor MU-MISO VLC setting, an optimal one based on a linear MMSE formulation and a simplified transceiver based on ZF precoding and evaluate performance in different user densities. They also report results for mean square error versus number of users.

MU-MISO precoding can help increase user data rates as well as the system throughput. However, there is much complexity on the transmit side that needs to be clarified. The transmitters are considered connected, synchronized and/or have channel information regarding the receivers in most works discussed here. Some works assume transmit precoding as well. The backhaul network must be able to handle such overhead, and as more devices enter the system, the technique does not scale gracefully. These systems appear promising, but more investigation is needed to establish scaling limits with respect to number of connected transmitters and user devices.

(iii) NOMA:

NOMA permits the full use of the channel bandwidth by any transmitter, relying on superposition coding at the source and successive interference cancellation at each receiver. There exists a lot of work on the topic of NOMA in 5G networks (Islam et al., 2017; Marshoud et al., 2018).

(Marshoud et al., 2016) propose a gain-ratio power-allocation (GRPA) scheme that factors each user's channel conditions in a NOMA downlink (DL) VLC system. This requires a central controller. They compare their scheme to static power and show an enhancement in system performance. They also study the effect of LED transmission angles, employing a technique similar to (Rahaim and Little, 2013), as well as receiver FOVs effects. However, the work does not consider receiver misalignment which can be introduced with device mobility.

(Kizilirmak et al., 2015) consider the impact of cancellation error in SIC receivers and compare the performance of NOMA in a DL VLC system to OFDMA. (Yin et al., 2017) study NOMA SIC error impact in a LiFi system. Meanwhile, in another work, (Yin et al., 2015) derive coverage probability and ergodic sum rate in DL VLC NOMA for two scenarios: (1) achieving a guaranteed quality of service and (2) an opportunistic best-effort service. They compare NOMA to TDMA and show results relating to the LED transmission semi-angle. Then in (Yin et al., 2016) they extend their work to provide a theoretical framework that analyzes the performance of VLC NOMA and characterizes its performance gains over orthogonal multiple access (OMA). (Marshoud et al., 2017) analyze BER performance in DL NOMA VLC for both perfect and imperfect CSI.

There are works that opt for solutions other than SIC such as (Guan et al., 2017) who study Joint Detection (JD) of VLC signals employing NOMA for the Uplink (UL). The authors suggest that transmitters use JD which is based on the maximum likelihood detection and provides enhanced BER results compared to SIC. They also maximize the minimum distance between constellations to improve performance by pre-distorting the phase of the CSI. Their work is confirmed experimentally using feedback channels from the receivers. (Wang et al., 2018) use joint detection and decoding in their energy efficient transceiver design for DL VLC NOMA systems where they propose a power allocation scheme based on finite alphabet inputs. (Chen et al., 2019) study SIC-free NOMA in DL VLC systems and use constellation partitioning coding and uneven constellation de-mapping.

(Yang et al., 2017) study a low complexity power control allocation that aims at fairness under optical intensity constraints by maximizing the sum log user rate. An efficient and low complexity power allocation is studied in (Chen et al., 2018) in MIMO NOMA VLC and a normalized gain difference power allocation is proposed as well.

NOMA advantageously allows full resource usage and therefore best spectral efficiency. While most works mention that NOMA is attractive for OWC systems, especially indoors, because the channel at a fixed location/orientation is nearly deterministic and the SNR is relatively high (in the absence of blockage), there is still a need for channel estimation as performance is impacted by shadowing, receiver mobility and orientation. The main drawbacks of this approach are complexity, error propagation, and latency added due to the use of SIC. There is room for new solutions that find a tradeoff between SIC and joint detection in terms of complexity while keeping a tolerable delay.

4.2.2 Multiple Access - Physical Layer (MA-PHY)

The implications of the physical layer characteristics on the nature of interference are considered in this section. This class includes sub-cases of (i) AP positioning, (ii) beam control and (iii) orthogonal multiplexing. Each is discussed in turn.

(i) Access Point Placement and Configuration

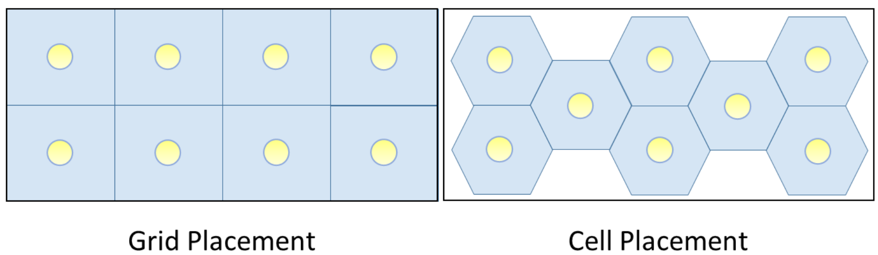

Figure 4·5: Lighting-Based APs Are Usually Grid-Like. But Cellular Arrangement Can Be Used Effectively

The traditional RF AP model is a single omni-directional unit spanning multiple rooms serving a locale (e.g., an apartment). Coverage of a larger space (building or campus) is realized by replication of APs. OWC access points, being primarily LOS-based and contained within walls, can service much smaller zones such as individual rooms, or can be replicated in larger rooms (e.g., open office seating). This causes important design considerations for the height, spacing, and beam width of the OWC APs especially if they are also intended to provide illumination (Fig. 4·5). Current work on AP placement and configuration explores this system design problem.

The authors (Wang et al., 2012) study the performance of 12 LED lamps placed in a circle at the center of a room with additional LED sources at the edges. They investigate this LED placement to reduce SNR fluctuation for a multi-user VLC setting in an attempt to maintain consistent user performance at all locations within a room. Their results show small SNR variability in comparison to the more expected LED placements in the center of the room. They also study how this placement increases ISI near the edges and propose a remedy using ZF at the receivers. (Stefan and Haas, 2013) focus on maximizing a room's ASE through optimal placement of APs. Their results show that for a receiver with wide FOV the transmitters are better placed far from each other while at lower FOVs, a receiver experiences less interference. The optimal configuration is found between these bounds. Their results also show that ASE is reduced when lighting constraints are imposed in the optimization. (Shashikant et al., 2017) propose different arrangements for placing the VLC APs and compare their coverage aspects. They define simple metrics, namely coverage, interference fraction and interference to coverage, to establish which arrangement is better. Results show that a hexagonal setup for VLC APs gives best coverage and least interference fraction. Meanwhile, (Vegni and Biagi, 2019) study optimal LED placement in indoor VLC networks under constraints of illumination and data rate outage. They propose two techniques 1) AttoCell Minimization (ACM) that aims to minimize the number of attocells that can serve a given number of users (to minimize unnecessary interference) and 2) AttoCell User Maximization (AUM) which maximizes the number of users that an attocell can serve. The results show that a large half-power semiangle and lower data rate per user requirement can realize an improved guaranteed performance. However, the authors did not study changing parameters on the receive side such as orientation or FOV which can highly affect their results.

AP placement is an interesting topic with more room to investigate, in particular, the impacts of mobility and device density. Steerable APs also add a new interesting dimension to improving system performance.

(ii) Beam Control and Steering

The cases we mentioned in Section 4.2.2(i) consider static lighting and AP deployment scenarios in which the source intensity parameters are decided for a particular operating point. With the use of beam control including beam width (transmitter FOV) and beam steering (directionality), new optimization problems emerge as well as more options to support adaptive performance for mobile devices and variable data traffic.

(Rahaim and Little, 2013) study SINR and VLC cell zooming while maintaining constant illumination in indoor VLC networks. The concept here is to adapt RF cell zooming but for OWC while operating within lighting constraints. The technique can be implemented through cell power reduction or by physically changing the emission pattern of the transmitter to allow a dynamic change of cell size. This allows for better communication for the users. Results indicate comparisons to frequency reuse scenarios and discuss combination scenarios of LOS versus NLOS regions. The technique can also be very useful in minimizing handover overhead if cells can grow to cover users in larger footprints. This system can also be very interesting if studied dynamically for randomly oriented mobile devices within a room to show more practical results.

(Valagiannopoulos et al., 2019) suggest a transmitter with a nanoslit metasurface that increases the directivity of the transmitted beams and therefore improves the received SIR. Here the nanoslits act as very directed transmitters with tiny cone beams that are able to concentrate the emitted power into small beams thereby suppressing interference between LEDs. The authors argue that while their system is susceptible to receiver rotations and misalignment, the angles and sizes of the receivers and the nanoslits demonstrate that these perturbations do not affect performance. Additional work will be required to establish viability under practical operating conditions.

Beam steering can also be used at the transmit side, either as a narrow or diffuse beam (Rahaim et al., 2017; O'Brien, 2019). By using a narrow beam, interference can be mitigated by source control delivering signal exactly to a receiver but running the risk of blockages and/or misalignment issues. With the use of high-speed control (mirrors or other spatial light modulators), rapid steering between receivers is possible with rates in the order of kHz for point-to-point cycles. (O'Brien, 2019) has successfully demonstrated such a system using IR signals. Once using a laser diode source, data rates can be very high relative to LED sources. However, this type of system is not appropriate for lighting and must factor eye safety requirements in its design.

(Chang et al., 2012) propose another MA-PHY technique involving a low-cost spectrum sensor array at the receiver intended to reject interference on incoming wavelength division multiplexing (WDM) signals. The receiver is also designed to cancel out ambient light interference. The technique is based on a filtering optimization formulation leading to optimal weights that allow SIR to be maximized. This approach requires timing synchronization between the employed sensors to work successfully.

In addition to controlling the directionality of a source, the FOV and pointing angle of a receiver can be controlled to improve interference rejection. (Abdalla et al., 2019b) propose a dynamic FOV receiver intended to isolate a channel through dynamic control of receiver FOV. Applications include responding to changes in device orientation, position, and velocity, and in supporting AP selection when traversing a larger set of OWC APs. An experimental system supports predicted performance improvements in realized SNR.

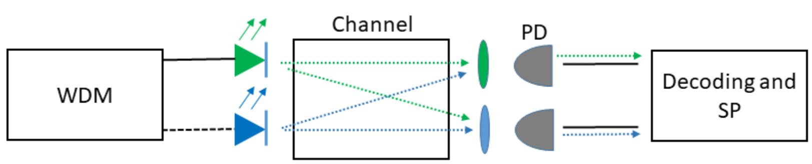

Figure 4·6: Typical MA-PHY Model with Two Optical Wavelengths

(iii) Orthogonal Multiplexing

This technique facilitates co-location of multiple non-interfering (orthogonal) signals that can be decoded selectively by independent receivers. (Note that the classifications of multiple access and multiplexing converge when considering only two endpoints, e.g., time division duplexing (TDD).)

(Liu et al., 2012) demonstrate a bi-directional LED VLC system using TDD protocol to mitigate reflection interference. Their system has LEDs for both uplink and downlink. To investigate the behavior of reflections they use mirrors. Their method addresses interference but at the cost of delays due to cycling the channel among participating devices. (Wu et al., 2012) consider specific modulation schemes for adjacent cells including On-Off-Keying (OOK), Pulse Width Modulation (PWM), and PPM. Experiments indicate error-free transmission at 1 Mb/s and 6.25 Mb/s. (Butala et al., 2014) propose a multi-wavelength VLC system design, including an analysis of the relationships among the source channel wavelengths, relative intensities, and optical filtering to realize maximum SNR while minimizing cross-talk at the receiver.

Exploiting WDM in OWC systems is an attractive means to gain capacity. However, it needs careful design to meet the relevant illumination requirements. These include 1) light distribution and intensity levels including minimizing glare, each dependent on the lighting use case; 2) providing satisfactory spectral power distributions for color rendering, essential for humans; and 3) avoiding visible temporal discontinuities in color or spatial distribution of light. Each of these is surmountable, but requires consideration when designing the modulation approach involving WDM or combinations of WDM with time division multiplexing (TDM).

4.2.3 Spatial Diversity

Diversity techniques exploit the ability to simultaneously source multiple signals that can be combined at a receiver, the ability to receive sources from multiple detectors at a receiver, or some combination of the two techniques. The diversity class of interference management includes sub-cases of (i) space time block coding, (ii) multiuser-MIMO, (iii) angular diversity, (iv) interference alignment, (v) differential detection, and (vi) spatial light modulators.

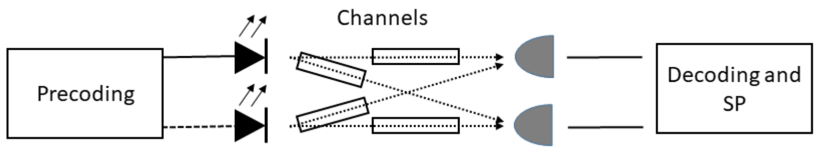

Figure 4·7: Typical Diversity Model

(i) Space-Time Block Coding

Space-Time Block Coding (STBC), first introduced for RF communications, has been established as a method to allow diversity in a system to achieve very low BER while saving power (Tarokh et al., 1999). The performance of STBC techniques in indoor diffuse optical wireless systems is analyzed in (Ntogari et al., 2009) in which the authors report that STBC schemes can increase system coverage and capacity and decrease the transmitted optical power required. Their scheme is to use discrete multi-tone modulation (DMT) to mitigate the effect of ISI caused by a channel impulse response. Their results come from comparing the performance of two Alamouti STBC schemes to SISO and maximum ratio combining (MRC) schemes. (Biagi et al., 2015) propose a MIMO-PPM-STBC in a VLC setup under the constraint of trace-orthogonal matrices focusing on achieving middle ground between high transmission rate and low BER. This performance contrasts with systems that only focus on one of the two sacrificing the other. The authors compare their system performance to other work (e.g., (Ntogari et al., 2009)) and show that they achieve middle performance trading off BER and transmission rate.

Meanwhile (Shi et al., 2015) construct an experiment to test the performance of MISO VLC networks using STBC where they employ two red, green and blue (RGB) LEDs as transmitters and a single receiver to test STBC-OFDM coding. They investigate performance in the overlapping region of the two transmitters. They report a total throughput of 500 Mb/s adding that the free space transmission range can be extended to 5 m. BER is reported at less than 10^{-5}. However, their system does not account for any mobility.

While STBC can be beneficial in achieving low BER, there is a relatively high complexity involved with this approach. This includes the complexity associated with achieving syncronization of distributed transmitters.

(ii) Multiuser MIMO

(Hong et al., 2013) investigate the performance of block diagonalization (BD) precoding to eliminate multi-user interference, reducing the receiver complexity level in a multi-user MIMO (MU-MIMO) setting. They test the performance on different receiver FOVs as well. Their simulation results show SNR up to 40 dB. The system is able to theoretically achieve 100 Mb/s at a BER of 10^{-6} while 70° and 50° are considered for receiver FOV.

(Pham et al., 2015) also employ BD. In this case for precoding of broadcast channels to find a lower bound for the sum-rate maximization of all users in an indoor space. Their results show the impact of photodiode (PD) rotations and user locations on interference. (Wang et al., 2015) investigate MU-MIMO OFDM for VLC systems. In their work they propose to evaluate a precoding matrix based on MMSE or ZF for each OFDM subcarrier with the goal of eliminating multiple user interference. Their results indicate that MMSE outperforms ZF when the optical power is low.

(Lian and Brandt-Pearce, 2017) study an indoor MU-MIMO VLC system using spatial multiplexing with a centralized power allocation and with four different decentralized transmitted power allocation algorithms. Each employs multiple LEDs and PDs, the latter having different orientation angles for better SINR. CDMA is used to accommodate the users, and receiver time-space MMSE filters are used to reduce the multiple access interference. They consider parameters such as shadowing, dimming control, illumination level, and transmitted power quantization. They also mention that the distributed techniques show an overall lower computational complexity. In terms of BER two of the distributed algorithms, Weighted Decentralized Multi-Detector Power Allocation Joint Optimization (PAJO) and Partial Decentralized Multi-Detector PAJO, outperform all other proposed methods. While using their centralized scheme helps in shadowing scenarios in getting twice the data rate compared to not knowing the shadowing information.

MIMO schemes support increases in system capacity and related performance but at the cost of complexity. Some of the systems mentioned above employ precoding which helps in relieving interference but assumes transmitter connectivity and the availability of CSI which is not always the case. Indoor VLC channels tend to be more deterministic but only in a static study. When device mobility and orientation are taken into consideration, CSI changes and static precoding matrices quickly become obsolete.

(iii) Angle Diversity Receivers

Angle diversity receivers (ADR) rely on the ability to discern the angle of arrival of an incident transmitted signal (Carruthers and Kahn, 1998). They are typically designed as a hemisphere with multiple PDs arranged on the surface (Fig. 4·8(a) and (b)) but other designs using masks suspended over array receivers can be used as well (Cincotta et al., 2018).

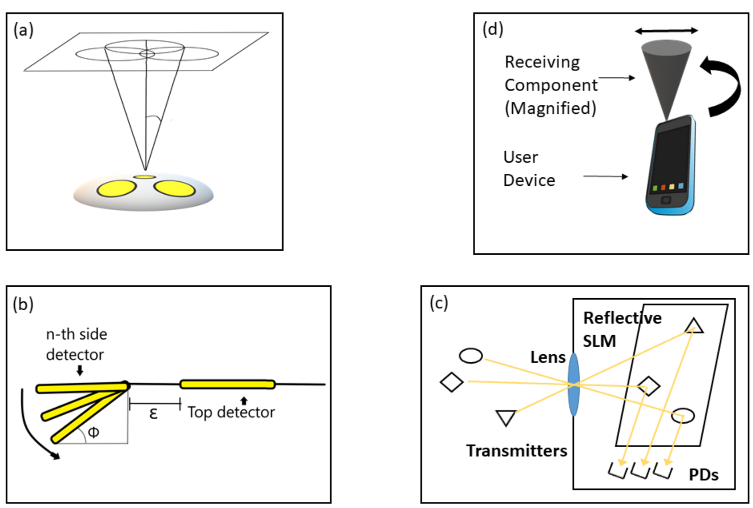

Figure 4·8: Proposed Receiver Designs: (a) 3 PD ADR Receiver, adapted from (Chen et al., 2014b), (b) Generalized ADR, adapted from (Chen et al., 2018), (c) Reflective MEMS SLM Optical Receiver (Chau et al., 2016), (d) Steerable DFOV Receiver (Abdalla et al., 2019a)

Most works use ADR receivers in MIMO settings specifically for optical channel decorrelation. ADRs can also be used to mitigate inter-cell interference (ICI). (Chen et al., 2014a) explore using an ADR receiver and signal combining schemes (from the many PDs on the receiver) to increase system SINR and achieve higher ASE. The authors report that the ADR employing MRC gives the best performance and provides 40 dB in SINR improvement over a single PD setting. Their results show that the ADR outperforms single PD receivers in both SINR and ASE.

A signal combining method named Optimum Combining (OPC) which incorporates interference correlation and studies non-LOS (NLOS) reflections is proposed in (Chen et al., 2014b). An interesting discussion in this work relates to NLOS reflections and their impact on SINR. The results indicate that first order reflections degrade performance only slightly because first order reflections bounce off the walls and fewer users are near the walls of a room. However, second order reflections emanating from the ceiling impact SINR negatively and cannot be completely eliminated through manipulation of FOV. To combat this effect from reflections they propose using ADRs and compare a single PD receiver to ADRs with multiple elements (3 and 7 elements) (Fig. 4·8(a)). Their results show that in their setup increasing the number of PDs (increasing diversity) improves the ability to reduce interference caused by reflections. And that the increased number of PDs degrades performance when reflections are not present due to the limited FOV of the PDs.

(Chen et al., 2018), study SINR variability in indoor multi-cell VLC systems by proposing an optimized ADR. This follows related work in SNR variability (Wang et al., 2012), (Section 4.2.2). The authors propose a generalized ADR structure comprised of a top detector with optimizable side detectors that can change their angles of inclination, ϕ (Fig. 4·8(b)). Results show promise in the ability to minimize SINR fluctuation through optimizing parameters such as number of detectors, inclination angle, and the combining scheme for the signals received by the PDs. However from their description of their ADR, they do not optimize ε, which they define as the gap between the top detector and the side one although that area where ε presides is very useful and important for communication quality, they also do not study NLOS reflections. Most importantly they do not study receiver orientation effects and so the proposed optimal inclination angle they reach through simulation is only optimized for a horizontally-fixed receiver.

Each of the works indicate that improvements in SINR can be achieved by employing more PDs. However, they do not account for the variations in receiver orientation, which is critical to link performance (Little et al., 2018; Abdalla et al., 2018; Dehghani Soltani et al., 2019).

(iv) Blind Interference Alignment

Blind Interference Alignment (BIA) (Jafar, 2012) is a variation on IA that does not require CSI and specifically the channel coefficient values at the transmitters. BIA only needs the knowledge of the channel coherence times (CSI is assumed to be known at the receiver). The transmitting LEDs do not need to cooperate which is a huge benefit. (Wu et al., 2017) analyze BIA for MU-MISO indoor VLC systems proposing a filter-pair-based scheme in which the receiver has a single PD and multiple receive filters, instead of reconfigurable antennas, which control the receive mode. They show that their system outperforms OMA schemes in terms of spectral efficiency and degrees of freedom.

(v) Differential Detection

(Ryoo et al., 2016) propose a differential optical detection system that engages both the transmit and receive elements. The transmitter consists of an LED and a polarizer; the receiver is comprised of two PDs each with a polarizer to provide differential detection. Then the transmitted polarized signal is received by one PD and blocked out of the other so that in the differential part of the system everything else cancels out except the desired signal and some noise. Experimental results verify their system for one or two interference sources but their EVM worsens when more interference sources are introduced but BER is still in the range of 10^{-3}.

Limitations of this approach exist when scaled to many user devices or in the presence of occlusions or variations in device orientation which may mask only a single channel. The use of a polarizer inherently limits incident signal strength as well.

(vi) Spatial Light Modulators

Spatial light modulators (SLMs) can be used reflectively or transmissively to manipulate or modulate optical signals. One approach leverages an array of mirrors to focus and enhance signal strength directed towards one or more PDs. The array of mirrors can be individually steered to reflect light from the target. By pointing all or a subset of the mirrors the signal strength of the target is increased and the noise from other sources is minimized. Bare PDs do not have this feature. (Chau et al., 2016) propose the use of SLM for MIMO VLC receivers as it has the ability to dynamically control the optical channel and to support its decorrelation. The design of the receiver is based on using an imaging receiver, a lens and a reflective SLM at the image plane that directs the incoming light signal in the direction of an array of photodetectors (Fig. 4·8(c)). This method has been successfully demonstrated. It shows promise in its ability to isolate the channels at the receiver, support diversity combining, and is relatively integratable into a working system.

4.3 Managing System Dynamics

The techniques discussed till here represent building blocks for the construction of high-performance OWC systems. The introduction of device mobility, orientation, density, and traffic use priorities each introduce new complexities for maintaining consistent performance. These factors motivate addressing the development of adaptive approaches that can react to changes in system state. The main topics considered here are 1) resource allocation and load balancing, 2) coordinated transmission, 3) combined beamforming, and 4) beam and FOV control.

4.3.1 Resource Allocation and Load Balancing

We focus our discussion on the works that aim to optimize resource allocation and load balancing with the end goal of interference management.

(Mondal et al., 2012) proposes a coordinator to estimate the interference level (IL) of users which the authors evaluate based on the SINR of the user and their distance from the AP. The coordinator then assigns a visible light multi-color logical channel based on the IL metric. Part of the channel set is reserved for control and hand-off purposes. Some priority is given to the lowest level interferers in getting the least interfering channel, as they form a queuing model and show results in case of low traffic, high traffic and prioritized traffic dropping probabilities as well as SINR cumulative distribution function (CDF). However, the results are not compared to a baseline scheme for a generalization of the system performance.

The work in (Li et al., 2015b) investigates different VLC cell formations with different frequency reuse (FR) patterns such as 1) Unity Frequency Reuse (UFR) which uses up all the resources and suffers from interference in cell edges. 2) Non-unity FR, where the reuse factor=2 in a hybrid VLC/wireless fidelity (WiFi) scenario. They then show the performance of different cell formations as 1) Combined Transmission where 2 VLC APs join to transmit the same data to the user, giving better SINR but less bandwidth efficiency which drives them to propose 2) Vectored Transmission (VT) where ZF is employed to serve many users in the interference region simultaneously. If cells are merged as well then it becomes JT with VT, example VT-16 is 16 cells merged together. They study centralized and distributed approaches for a proportionality fairness scheduler focusing on throughout, fairness and area spectral density. The proposed VT-16 shows the most promising results but the most overload on the system to use all 16 LEDs for a single user and so no interference would be experienced since the system has 16 APs total. The system is static and is not considering user mobility as well as device orientation. To accomodate system dynamics, (Li et al., 2016) build a user-centric system, as opposed to a network-centric system, that employs VT to mitigate ICI. Their results show that VT-user centric clusters outperform network centric ones in average user throughput bearing in mind the presence of impending issues that need to be accurate/solved for the system to perform well such as user position estimation and possible system blockages.

To improve load balancing results, (Dehghani Soltani et al., 2016) consider two metrics, Signal Strength (SS) and AP traffic, in making an AP selection in LiFi cellular networks while assuming random receiver orientation. They assume that the receiver angles are uniformly distributed along their dynamic ranges which is not practical in a real life setting and draws attention to a much needed accurate statistical modeling of user device orientation angles. They also analyze LOS and NLOS cases in their SINR study. The authors propose a central controller to carry out the load balancing and discuss their results in terms of average user throughput, satisfaction level and fairness index showing an improvement in their proposed metric when compared to only using SS as a metric.

(Wang et al., 2017) study load balancing under device orientation and shadowing in indoor hybrid LiFi/RF networks. Their results show better performance than other load balancing schemes, such as joint optimization algorithm, threshold-based access algorithm and random access algorithm, in terms of user quality of service level while attaining lower complexity as well. A two-step resource allocation process to allocate both zone and user level resources evaluating ASE and fairness is performed in (Hammouda et al., 2018). They study their system performance in a room-scale transmission scenario using the simulation tool CandLES (Rahaim et al., 2010). However, they assume fixed receiver orientation. (Zhang et al., 2018) propose a predictive system that exploits location and delay information to achieve a better delay-throughput trade-off, through anticipating user association in an indoor VLC network. They assume perfect knowledge of the users' locations as well as a priori knowledge of the users' wireless traffic distribution and then form an optimization problem that maximizes the sum rate for the duration of several future time slots weighted by the evolving queue backlog of each user over many future time slots. They compare their anticipatory association (AA) with responsive association (RA), which maximizes the sum rate at a current time slot weighted by the current queue backlog of the user. They report that their system outperforms RA achieving better trade-off between the average system queue backlog and the average per user throughput. They also note that their study indicates that the overall system average delay can be reduced when AA is employed. However, their choice of mobility model was the random waypoint model which is not practical and the assumption of perfect receiver location is not quite robust.

Designing a predictive system is a step in the right direction but much more analysis and study is needed to delve deeper in the variations of this dynamic system and its reliability. There is definitely room for innovation and exploration in this area.

4.3.2 Coordinated Transmission

Coordinated transmission involves multiple transmitters working together to produce signals decoded by one or more receivers. This includes 1) coordinated and non-cooperative cases and 2) coordinated and cooperative cases.

Coordinated Non-Cooperative Transmission

Self-organizing interference coordination in optical wireless networks is the topic of the work of (Ghimire and Haas, 2012). The authors investigate interference coordination in an aircraft cabin scenario with an OFDMA/TDD system. A busy burst (BB) scheme in which APs are required to share common channels is investigated. Transmitters intending to reuse a resource need to listen in on BB messages without centralized controllers aiding them and evaluate the CCI they would cause to a user and decide based on that whether to transmit or wait. They also add a heuristic that stops a user from reserving the resource after the user has had a fair share of resources. The authors compare their approach to static resource partitioning and reveal improvement in fairness and spectral efficiency. However, it would be useful to see how many users are allowed in the system, how much delay is caused due to contention and the overall system dropping probability.

Meanwhile fractional frequency reuse (FFR) is studied in (Chen et al., 2013a) which is considered a compromise between full frequency reuse and static partitioning schemes. In FFR the entire bandwidth is partitioned into several sub-bands depending on the reuse factor which the authors choose to be 3. The cell is divided into an interior region and an exterior region based on an SINR threshold. If a SINR is above the threshold then the device is considered to be in the interior and may use the full frequency band otherwise the device is in the exterior region and can use a sub-band (Fig.4·9(b)). Due to this partitioning they provide a power control factor β to help edge users get higher power than center ones. This method improves the cell-edge user and overall system throughput.

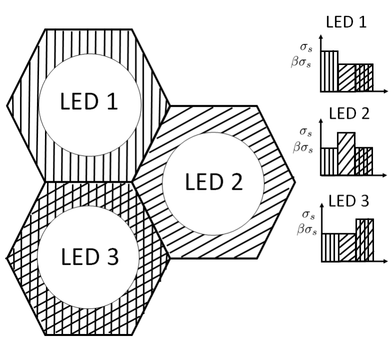

(a) Color Cell Planning (Zhou et al., 2017)

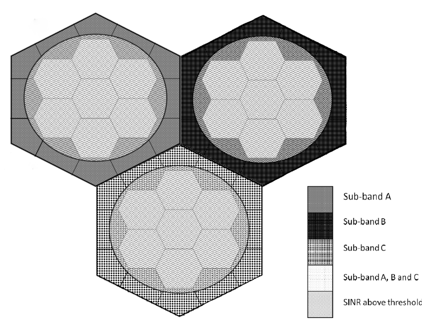

(b) FFR (Chen et al., 2013a)

Figure 4·9: Cell Planning

(Zhou et al., 2017) analyze a multi-color VLC system adopting Soft Frequency Reuse (SFR) based interference coordination but performed on color planning. They divide the VLC attocell hexagon into an inner circle which uses two colors then the outer region would use the third color of the RGB division making sure the neighboring cell gets a different cell edge color (Fig. 4·9(a)). While accommodating illumination requirements, they propose a static scheduler that adjusts power control to give center cell users the minimum required communication performance to mitigate interference for cell edge users, as well as a dynamic scheduler for dense scenarios when the static scheduler is not sufficient to combat interference for the cell edge users. The dynamic scheduler limits color usage in some attocells according to interference intensity and under SINR demands of all the user devices. It is intended to function in one of two modes: 1) a distributed stage followed by a centralized stage jointly to adjust color usage, or 2) a greedy approach based on dividing the hexagon cell into rings which would then get colors according to their location. They compare their results with CD which is the one color per cell plan and NoICIC which is the plan where a cell is allowed to use all colors. They show results based on inter-LED distances but the system has a very high overhead, requires two scheduling phases which can provide delays for highly mobile users, and also depends on reliable feedback channels which may not be practical.

Of the works that study interference coordination employing NOMA (Section 4.2.1), (Kashef et al., 2015) study an interference coordination scheme that entails two transmission schemes to maximize a network utility function; one which uses Orthogonal Multiple Access and the other uses NOMA. A central controller decides which scheme to use based on user location and other system parameters. Another example is (Zhang et al., 2016) who explore grouping users based on their locations to reduce interference then they optimize power allocation for NOMA taking residual SIC interference into account.

Coordinated and Cooperative Transmission

A coordinated transmission scheme based on a bipartite graph formed in the downlink is proposed in (Bai et al., 2015). They form a max-min problem to maximize the minimum user rate and perform an allocation scheme derived from the optimization problem. They divide the possible scenarios into two cases 1) when a device is in an overlapping region between two cells and so the cells would allocate the same sub-carriers, labeled “coordinated transmission,” and 2) when the device is not in an overlapping region and thus the same sub-carrier is not assigned as in an overlapping region. This case is labeled “interference mitigation.” They use their graph theoretic algorithm Backward Forward Marking (BFM) to do the allocation. They then compare their throughput and fairness results to Round Robin and Proportional Fairness Schemes and show that BFM gives better performance. They consider first-order reflections in their work but make the assumption of perfect CSI at both transmitter and receiver which is not a robust assumption.

These areas are very interesting; methods that realize maximum performance obtainable from the diverse set of physical layer techniques under dynamic conditions are needed. Potential works that could define upper bounds on number of supported users on repeatable benchmark traffic and mobility configurations would be extremely useful. We also note that some of the aforementioned techniques will be challenging to scale to many transmitters (e.g., the use of synchronized transmitters).

4.3.3 Combined Beamforming

Combined beamforming (Fig. 4·10) employs cells comprised of multiple LEDs. Within each cell the individual LEDs are modulated to deliver one signal to a user device depending on their location.

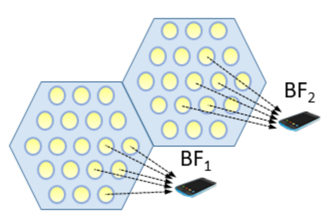

Figure 4·10: Combined Beamforming Scenario

(Ma et al., 2018) suggest that since JT required too much overhead and high synchronization between transmitters, coordinated beamforming (CB), adopted from RF, would allow for less transmitter collaboration for interference mitigation. This concept is studied in a downlink multi-cell MU-MISO VLC system. They assume that an attocell consists of a single transmitter with multiple LEDs and can serve a number of users each having a receiver with a single PD and each user is served by a single attocell. Taking intra-attocell and inter-attocell interference as well as illumination requirements and receiver noise into consideration, they form an optimization problem to find the best linear MMSE beamforming design. The authors employ linear beamforming design in a perfect CSI setup and a more robust imperfect CSI setting. While their CB scheme exploits the spatial domain for multiplexing and interference mitigation, the results show that in comparison to JT, CB is sometimes close to performance of JT when there are many transmitters but for specific user distributions it is very limited in comparison to JT. The closer users are together, the harder it is to beamform messages intended to specific users specially when they are served by only a single attocell. The authors provide a possible solution to add coordinated scheduling to alleviate this problem for certain user distributions by serving them in different time slots in order to achieve resource partitioning. Based on the results in the paper, solving the high density case needs more study and analysis.

4.3.4 Beam and FOV control

Beam and receiver field of view control can also be used to address dynamic user behavior. Examples include aforementioned work (Abdalla et al., 2019b) and (Rahaim et al., 2017; O'Brien, 2019; Rahaim and Little, 2013) which can be considered dynamic as they adapt to system changes to fulfill the user requirements. In (Abdalla et al., 2019b) the receiver adapts to changes in the user location, orientation and velocity by evaluating the best (transmitter-FOV) pair per receiver dynamic change to allow it to receive the best SNR. While (Abdalla et al., 2019a) (Fig. 4·8(d)) is more active in adapting the FOV and orientation to allow the user the best SNR quality and is able to change them dynamically with system changes. In contrast, work that proposes dynamic beam and steerability adapt the transmit side to change along with the user density, location and overall motion within the room to allow for better coverage and communication quality. Both areas are very interesting and have room for more analysis in the system scale.

Combinations Here we discuss systems that generally combine some of the building blocks discussed in Section 4.2. A strategy that jointly employs a color and code strategy to mitigate interference in indoor VLC femtocells is proposed in (Cui et al., 2013). First the authors use WDM between different VLC cells from the colors red, green and blue, then they assign phase-shifted maximum length pseudo noise (PN) sequences to LEDs that have the same wavelength. They also use orthogonal Walsh-Hadamard (WH) code for different users within a cell to combat intra-cell interference. According to their design they have no intra-cell interference but inter-cell interference is limiting the system. They evaluate their system performance in relation to parameters such as closest LED distance, user density in a cell and the dimming level of the LED. However, their system complexity is relatively high and requires accurate synchronization.

(Adnan-Qidan et al., 2019) study user-centric BIA design in a VLC system to relieve the transmitters from complexity of designing a precoding matrix in which they employ a reconfigurable PD in an ADR configuration (Section 4.2.3). They propose two schemes depending on how the user clusters are connected. One scheme considers a broadcast channel for each cluster named KM-sBIA and the other scheme, KMtopBIA, allows each cluster to divide into graphs that depend on the users' connectivity. They report that their schemes outperform ZF (Transmit Precoding method) in both network and user centric settings in BER and user rate.

Key Takeaways We offer a few key takeaways from reviewing the state-of-the-art in OWC interference management:

1. VLC provides links that have unique properties of light leading to methods and performance unique to OWC.

2. When adopting and replicating VLC for APs, one needs to address interference among user devices and among the multiple APs.

3. Many interesting techniques exist (spatial multiplexing, WDM, ADR, etc.) each with different considerations for interference.

4. Techniques can be combined and optimized for static scenarios, but ultimately a study of how they interact and can adapt to follow the dynamics introduced by device mobility, orientation, and data traffic models is needed for accurate system performance prediction.

5. Future work should address system dynamics including optimization and management in the context of overall network performance adaptation.

4.4 Multi-User Interference Case Study Using Dynamic FOV Receivers

Increased density of networks potentially leads to increased interference among APs and possible reduced service quality. Most works in the literature focus on studying cell edge users (Chen et al., 2013a; Chen et al., 2013b; Zhou et al., 2017), because interference is primarily an issue at these boundaries. Dense optical networks, especially ones implemented as VLC, in contrast, are more likely to have wide intersecting coverage ranges. This causes interference to become a more significant issue throughout the whole space. We propose to manage interference in these regions through dynamic FOV receivers, as they have the ability to meet best performance in both reuse and interference mitigation. We consider this case study as a strong motivator for our work in Chapter 6.

Using the SINR definition in eq. (2.11), we analyze interference mitigation under four different receivers: (1) DFOV receiver, (2) SDFOV, (3) A baseline FFOV (90°) receiver without tracking and (4) SFFOV; a fixed FOV (90°) receiver with steering capabilities. Note that we interchange the use of the term tracking or steering to describe a receiver pointed at the center of a target transmitter.

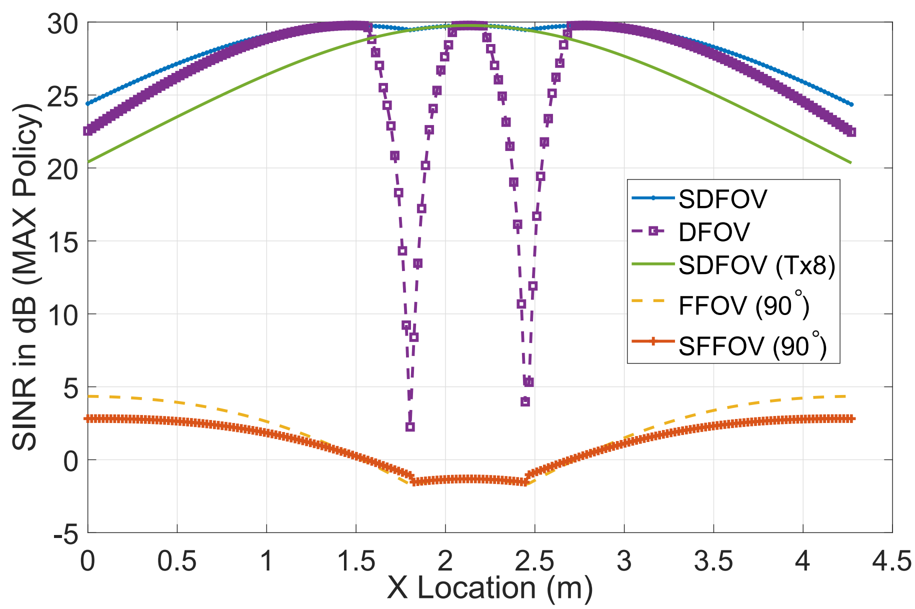

Figure 4·11: Interference Analysis under Four Different Receiver Configurations

Fig. 4·11 shows each receiver flat and moving along a single path under three transmitters, T_{x5}, T_{x8} and T_{x11} from the general layout in Fig. 3·1b, and compares the results of the above mentioned receivers which all aim at connecting to the highest SINR in the room. The figure also shows the SINR if an SDFOV receiver had a certain transmitter desired (namely, Track T_{x8}) for the length of the communication which is an added benefit available to this receiver. It is clear that the two fixed FOV receivers do not benefit the user. It is also worth noting that the SFFOV performs worse than the non-steerable FFOV in the locations away from the active transmitters. This is due to the fact that in the SFFOV receiver's pointing phase, without the ability to tune the FOV to get smaller, it receives more noise/interference through pointing at the whole grid of lights. On the other hand the non-steerable FFOV being oriented away from the lights helped in chopping of some of the undesired noise and signals.

The DFOV receiver suffers from areas of coverage holes due to its inability to change its orientation but is still a better option than the fixed FOV receivers. The SDFOV receiver outperforms all of the other receivers. These results show that the SDFOV is superior in terms of SINR and allows tracking a single transmitter during path traversal while maintaining an uninterrupted connectivity experience. It has high potential of achieving seamless connectivity (assuming no blockages exist). This motivates the employment of dynamic field of view receivers in multi-user networks.

4.5 Chapter Conclusion

Optical wireless communications promise to provide a huge boost to the capacity of indoor dense access point networks including those coupled to the lighting function as VLC. However, the properties of the optical spectrum and the anticipated increase in density of mobile user devices requires a revisit to interference management for this media type. In this chapter we explore the state-of-the-art with respect to multiple user optical access and develop a classification of current technical approaches for exploiting this technology and managing interference. This proves to be useful to the community in offering a compact and concise critique of the work done to date. It also amplifies the missing aspects of analyses through pointing out open problems which provides further research opportunities.

Finally, we study a multi-user interference scenario while employing DFOV and SDFOV receivers and compare them to FFOV receivers. The superior results of the dynamic FOV receivers give a flavor of their anticipated gains in performance. We consider this a strong case towards analyzing them further in Chapter 6.

Chapter 5

Multi-Cell Coverage under Illuminance Constraints

In this chapter we show the importance of satisfying the dual-use requirements of indoor VLC systems. This is done through proposing a novel dual optimization problem that constrains the communication aspect with the illuminance requirement. We start by defining the problem and design challenges, then we formulate the constrained dual optimization. Finally, we show the optimization impact on performance through varying multiple system parameters.

5.1 Illuminance Constrained Multi-Cell Coverage and Transmission Power Dual Optimization

One of the motivations to using VLC technology is its dual-use. Exploiting the presence of luminaires that are already in place by swapping them out for LEDs or micro-LEDs is very appealing in terms of infrastructure planning and overall system deployment cost. However, this imposes constraints in both the communication aspect as well as the illumination aspect that should be addressed in the design phase. Lighting standards indicate illuminance levels for different settings and supported tasks. For example, standards require that office spaces illuminance should be kept within 300-500 lux at the working surface (Richman, 2015; Rae, 2000). If illuminance is less than 300 lux, this is considered insufficient for a working space and going beyond 500 lux introduces too much brightness which may cause irritations to the human eye.

5.1.1 Design Challenges

There are two trade-offs that spin off from this design requirement. First is the impact of the light emission pattern. Changing it from "wide" to "spot" (Fig. 5·2) at a fixed transmit power, concentrates the transmitted power over a smaller area on the working surface. Thereby changing both the luminous intensity and luminous flux which causes an increase in brightness. This can easily cause a violation of the standard lighting requirement. Second, the impact of light reflections also plays a role in complicating the situation. A wider emission profile creates a more uniform illuminance pattern but also causes more reflections. In turn, reflections increase the desired received power but also increase the total illuminance which is subject to a maximum value.

This motivates us to propose a novel formulation that jointly optimizes the transmission power and emission profile for a VLC deployment in order to maximize minimum irradiance (essentially relating to received power) while guaranteeing an illuminance distribution that falls within the required illuminance specifications. Because we are concerned with indoor office spaces, in our optimization we require the illuminance CDF mass to be between 300 and 500 lux with a probability I_d of the total CDF mass.

In (Raj et al., 2019) the authors vary the transmitter semi-angle to reduce the spatial variations in power. (Wu et al., 2012; Wu et al., 2016) explore optimizing the Lambertian order to maximize the minimum power in a room as well; however, the work does not consider the illuminance constraint, keeping the transmit power constant while focusing only on optimizing the Lambertian order. This approach can lead to an illuminance violation which we consider in our work.

We also show the importance in performing a dual-optimization under the illuminance constraint; confirming that the single optimization can lead to compromised performance or infeasible solutions. Optimizing based on only the Lambertian order results in a solution that must be later adjusted for the illuminance constraint. We show that this approach produces a reduced average illuminance and a reduced minimum received signal power, dropping to about $55-72\%$ of its optimal value.

We form a general model for our problem and plug in an instance layout to show the impact of the dual optimization. We assume a rectangular volume with four access points distributed symmetrically at ceiling height and an observed working surface as shown in Fig. 5·1. One might choose different working areas of interest, the same model can be used by applying it to each of the considered areas. In terms of communications modeling, we use the model previously discussed in Section 2.1.1.

We study the effect of the LOS optical channel gain while also considering the first order reflection ($k=1$ bounce) effect on the received power using the model in Section 2.1.3. Also, the area of the working surface A_s, highlighted in Fig. 5·1, avoids the potential impact of higher order reflections as it is 0.5 m away from all walls. This is why we do not study higher orders because their effect can be neglected in most environments (Kahn and Barry, 1997).

Radiant intensity is defined as

$$R(\phi) = P_t * G_T(\phi) \tag{5.1}$$

and P_t is the transmitted power. In Fig. 5·2 we show the relation between Lambertian order and beam width, while Fig. 5·3 shows radiant intensity of different orders. To obtain the transmitter semi-angle at half power ($\phi_{\frac{1}{2}}$) simply use the following equation, (Kahn and Barry, 1997): $\phi_{\frac{1}{2}} = \cos^{-1}(\exp(\frac{-\ln 2}{m}))$.

5.1.2 System Power

We focus on the LOS channel when maximizing the minimum power received assuming that the effect of reflections can be neglected through the receiver's optics (Abdalla et al., 2019b; Abdalla et al., 2019a). To calculate the lowest LOS received power, P_{min}, we can

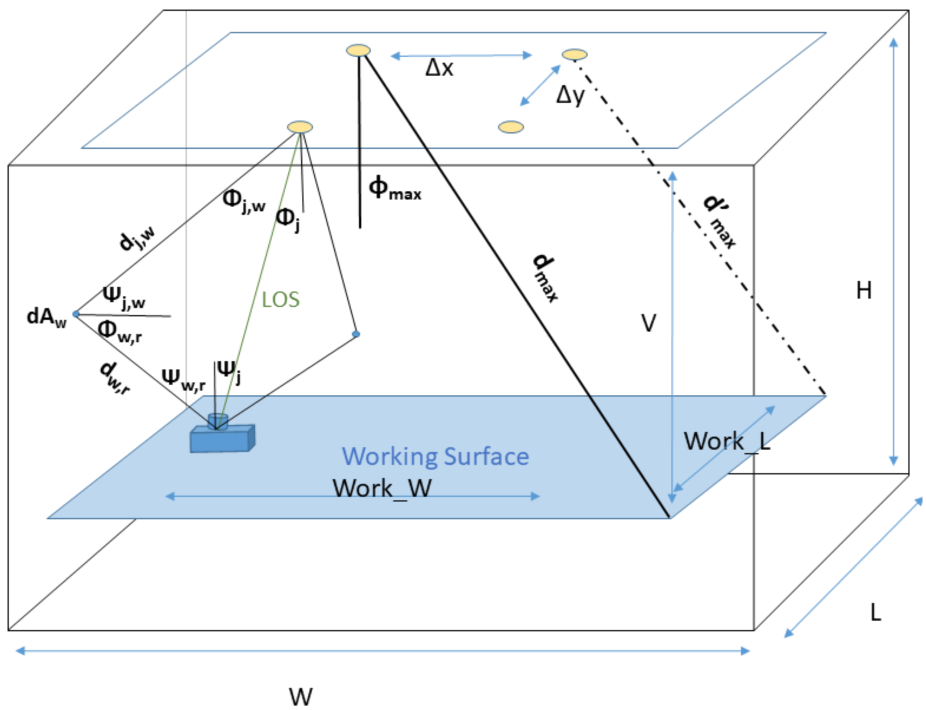

Figure 5·1: Example Room Setup

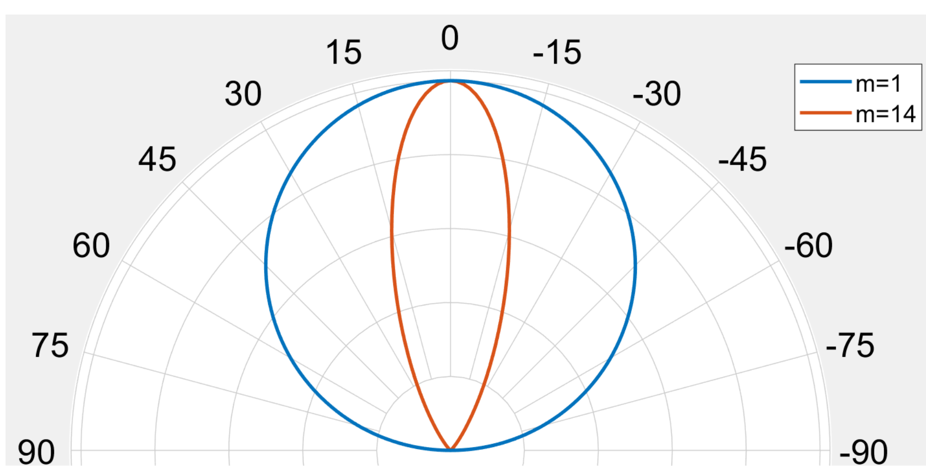

Figure 5·2: Relation Between Lambertian Order vs. Beam Width Normalized to Peak Intensity

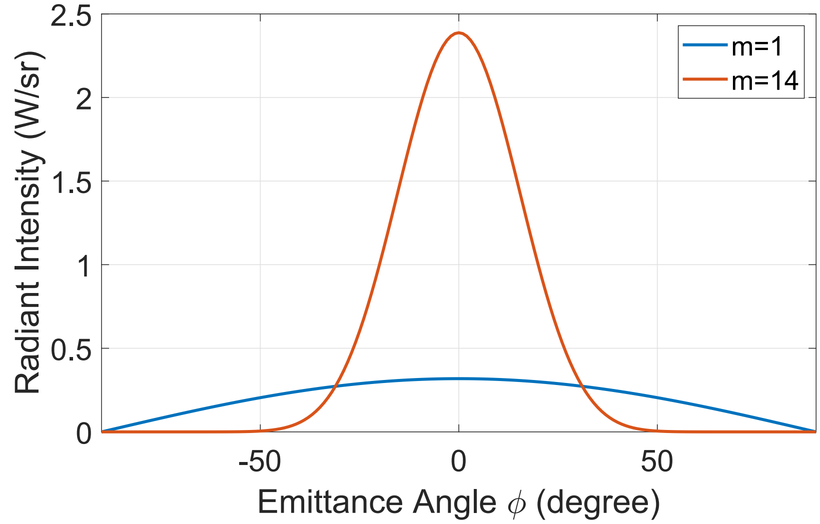

Figure 5·3: Radiant Intensities of Small vs Large Lambertian Orders

substitute d for the largest distance between a transmitter and the receiver in the room d_{max}, shown in Fig. 5·1 which creates the largest angle between the transmitter and the receiver ϕ_{max}, its cosine is defined as $\cos(\phi_{max}) = \frac{V}{d_{max}}$.

This particular d_{max} is chosen to allow receivers to connect to any of the transmitters in the ceiling. Define this as Connect Any mode. This mode allows the receiver to take any random orientation and connect accordingly which confirms the practicality of this setup. In a different system with different connection assumptions, d_{max} differs accordingly. We compare our findings with a mode which assumes the receiver has to connect to the AP it is under, mentioned in (Wu et al., 2012). This mode in our setup gives d'_{max} in Fig. 5·1, we refer to it as the One Cell mode for simplicity. We optimize:

$$P_{min} = \frac{P_t^{(j)}(m+1)A\cos^m(\phi_{max})cos(\psi_j)}{2\pi d_{max}^2} 1\{\psi_j < \chi\} \tag{5.2}$$

where j in this case is the AP connected to the receiver through either d_{max} or d'_{max}. To maximize P_{min} with respect to m, we need to constrain this problem with the standard illuminance required at the working surface. If this is not the case the brightness level can quickly rise to become too irritating to the human eye or decrease abruptly reducing the quality of the user experience. This is another reason why $P_t^{(j)}$ has to be involved in the optimization as well. P_{min} also depends on the receiver FOV and orientation. Our objective in deployment is to maximize the irradiance at the surface of a receiver directed towards the light. Therefore, without loss of generality, in the communication analysis we consider $G_R = 1$. Setting $A = 1$ m^2 gives the results in terms of power per unit area (i.e., irradiance).

5.1.3 System Illuminance

Illuminance is evaluated by summing the received power by the human eye from all transmitters and their reflection paths. In the illuminance analysis, we consider $G_R = \cos(\psi)$. This helps capture illuminance effects from all transmitters while providing a tighter constraint on it. Illuminance describes the quantity of luminous flux Φ per unit area (Zumtobel Lighting GmbH, 2018). Luminous flux is defined as (Rahaim et al., 2010):

$$\Phi = K_m \int_{380}^{720} P_s V_L(\lambda) PSD(\lambda) d\lambda \tag{5.3}$$

where K_m is maximum visibility which is about 683 lm/Wt at λ =555 nm (Komine and Nakagawa, 2004), $V_L(\lambda)$ is the standard luminosity curve and $PSD(\lambda)$ is the spectral content of the light incident on the receiver. We assume a constant PSD for the source as well as a flat spectrum reflectivity for the wall surfaces. This allows eq. (5.3) to become $\Phi = P_s L$ where L is a constant in Lumens per Watt. P_s in the context of this equation is the radiant power received from all the transmitters, defined as:

$$P_s = \sum_j \frac{P_t^{(j)}(m+1)\Delta A_s \cos^m(\phi_j)\cos(\psi_j)}{2\pi d_j^2} \tag{5.4}$$

We assume that illuminance is approximately constant over a small enough area. It is then evaluated as luminous flux over this area in which it was observed ΔA_s, as $I = \frac{\Phi}{\Delta A_s}$. We consider the area of interest to be the working surface A_s across which illuminance varies.

A_s in our observed instance is the space 0.5 m from each wall and 0.72 m from the floor, highlighted in Fig. 5·1.

5.1.4 Constrained Dual Optimization

Here we discuss the formulation of the optimization problem that maximizes the minimum LOS power received while keeping the illuminance in the required standard range (Abdalla et al., 2020a). Our formulation is as follows:

$$\begin{aligned} \max_{P_t^{(j)},m} \quad & P_t^{(j)}(m+1)\cos^m(\phi_{max}) \\ \text{s.t.} \quad & P\{300 \leq I \leq 500\} \geq I_d \\ & 0 \leq P_t^{(j)} \leq P_{max} \\ & m > 0 \end{aligned} \tag{5.5}$$

where P_{max} is the maximum transmit power. The optimization variables are the transmitted power ($P_t^{(j)}$), which has to be restricted to the values that allow the transmitter and the receiver to operate in their linear ranges, and the Lambertian order m. Illuminance, I, is a random variable that depends on the receiving eye location along the working surface (x_e,y_e), another random variable. Both x_e and y_e are uniform random variables over the plane. Note that in eq. (5.3), P_s is the power received from all transmitters. The first constraint requires the illuminance CDF mass between 300 and 500 lux to have a minimum acceptable probability I_d of the total CDF mass. Increasing I_d decreases the feasible set for the problem. It is worth noting that this optimization problem is convenient for designing any general room. In case the focus is not an office, the designer is able to switch out the illuminance ranges to fit the requirement.

The more transmitters are present in the system, the more random variables based on the location of each transmitter are considered. This makes finding a closed form for the CDF formulation an intractable challenge. This is why we evaluate the CDF numerically to solve

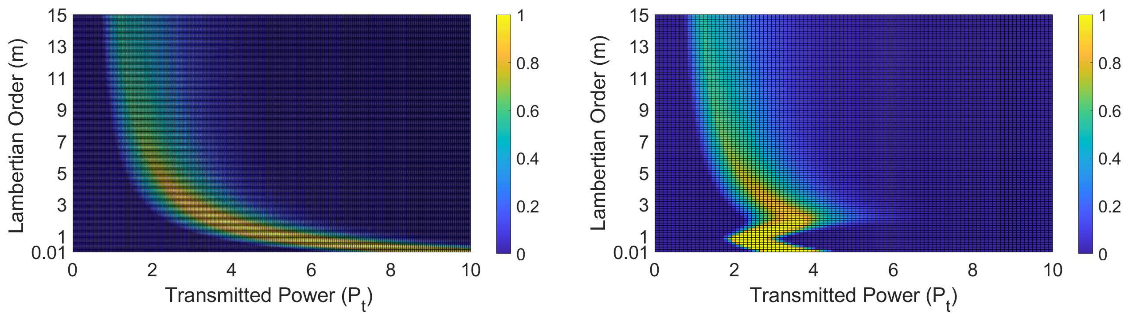

(a) **(b)**

Figure 5·4: Standard Illumination Probability Heat Map, Room 1. (a) $\rho = 0$; (b) $\rho = 0.8$.

the optimization problem. Due to the fact that this problem is evaluated once before designing the room/transmitters at the deployment stage, we are not concerned with the computational complexity. The solution depends on room dimensions, number of transmitters, their locations, the desired illuminance probability and the allowed maximum transmission power.

5.1.5 Dual Optimization Impact and Performance

We discuss the optimization performance on the received power and its implications on illuminance. In our simulation setup, we assume a symmetric placement of the APs as well as equal transmit powers and Lambertian orders for each transmitter. We show results for different 1) Wall reflectivities: we simulate $\rho = 0$ (no reflections), $\rho = 0.2$ and $\rho = 0.8$, 2) Room dimensions, 3) Transmit modes: both of the aforementioned modes Connect Any and One Cell, 4) Transmitter Inter-spacings and 5) Transmitter count. Our simulation parameters can be found in Table 5.1. We also show the effect of ignoring the dual optimization on illuminance.

We introduce the illuminance uniformity metric (U) defined in (Philips, 2014) to assess the system illuminance. It is the ratio between the minimum illuminance to the average illuminance. The average illuminance for an office space should be around 400 lux accord-

Table 5.1: Dual Optimization Simulation Parameters

Parameter	Parameter Description	Value
Room 1	L × W × H	$4\times4\times4$ m^3
Room 2	L × W × H	$4\times4\times3$ m^3
Surface Area	WorkW×WorkL×Rx height	$3\times3\times0.72$ m^3
Δ_x	Spacings between Tx in x-axis	1.3 m
Δ_y	Spacings between Tx in y-axis	1.3 m
dA_w	Wall Element Area	0.04 m^2
ρ	Wall Reflectivity	0.2/0.8
P_{max}	Maximum transmitter power	10 W/ 3.5 W
Room 1 V1	Vertical height bet. Tx and Rx	3.28 m
Room 2 V2	Vertical height bet. Tx and Rx	2.28 m

ing to (Richman, 2015). As for U, ideally $U = 1$ but it is also declared in (Philips, 2014) that a minimum of $U = 0.6$ is acceptable.

Room 1 is used in most simulations unless otherwise stated. It's volume is 4×4×4 m^3. The vertical height V, between the receiver and the transmitter is $V1 = 3.28$ m. In this room the maximum distance $d_{max} = 4.98$ m.

Effect of Reflections

In Fig. 5·4a, we show a heatmap of the probability of the desired CDF mass at different Lambertian orders and different transmission powers for Room 1 while $\rho = 0$, in Fig. 5·4b we show the CDF at $\rho = 0.8$. The figures confirm 1) that reflectivity plays a role in changing the illuminance specifically in lower Lambertian orders, 2) that there exists a limited set of (m, P_t) pairs that can satisfy the illuminance constraint. The feasible set of m and P_t comes from slicing the function at the desired I_d. This set changes with different ρ, I_d and P_{max}. Fig. 5·5 shows the feasible set for P_{min} at different reflectivities $\rho = 0, 0.1, 0.8$ and $I_d = 0.6$. It highlights the reflectivity effects on the feasible set and subsequently the optimal minimum power. This is also confirmed in Figs. 5·6a and 5·7a which show different optimal power performance for different reflectivities. We elaborate more on

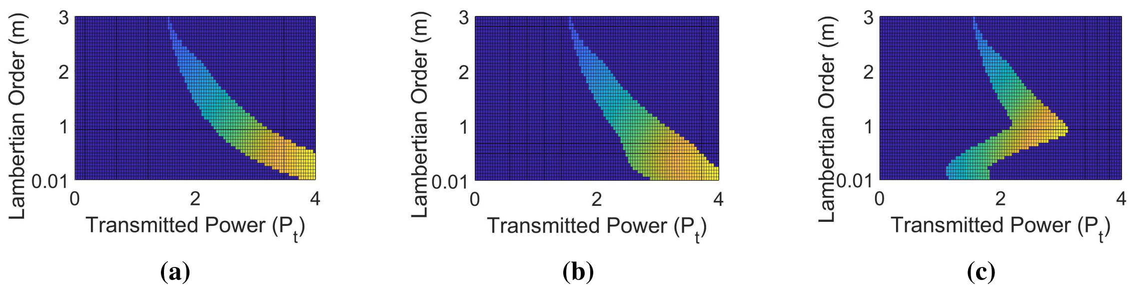

Figure 5·5: Feasible Region at $I_d = 0.6$ and $P_{max} = 4$ W. (a) $\rho = 0$; (b) $\rho = 0.1$; (c) $\rho = 0.8$.

these figures in the transmit modes discussion.

Different Room Heights

For Room 1, the optimal solution for $I_d = 0.85$, $\rho = 0$ and $P_{max} = 10$ W is $P_{min} = 0.067$ W resulting from the pair ($m = 0.1, P_t = 9.8$ W). This gives the illuminance CDF left of Fig. 5·6b. If illuminance is disregarded in this optimization, the solution using only the optimized m and max transmit power results in the illuminance CDF on the right in Fig. 5·6b which clearly violates the standard illumination ranges. However, ignoring the illuminance constraint in optimizing m and then reducing power to achieve the required illuminance gives $m = 1.39$ and $P_t = 4.83$ W. This has two drawbacks: (1) an illuminance with a lower average of 426 lux (Main Illuminance results can be found in the right column in Table 5.3), and (2) the resultant minimum received power in this case is $P_{min} = 0.04$ W which is 59% of the optimal value calculated from the dual-constrained optimization. Additional cases are shown in Table 5.2.

We simulated the problem for a room with a lower ceiling. Room 2 is $4 \times 4 \times 3$ m^3, has a vertical height between the transmitter and the receiver $V2 = 2.28$ m and $d_{max} = 4.39$ m. In this case the standard illuminance probability has a smaller feasible region.

Table 5.2: Different Room Results

$I_d = 0.9, \rho = 0$	Room 1		Room 2	
Dual Optimization	No	Yes	No	Yes
$P_{max} = 10$ W				
m	1.39	0.14	Infeasible	0.01
P_{min}	0.04	0.06		0.05
P_t	4.75	9.4		5.63
U	0.67	0.7		0.6
$P_{max} = 3.5$ W				
m	Infeasible	2.04	Infeasible	Infeasible
P_{min}		0.03		
P_t		3.5		
U		0.6		

In Table 5.2 we show results for two different room heights, different maximum transmit power capabilities and a stricter desired illumination I_d. The reason behind this analysis is to show that the room design, the illuminance requirement, the transmitter properties i.e., Lambertian order, maximum transmit capability all play a role in the design decision. It is logical to investigate each to avoid pitfalls that are highlighted in Table 5.2 where infeasibility is inevitable. Otherwise a designer will need to sacrifice one property based on the importance of another. This is clearly shown in Table 5.2 where there was no possible m, P_t pair in that room able to reach the required $I_d = 0.9$ with a maximum transmit power 3.5 W. One would either reduce illuminance requirement to 0.85 or look into ways to push the max transmit power higher if insisting on $I_d = 0.9$.

Transmit Modes

Here we show the effect of choosing Connect Any mode transmission versus One Cell mode on the design. The effect of the illuminance constraint on the optimization problem, therefore the optimal P_{min}, is shown in Fig. 5·6a. The figure shows the best P_{min} per Lambertian order when employing the Connect Any Mode and highlights the optimal one and the transmitted power that achieved it, all for different reflectivities as well as a case where

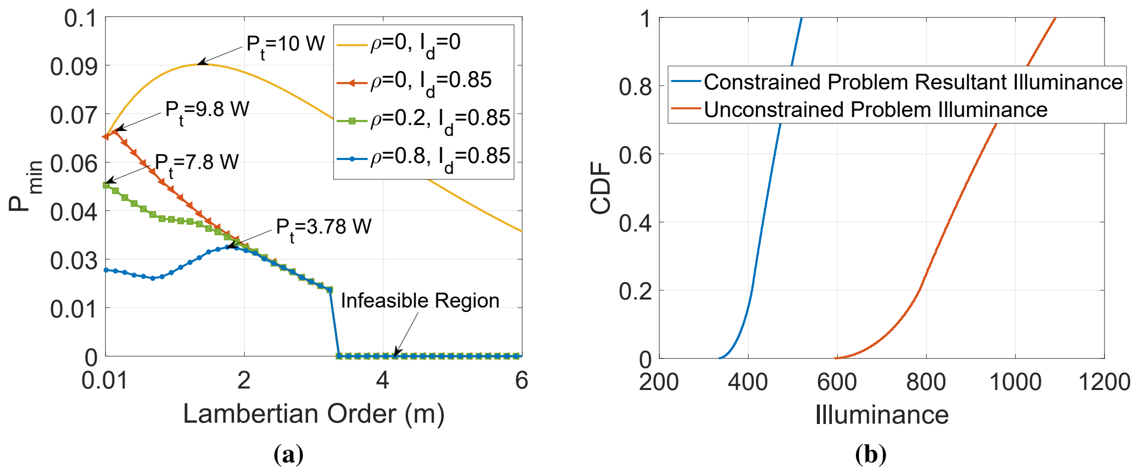

Figure 5·6: Room 1 P_{min} and Illuminance Results when Employing Connect Any Mode. (a) Optimal P_{min} at Different Lambertians for Different ρ; (b) Illuminance CDF Room 1, $I_d = 0.85$.

the illuminance constraint is dropped $I_d = 0$. The effect of the illuminance constraint is also observed through the sharp drop in the received power curves caused by the infeasibility region.

In Fig. 5·7a we show the optimal P_{min} at different wall reflectivities and show the transmit power that achieves the optimal values as well but for the One Cell mode. The main difference in these modes is that One Cell will allow higher Lambertian order, as d'_{max} is smaller than d_{max}. While this may appear beneficial because higher m means smaller transmitter half angle and so a possible reduction in the effect of reflections on illuminance, the growth in concentrated power with m as shown in the radiant intensity curve (Fig. 5·3) causes a higher possibility of illuminance violation as well as less uniformity. This is confirmed in Fig. 5·7b where designing the system without considering illumination causes the illuminance to approach 4000 lux. Another drawback in this transmit mode is the assumption that receivers will be able to connect to the cells they reside in, ignoring their device orientations.

The illuminance values for different ρ and different transmit modes are populated in

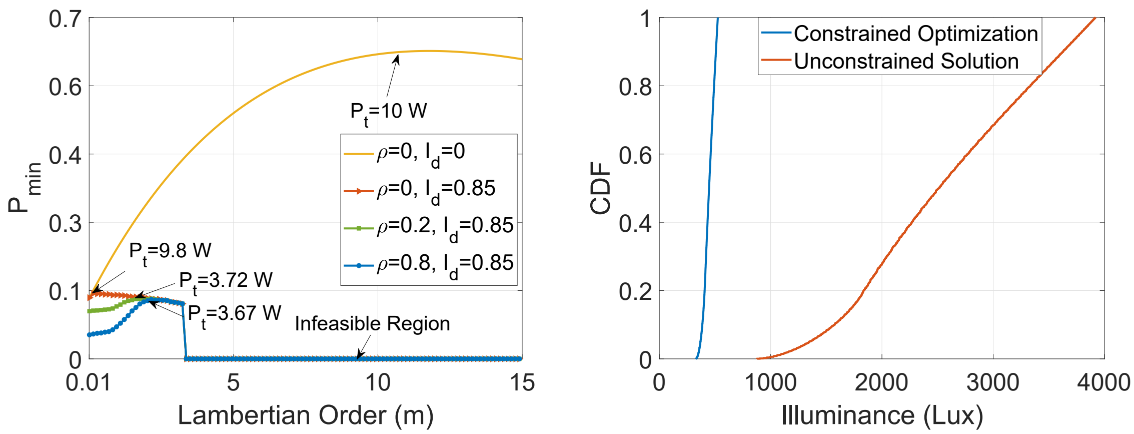

(a) (b)

Figure 5·7: Room 1 P_{min} and Illuminance Results when Employing One Cell Mode. (a) Optimal P_{min} at Different Lambertians for different ρ; (b) Illuminance Violation in The One Cell Mode.

Table 5.3: Illuminance Results (Room 1)

$P_{max} = 10$W	One Cell Mode	Connect Any Mode
	uniformity @ average illuminance	
$\rho = 0, I_d = 0.85$	0.7@447	0.7@447
$\rho = 0.2, I_d = 0.85$	0.6@414	0.9@477.6
$\rho = 0.8, I_d = 0.85$	0.5@421	0.6@444
$\rho = 0, I_d = 0$	0.2@2540.2	0.6@884.7

Table 5.3. We note that with the increase in reflectivity, the One cell mode tends to get worse in uniformity. Connect Any has variations in uniformity as well but all are within the acceptable range, 0.6 and above.

Table 5.4: Transmitter Inter-spacings and Count

	A) Tx Inter-spacings			B) Tx Count		
	0.8 m	1.3 m	2 m	4	6	8
m	0.04	0.1	0.2	0.1	0.01	0.01
P_{min}	0.071	0.067	0.061	0.067	0.038	0.027
P_t	9.8	9.8	10	9.8	7.69	5.48
U	0.73	0.75	0.79	0.75	0.78	0.81

Inter-spacings and Number of Transmitters

We show how varying the number of transmitters affects the problem as well as changing their separation distances. We simulate employing four, six and nine transmitters with the same inter-spacings in Table 5.4B and compare their results. We also report the result of having four transmitters in the system but with different separation distances in Table 5.4A. These results are evaluated at $I_d = 0.85$, $\rho = 0$ and $P_{max} = 10$ W. As expected, the more transmitters deployed, the quicker the illuminance constraint is met and the system needs to back off the transmitted power to meet the constraint. This directly affects the minimum power received. However illuminance uniformity is slightly enhanced with transmitter count.

With respect to separation distances, we note that the further the transmitters are from each other, uniformity is slightly enhanced and the power allowance increases. This makes sense because light gets spread out over more area decreasing the brightness of the middle overlap region between the transmitters. However, this causes the distance d_{max} to increase and so decreasing the minimum power received. In case of d'_{max} it would actually help in increasing the minimum power. This all circles back to how the system designer envisions connectivity and finally decides on the intricate details between illumination and communication in the system.

Results show that using the constrained dual optimization is better for optimizing the minimum received power in the space. A single optimization causes losses ranging from $29-45\%$ in two different room scenarios. Otherwise ignoring illumination can cause violations to up to 2,000-4,000 lux in the working surface instead of the standard 300-500 lux range as well as non-uniformity in illuminance.

5.1.6 Infrared Optimal Lambertian Order

While this work does not specifically cover IR sources, we note that our analysis framework also extends to IR deployment scenarios. In this case the overall illuminance is not a constraint; however, IR has eye-safety limits that must be considered.

The formulation changes as follows. The problem reduces to the term that optimizes P_{min} which is found by getting the second derivative of eq. (5.2) ($\frac{\partial^2 P_{min}}{\partial^2 m} = 0$) which gives the result:

$$m_{opt}^{Infrared} = \frac{-1}{\ln(\cos(\phi_{max}))} - 1, \phi_{max} < 68.4^{\circ}$$

Evaluating this Lambertian order in eq. (5.2) and using the maximum allowed power gives the max-min received power for this case. The main concerns for IR are eye safety and power consumption. In (Kahn and Barry, 1997), the authors indicate that LED IR sources are generally considered to be eye safe; however, as IR sources become increasingly collimated, there is increased potential to exceed safety limits.

5.2 Chapter Conclusions

We formulate a dual optimization VLC deployment problem that aims to maximize the minimum received power (a communication aspect) while keeping illuminance within the desired range suggested by many standards while taking first order reflections into consideration. The proposed technique is flexible, allowing illuminance to be tuned according to the needs of lighting design and provisioning. The optimization problem reveals how illuminance limits the feasible set of optimal emission pattern and transmitted power solutions. We also describe how the problem differs if infrared sources are used.

Finally, we simulate different environments (room sizes, wall reflectivities, transmit modes, number of transmitters and their inter-spacings) to show the optimal minimum received power and the resultant illuminance CDF, while discussing the drawbacks of single optimization (Lambertian order only). Results indicate losses between 29-45% in minimum received power when using the single optimization instead of our proposed dual constrained formulation as well as overall lower average illuminance. The results also confirm that illuminance needs to be constrained during the design and provisioning phase to mitigate scenarios of reduction in either the communication quality or the illuminance requirement. This serves as a novel dual optimization that may be utilized to optimize various communication purposes while assuring that the dual-use requirements are upheld for best user experience in both aspects.

Chapter 6

Standalone VLC: Multiple Users

In this chapter, we tie what we observed in our previous analyses to build a more coherent VLC system and optimize it for future integration with an RF system. First we discuss challenges within the system and define our system model. Second we focus on the transmit side where we propose a variation of the constrained dual optimization in Chapter 5 by forming a constrained joint optimization of minimum received power and illumination. Third we talk about the receive side parameters where we employ SDFOV and DFOV receivers and formulate a user association with FOV optimization. Fourth, we show the system simulation results for optimizing fairness and sum throughput in both a centralized as well as a distributed greedy architecture. Sixth, we propose algorithms and heuristics for the optimization of the SDFOV receiver as well as a heuristic for the DFOV fairness problem. Finally, we evaluate the effect of self-blockage as well as random human blockers on the system performance.

We study a dense indoor VLC network. AP density increases the possibility of interference between cells. It also poses the question of how to balance the load across the APs. There exists work, relevant to the interference problem, that focuses on power allocation, user association, load balancing or multiple access techniques (Li et al., 2016; Zhang et al., 2016; Obeed et al., 2018; Li et al., 2015). We discuss interference mitigation in indoor optical wireless networks in (Abdalla et al., 2020b). We also study dynamic receiver FOV performance and advantages in prior work (Abdalla et al., 2019b; Abdalla et al., 2019a; Little et al., 2018; Abdalla et al., 2020d; Abdalla et al., 2018) providing important insights

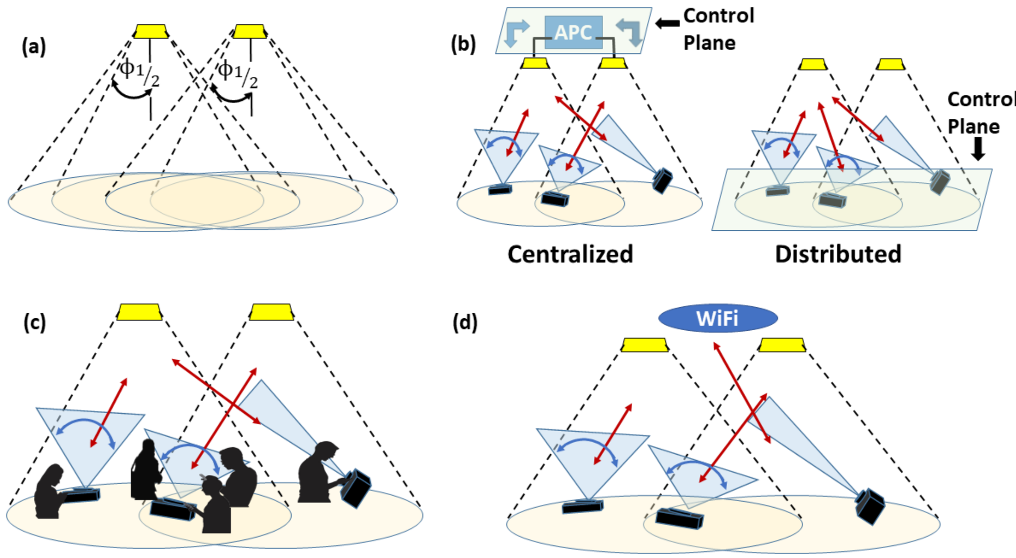

Figure 6·1: Sequence of System Analysis. (a) Deployment Optimization for VLC Coverage and Illumination; (b) User Association and FOV Optimization in a Multi-user Setting Under Two Different System Architectures ; (c) Evaluation of Occlusion Effects on the VLC System; (d) Analysis of the Hybrid Setup of the Optimized VLC System and WiFi in Chapter 8.

to its usages theoretically and through experimentation.

Based on these two dimensions; the need for balanced illumination, and the need to mitigate interference between users, we aim to 1) optimize luminaire emission, as discussed in Chapter 5 and 2) optimize signal quality and user association in a multiple AP setting. We also address how this will be managed practically in either a centralized or distributed way. The sequence of our analysis is illustrated in Fig. 6·1. Variables and dynamics that affect this system include transmitter parameters: transmitter layout, coverage (emission pattern), illumination, and power. Receiver-side parameters include: receiver orientation, location, FOV, density, and blocking. Finally, system parameters include the system architecture: whether via a central access point controller (APC) or by distributed greedy receivers.

With the motive of enhancing user signal quality and user experience in the presence of interference we 1) optimize the multi-cell AP transmit power and emission pattern to satisfy a joint objective for maximizing the minimum received power and an illumination

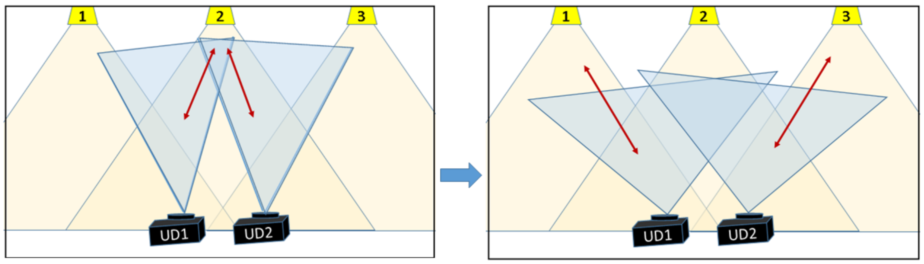

Figure 6·2: Importance of FOV Optimization and User Association.

probability γ; 2) propose a novel user association and FOV optimization taking load balancing into account; 3) analyze the effect of receive parameters as well as different system architectures; 4) show the effect of both self-blockage as well as random human blockages on the communication quality (Abdalla et al., 2020c).

6.1 Challenges in the Novel User Association and FOV Optimization

The user association and FOV optimization are tightly coupled. We show a simple example of this in Fig. 6·2 where both users are located closer to transmitter 2 (Tx_2). It may seem that the association solution would be to have them both connect to Tx_2 and share the cell resources or suffer from interference generally. However, if we allow their FOVs to grow so each one can see the more distant transmitter closest to it as in Fig. 6·2 (right), then User 1 connects to Tx_1, User 2 connects to Tx_3 and Tx_2 is turned off. The result is better individual and system throughput. The problem also depends on the user density; if there were a third receiver that would cause Tx_2 to be on, then it would cause the highest interference on users 1 and 2 and the best allocation/FOV solution would be different.

Fig. 6·3 shows the challenge of FOV optimization specifically for the non-steerable dynamic FOV receiver through another example. In this case the receiver is shown centered in a FOV with a flat orientation and connected to Tx_1. In case of point-source transmitters, the solution is easier because the optimized FOV will just be the minimum FOV that allows the receiver to see the transmitter. In our configuration, we assume a more practical non-

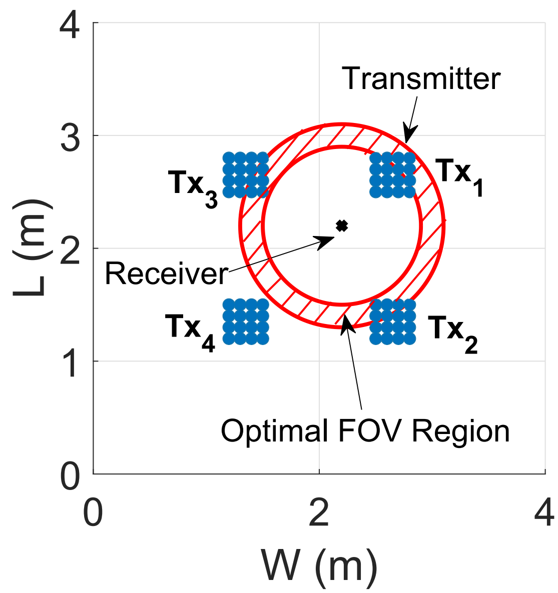

Figure 6·3: FOV Optimization Challenges in a Multi-Element Transmitter Configuration

point-source transmitter that we model as consisting of a grid of point-source elements. If the receiver sees all the transmitters, interfering components come into view from both Tx_2 and Tx_3. To remove interference completely, the FOV must reduce to the smaller illustrated circle. However, this is not necessarily the best solution because of the trade-off between signal strength and interference. This is why the region between these two circles is the optimal FOV region. The optimal FOV is the one that finds the right combination of desired and interfering elements that gives the best signal to interference plus noise ratio (SINR). Other factors that determine the best solution include: which transmitters are actually on, the receiver location and orientation, user density, and transmitter spacing.

6.2 System Model

In this Section we describe the details of our standalone VLC system model including our assumptions and system performance metrics. In our work we are concerned with average optical transmitted and received power because average power is what constrains the transmit signal and also defines illuminance, both vital to our analysis.

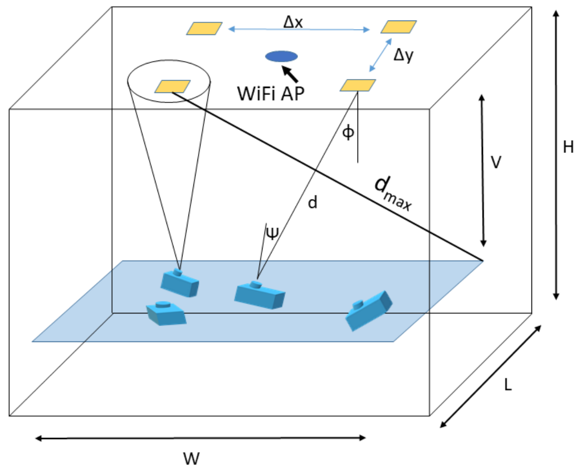

Figure 6·4: Room Layout Emphasizing Variable Device Orientation, Location, and FOV in a Hybrid RF/VLC Network.

Fig. 6·4 shows the hybrid RF/VLC network, the variable receiver location, orientation, FOV, and the parameters involved in our analysis, described later on in this Section. Our focus in this chapter is the VLC system, the integration of both media follows in Chapter 8. We study the LOS optical channel gain. We do not study the effect of reflections as in most environments their effect can be neglected (Komine and Nakagawa, 2004). We use the channel model in Section 2.1.1 and consider a Lambertian emission with order m and model a PD with area A and no filter or optical lens. χ is the receiver's FOV.

In a multi-user setup, we define the SINR of user u connected to the jth transmitter as:

$$SINR_u^{(j)}(\chi) = \frac{\sigma_j^2}{\sum_{q,q\neq j}\sigma_q^2 + \sigma_a^2} = \frac{(RP_r^{(j)}(\chi))^2}{\sum_{q,q\neq j}(RP_r^{(q)}(\chi))^2 + \sigma_a^2(\chi)} \tag{6.1}$$

σ_j^2 is the variance of the desired signal from the associated transmitter j, σ_q^2 is the interfering signal variance and we sum over q depending on the number of interference signals. σ_a^2 is the noise current variance and R is the receiver responsivity.

In our shot noise dominated system, we model σ_a^2 as (Ramirez-Iniguez et al., 2008):

$$\sigma_a^2 = \overline{i_q^2} + \overline{i_d^2} \tag{6.2}$$

where $\overline{i_d^2}$ is the dark current noise and $\overline{i_q^2}$ is the quantum noise. $\overline{i_q^2} = 2qRP_nB_{VLC}$, q is the electron charge, B_{VLC} is the VLC AP bandwidth and P_n is the optical power incident on the photodiode, as in Section 2.1.1. Meanwhile, $\overline{i_d^2} = 2qI_dB_{VLC}$ where I_d is the dark current.

Analysis Assumptions:

1. User devices are assumed to move in a uniformly random fashion throughout the x-y plane at a fixed receiver height (the working plane, highlighted in Fig. 6·4). We choose to fix the receiver height for simplicity but realize that performance varies with different receiver heights as we discussed in Section 3.5 where we show that variable height can cause changes to the optimal FOV.

2. Devices are allowed to have variable orientation. The azimuth angle can take a uniformly random angle between (0-360) degrees as well as the elevation which is between (30-150) degrees. We choose these ranges to ensure that the receiver has visibility to at least one transmitter.

3. Interference is assumed to exist among different APs but for users connected within an AP the resources are divided equally. In terms of individual throughput[1], assuming no overhead for division of resources, the equation within an AP j for a user u becomes

$$T_u^{(j)} = \frac{B_{VLC}}{2N_{VLC,j}} log(1 + SINR_u^{(j)}) \tag{6.3}$$

where B_{VLC} is the VLC AP bandwidth and $N_{VLC,j}$ is the number of users connected to VLC AP j.

[1] The Shannon representation of throughput serves as a tractable model, that is not concerned with specific modulation, for a good approximation of VLC link performance (Kashef et al., 2016; Guo et al., 2013).

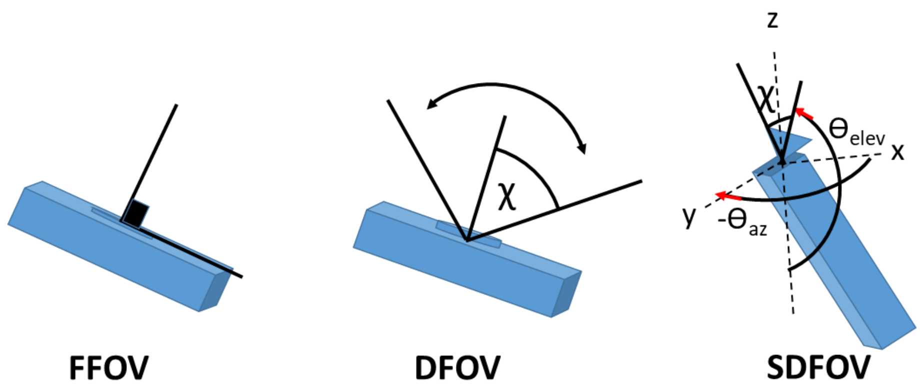

Figure 6·5: Receiver Structures; Fixed Field of View (FFOV), Dynamic Field of View (DFOV) and Steerable Dynamic Field of View (SDFOV).

We employ the receivers we proposed in Sections 3.3 and 3.4, illustrated in Fig. 6·5, and compare their results to the baseline FFOV receiver (Section 3.2).

Performance Metrics We consider the following performance metrics in evaluating the proposed work.

1. **Fairness:** In the coordinated setting, we solve a max-min problem to get the highest minimum individual throughput. (This considers the user throughput after the cell resources have been shared between users within one cell). If this max-min solution can be achieved through multiple user allocations, the one that gives the highest sum is then chosen. This helps the other users not lose performance gains unnecessarily allowing better total system throughput as well. In case of the greedy association, we look at the resultant minimum rate.

2. **Total System Throughput:** The sum of each user throughputs.

3. **Transmitter Utilization Percentage:** The number of active transmitters on average within the system.

4. **Outage Probability:** For a fixed system required throughput, we evaluate the probability that each receiver is unable to meet the requirement. We define an outage as the case when this happens.

6.3 Deployment Optimization for VLC Coverage and Illumination

We employ a variant of the formulation in Chapter 5 to optimize deployment in a dense network with multiple users. For the room shown in Fig. 6·4, we change the coverage patterns by tuning the transmitter Lambertian order m. Controlling m changes the semi-angle of the transmitter ($\phi_{1/2}$) and so changes the inter-cell interference pattern. The trade-off involved is that although having smaller beams creates less interference, the power transmitted has to be reduced to keep the illuminance level in the standard range 300-500 lux (Rae, 2000) at the working plane of an office space.

We analyze the effect of changing the coverage pattern on the multi-user scenario when three different receivers are used: the FFOV, DFOV and SDFOV receivers and consider the area of interest to be the working surface A_s across which illuminance varies. A_s is highlighted and shown in blue in Fig. 6·4.

In Chapter 5 the maximum minimum power received in a space is optimized subject to an illuminance constraint. The minimum power is received from the furthest transmitter away from the edge of the working surface at d_{max}, as shown in Fig. 6·4. However, in our design here we focus on jointly optimizing a weighted sum of the minimum power received and the probability that illuminance lies between the standard ranges, $P_{ill} = P(300 < I < 500)$. The optimization is formulated in eq. (6.4), where the difference from Chapter 5 is the addition of weighted P_{ill} in the objective.

We continue our discussion by choosing equal weights $w_1 = w_2$. This way illuminance will not only be constrained (such that the solution will reside at the threshold) but also maximized to provide better user viewing experience. Our system does not assume a dynamically changing Lambertian order hence for each m we aim at giving the users the best illuminance ranges as well as max-min power received. We also simulated results for only maximizing the minimum power received ($w_2 = 0$) and note that the results do not significantly change. Assuming $d_{ji} = d_{max} \forall i$ for the furthest AP j, recalling that $P_{t,e}^{(ji)} = \frac{P_t^{(j)}}{wl}$

and looking at the relevant terms containing the optimization variables, the optimization problem becomes:

$$\begin{aligned}
\max_{P_{t,e}^{(ji)},m} \quad & w_1 \sum_{i}^{wl} \frac{P_{t,e}^{(ji)}(m+1)V^m}{d_{ji}^m} + w_2 P_{ill} \\
\approx \max_{P_t^{(j)},m} \quad & w_1 \frac{P_t^{(j)}(m+1)V^m}{d_{max}^m} + w_2 P_{ill} \\
\text{s.t.} \quad & P_{ill} \geq \gamma \\
& 0 \leq P_t^{(j)} \leq P_{max} \\
& m > 0
\end{aligned} \tag{6.4}$$

γ in this case is the least allowed standard illuminance probability. The first constraint ($P(300 < I < 500) \geq \gamma$) is to guarantee that the illuminance CDF mass between 300 and 500 lux has a probability γ of the total CDF mass.

6.4 Interference Management Through Receiver FOV Optimization and User Association

Here we investigate the problem of allocating users to transmitters to yield the best fairness and system sum throughput. The solution and the optimization problem differ based on the receiver used.

For each receiver, we show two possible optimization methodologies, solving it jointly and through decoupling. The results are rendered through Monte Carlo simulations; however, we provide heuristics and show their performance and discuss the limitations of each methodology. The general joint allocation/FOV optimization formulation, for M receivers and N VLC APs, to maximize fairness in this model can be expressed as:

$$\max_{\substack{x_{uj},\chi_u^{(j)},\\ j=1,\ldots,N,\\ u=1,\ldots,M}} \quad \min_u \sum_{j=1}^{N} \frac{B_{VLC} x_{uj}}{\sum_{k=1}^{M} x_{kj}} \log(1 + SINR_u^{(j)}(\chi_u^{(j)}))$$

$$\begin{aligned} \text{s.t.} \quad & x_{uj} \in \{0,1\} \quad \forall u, j \\ & \sum_{j=1}^{N} x_{uj} = 1 \quad \forall u \\ & \chi_u^{(j)} \in \mathcal{F} \quad \forall u, j \end{aligned} \tag{6.5}$$

where $SINR_u^{(j)}(\chi_u^{(j)})$ and $\chi_u^{(j)}$ are the SINR (from eq. (6.1)) and the FOV of user u connected to transmitter j respectively. Meanwhile, x_{uj} is a binary connection variable; if transmitter j is connected to user u then $x_{uj} = 1$ otherwise it is 0. The second constraint allows the receiver to connect to only a single AP. The last constraint states that χ should be between the allowed ranges within FOV set $\mathcal{F} \triangleq [\chi_{min}, \chi_{max}]$. χ_{min} and χ_{max} are the smallest and largest FOVs achievable by the receiver respectively. The general problem for maximizing the sum throughput resembles eq. (6.5) but instead the objective function is:

$$\max_{\substack{x_{uj},\chi_u^{(j)},\\ j=1,\ldots,N,\\ u=1,\ldots,M}} \quad \sum_{u=1}^{M} \sum_{j=1}^{N} \frac{B_{VLC} x_{uj}}{\sum_{k=1}^{M} x_{kj}} \log(1 + SINR_u^{(j)}(\chi_u^{(j)})) \tag{6.6}$$

Both objective functions inherently penalize the connection of multiple users to the same AP to promote a more balanced load. The search space S for both set of variables is $S \triangleq |\{0,1\}|^{MN} \times |\mathcal{F}|^{MN}$, the first term results from the association problem and the second from the FOV optimization. $|\{0,1\}| = 2$, χ on the other hand is continuous. This makes $S = 2^{MN}|\mathcal{F}|^{MN}$. When applying the constrains on x_{uj} such that 1 receiver is served by 1 AP at most, the association space reduces to N^M. As for the FOV space, for a specific association $\{x_{uj}, \forall j, \forall u\}$, it reduces to $|\mathcal{F}|^M$ since each receiver has a single non-zero FOV associated with a single specific transmitter. This is further reduced to $M|\mathcal{F}|$ because there are no dependencies between different receivers FOVs. We then discretize the FOV by Δ_χ to search the continuous space, bringing the overall space (complexity) to $S = N^M M^{\frac{\chi_{max}-\chi_{min}}{\Delta_\chi}}$.

FFOV analysis

Because the FOV is fixed, the problem reduces to a nonlinear resource division association among users.

DFOV analysis

The user association and FOV optimization are tightly coupled. This is clear within this formulation. From eq. (6.1), the FOV variable $\chi_u^{(j)}$ is present in both the numerator and the denominator of the SINR term. The interference term adds to the complexity of the problem. Also if the interference terms were neglected the problem in terms of FOV only would still be non-convex. The presence of the association variables x_{uj} cause the problem to be a mixed-integer nonlinear program which is known to not have efficient solving techniques.

Unfortunately, methods like the work in (Zabini et al., 2017) do not apply in our formulation as the performance function is non-differentiable with respect to FOV and the performance function per a single user depends on the resources of the other users which causes strong coupling in the optimization, both of which are requirements that are not met to allow usage of the solution in (Zabini et al., 2017).

SDFOV analysis

The problem remains similar to the DFOV analysis in terms of variables. However, due to the presence of the pointing and acquisition capabilities of this receiver the SINR term reduces to the SNR. Therefore decoupling the problem, through solving the association problem then optimizing the FOV, can give close sub-optimal solutions.

Table 6.1: System Overhead

Overhead	Coordinated At the Tx side:	Distributed At the receive side:
FFOV	Receiver Location Info Receiver Orientation Info	Connecting to highest SINR
DFOV	Receiver Location Info Receiver Orientation Info	Scanning FOV for highest SINR
SDFOV	Receiver Locations	Steering and scanning for highest SNR

6.4.1 Coordinated System

This system assumes the usage of a controller. The controller is assumed to know the location of the receivers. In case of FFOV and DFOV receivers, it needs to know the receiver orientation as well. It is able to send the best elevation and azimuth angles to the SDFOV (if necessary). The receivers however are assumed to be able to tune their FOVs on their own. In turn the controller is able to evaluate the best associations between transmitters and receivers for different FOVs. This shows the best performance that the system can achieve in terms of fairness and sum throughput. However, its computational complexity is $O(MN^M)$. It is NP-hard and cannot be solved in polynomial time.

6.4.2 Distributed System

In this system the problem is decoupled. Both the association and FOV optimization problem are done at the receivers. We consider the greedy method where each receiver tries to connect to its best channel. The receiver scans the room for best SINR then, when applicable, it changes its FOV to zoom to the best connection. In case of SDFOV, the receiver searches for best SNR. This is highlighted in Table 6.1.

6.5 Systems Performance Results

We demonstrate the performance of the different systems in terms of the metrics described above. Simulation parameters are shown in Table 6.2. The results we show are averaged over 10,000 iterations. We set the number of transmitters N to 4 as well as the receivers M unless otherwise stated. A_s is 0.5 m away from each wall and 72 cm away from the floor level. For the dynamic FOV receivers, the dynamic FOV range is $\mathcal{F} = [0, 90]$ and for the FFOV, we set $\chi_{FFOV} = 90°$ to be able to see all transmitters in any room and at any orientation.

6.5.1 VLC Deployment

For our simulation setup (room dimension, transmitter spacing, maximum transmit power, and transmitter count, in Table 6.2), the optimal (m, P_t) pair is (0.3,3.8 W). To test different room coverage, we evaluate the transmit powers to a set of Lambertian orders that exist within the feasible range of the problem in eq. (6.4), $m = \{0.01, 0.3, 1, 2, 5, 10, 15, 20\}$. $P_t = \{4, 3.8, 2.5, 1.8, 1.2, 1, 0.8, 0.77\}$ W are the resultant transmit powers.

6.5.2 System Throughput

Fig. 6·6 compares the average sum throughput of the two systems at different coverage for the three proposed receivers. In the figure, at each point the illuminance CDF mass is centered around 300-500 lux (with the highest possibility that can be reached given this room model and the Lambertian order) by reducing the power for larger Lambertian orders, to allow for best user experience on the working surface in the space. SDFOV has the best performance but it decreases with higher Lambertian order, followed by DFOV which decreases as well. Meanwhile, the FFOV performance is enhanced when the Lambertian order is increased. This is owing to less overlap and less interference. Meanwhile the other two receivers already mitigate interference; thus they are mainly affected by the power drop

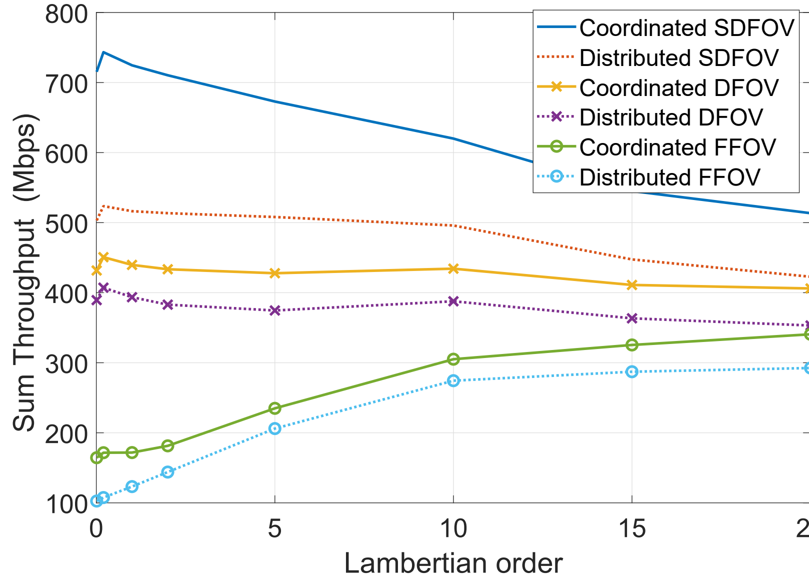

Figure 6·6: Sum Throughput of Coordinated vs. Distributed for Different Coverage Patterns.

to maintain illuminance levels.

6.5.3 System Fairness

In terms of minimum individual throughput, the receivers still attain their rank in terms of performance as shown in Fig. 6·7. It is notable that the FFOV receiver does not outperform the greedy association performance of the DFOV receiver. This relationship is maintained as well between the DFOV receiver and the SDFOV receiver. This is due to the FFOV receiver being a strict special case of the DFOV receiver; a lower bound. Likewise the DFOV receiver is a lower bound on the performance of the SDFOV receiver.

Another important result here is that jointly optimizing the Lambertian order for max-min received power and illuminance can enhance the max-min fairness of a system. This optimization result is not normally attained in a multi-user scenario. However when the right receiver is employed, this can change. In this design, the optimal m is 0.3 for highest minimum power received and standard illuminance probability. FFOV receivers do not

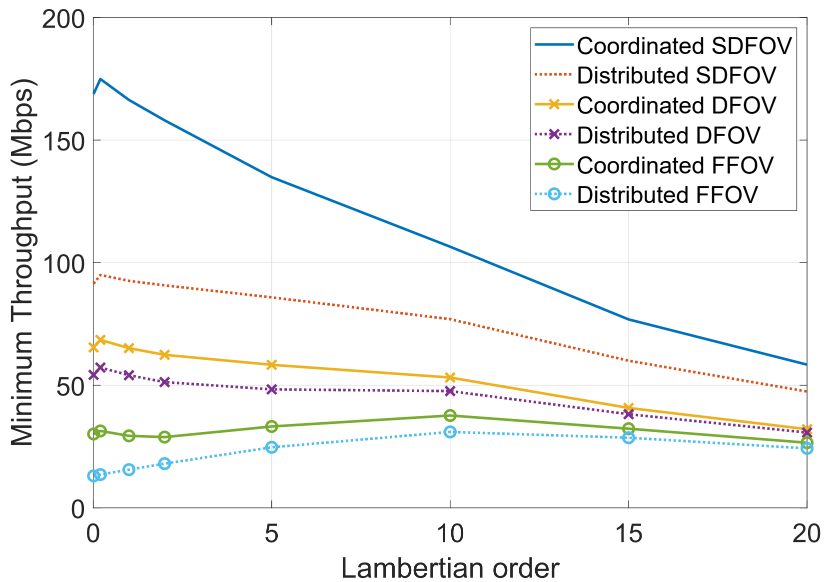

Figure 6·7: Fairness of Coordinated vs. Distributed for Different Coverage Patterns.

attain the optimal m simply because the interference effect dominates. In our analysis $m = 10$ gives the best performance for the FFOV minimum rate. However, the SDFOV and DFOV receivers have the ability to mitigate interference much better which enhances their ability to attain best fairness results at the optimal m. This is mainly guaranteed for the SDFOV receiver which completely isolates interference.

Analyzing the results, we see that the distributed and coordinated performance for both the FFOV and the DFOV receivers in this setup are closer than their counterpart performance for the SDFOV receiver. The greedy association for the SDFOV receiver substantially fails to meet the coordinated system performance which confirms that the greedy approach does not uncover the full potential of this receiver.

We investigate heuristic approaches to allow the controller to use reduced information about the receivers and still maintain a performance better than the greedy association method in Sections 6.6.1 and 6.6.2.

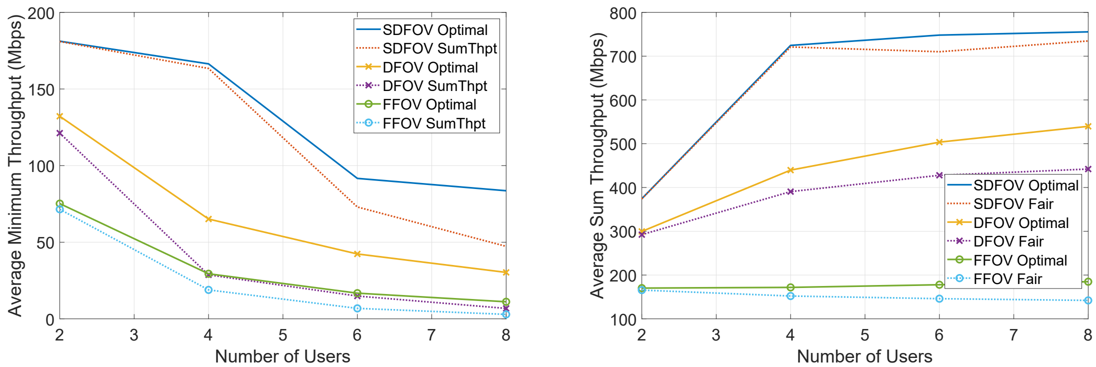

(a) **(b)**

Figure 6·8: Sum Throughput Results: (a) Fairness of Sum Throughput Optimal Mode; (b) Sum Throughput of Fairness Optimal Mode.

6.5.4 Fairness vs. Sum Throughput Tradeoff

Here we discuss the effects of targeting fairness on the system sum throughput and vice versa. Fig. 6·8a shows the system average minimum throughput for a coordinated system that optimizes sum throughput plotted for different number of users. The results for all receivers start to diverge from each other as soon as four users are in the system. However, Fig. 6·8b shows the system average total throughput of a coordinated system that optimizes fairness as defined in Section 6.2. In this figure the curves diverge at a slower rate with the worst case being the DFOV in terms of divergence away from the optimal, but the other two receivers show that maximizing fairness, specially using either SDFOV or FFOV, shows a promising total system throughput as well. Results are plotted for $m = 1$.

6.5.5 Transmitter Utilization Performance

Transmitter utilization is an important metric to help understand if the system is balanced in terms of resource sharing and can help a designer understand where the system can reach its limit in terms of user access. The results we show have been averaged over $10,000$ trials that fully covered the room and different device orientation uniformly to provide sound

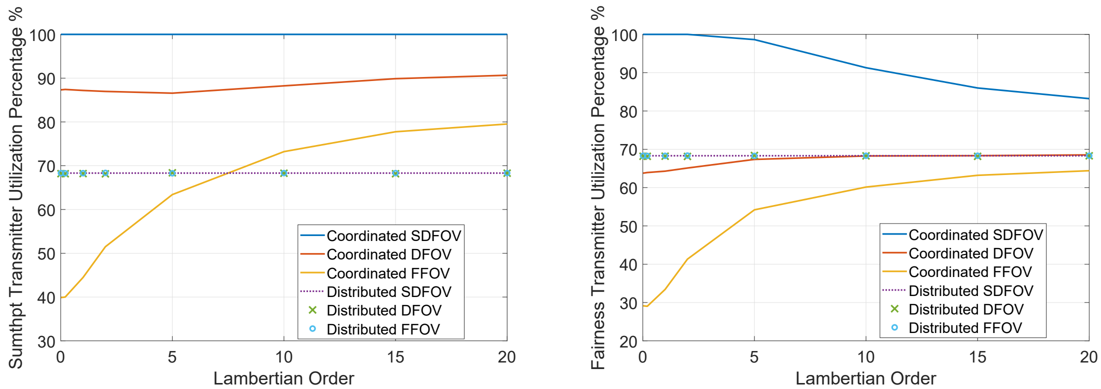

(a) **(b)**

Figure 6·9: Throughput vs. Fairness Transmitter Utilization Results: (a) Transmitter Utilization Percentage in Sum Throughput Optimal System; (b) Transmitter Utilization Percentage in Fairness Optimal System.

statistical conclusions.

Fig. 6·9a shows the average transmitter utilization percentage of the sum throughput optimizing coordinated system for different room coverage plotted along with the results of the distributed system. This figure also tells us information about the system load balancing for each receiver employed. The SDFOV receiver utilizes all transmitters (one Tx per each Rx) to achieve best sum throughput and also gives best load balancing performance. Second in performance is the DFOV receiver which utilizes almost 90% of the receivers at all Lambertian orders. Its inability to steer to a transmitter causes the difference from the SDFOV receiver. As for FFOV utilization, it is highly dependent on the Lambertian order. This is mainly due to the presence of high interference in the lower Lambertian orders which takes away its ability to freely choose transmitters. Finally, the distributed system shows similar transmitter utilization percentages for all receivers and all Lambertian orders around 68% of transmitters are used on average.

Fig. 6·9b shows these statistics for a coordinated system optimizing fairness instead. In this case all the receivers show variable performance with different Lambertian orders. The SDFOV receiver is able to achieve best load balancing results at lower Lambertians

Table 6.2: Hybrid Simulation Parameters

Parameter	Parameter Description	Value
Room Size	W×L×H	4×4×3 m^3
B_{VLC}	Bandwidth	5×10^7 Hz
A	Receiver area	785×10^{-9} m^2
Δ_x	Spacings between Txs in x-axis	1 m
Δ_y	Spacings between Txs in y-axis	1 m
P_{max}	Maximum Transmitter power	4 W
$w \times l$	T_x Element grid width × length	4 × 4
R	Responsivity	28 A/W
V	Vertical height between Tx and Rx	1.96 m
γ	Desired illuminance probabiliy	0.4
i_d^2	Dark current noise	68×10^{-20} A^2
P_{txDC}	Noise DC power	0.0022 V
No_{WiFi}	Noise power spectral density	-174 dBm
P_{WiFi}	Transmitted RF power	27dBm
B_{RF}	RF WiFi Bandwidth	20 Mhz
d_h	Head diameter men/women	18/17.5 cm
d_b	Body diameter men/women	41/36 cm
v_l	viewing distance	36 cm
d_h	Head diameter men/women	18/17.5 cm
l_h	Head and neck length men/women	31.2/29.8cm
l_{bd}	Distance between device and body	20 cm

but higher ones give less flexibility for the minimum throughput user and so load balancing is sacrificed. The same happens to DFOV receivers and the FFOV mostly shows the same performance. Overall the load balancing results are better in the sum throughput optimizing scheme, seen in Fig. 6·9a. This is because the scheme tends to be greedy, by allocating the poorest signal to a transmitter that balances the load instead of a transmitter that helps the minimum throughput user. This does not happen in the max-min allocation and so users may have to share transmitters more often which causes less load balancing.

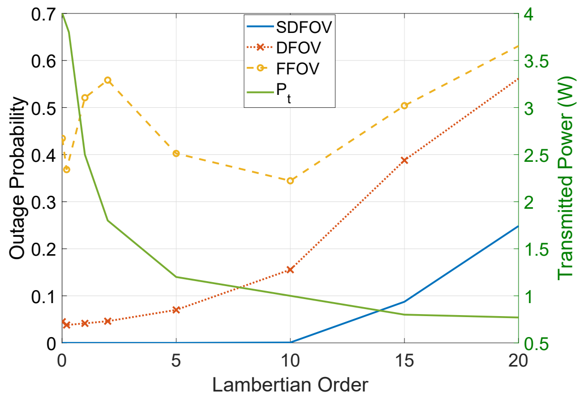

(a)

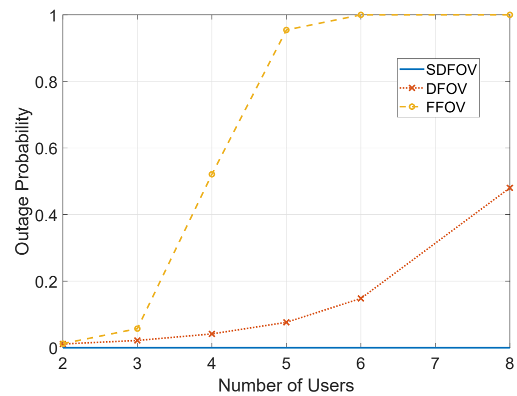

(b)

Figure 6·10: Outage Probability Results: (a) Outage Probability for 4 Users at Different Lambertian Orders; (b) Outage Probabilty for $m = 1$.

6.5.6 Outage Probability

We define outage as the system not meeting a required throughput at a certain user device. Once a user throughput is less than target throughput T_{out}, this user is declared in outage $P_{Outage} = P\{T_u^{(j)} < T_{out}\}$. We set T_{out} to 30 Mbps and evaluate how the receivers perform at different Lambertian orders as in Fig. 6·10a and at a fixed Lambertian order $m = 1$ for different number of users, Fig. 6·10b.

Fig. 6·10a shows that the SDFOV receiver outperforms the other two receivers but generally deteriorates at large Lambertians due to the lower power transmitted for maintaining acceptable illuminance (also plotted in the figure). The DFOV receiver has the lowest outage probability at the optimal m obtained for the system and the FFOV receiver has worst performance. FFOV has a variable performance when plotted against the Lambertian order; first it starts off in a high interference-high transmit power region ($0.01 < m \leq 0.3$) and so P_{out} is low, second it enters a region of high interference-low transmit power ($0.3 < m \leq 2$) which in turn causes P_{out} to go up, then a low interference-lower transmit power region ($2 < m \leq 10$) and in this case we observe the lowest P_{out}, finally the last region ($m > 10$) has the least transmit power coupled with the effect of high Lambertian orders on the channel gain and so P_{out} continues to grow. Fig. 6·10b shows the outage probability at a fixed Lambertian order $m = 1$ for 2 to 8 users in the system. We notice the same trends and ordering of the receivers with SDFOV outperforming the other two receivers, showing no outage at that m and FFOV outage growing fastly with the increase in number of users.

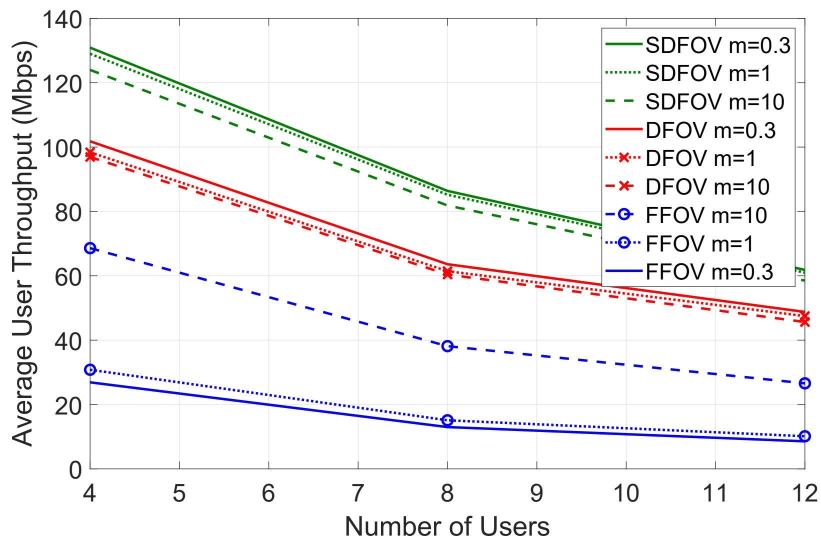

Figure 6·11: Distributed System Average Rate at Different Lambertian Orders with Increased User Count.

In Fig. 6·11 we show a result related to the distributed system that confirms the relationships between m and average system rate for each receiver. The figure shows the performance of the greedy association for different numbers of users. It also shows the consistency of the performance of each receiver with increasing the number of users in the system. The FFOV receiver shows variable performance with Lambertian orders. In this case better performance with $m = 10$ because of the reduced interference in the system.

6.5.7 Angle Sensitivity

In a practical setup, it is conceivable that attaining an exact FOV indicated by the optimization might not be possible due to the limits of FOV actuator precision. We tackle this problem for a single user in (Abdalla et al., 2019a, Fig. 6), explained in Section 3.4, showing that inaccurate FOV precision, within less than 2° difference, may cause up to 1.3 dB losses in the signal quality. However, we also mention that this can be adverted as long as the practical FOV does not fall lower than the optimal value and is either equal to or slightly larger than the optimal value. In this setup though one must take precaution in going too high in FOV increase because this may cause a reduction in performance due to allowing more interfering elements into view.

6.6 Algorithm and Heuristic Performance

Here we consider heuristic approaches for the optimization problems in eq. (6.5) and eq. (6.6) for the SDFOV receiver as well as a fairness heuristic for the DFOV receiver.

6.6.1 SDFOV Heuristic Approach for Fairness

Instead of identifying the exact location of the receiver, the heuristic we propose settles for less information at the controller. We disregard the redundant terms in eq. (2.2), keeping only the distance between the transmitter and the receiver and the angle of emittance. Both pieces of information are expected to be available on the transmit side without the need for feedback from the receiver (reducing overhead). Then the MINLP problem in eq. (6.5) becomes decoupled into the binary linear program, defined next in eq. (6.7), for user association and then FOV optimization can be done at the receiver. Then the controller solves:

$$\begin{aligned}
\max_{\substack{x_{uj},\\ j=1,\dots,N,\\ u=1,\dots,M}} \quad & \sum_j \sum_u \frac{x_{uj} r_{uj}}{\sum_k r_{kj}} \\
\text{s.t.} \quad & x_{uj} \in \{0,1\} \quad \forall u, j \\
& \sum_j x_{uj} = 1 \quad \forall u \\
& \left\lfloor \frac{M}{N} \right\rfloor \le \sum_u x_{uj} \le \left\lceil \frac{M}{N} \right\rceil \quad \forall j
\end{aligned} \tag{6.7}$$

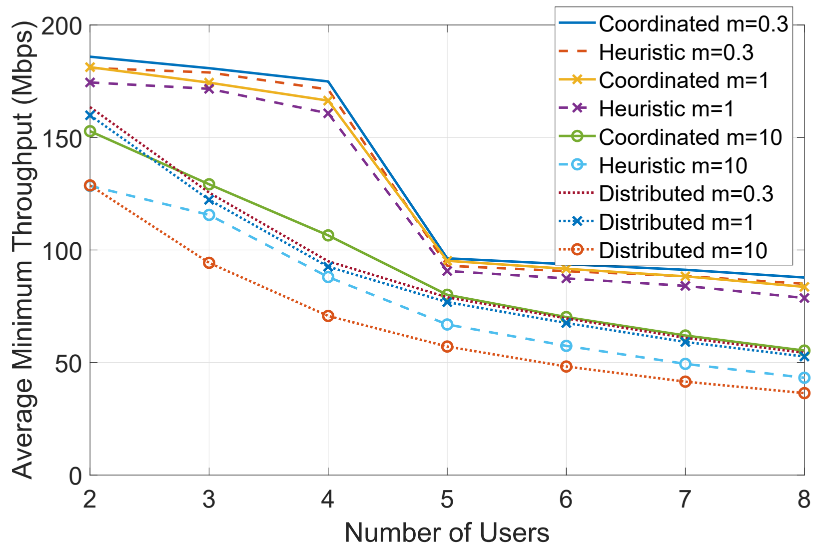

Figure 6·12: SDFOV Fairness Heuristic Approach, Optimal and Distributed Solutions.

where $r_{uj} = \log(1 + \frac{\cos^m(\phi_{uj})}{d_{uj}^2})$ is a metric concerning receiver u and AP j. The denominator introduces a penalty to reduce the number of receivers connected to the same transmitter. It resembles the sum of number of users from the original problem but it only sums their partial rates if they were connected to the same AP. In this way using the same AP for several users is reduced, load balancing is enhanced and the problem is now linear in the variable x_{uj} instead of the non linear original. This problem encapsulates both the user association among APs as well as system AP load balancing.

The last constraint helps spread the receivers across the transmitters to allow better fairness results and higher minimum throughput per user. This constraint is removed in the case of large Lambertian orders ($m > 5$) because with smaller transmitter semi-angles, it will prove non-beneficial to try to constrain a certain number of users on the transmitters because there is no longer a guarantee that any transmitter can provide signal everywhere.

We solve this problem using `intlinprog tool` (Copyright 2013-2019 The MathWorks, Inc.). The results for this heuristic show near optimal performance in smaller Lambertian scenarios and more overlap (i.e., higher interference scenarios). Performance for larger Lambertian orders is not as close; however it still outperforms the greedy approach association and in this scenario most system results show better performance at lower Lambertian orders. Fig. 6·12 shows the average minimum throughput performance of the heuristic and compares it with the coordinated and distributed approaches for each of the proposed receivers. This is performed for three Lambertian orders $0.3, 1, 10$ to show the extremes in performance. The heuristic shows near optimal performance in the lower Lambertian orders and starts to diverge when $m = 10$ but it still performs at or above the performance of the distributed method. This figure is plotted for $N = 4$ and M in the range of 2 to 8 receivers.

6.6.2 SDFOV Heuristic Approach for Sumrate

Here we seek to find the association that leads to best system sum throughput in another attempt to reduce the overhead at the controller. We introduce a weighted binary linear program that only needs the distances between the transmitter and the receiver. The program is defined below:

$$\begin{aligned}
\max_{\substack{x_{uj},\\ j=1,\dots,N,\\ u=1,\dots,M}} \quad & \sum_u \sum_j x_{uj} w_{uj} r^*_{uj} \\
\text{s.t.} \quad & x_{uj} \in \{0,1\} \quad \forall u, j \\
& \sum_j x_{uj} = 1 \quad \forall u \\
& \left\lfloor \frac{M}{N} \right\rfloor \le \sum_u x_{uj} \le \left\lceil \frac{M}{N} \right\rceil \quad \forall j
\end{aligned} \tag{6.8}$$

where $r^*_{uj} = \log(1 + \frac{1}{d^2_{uj}})$. $w_{uj} = 1$ for small Lambertian orders and $w_{uj} = \frac{1}{\sum_k r^*_{kj}}$ for $m > 5$.

We also solve this problem using `intlinprog`. The results for this heuristic are very promising as shown in Fig. 6·13. The data indicate very close performance to the coordinated system at small Lambertian orders. This is due to the SDFOV receiver's ability to eliminate the interference and so the problem reduces to user association according to

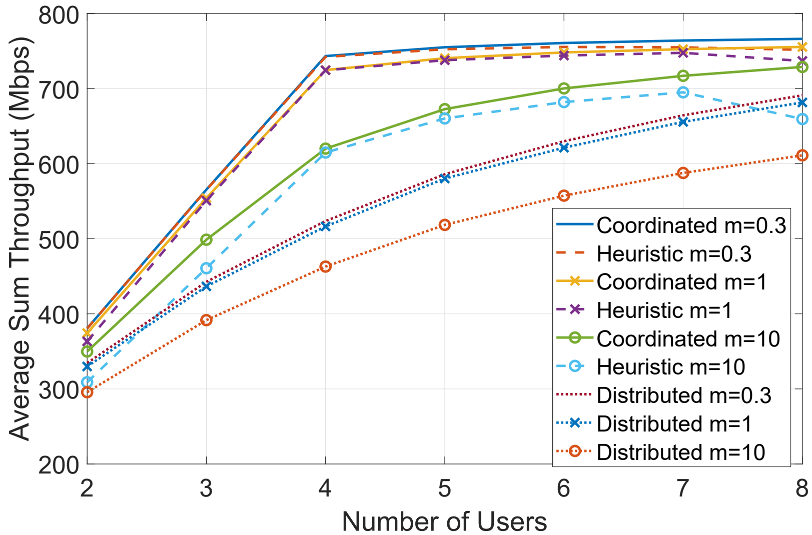

Figure 6·13: SDFOV Sum Throughput Heuristic Approach, Optimal and Distributed Solutions.

SNR and FOV optimization without interference. The results degrade with larger Lambertian orders but still outperform the greedy approach. The results plotted are for $N = 4$ and receiver count M between 2 and 8 receivers.

6.6.3 DFOV Fairness Heuristic

Here we focus on the fairness problem defined in eq. (6.5). It has a computational complexity on the order of $O(MN^M)$ which cannot be solved in polynomial time and quickly grows in the number of users and transmitters. The problem is tightly coupled to the variables. Trying to associate the users without adjusting what the receiver sees and vice versa gives sub-optimal solutions.

However, due to the directionality of the optical medium, we can reduce the complexity of the optimal problem to become on the order of $O(M2^M)$ which still grows exponentially but at a slower rate. We also show that with larger number of receivers M the problem grows even closer to the optimal solution. The reason behind this is shown in Fig. 6·2. The presence of only two receivers in the room gives more free transmitters to choose from and

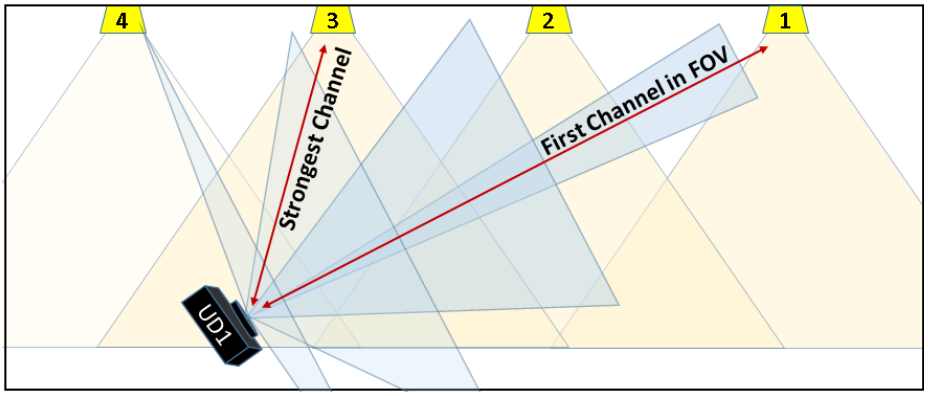

Figure 6·14: Difference Between Strongest Channel and First Channel in FOV.

turn ’off’ but with the increase in number of receivers, the likelihood that more transmitters are ’on’ grows. If (Fig. 6·2) transmitter 2 is ’on’ due to the presence of more receivers, then the receivers UD1 and UD2 would need to connect to transmitter 2 because otherwise it would cause the highest interference on their communications.

Closest Channel vs Strongest channel

A combination of system variables triggers the decision of best user-AP association. The receiver location, orientation, transmitter coverage and user density have key roles. In Fig. 6·14 we show two different definitions, the first channel seen by a receiver FOV as opposed to the stronger channel relative to that receiver. To clarify how we get the best channel in variable FOV scenarios; the receiver scans different FOVs to get the best channel. If the FOV is fixed at 90° when searching for the best channel then this gives the worst solution on average. This is because this methodology takes away the channel isolation capability and interference isolation. The association based on it is misleading.

The best solution in regards to fairness is not always connecting to the strongest channel. In fact if two receiver were closely located under Tx2 from Fig. 6·2 then as we showed in the previous example, they are better off connecting to other transmitters.

Through our analysis we have uncovered that for best fairness associations given the

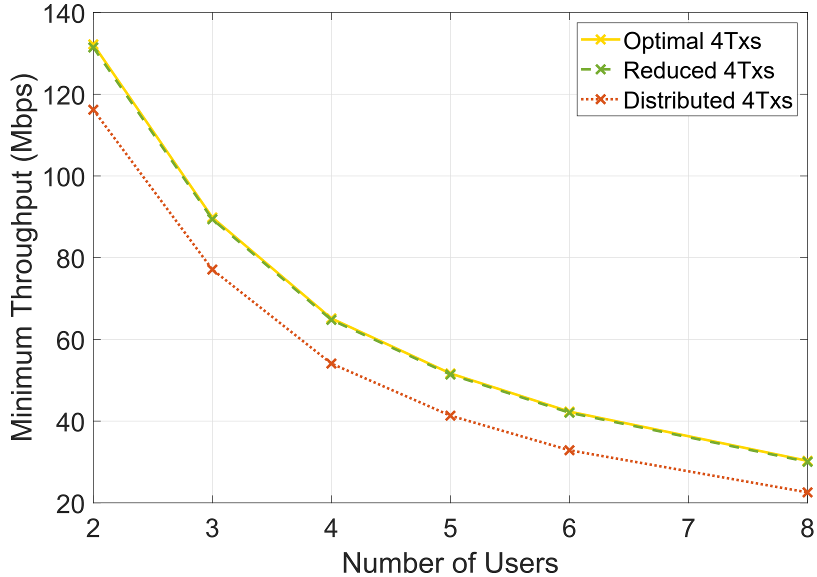

Figure 6·15: Performance of Reduced Complexity in Four Transmitters Scenario.

system assumptions, the two closest channels (channels with smaller incidence angles) give better performance on average than the two strongest channels (depicted in Fig. 6·14). This is mainly because the first few channels seen by the FOV give the best possibility of complete isolation from other interferers. Also, narrow FOV allows for higher signal quality and less noise and interference (discussed in Chapter 3). The other advantage in terms of overhead is that scanning different FOVs for the best channel strength might take longer than only finding the first two transmitters in sight. One should note that, on some occasions the strongest channel is also the first in sight.

We test this observation in a room with four transmitters (Fig. 6·15). Here we plot the average minimum user throughput with increasing number of users in the optimal coordinated system, the reduced method, and a distributed system that picks the best channel. Here the worst accuracy is 99%. In Fig. 6·16 we assume 6 transmitters (with the same inter-spacings). In this figure we plot the optimal minimum user throughput along with the reduced method when the first three, two and only one channels are used for association,

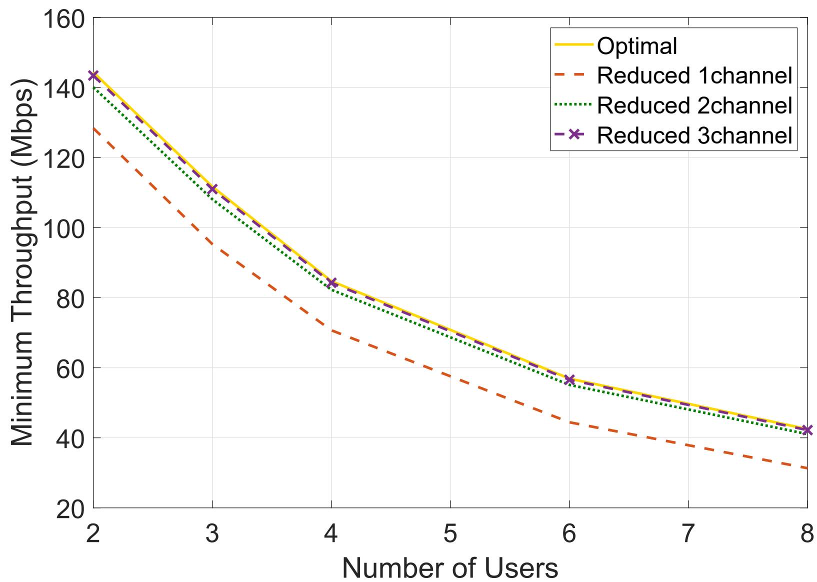

Figure 6·16: Performance of Reduced Complexity in 6 Transmitters Scenario.

the worst accuracy is 97% at complexity $O(M2^M)$ instead of $O(M6^M)$. It is also noted that if only one channel information is available then the strongest channel provides marginally better average results).

The worst accuracy is at the lowest number of receivers. The more receivers there are in the room, the better the accuracy. Based on this observation we plotted the worst case of both four and six transmitters along with nine in Fig. 6·17 to show the accuracy of the worst case compared in growing transmitter number. We did not add more than nine transmitters because we assume 1 m separation in the transmitter grid and any more would be physically impractical. This reduction is even more accurate when transmitters are placed in a line (as opposed to a grid placement). Also, accuracy increases if the separation between the APs is greater than 1 m. We conclude that this analysis approach introduces a novel association method based on device orientation.

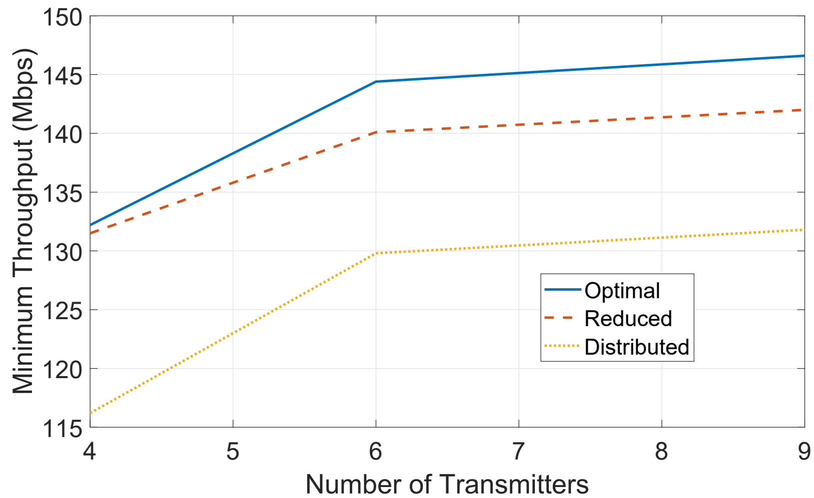

Figure 6·17: Reduced Complexity Performance with Growing N at Worst Case Two Receivers.

6.7 Line of Sight Blockage Effects

Channel blockage can be characterized by three factors discussed in (Wu and Haas, 2017): occurrence rate, occupation rate and blockage degree. Occurrence rate defines the presence of channel blockages per unit time, modeled here as Poisson arrivals with arrival rate λ_h. Occupation rate defines the length of time the blockage remains in place. In our model, we assume once the blockage is present it persists throughout the random trial. The unit time is the single random trial time. Finally, the blockage degree is a fraction between 0 and 1 describing how much of the signal gets blocked, with 0 meaning no blockage and 1 meaning full blockage. Most models assume it to be either 0 or 1, for simplicity, our model allows it to be non binary due to the non-point-source assumption. This allows for more practical results.

In our model we consider the blockage effect of user 1) self blockage as well as 2) randomly placed blockers (humans) in the room. Users and blockers are assumed to be seated and using their devices at the working surface. We assume that the difference between all users sitting or all standing is negligible. A mix between standing and sitting constitutes

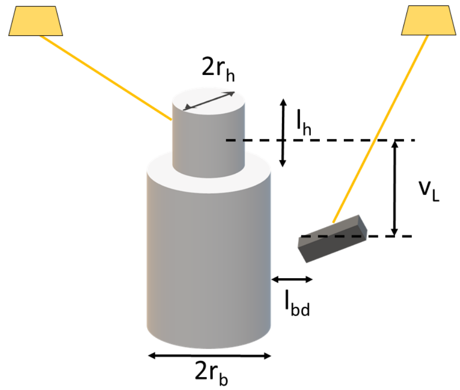

Figure 6·18: Approximate Human Holding Smart Phone.

a different model not studied in our work. We show LOS blockage effects on the average performance of the three receivers introduced in Sections 3.2, 3.3 and 3.4.

The blocker we model is an approximation of a typical person, Fig. 6·18. The blocker is modeled as two cylinders on top of each other, one represents the head with radius r_h and the other represents the body trunk r_b. Variables are picked according to the average human head and neck width and length as well as the average human shoulder width respectively. Body size varies according to men and women according to the medical studies/statistics in (Wikipedia, 2020a; Fryar et al., 2018). Therefore we give a probability of 0.5 for each and model accordingly. As for the distance between the user and the phone, viewing distance v_L, we use numbers provided in the optometry study in (Bababekova et al., 2011). All parameters are in Table 6.2.

We analyze a *passive system* that gets affected by blockage and has no feedback about its whereabouts, as well as an *active system* that gets either feedback information from the receivers or is able to detect human presence and associate the users accordingly. In Fig. 6·19a we show the average user throughput performances when no blockage and self-blockage are assumed in both the active and passive systems in a coordinated scheme for all three receiver types and two different emission patterns when four users are in the room. Performance of the minimum user throughput under the same conditions is plotted in Fig.

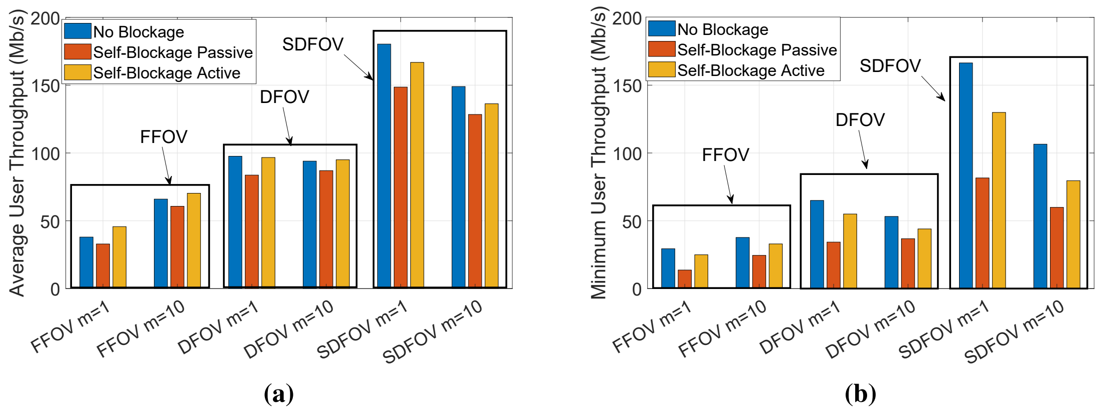

Figure 6·19: Self-Blockage Impact on Average and Minimum Throughput. (a) Average Throughput Under Different Blockage Systems; (b) Minimum Throughput Under Different Blockage Systems.

6·19b.

Fig. 6·19a and Fig. 6·19b entail a lot of interesting results. We observe that: 1) Self-blockage has an apparent effect on throughput performance, however each receiver sees a different grade of impact. The SDFOV is the most affected receiver specifically in the minimum throughput results. The active system helps in enhancing the performance but not as much as in the other receivers. But even in the worst performance case, SDFOV does better on average than the other two receivers. 2) The FFOV receiver performs better in smaller beam width due to decreased interference. We also note that in the active system which is able to correct the associations based on the presence of blockage, the average user throughput from the FFOV receiver is enhanced even compared to the blockage-free case. This is because blockages potentially remove interference sources from its view. 3) The DFOV is well balanced, on average the active system is able to provide throughput enhancements.

So far we discussed the results of no-blockage versus self-blockage. In Fig. 6·20 and Fig. 6·21 we show the effect of self-blockage in the presence of random human blockers in the room. Their arrival is modeled as poisson with rate λ_h. When $\lambda_h = 0$ we revert back to

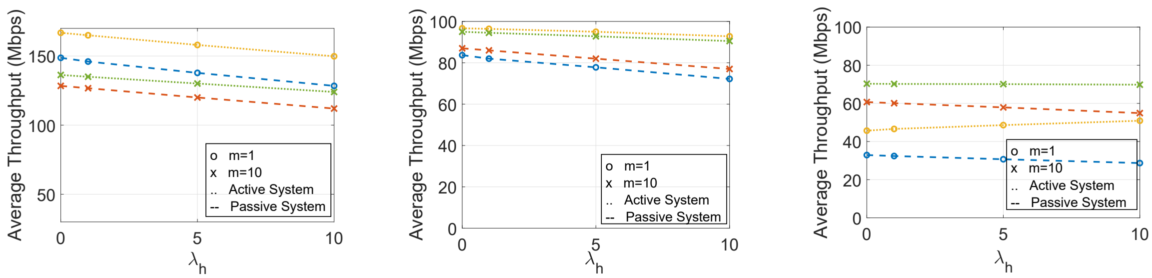

(a) **(b)** **(c)**

Figure 6·20: Active and Passive Blockage Average User Throughput Performance for All Receivers at Different m and λ_h. (a) SDFOV; (b) DFOV; (c) FFOV.

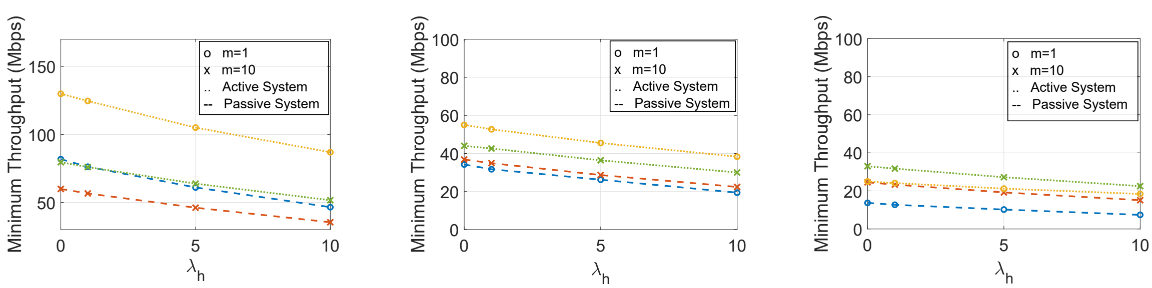

(a) **(b)** **(c)**

Figure 6·21: Active and Passive Blockage Minimum User Throughput Performance for All Receivers at Different m and λ_h. (a) SDFOV; (b) DFOV; (c) FFOV.

the self-blockage-only case. The results plotted in Fig. 6·20 show the effect of shadowing on the receivers' average throughput for two different lambertian orders. We also show the effect of active and passive systems. Fig. 6·21 shows the effects on minimum throughput.

Our general observations from Figs. 6·20 and 6·21 are: 1) The effect blockage has on minimum throughput is much worse. It causes around 40-50% drops in throughput, depending on the receiver used. 2) Higher Lambertian orders show less throughput reduction due to blockages in comparison to the wider beam case but this is not an indication on the actual performance numbers. 3) DFOV receivers throughout our analysis have better performance with wider beam emissions however only in blockage scenarios in the passive systems, the smaller beam emission gives marginally better results.

6.8 Chapter Conclusions

After studying this optimized transmit-receive analysis, we can summarize the accomplishments of this chapter to be:

- Studying the user association and FOV optimization in a multi-user indoor OWC system under two different FOV receivers; namely, a dynamic FOV (DFOV) receiver and a steerable dynamic FOV (SDFOV) receiver. Then comparing the performance to a baseline fixed FOV receiver (FFOV).

- Comparing the performance of different system architectures in terms of multiple system metrics.

- Comparing the performance of the proposed system under different coverage patterns created through changing the transmitter beam width while maximizing the minimum power received as well as the probability of maintaining illuminance at the standard range.

- Proposing heuristics for the SDFOV receiver as well as proposing a novel orientation based association method for DFOV fairness performance.

- Analyzing the effect of self-blocking as well as randomly located human blockers within the room showing their effect on minimum as well as average user throughput for different Lambertian orders and different system blocking responses (active versus passive).

- Comparing the minimum user throughput as well as the aggregate sum throughput of a dynamic FOV VLC-only system to a hybrid RF/VLC system.

As outcomes of the novel analysis described above, we find the following key results:

- SDFOV outperforms DFOV by up to 2.6x in average minimum throughput gain (5.6x gain over FFOV); DFOV receivers achieve up to 2.2x gain over FFOV receivers in the evaluated configuration.

- The distributed greedy system may reach a lower performance up to 46% less on average (in terms of minimum user throughput) than the coordinated system for SDFOV, 16% for DFOV and 57% for FFOV at a computational complexity reduction from $O(MN^M)$ to $O(MN)$.

- The heuristic we propose for DFOV fairness reduces the optimal search space down from $O(MN^M)$ to $O(M2^M)$ with $97-99\%$ accuracy.

All these results point us towards the anticipated analysis of integrating this successful system into a hybrid RF/VLC setup to see how the hybrid performance will be affected. This hybrid setup is studied in Chapter 8.

Chapter 7

Outage Analysis and AP Deployment

In this chapter we focus on analyzing the outage probability of the VLC system and do so using two different methods. First method: we propose a probabilistic model characterizing where to deploy indoor VLC APs by tying outage to handover delay and user velocity. Then we provide a closed form upper bound on outage probability that guarantees outage-free regions for devices attempting handover. The model is used to demonstrate the impact of different VLC AP cell separations and to show how the system parameters impact outage probability. Second method: we derive an exact closed form outage probability for SDFOV receivers in a multi-user environment where users equally share the system resources.

7.1 Single User: Outage Probability and AP placement for Seamless Connectivity

When considering mobility of devices in VLC deployment, a narrow beam VLC AP becomes a liability as the user can quickly exit from the coverage area causing a loss of connectivity. But with multiple overlapping VLC APs we have an opportunity to handover a user connection to a neighboring AP in order to maintain continuous or "seamless" connectivity. How to design the layout of overhead dual-use APs to meet the lighting and communications needs to mobile users across a wide, diverse indoor environment is an important question. We explore answering this question and propose a probabilistic model (Abdalla et al., 2019c) that characterizes where to deploy indoor VLC APs while considering the impact of handover delay and user velocity. We also provide a closed form upper

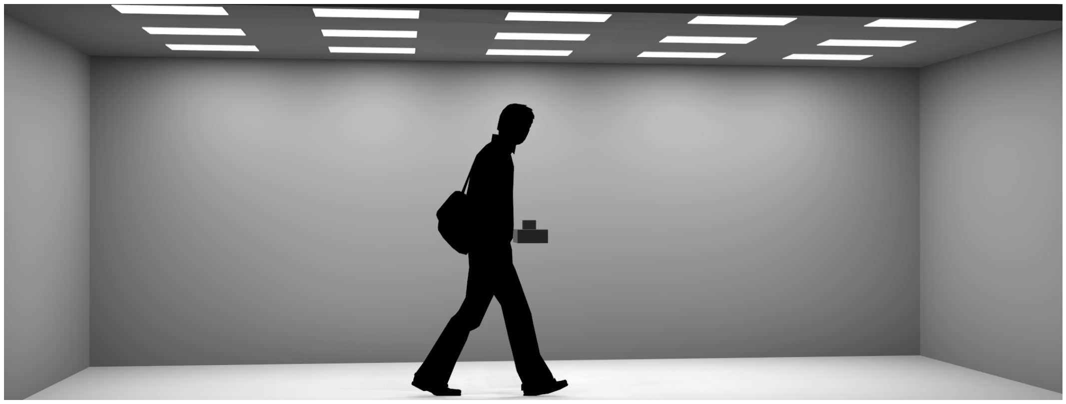

Figure 7·1: User Moving along a Dense Indoor VLC Network.

bound on outage probability that guarantees outage-free regions for devices attempting handover. Finally, we provide analysis and simulation under different scenarios.

Consider the scenario illustrated in Fig. 7·1. A mobile device requires handover from cell to cell as the user moves between cells. The simplest handover technique tracks RSS values. In RSS-based handover, once a stronger signal is detected in a different cell, handover is initiated. Robustness is improved with a variety of techniques including adding a delay in switching to achieve hysteresis to prevent a "ping-pong" effect at cell edges. This delays the handover until a difference between the two signal levels is met. Another source of handover delay in a VLC system, as illustrated in Fig. 3·2, is the handover decision time that arises from the variable receiver orientation and FOV. Both factors will impact the handover decision based on RSS alone. Lastly, occlusions (whether introduced by the user or the environment) will impact the reliability of the RSS interpretation. For our model, we define handover delay t_{HO} to account for both the handover decision time and the hysteresis delay.

The impact of factors that affect coverage probability of a VLC network inside an empty room, such as number of APs, room area and source height from the floor is studied in (Vavoulas et al., 2015). (Jian-Hui Liu and Zhang, 2014) investigate the communication and illumination coverage in VLC; their results show the relationship between coverage and LED arrangements (lattice versus hexagon structures), semi-angles at half-power and heights. In (Vegni and Little, 2012), the authors propose an approach to manage handover that provides cooperation and coordination between VLC terminals in two scenarios of overlapping versus non-overlapping sources to achieve seamless connectivity. However, the previously mentioned bodies of work do not study the room layout effect in terms of handover delay. In RF, there exists work that considers this. For example, (Emmelmann, 2005) analyzes handover delay and finds the minimal overlap between cells needed to achieve seamless handover. The unique contribution of our work is the design and analysis of VLC AP placement based on a probabilistic handover outage model intended to mitigate handover effects. We also show trade-offs with respect to user velocity, handover delay, light placement distances, and outage probability.

System Assumptions and Geometry: In this work, we assume all sources are the same and have the same height from the floor. This would cause their coverage range (as well as coverage radius, R) to be identical. In Fig. 7·2, we define S as the distance between the centers of the two light sources, which we are interested in optimizing and L which is the length of the midline J dividing the overlap region of the cells. In an omni-directional medium utilizing RSS-based handover, this line is theoretically where the handovers are triggered because crossing it in any direction switches users to the cell that has the stronger signal within that overlap region. However, in directional systems such as VLC, receiver orientation and FOV can change where your highest signal might come from (Fig. 9·13 highlights this effect). For the purpose of designing the room, we will consider an upward facing receiver scenario. Assume that the user crosses the line J at point m. Point m defines $l(m)$ which is the distance from the intersection of the two cells to the point m. Assuming that the user is equally likely to cross at any point on J, $l(m)$ is uniformly distributed with PDF/CDF respectively as follows:

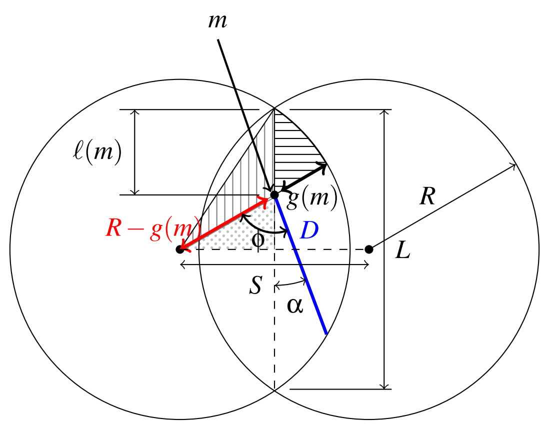

Figure 7·2: Two Overlapping VLC Cells

$$f_{l(m)}(k) = \frac{1}{L}, 0 < k < L, \qquad F_{l(m)}(k) = \int_0^k \frac{1}{L} dx = \frac{k}{L}.$$

The distance S impacts the size of the overlap region and controls L, the length of J. In our design, once the user crosses the midline, we assume he subsequently exits from the cell. The shortest path from the midline to the neighboring cell is $g(m)$. $g(m)$ can also be defined as the distance perpendicular to the exit arc traveled by the user within the overlap region starting at any point m on line J and ending at the tangential point at which he exits the primary cell he was connected to. D is the distance traveled by the user from point m and α is the angle that the user takes when moving out of m to exit the cell. α is uniform over π and independent of $\ell(m)$.

We employ geometric manipulations and deductions to reach the following relations which are important in our analysis:

- $L = \sqrt{4R^2 - S^2}$ which ties S to L, we can derive this from the right-angled triangle in Fig. 7·2 that consists of the vertically shaded and dotted triangles, where the hypotenuse is R and the two remaining sides are $\frac{L}{2}$ and $\frac{S}{2}$.
- $g(m) = R - \sqrt{\frac{S^2}{4} + (\frac{L}{2} - l(m))^2}$ which ties $g(m)$ to $l(m)$, this can be deduced from

the dotted right angle triangle Fig. 7·2, with hypotenuse $R - g(m)$ and the two sides $\frac{L}{2} - l(m)$ and $\frac{S}{2}$.

- $\phi = \alpha + \tan^{-1}\left(\frac{S}{L-2l(m)}\right)$.

- Employing the law of cosines (Wikipedia, 2020b), we get
  $R^2 = (R - g(m))^2 + D^2 - 2(R - g(m))Dcos(\phi)$.

Solving the last equation for D we get

$$D = (R - g(m))\left(cos(\phi) + \sqrt{cos^2(\phi) + \frac{g(m)(2R - g(m))}{(R - g(m))^2}}\right)$$

where we rejected the negative term since D is a distance.

Next we move on to derive an exact outage and an upper bound.

7.1.1 Exact Outage Probability

Given the model above, outage occurs when the user fails at achieving a seamless handover. This happens if the time it takes to establish the actual handover, t_{HO}, is greater than the time the user takes to cross the distance from line J to his current cell's exit arc. This is interpreted as losing the current connection before getting a chance to establish a new one with the cell in one's path. Let v_u be the user's velocity.

Finally, to get the outage probability, we consider the outage of our model as:

$$P_{outage} = P\left(t_{HO} > \frac{D}{v_u}\right) = P\left(D < t_{HO}v_u\right)$$

where the probability is taken w.r.t $\ell(m)$ and α.

We use simulations to compute the exact outage probability as a closed form solution is not immediately available but will be studied in a future work.

7.1.2 Upper Bound on Outage Probability

We get a closed form for an upper bound to the outage probability by designing our model for the worst case scenario, $g(m)$. At any point m, a user can cross to the exit arc using infinite possible paths. We define the minimum path as $g(m)$. By doing so we evaluate an upper bound for the outage probability, as the shorter distance imposes a tighter constraint on the handover time. If it can guaranteed for a certain m that there is no outage caused from traversing the minimum path generated at it ($g(m) > t_{HO}v_u$) then all paths greater than it at this point will not cause outages as well. We evaluate the upper bound on outage probability of our model to be:

$$P_{outage} < 1 - \sqrt{\frac{(R - t_{HO}v_u)^2 - \frac{S^2}{4}}{R^2 - \frac{S^2}{4}}}$$

Details of the proof are in Appendix A.1.

The derived upper bound captures the design trade-offs for dual-use VLC including light spacing. The closer the lights are together the more overlap exists and therefore there is less probability of outage; but this is also dependent on the speed of the user and the actual handover time. This model provides a guaranteed outage-free region and small regions where there could be possible outages, such as the region horizontally shaded in Fig. 7·2. Note that from the symmetry of the shape, another mirrored outage region occurs on the bottom of the arc. This region shows the area where you can possibly get paths shorter than $t_{HO}v_u$.

This approach designs for the worst case scenario; it is possible to guarantee not to cross a certain outage probability determined in advance. Using the upper bound formula derived one can deduce where to place the APs, by determining S, for a predefined tolerable outage probability. For example, if the two sources were at the maximum allowed separation distance which is $S = 2(R - t_{HO}v_u)$ in this model, this results in an upper bound of 1 on the outage probability. On the other hand, for the case where you allow the two sources to completely overlap, $S = 0$, the minimum outage probability becomes $\frac{t_{HO}v_u}{R}$ (not 0 as this is an upper bound).

The main differences between the exact outage and the upper bounds are: 1) The outage probability upper bound is derived in closed form and this bound gives the designer regions of guaranteed outage free zones. 2) The exact formula does not guarantee outage free regions.

We now provide some numerical examples for the upper bound outage model.

7.1.3 Outage Upper Bound Performance

For our simulations, we assume practical numbers for the parameters. We let the coverage radius $R = 1\ m$ and $v_u = 2\ m/sec$ which is an upper bound on the indoor user velocity. We note that there are several regimes for indoor mobility when there is overlapping coverage: (1) quasi-static slower users with low or intermittent velocity in which there is ample time to address handover, (2) faster users with very high velocity that are best supported by omni-directional media (RF), and (3) the intermediate ones which hope to exploit the availability of the VLC channels without handover to RF.

In Figs. 7·3 and 7·4, the user is assumed to be moving from cell 1 (left) to cell 2 (right). The dotted regions show the possible outage regions for two scenarios in which the lights are spaced at 0.5 m versus at 1 m while $t_{HO} = 0.2$ s and $t_{HO} = 0.1$ s respectively. It is clear that spacing the sources too far from each other strongly affects the outage probability but what also plays a vital role is the handover time t_{HO} where in Fig. 7·4 when it decreased to 0.1 s for the same S values as in Fig. 7·3, we realized much better results and the difference in outage probability was much closer than in Fig. 7·3, results are listed in Table 7.1. We are able to calculate the minimum outage probability for each of these scenarios; which are 0.4 for Fig. 7·3 and 0.2 for Fig. 7·4. This will change with user velocity as well. In these

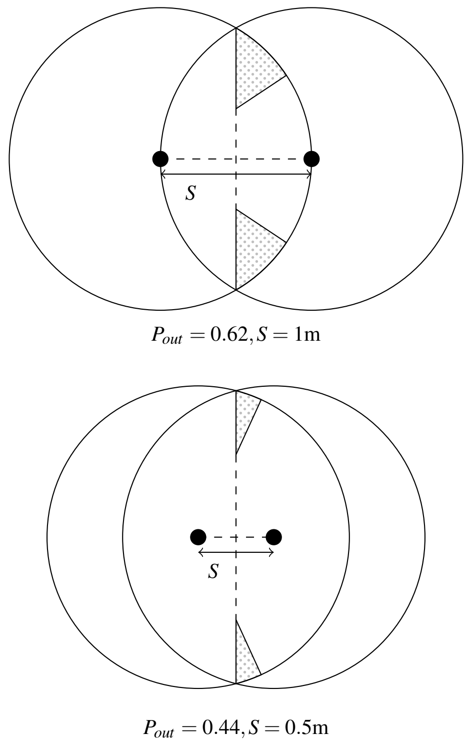

Figure 7·3: Possible outage regions at $t_{HO} = 0.2$ Sec for different S

Table 7.1: Upper Bound Numerical results

	At $t_{HO} = 0.2$ s	At $t_{HO} = 0.1$ s
S	0.5 m	0.5 m
P_{outage}	0.44	0.32
S	1 m	1 m
P_{outage}	0.68	0.37

cases we only show the worst case scenarios. One can also show improved performance with a source with a wider coverage region.

The key observation from these results is the importance of lighting placement with respect to user mobility and the resulting handover delays.

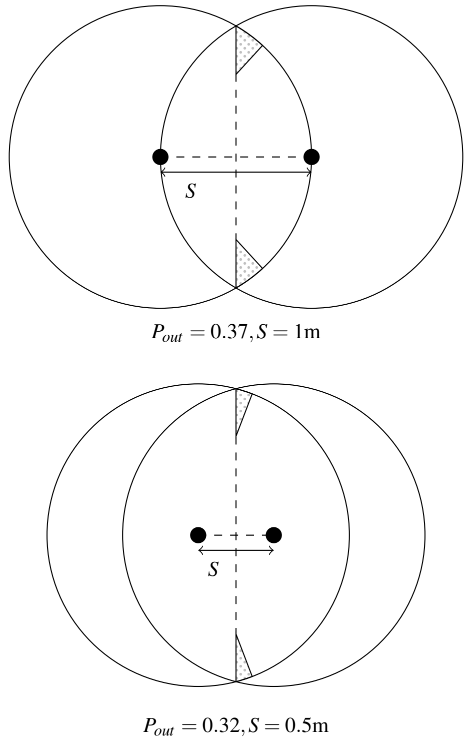

Figure 7·4: Possible outage regions at $t_{HO} = 0.1$ Sec for different S

7.1.4 Analysis of Trade-Offs

We discuss possible applications for the proposed model and show the results for both the exact and upper bound on the outage probability. This allows for a closer analysis of the trade-offs involved in the overall system.

Impact of Source Coverage Radius R on Outage Probability

Suppose a lighting system is constrained to use legacy wiring, i.e., the VLC fixtures are constrained to use pre-existing locations. We let $S = 1\ m$ and a user velocity of $v_u = 2\ m/s$. In this scenario it is possible to select the light sources to realize desired performance. Fig. 7·5a shows options of possible coverage radii R at the receiver plane. The results also show how performance is affected by different handover delays. Fig. 7·5a shows that with the increase in R while maintaining a low t_{HO}, we get better performance in terms of

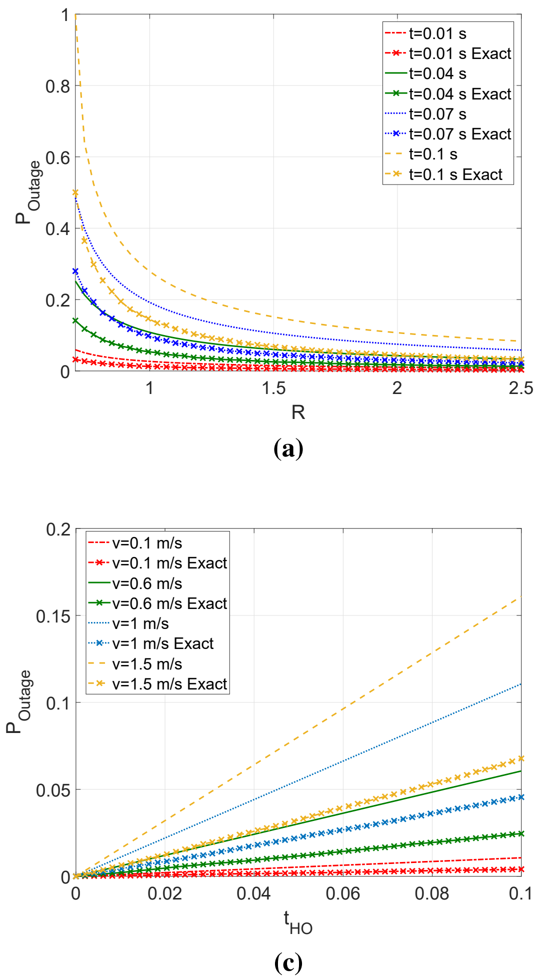

Figure 7·5: AP Placement Analysis: Impact of Source Coverage and Separation Distance on Outage Probability: (a) Source Coverage Effect for Fixed S and v_u; (b)Source Inter-Spacing Effect for Fixed R and v_u; (c) Handover Time Effect for Fixed R and S;(d) User Velocity Effect for Fixed R and S.

outage probability.

Impact of Source Separation Distance S on Outage Probability

The explored scenario here deals with having a fixed $R = 1\ m$, assuming $v_u = 2\ m/s$ and trying to find how to place the lights to achieve the tolerable outage probability. Fig. 7·5b shows the relationship among the parameters and the outage probability; by increasing S, the outage probability increases but when the handover time t_{HO} decreases, the performance quality increases.

Impact of Handover Time t_{HO} on Outage Probability

Room dimensions in this case are considered to be constrained. Here we assume that the sources are in place and we set out to find a bound on the performance of the system, allowing study of how to optimize the handover delay based on the required performance. Fig. 7·5c shows, for a fixed $R = 1\ m$ and $S = 0.5\ m$, how the handover delay and user velocity play an important role in deciding how the system will perform. Of course, the lower the handover time or the lower the user velocity, the lower the outage probability.

Impact of user velocity v_u on Outage Probability

This case follows from the case above ($R = 1\ m$ and $S = 0.5\ m$) and is plotted to show, in Fig. 7·5d, that the impact of user velocity is close to the impact of handover time, confirming that the lower the user velocity, the lower the outage probability.

Exact Versus Upper Bound Figures [7·5a - 7·5d] show that the upper bound is tight at lower handover times or lower velocities. The higher t_{HO} or v_u get, the more the bound becomes loose.

In the following section, we look at deriving the outage probability in a multiple user setup while employing SDFOV receivers.

7.2 Multiple Users: SDFOV Closed Form Outage Probability

Here we analyze the outage probability of a multi-user scenario specifically when SDFOV receivers are utilized. For this receiver, we take a different approach to derive a closed form for outage probability. We define the outage as the probability that a typical individual user throughput (from eq. (6.3)) falls below a target throughput T_{out}. $P_{Outage} = P(T < T_{out})$. Assuming that the number of users follows a homogeneous Poisson Point Process (PPP), the number of users connected to a VLC AP, N_{VLC}, can be modeled as a Poisson random variable with mean λ_t.

$$P(N_{VLC} = n) = \frac{\lambda_t^n e^{-\lambda_t}}{n!} \tag{7.1}$$

where $\lambda_t = \frac{\lambda_u}{L_v}$. The Poisson arrival of users per m^2 is modeled by λ_u and L_v is the number of VLC APs present per m^2. The VLC APs are modeled as non-point sources as well.

Fig. 7·6 shows the general VLC cell connectivity model where x marks the center of the transmitter, Δ_x is the distance between the centers. We derive the SDFOV receiver individual user outage where each user connects to the strongest channel. This causes each cell's association region to be the closest users in terms of Euclidean distance as Fig. 7·6b illustrates.

Lemma 1: The per user outage probability for an SDFOV device in a multi-cell VLC network with user density λ_u users per m^2 and equal resource division between the users

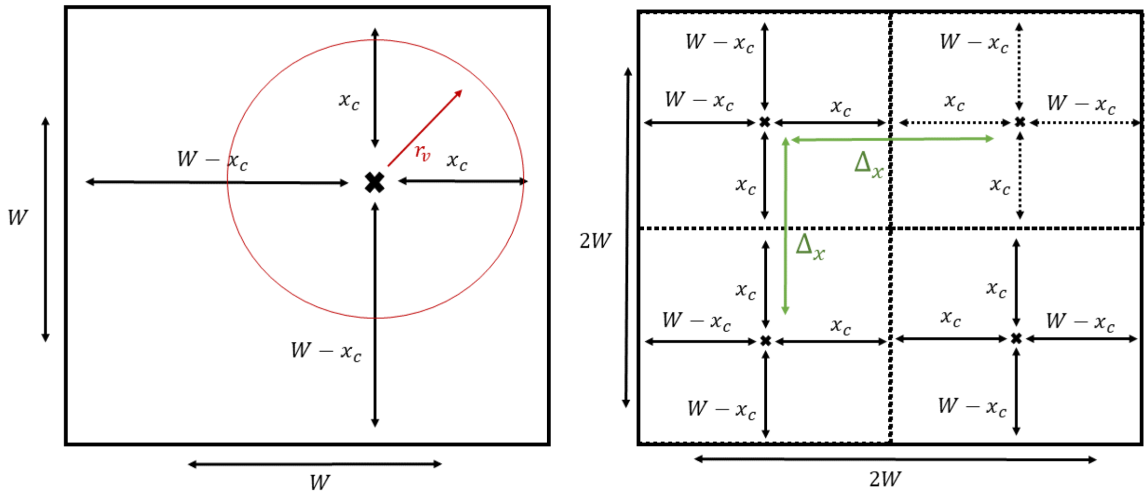

Figure 7·6: VLC Cell Model: (a) Generalized Symmetric Single Cell; (b) Simulated Scenario for 4 VLC APs.

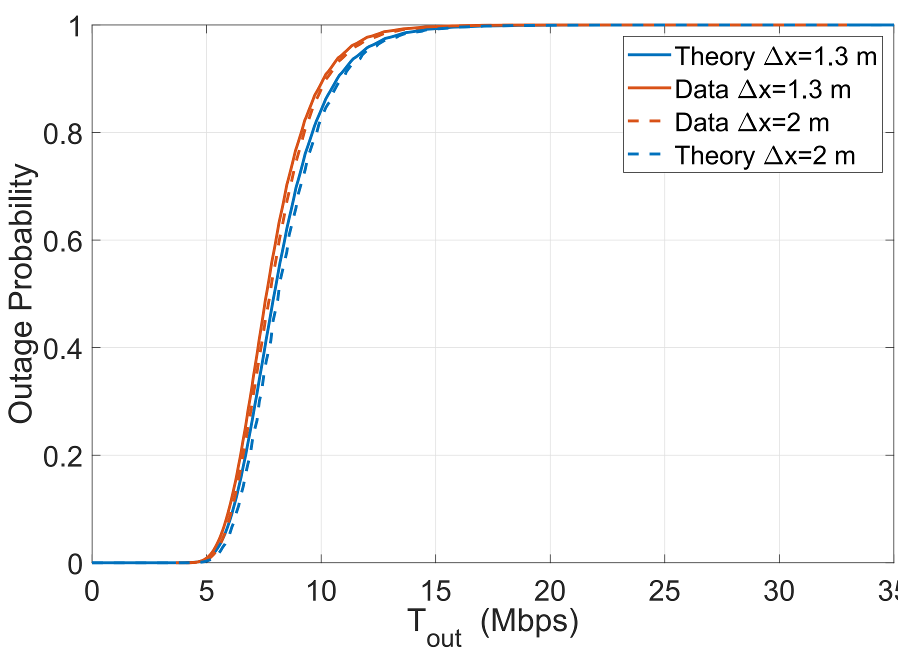

Figure 7·7: Individual User Outage Probability in VLC-Only System.

Table 7.2: VLC Outage Simulation Parameters

Parameter	Parameter Description	Value
Room Area	W×W	4×4 m^2
B_{VLC}	VLC Bandwidth	5×10^7 Hz
A	Receiver area	785×10^{-9} m^2
P_t	Transmitter power	2.5 W
$w \times l$	T_x Element grid width × length	4 × 4
R_r	Receiver Responsivity	28 A/W
V	Vertical height between Tx and Rx	1.96 m
L_v	VLC APs per m^2	0.25
σ_n^2	Noise variance	2.3×10^{-5}

connected within the same VLC AP is:

$$P_{outage-SDFOV} = \sum_{n=1}^{\infty} \left(1 - F_{r_v|N=n}\left(\sqrt{ \left(\frac{(m+1)AV^m}{2\pi} \sqrt{ \frac{R_r^2 P_t^2}{\sigma_n^2 (2^{\frac{2nT_{out}}{B_{VLC}}} - 1)} } \right)^{\frac{2}{m+2}} - V^2 } \right) \right) P(N_{VLC} = n) \quad (7.2)$$

where m is the lambertian order, A is the receiver area, R_r is the receiver responsivity, V is the vertical distance between the transmitter and the receiver and B_{VLC} is the VLC bandwidth. F_{r_v} is the CDF of the horizontal distance (r_v) from the VLC AP to the user. Details of the proof are available in Appendix A.2.

Fig. 7·7 shows the result of the simulated data at $\lambda_u = 6$ plotted against the theoretical formula derived in Lemma 1. Simulation parameters are in Table 7.2. Note that σ_n^2 may be considered constant due to the small FOV resolution when employing SDFOV receivers. We show the results of close (dense) APs, $\Delta_x = 1.3$ m, as well as centered VLC APs at $\Delta_x = 2$ m. The individual user outage probability is slightly reduced when the APs are further apart. We use this result later on in our hybrid setup.

7.3 Chapter Conclusion

In this chapter we focus on outage probability; first for a single user crossing between two VLC cells. Lighting requirements usually dictate providing a mix of broad light and direct, line-of-sight spot lighting, which are not ideal for VLC. Dual-use systems need to reconcile these requirements in overall system design and operation as both the lighting and user mobility are considered, especially when devices move through the lighting field. This prompted us to investigate the impact of device mobility in a dual-use system with a focus on data outage probability due to lighting design parameters. We develop a probabilistic model that provides an exact outage probability and derive a closed form upper bound on outage probability under the constraint of outage-free zones. The models are used to show how design parameters affect system performance and illustrate trade-offs for dual-use VLC systems and lighting designers.

Next, we derive an exact formulation of the outage probability of an indoor symmetric VLC setup where users equally share the system resources and SDFOV receivers are employed. The results show promise in the ability to design a system for a desired individual user throughput while taking many system parameters into consideration such as AP load.

Chapter 8

Hybrid RF/VLC

Building on the multi-user VLC system proposed in Chapter 6, here we study a hybrid RF/VLC system and analyze its performance. First we look into 1) integrating the VLC system, discussed previously, with a WiFi AP, 2) evaluating the performance of two load balancing algorithms focused on i) sum throughput and ii) minimum user throughput and 3) discussing their results and implications. Second we dive into deriving the outage probability of a hybrid RF/VLC system employing SDFOV receivers and show results for different user association methods.

8.1 Hybrid RF/VLC

In this section we combine our VLC system performance analysis with the integration of an RF component to yield a hybrid system. The configuration here includes the use of a WiFi AP located at the center of the set of VLC transmitters, see Fig. 6·4. Keeping RF congestion in mind, the way we design our system is to try to optimize the user association on the VLC network first then according to a design metric, i.e., fairness or throughput, we start to allocate the users who cannot be accommodated on the VLC to the RF network. Users migrate to RF only if they cannot be supported on any of the VLC APs in the VLC network. The goal in this analysis is to better understand the performance characteristics of such a hybrid model.

8.1.1 RF Indoor Channel Model

We consider a single WiFi AP. The WiFi channel gain at user u is given by:

$$g_u^{WiFi} = |h_u^{wifi}|^2 10^{\frac{-L(d_u)}{10}}$$

where h_u^{WiFi} is the channel transfer function whose magnitude is Rayleigh distributed. As for the log distance path loss $L(d_u)$, where d_u is the distance between the transmitter and receiver in meters, we follow the JTC indoor path loss model detailed in Section 2.2.1. In an office setup, $A_e = 38$ dB, $B_l = 30$ and $L_f(n) = 15 + 4(n-1)$ dB with $n = 0$.

The users equally share the single WiFi AP bandwidth B_{WiFi} and so do not interfere with each other. Therefore, the SNR and the rate of a WiFi user u respectively are:

$$SNR_u^{WiFi} = \frac{g_u^{WiFi} P_{WiFi}}{B_{WiFi} No_{WiFi}} \tag{8.1}$$

$$T_u^{WiFi} = \frac{B_{WiFi}}{N_{RF}} log(1 + SNR_u^{WiFi}) \tag{8.2}$$

where P_{WiFi} is the transmitted WiFi power and No_{WiFi} is the power spectral density of noise at the receiver.

8.2 Hybrid Algorithms and Results

In this section we show the results of employing two different load balancing algorithms on the RF/VLC system. Both are focused on enhancing the weakest user throughput performance.

8.2.1 Minimum Throughput Enhancing Design Rule

In this design, we care about the minimum user throughput (T_{min}) and so the priority goes to users with outages due to device orientation or location with an ordering from lower to higher rates. A user is removed from the VLC network until either there are no more outages or until the minimum rate calculated in the whole network is the highest achieved. Once a user is removed from the VLC network, this frees up bandwidth in a specific VLC AP which in turn helps in alleviating the outage. However, we only give the user the needed rate, the goal is not to give users the highest rates they can achieve. This is to keep the RF free for users that really need it and to not allow excess unnecessary handovers between the two media.

We define the set of users connected to RF and VLC as $\mathcal{WiFi}$ and $\mathcal{VLC}$ respectively. Recall that $N_{RF} = |\mathcal{WiFi}|$ and $N_{VLC,j} = \sum_u x_{uj}$

The algorithm is shown as Algorithm 2.

Algorithm 2 Min Throughput (T_{min}) Algorithm

1: **Input:** $T_k \triangleq \sum_j x_{kj} T_k^{(j)}$, $\mathcal{VLC} = \{1, 2, \cdots, M\}$, $\mathcal{WiFi} = \emptyset$, $x_{uj} \forall u, j$, T_{out}
2: $T_{min}(0) = \min_k T_k$, $u_{min} = \arg\min_k T_k$
3: **for** i=1:M **do**
4:     $T_{min}(i) = \min_k T_k$, $u_{min} = \arg\min_k T_k$
5:     $\mathcal{WiFi} = \mathcal{WiFi} \cup u_{min}$.
6:     $\mathcal{VLC} = \mathcal{VLC} \setminus u_{min}$
7:     Recalculate $T_k \forall k \in \mathcal{VLC}$ using eq. (6.3) and $T_k \forall k \in \mathcal{WiFi}$ using eq. (8.2). Set $x_{u_{min}j} = 0 \forall j$
8:     **if** $T_{min}(i) < T_{min}(i-1)$ **then**
9:         Reverse lines (5-6) then Break.
10:     **else if** $T_{min}(i) > T_{out}$ **then**
11:         Break.
12:     **end if**
13: **end for**

Fig. 8·1 shows the CDF of the minimum individual throughput in case of VLC-only and as well as in the hybrid RF/VLC system at a Lambertian order $m = 1$. A user declares an outage if $T_u^{(j)} < T_{out}$, $T_{out} = 30$ Mbps in this case. At first look, notice that the SDFOV does not experience outage and thus does not need to use the hybrid mode. This is by design, as long as all users meet their needs there is no need for unnecessary handovers. This behavior alleviates the load on the RF network as well as removes unnecessary latencies. As for the FFOV and the DFOV, if the users can tolerate an outage probability of 0.2, then the hybrid

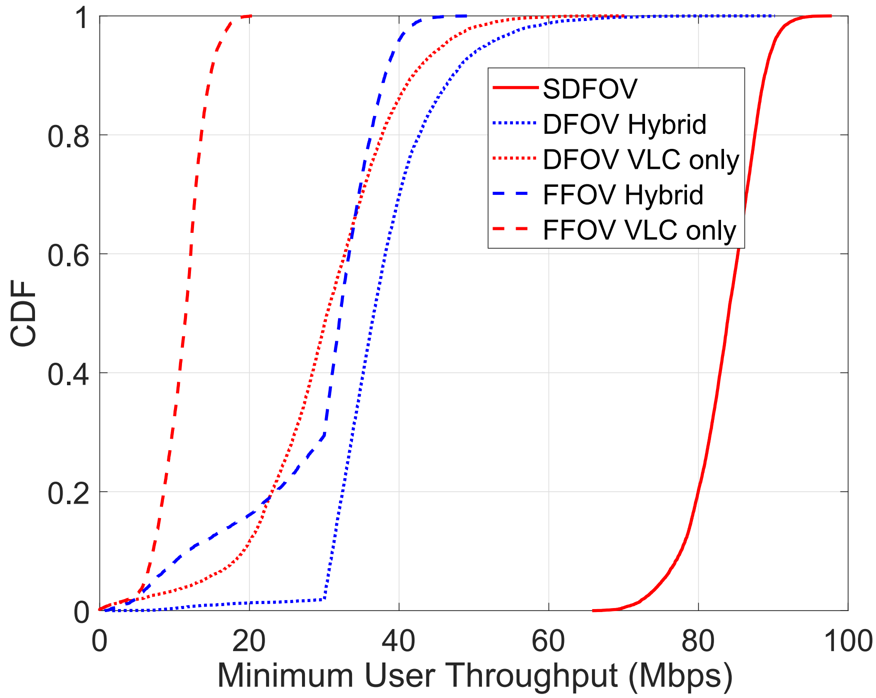

Figure 8·1: Minimum User Throughput Hybrid vs. VLC Downlink Only at $m = 1$ under Minimum Throughput Enhancing Design.

network adds a gain of 175% in FFOV case and 41% in case of DFOV.

Meanwhile, Fig. 8·2 shows the percentage of users that switch to RF. In the case of SDFOV there are none. For DFOV mostly 50% are under 15% of the users in the system (8 users total). Finally the FFOV has the highest percentage of transfers.

Fig. 8·3 shows the minimum user throughput CDF as well but at $m = 15$ (with a narrower beam). We show the performance of the standalone VLC downlink against the hybrid RF/VLC which is focused on lifting the minimum throughput out of outage. This approach does not allow unnecessary VHOs. In this case, SDFOV has outages due to the usage of lower transmission power to attain the illuminance constraint. DFOV performs worse at $m = 15$ than at $m = 1$ which can be seen in the VLC-only result but the hybrid system is able to enhance the performance by 255% on average. As for the FFOV, the individual user throughput has higher ranges in the $m = 15$ case but the minimum throughput is worse;

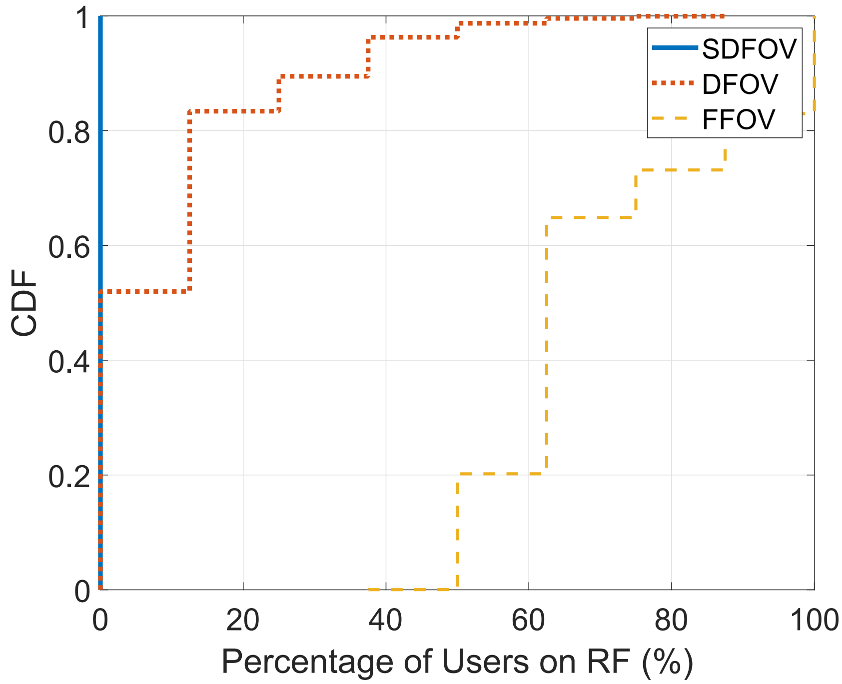

Figure 8·2: Percentage of Users that Transfer to RF when $m = 1$ under Minimum Throughput Enhancing Design.

however, its hybrid mode in $m = 15$ is able to achieve better minimum throughput than in the larger emission pattern $m = 1$.

We show the results of transferred user percentage in the $m = 15$ case in Fig. 8·4. The percentage of transferred users agrees with the overall conclusion that with higher Lambertian order FFOV is enhanced, while the other two receivers perform worse. This is confirmed in Fig. 8·4 where the percentage of users that transfer to RF when using DFOV and SDFOV increased yet the FFOV percentages decreased.

8.2.2 Sum Throughput Enhancing Design Rule

In this case, we try to enhance throughput as well as the minimum user rate by moving the weakest users in the VLC network first to the RF network until the sum throughput (T_{sum}) is maximized. Once the addition of a user reduces the sum throughput, the algorithm stops adding users to the RF. Details are shown in Algorithm 3.

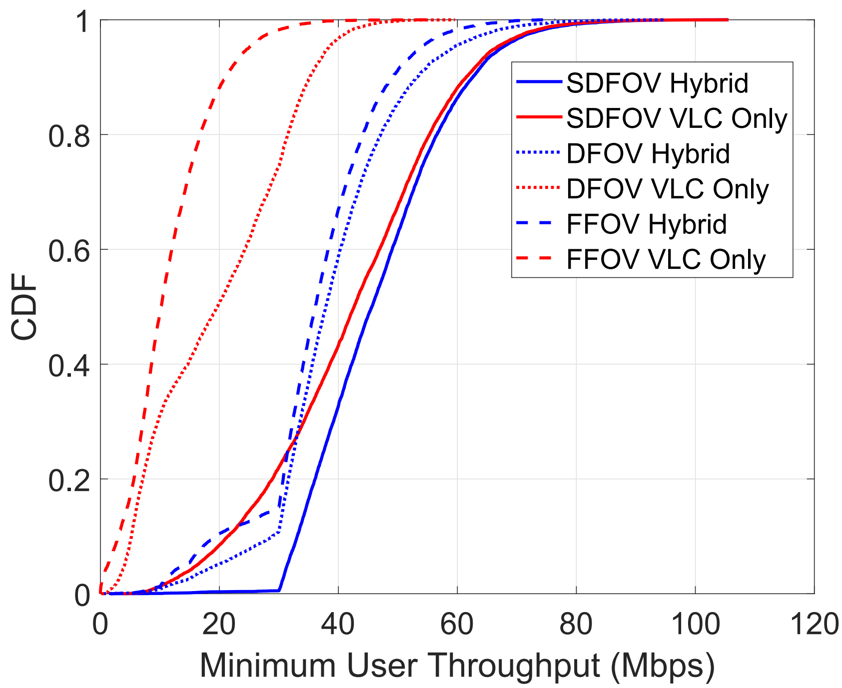

Figure 8·3: Minimum User Throughput Hybrid vs VLC Downlink Only at $m = 15$ under Minimum Throughput Enhancing Design.

Algorithm 3 Sum Throughput (T_{sum}) Algorithm

1: **Input:** $T_k \triangleq \sum_j x_{kj} T_k^{(j)}$, $\mathcal{VLC} = \{1, 2, \cdots, M\}$, $\mathcal{WiFi} = \emptyset$, $x_{uj} \forall u, j$.

2: $T_{sum}(0) = \sum_k^{|\mathcal{VLC}|} T_k^{VLC} + \sum_k^{|\mathcal{WiFi}|} T_k^{WiFi}$

3: **for** i=1:M **do**

4: $\quad T_{min}(i) = \min_k T_k$, $u_{min} = \arg\min_k T_k$

5: $\quad \mathcal{WiFi} = \mathcal{WiFi} \cup u_{min}$.

6: $\quad \mathcal{VLC} = \mathcal{VLC} \setminus u_{min}$

7: $\quad$ Recalculate $T_k \forall k \in \mathcal{VLC}$ using eq. (6.3) and $T_k \forall k \in \mathcal{WiFi}$ using eq. (8.2). Set $x_{u_{min} j} = 0 \forall j$

8: $\quad T_{sum}(i) = \sum_k^{|\mathcal{VLC}|} T_k^{VLC} + \sum_k^{|\mathcal{WiFi}|} T_k^{WiFi}$

9: $\quad$ **if** $T_{sum}(i-1) > T_{sum}(i)$ **then**

10: $\quad\quad$ Reverse lines (5-6) then Break.

11: $\quad$ **end if**

12: **end for**

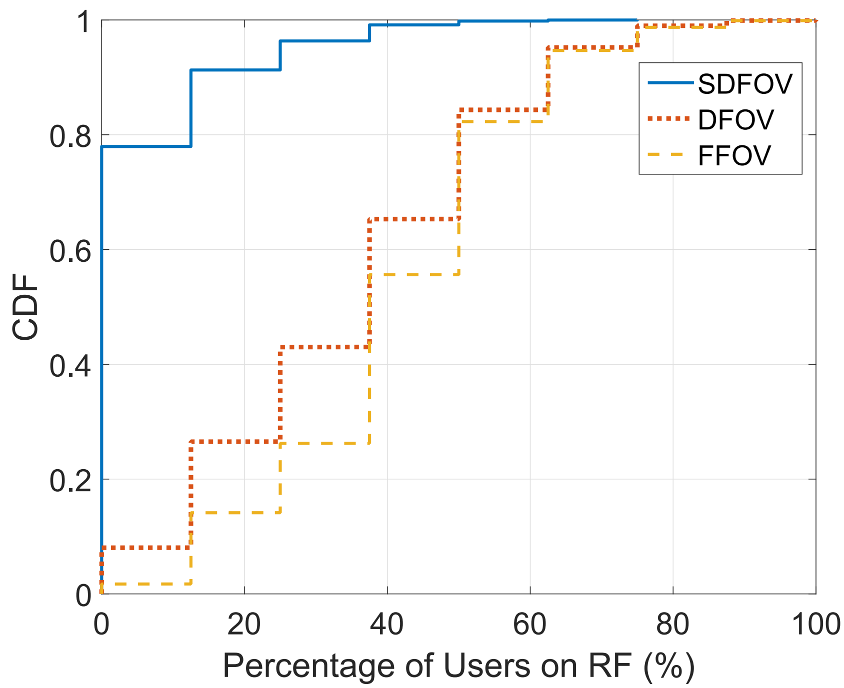

Figure 8·4: Percentage of Users that Transfer to RF when $m = 15$ under Minimum Throughput Enhancing Design.

Fig. 8·5 shows the results for the sum throughput enhancing RF/VLC system design. It also confirms that the gains from the hybrid RF/VLC system are large in all three receivers. FFOV sees an average sum throughput gain of 136%, DFOV 49% and SDFOV 32%. Meanwhile in Fig. 8·6 we see that each of the three receivers transfers a high amount of users to the RF AP to achieve such gains. SDFOV transfers up to half the users. DFOV transfers around up to 60% and FFOV up to 90% which in that case leaves one user (8 users total in this simulation) on the VLC network. The fact that the dynamic field of view receivers achieve lower hybrid gains than the fixed field of view receiver show that they depend less on the RF network which is ideal for the concept of offloading crowded RF networks.

The drawback of this design lies in allowing a frivolous number of vertical handovers, which can be problematic when more users enter the system. Users who need RF may

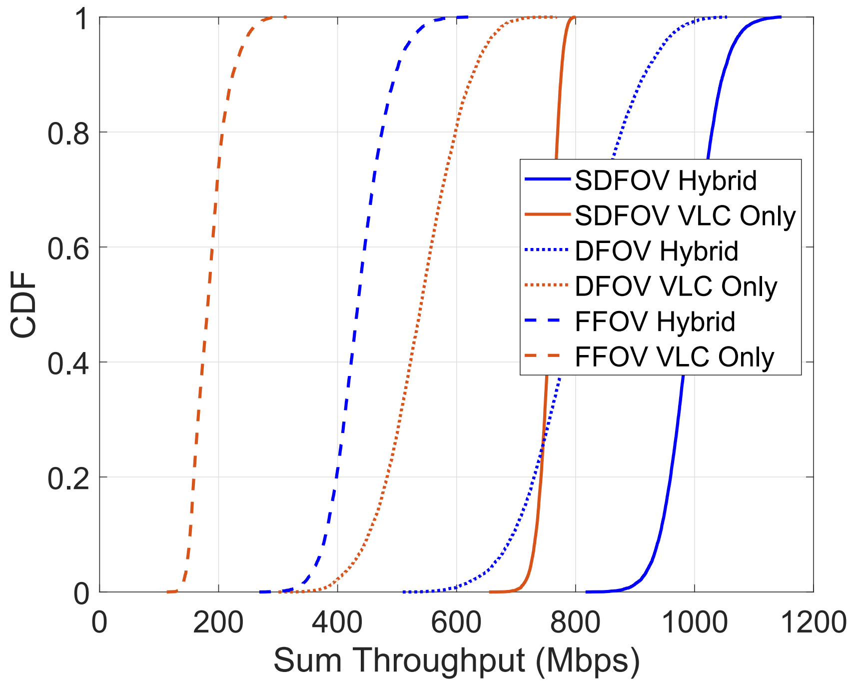

Figure 8·5: Aggregate Sum throughput VLC-Only vs. Hybrid under Sum Throughput Enhancing Design at $m = 1$.

be categorized into 1) fast-moving users (which we do not study here but this is discussed in (Abdalla et al., 2019b; Abdalla et al., 2019c)) because they risk extensive HHOs along their path; 2) orientation-based outaged users; 3) location-based outaged users; 4) LOS-blocked users; and 5) users in high-density spots which either face high interference from other users or in our case need to share the bandwidth to a degree that affects their service quality.

Lastly, we expect VHOs to have higher latency than HHOs. In the hybrid design process we argue for making VHOs only as needed. Figs. 8·5 and 8·6 do not represent the case of minimizing handovers. Fig. 8·5 shows the huge throughput gains without details. Fig. 8·6 shows the large percentage of users that migrate to RF to create these high gains.

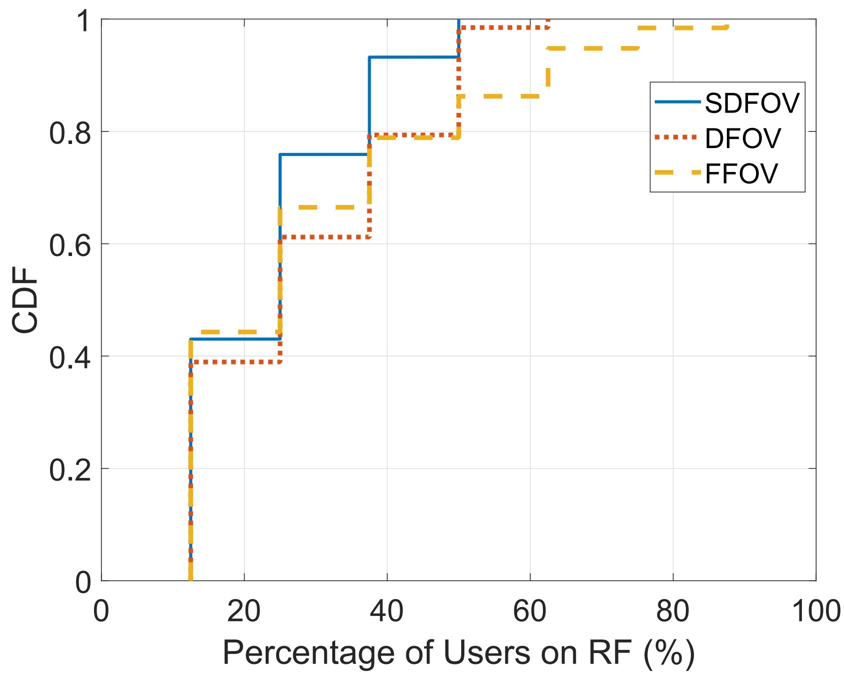

Figure 8·6: Percentage of Users that Migrate to RF Under Sum Throughput Enhancing Design at $m = 1$.

8.3 Hybrid System Outage Probability Analysis

We build upon the results obtained in Section 7.2 for the VLC-Only network where SDFOV receivers are employed. First, we discuss the individual user outage in an RF-Only network. Second, we propose a hybrid setup that combines both systems and derive an approximation for the individual user outage probability (rate coverage).

8.3.1 RF-Only Outage Analysis

Assuming a Nakagami-m fading channel, modeled in Section 2.2.2, with $\Omega = 1$ and the path loss G as follows (Rappaport et al., 1996):

$$G = \left(\frac{4\pi d_o}{\lambda_c}\right)^2 \left(\frac{d}{d_o}\right)^{\gamma_{nak}} \tag{8.3}$$

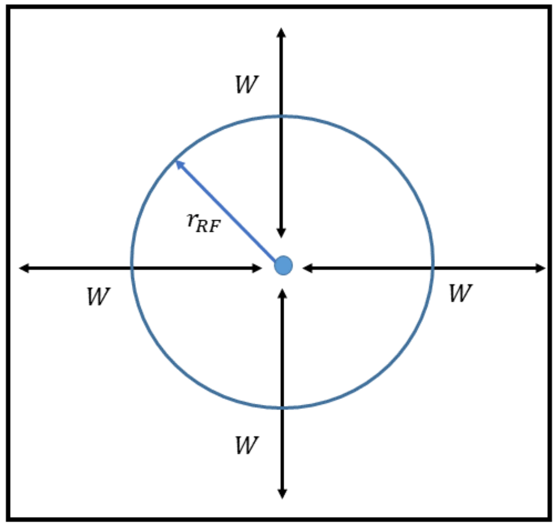

Figure 8·7: RF Cell Model.

where d is the distance between the RF AP and the receiver, d_o is a reference distance, normally 1 m indoors, λ_c is the carrier frequency and γ_{nak} is the path loss exponent, typically a value between 1.6 and 1.8 indoors (Cebula III et al., 2011; Rappaport et al., 1996). The number of RF users, N_{RF}, is modeled by a Poisson distribution with rate λ_{RF}. The users are assumed to be uniform over a circle with radius r_{RF} (Fig. 8·8), creating a homogeneous PPP. The RF user throughput can be defined as:

$$T_{RF} = \frac{B_{RF}}{N_{RF}} log(1 + \frac{P_{RF}|h|^2}{GN_oB_{RF}}) \tag{8.4}$$

Fig. 8·7 shows the radius of connectivity for the RF AP where r_{RF} represents the maximum connectivity radius. This brings us to a per user device outage probability of:

$$P_{outage-RF} = \mathbb{E}_{N_{RF}}\left[\frac{1}{r_{RF}^2\Gamma(m_{nak})}\left(x\Gamma(m_{nak}, m_{nak}n_o x^{\frac{\gamma_{nak}}{2}}) - \frac{\Gamma(m_{nak}+\frac{2}{\gamma_{nak}}, m_{nak}n_o x^{\frac{\gamma_{nak}}{2}})}{(m_{nak}n_o)^{\frac{2}{\gamma_{nak}}}}\right)_{x=V^2}^{x=V^2+r_{RF}^2}\right] \tag{8.5}$$

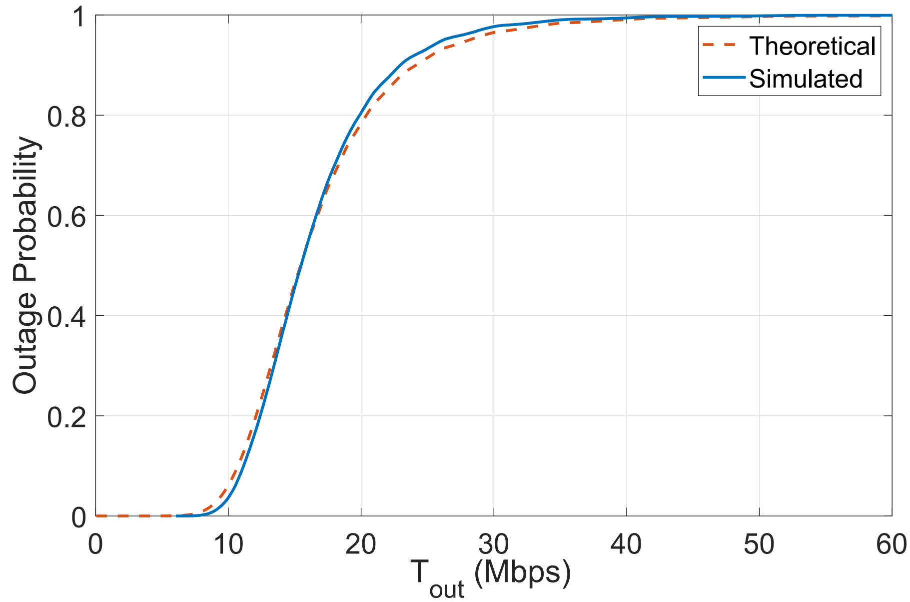

Figure 8·8: RF-Only Individual User Outage Probability.

where $n_o \triangleq \frac{16\pi^2 B_{RF} N_o}{\lambda_c^2 P_{RF}} (2^{\frac{nT_{out}}{B_{RF}}} - 1)$, $\Gamma(.)$ is the gamma function and $\Gamma(.,.)$ is the lower incomplete gamma. Proof is available in Appendix A.3.

We show the results of the simulated data vs. the theoretically derived outage probability for a typical user moving uniformly at random across the space in Fig. 8·8. The curves are plotted for different different rate thresholds and show that the derived outage conforms with the simulated results. The simulation parameters used for this figure are available in Table 8.1.

8.3.2 Hybrid RF/VLC System Outage

Here we assume that the hybrid RF/VLC system is composed of a basic unit that can be easily replicated depending on space/design requirements. This unit contains a single centered RF AP and 4 centered VLC APs as illustrated in Fig. 8·9. The radius of the RF AP connectivity r_{RF} is variable and can be optimized for a desired hybrid outage performance. This assumption inherently poses either the assumption that the system is aware of user location and is able to discern the users within its connectivity radius or a possible beam

Table 8.1: RF-Only System Simulation Parameters

Parameter	Parameter Description	Value
W	Room Dimension	2 m
P_{RF}	RF Transmitter Power	0.01 W
N_o	System Noise	4×10^{-21} W/Hz
B_{RF}	RF Bandwidth	25 MHz
f_c	Carrier Frequency	2.5 GHz
V	Height Between Transmitter and Receiver	1.96 m
γ_{nak}	Path Loss Exponent	1.6
m_{Nak}	Nakagami-m parameter	1

shaping capability at the RF AP (such as mmWave). This setup helps the system attain the load balancing solution needed to enhance the user throughput.

The main assumption is that VLC is the primary system. Users attempt to connect to VLC first, then only the outaged users that lie within the RF connectivity switch to it. We assume no interference between users connected to the same AP in each of the technologies. The users are assumed to share the AP resources. Interference is only considered between cells. The VLC APs are non-point-source and due to the usage of SDFOV receivers, we can assume that the receivers can connect to the nearest AP. Therefore, the connection regions as seen in Fig. 8·9b show the nearest Euclidean distances. Using the VLC throughput definition in eq. (6.3) and RF throughput definition in eq. (8.4) we define the user outage as the probability that a user throughput goes below a certain threshold $P(T < T_{out})$.

Users are assumed to be uniformly distributed over the room. The number of users in the system forms a homogeneous PPP with a density $\lambda_u = \frac{N_a}{A_r}$ where N_a is the average number of users in the whole space and $A_r = 4W^2$ is the total area of the room.

We derive the hybrid network typical individual user outage probability. Let the VLC outage be termed as V_o while the RF outage is RF_o. The RF connections reach a circle of radius r_{RF} with area $A_{RF} = \pi r_{RF}^2$ and $a_1 = \frac{A_{RF}}{4}$ (shown in Fig. 8·9a). There are two user occurrence events, $A1$ which is the event that the user is in area a_1 and $A2$ which is the

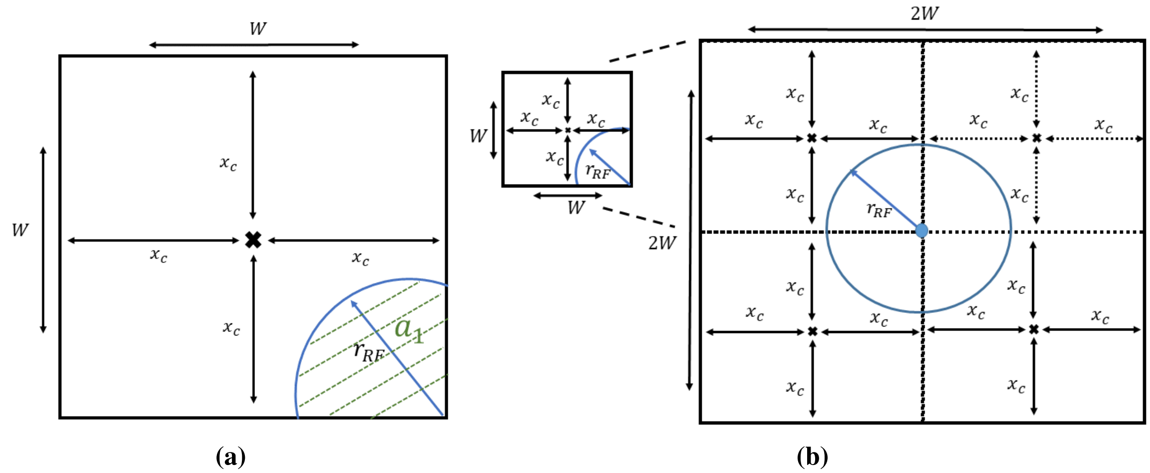

Figure 8·9: Indoor Hybrid Model: (a)Magnified Cell Connectivity; (b) Total Room Hybrid Connectivity Model .

event of the user being in the remaining area $a_2 = W^2 - a_1$.

Lemma 2 The hybrid outage probability for a typical user in a hybrid RF/VLC network with total user density λ_t, RF user density λ_{RF} and VLC user density λ_{VLC} under the discussed system assumptions can be approximated as:

$$P_{Outage-Hybrid} \approx \left[\sum_{n'=1}^{\infty} P(V_o|A1, N_t = n') P(N_t = n') \sum_{n''=1}^{\infty} P(RF_o|A1, N_{RF} = n'') P(N_{RF} = n'') \right] P(A1) + \sum_{n=1}^{\infty} P(V_o|A2, N_{VLC} = n) P(N_{VLC} = n) P(A2) \tag{8.6}$$

where N_t is a Poisson random variable with $\lambda_t = \frac{\lambda_u}{\lambda_{VLC-AP}}$ and $N_{VLC} \triangleq N_t - N_{RF}$. Our model causes the VLC AP density λ_{VLC-AP} to be fixed at $\frac{1}{W^2}$ (1 AP per W^2 m^2). We approximate N_{RF} and N_{VLC} to be Poisson random variables. N_{RF} has mean $\lambda_{RF} = \lambda_u P(V_o|A1, N_t) A_{RF}$.

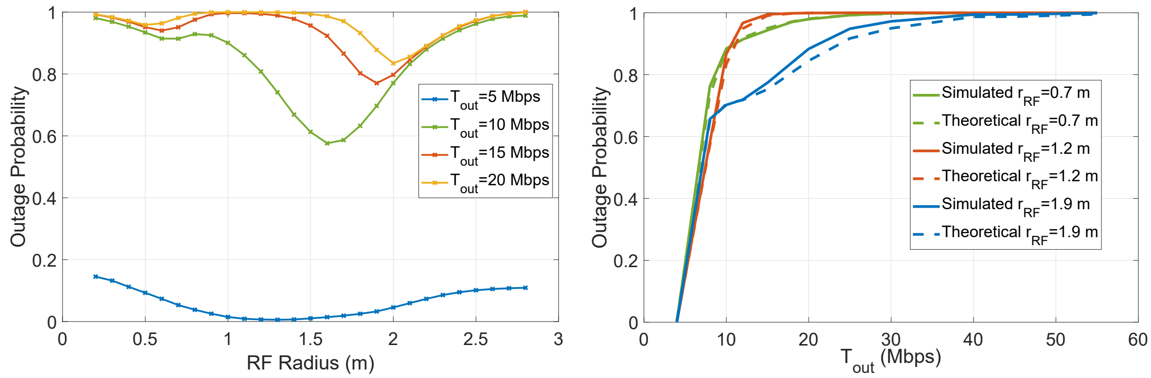

(a) **(b)**

Figure 8·10: Hybrid Outage Probability: (a) Hybrid Outage Probability Simulated Data Plotted with Different r_{RF};(b) Hybrid System Outage Probability Simulated Data vs. Theoretical Results For Different T_{out} at $r_{RF} = 0.7, 1.2$ and 1.9 m.

Finally, the last Poisson variable considered is N_{VLC} which has a mean $\lambda_{VLC} = \lambda_t - \frac{\lambda_{RF}}{4}$. Details of the proof are in Appendix A.4. Each term is defined below and the details of deriving each term is in the appendix as well. The VLC outages are somewhat similar to the formula derived in Section 7.2 but are evaluated on different areas in this case.

The steps of the solving eq. (8.6) are to first evaluate the VLC outage within the area a_1 using eq. (8.7), then the RF outage within the same area (using eq. (8.8)) after the RF Poisson mean gets updated. Finally, the VLC outage in area a_2 from eq. (8.9) after λ_{VLC} is evaluated.

$$P(V_o|A1, N_t = n') = 1 - F_{r|N_t,A1}\left(\sqrt{\left(\frac{(m+1)AV^m}{2\pi}\sqrt{\frac{P_t^2R^2}{\sigma_n^2(2^{\frac{2n'T_{out}}{B_{VLC}}}-1)}}\right)^{\frac{2}{m+2}} - V^2}\right) \quad (8.7)$$

$$P(RF_o|A1, N_{RF} = n'') =$$

$$\frac{1}{r_{RF}^2\Gamma(m_{nak})}\left(x\Gamma(m_{nak}, m_{nak}n_o x^{\frac{\gamma_{nak}}{2}}) - \frac{\Gamma(m_{nak}+\frac{2}{\gamma_{nak}}, m_{nak}n_o x^{\frac{\gamma_{nak}}{2}})}{(m_{nak}n_o)^{\frac{2}{\gamma_{nak}}}}\right)\Bigg|_{x=V^2}^{x=V^2+r_{RF}^2} \quad (8.8)$$

Table 8.2: Hybrid Outage Simulation Parameters

Parameter	Parameter Description	Value
x_c	Room Dimension	1 m
W	Room Dimension	2 m
P_{RF}	RF Transmitter Power	0.01 W
V	Vertical height bet. Tx and Rx	1.96 m
m	Lambertian Order	1
B_{VLC}	VLC Bandwidth	50 MHz
A	Receiver Area	785×10^{-9} m^2
R	Receiver Responsivity	28 A/W
σ_n^2	Noise Variance	2.3426×10^{-7}

$$P(V_o|A2, N_{VLC} = n) = 1 - F_{r|N_{VLC},A2}\left(\sqrt{\left(\frac{(m+1)AV^m}{2\pi}\sqrt{\frac{P_t^2 R^2}{\sigma_n^2(2^{\frac{2nT_{out}}{B_{VLC}}} - 1)}}\right)^{\frac{2}{m+2}} - V^2}\right) \tag{8.9}$$

Fig. 8·10a shows that different RF radii give variable outage performance when varying T_{out}. If a system is adjusted for a specified T_{out} then the connection RF radius may be evaluated beforehand for a specific user arrival rate. We show the performance of different hybrid systems at different r_{RF} in Fig. 8·10b. This figure clearly shows how each radius performance varies at different thresholds. In this figure $P_t = 2.5$ W and $m_{Nak} = 1$, other parameters are in Table 8.2.

Fig. 8·11a shows the individual user outage probability for different throughput thresholds in the RF-Only $m_{Nak} = 1$ system, the VLC-Only system (if only the VLC APs in the space are used to provide communications) and finally the performance of opportunistically using both technologies together. The figure shows the enhancement the hybrid system provides over both the single RF cell or the 4 VLC AP system. In this figure $B_{RF} = 25$ MHz, VLC transmit power $P_t = 2.5$ W and $\lambda_u = 10$.

We show the effect of different RF channels in the hybrid outage in Fig. 8·11b where the VLC power $P_t = 5$ W. $m_{Nak} = 1$ models a Rayleigh fading while $m_{Nak} = 5.7$ approximates

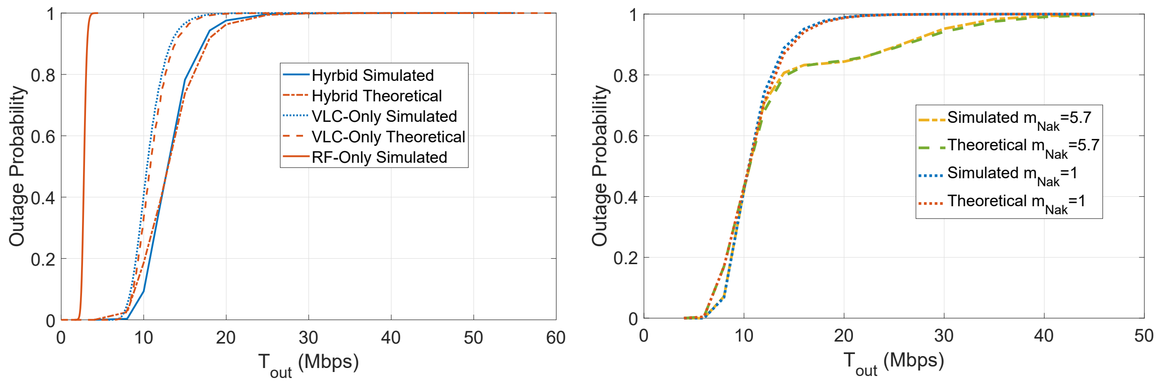

(a) **(b)**

Figure 8·11: Hybrid Outage Probability Simulated Data vs. Theoretical Results For Different T_{out} Thresholds at $r_{RF} = 0.9$ m: (a) Comparison of The Standalone Systems with their Hybrid at $m_{Nak} = 1$; (b) Different RF Channel Models.

the Ricean-k with $K = 10$ dB (using the relation in eq. (2.17)) which is a typical assumption in indoor mmWave systems (Sarris and Nix, 2007). The systems also differ in operating frequencies as well as the bandwidths. We assume $B_{RF} = 25$ MHz and $f_c = 2.5$ GHz for $m_{Nak} = 1$; and $B_{RF} = 100$ MHz and $f_c = 60$ GHz for $m_{Nak} = 5.7$. Results show the improvements added by the mmWave channel. We note that the approximation is further from the data at thresholds T_{out} which are very close to the average VLC user throughput (seen here at 8 Mbps, VLC user mean throughput is 6.5 Mbps in this simulation). This case is explained in the derivation in the appendix A.4. The figure otherwise shows that the hybrid outage approximation conforms well to the simulated outage.

8.3.3 Association Policies

We discuss two main association policies:

- Distance Association (DA) is the common association we show in our results and derived the outage formulas for. It basically assumes that each receiver connects to the nearest transmitter.

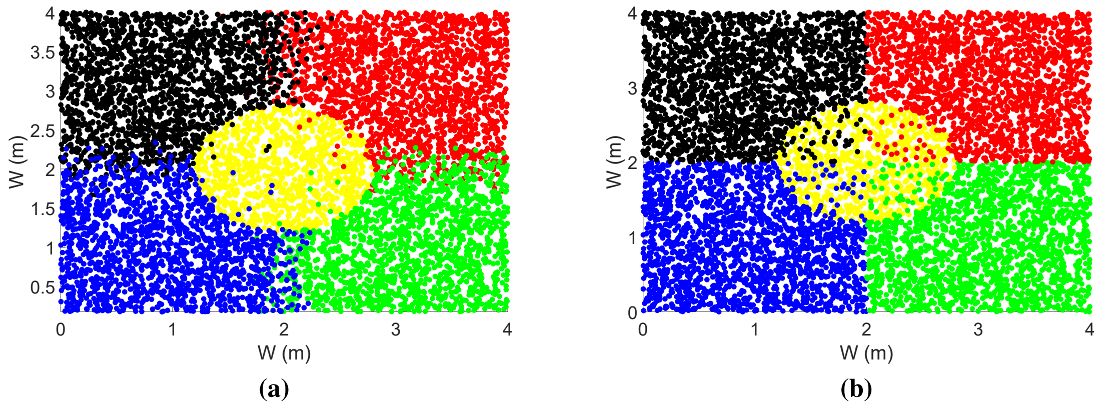

Figure 8·12: Connected Users Under Different Association Policies at $T_{out} = 10$ Mbps, $m_{Nak} = 1$ and $r_{RF} = 0.7$ m: (a) FA Policy; (b) DA Policy.

- Fairness Association (FA) is an association based on the optimization problem we proposed in eq. (6.7) that promotes max-min fairness for SDFOV receivers.

As shown in Fig. 8·12a, when using the FA policy, one can no longer assume perfect uniformity of the users in the Euclidean spaces tied to each AP (as is the case in Fig. 8·12b representing DA connections). There exists a minimal leakage of users connected to APs outside these regions however the figure also shows that they are a few and can be approximately considered uniform. However, the pmf of the number of users connected to RF in this case does not follow the Poisson distribution and in this case we obtain the pmf empirically and use the formulas derived.

Fig. 8·13 shows the performance of both policies in the VLC-Only system as well as the hybrid. One important thing to note is how the FA policy shows lower outage probability in the lower individual user rate region but the price comes at the higher rates where it shows worse performance than DA. Both hybrid setups show an improvement over their counterpart VLC standalone systems. In this figure $\lambda_u = 10$, $r_{RF} = 0.8$ m, $P_{VLC} = 5$ W and $m_{nak} = 1$.

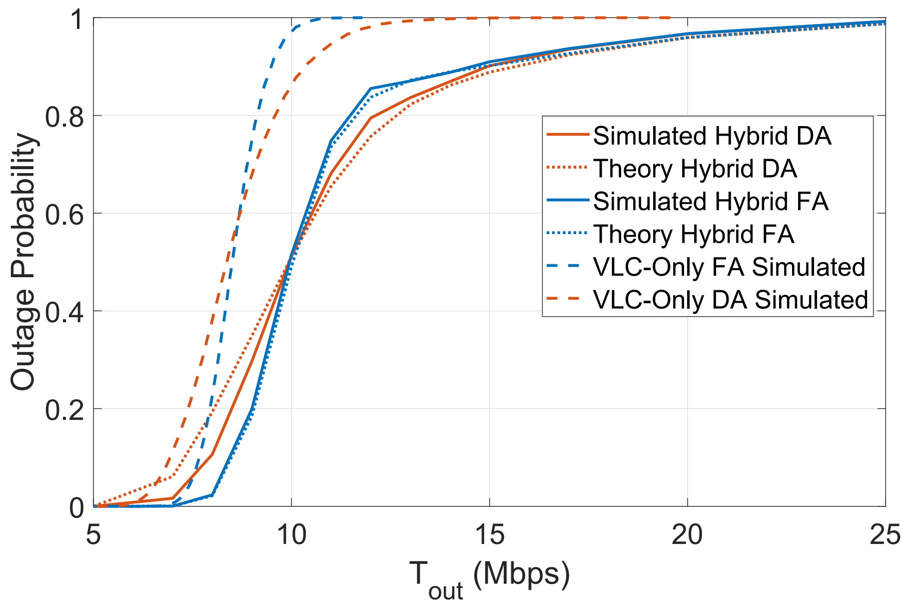

Figure 8·13: User Outage Probability of DA and FA Policies at Different T_{out} in Hybrid System vs. Standalone VLC FA and DA System.

8.4 Chapter Conclusions

In this chapter we build on the VLC system we worked on optimizing throughout the previous Chapters 3-7 to analyze it in a hybrid RF/VLC system. We propose two different load balancing schemes: a minimum throughput enhancing design as well as a sum throughput enhancing one. We discuss that in terms of load balancing and unnecessary handover reduction, protocols that only lift the system from outage are best in keeping VHOs reduced as well as helping the overall system in terms of delay and RF congestion. We also derive an approximation for the per user outage probability of a hybrid system that employs SDFOV receivers (employing of the VLC-only outage derived in Section 7.2). A system that helps in balancing the load between RF and VLC APs to help a user achieve a target throughput. We simulate results for two different association schemes FA and DA which enhance fairness and throughput respectively. The results reached reveal information on how to optimize the system and analyze the interactions between the system parameters and the outage probability (rate coverage).

Chapter 9

Proof of Concept and Experimentation

In this chapter we focus on the experimental aspect of our study. First, we discuss our lab setup, with detailed information about our testbed, utilized receiver as well as the mobility schemes we devised to achieve receiver dynamic control within the space. Second, we compare our empirical model to the measured data and quantify the error between the simulated and measured optical power received. Third, we explain the experiments we ran to get our data and the importance of their results. Finally, we end the chapter with our implementation of the hybrid RF/VLC asymmetric link with handover.

9.1 System Blocks

Our system consists of the following blocks: 1) Signal Processing; 2) Signal Conversion; 3) Optical Conversion and 4) Receiver with dynamic control. This can be seen in Fig. 9·1. Each of these essential blocks is discussed next:

9.1.1 Signal Processing: PC

To be able to transmit modulated signals we run a software defined radio (SDR) system; namely GNU Radio software (GNU Radio, 2020) which is an open-source software that provides signal processing blocks to implement software radios, on a personal computer (PC) to be able to process the signal at the computer's end. This goes on to be fed to the Universal Software Radio Peripheral (USRP), discussed in the next block. GNU Radio provides standard blocks, including Fourier transforms, and graphical user interfaces (GUIs)

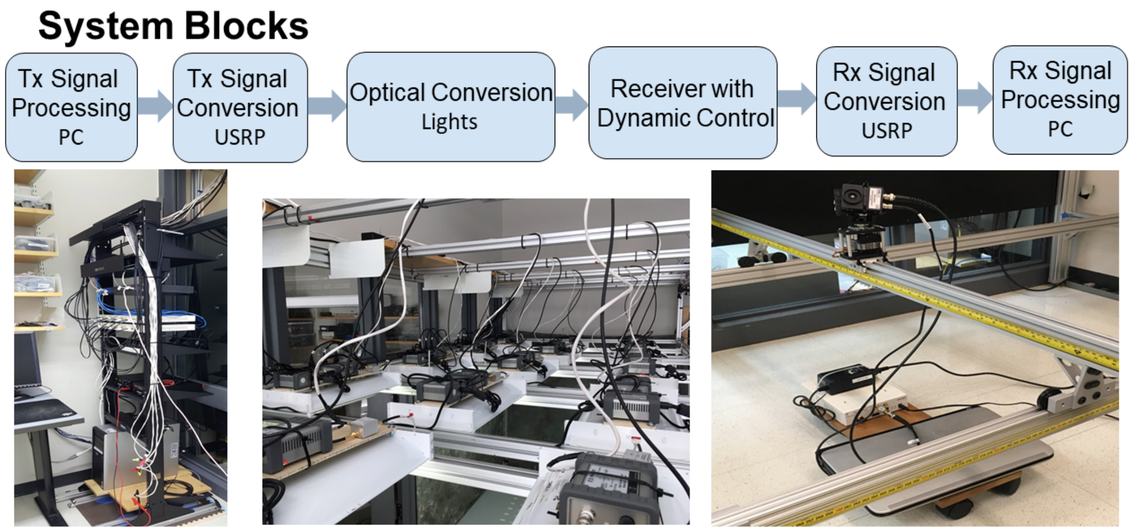

Figure 9·1: System Blocks

that can be used to build flowgraphs. C++ is used for performance intensive operations while Python is used for rapid development. We use a flowgraph to drive output signals (i.e., fixed frequency sine waves) through multiple USRPs to modulate the 15 luminaires that make up our lighting array. At the receive side more signal processing occurs where another flowgraph on a laptop connected to the receiver (through another USRP) performs RSS analysis while saving the recorded signals and raw data for later analysis.

9.1.2 Signal Conversion: USRP

We setup 4 X-series USRPs from Ettus Research (Ettus Research, 2020) which allow the transmission of 8 complex signals or 16 real valued ones. This gives us the ability to uniquely control 15 arbitrary signals to modulate the 15 luminaires in our grid. We are able to transmit up to 15 pure sine waves in the frequency ranges 100 kHz to 800 kHz with 50 kHz separations. We do this to be able to isolate each signal in the frequency domain later on for further testing. We do not consider this an actual data transmission method for an employed system as this clearly has reduced spectral efficiency.

At the receive side an N210 USRP is attached to an additional computer running GNU

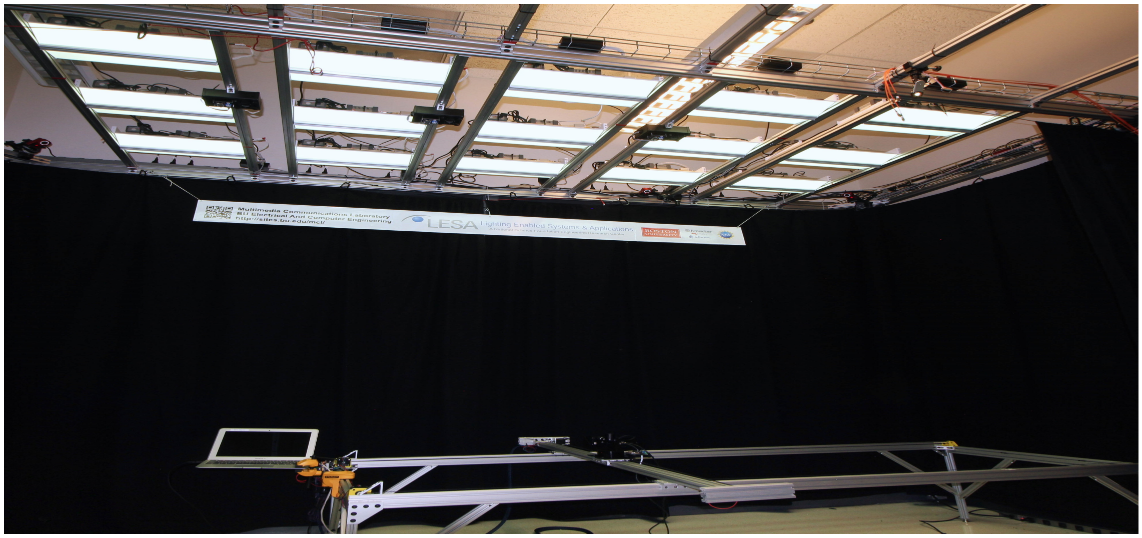

Figure 9·2: Boston University VLC Testbed and the Data Collection Apparatus MATT

Radio software and is automated to collect measured raw data and calculate the electrical power corresponding to each received sinusoid through an FFT operation using the USRP/GnuRadio framework, producing the peak-to-peak voltage of the received sinusoids and then the peak-to-peak optical power. We directly relate the received optical power to the received amplitude as optical power is directly proportional to current in the optical domain.

9.1.3 Optical Conversion: Testbed

Our testbed at Boston University (Fig. 9·2) consists of 15 off-the-shelf CREE luminaires[1] (#CR22-32L-35K-S) in a 3×5 grid. Each luminaire's dimensions are $0.24\ \text{m} \times\ 0.46$ m. They are placed in the center of the room with spacings of 0.5 m in the x-axis (room width) and 0.7 m in the y-axis (room length). The room dimensions are $4.27\ \text{m} \times 1.62$ m. The lights are at a height of 2.68 m from the floor while the receiver is 1.96 m away from the lights. We wrapped the testbed area in dark, non-reflective fabric, to suppress effects of

[1] The CREE luminaires have a limited frequency response that is apparent within the set of test frequencies used to identify each transmitter, but is not germane to the experiments. In practice each transmitter will exploit the full viable frequency range of the luminaire used.

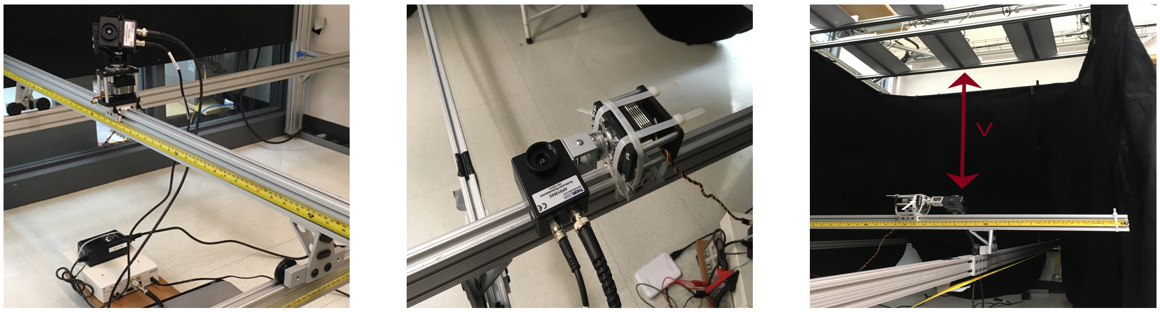

(a) (b) (c)

Figure 9·3: Data Collection Apparatus Version 1: (a) APD Receiver with No Filter or Lens; (b)Close-up of Receiver and Servo; (c) Vertical Distance Between the Receiver and the Lights.

ambient lighting.

9.1.4 Receiver Control-MATT/PATT

The signals transmitted through the blocks aforementioned are received using a Thorlabs Avalanche Photodiode (APD, ThorLabs unit (#APD120A2)), shown in Fig. 9·3b. Part of the receiving control is the method with which we collect our data. Next, we describe the control system evolution in Subsection MATT/PATT.

MATT/PATT

We first started the data collection process with the system in Fig. 9·3. The receiver and servo mount are set for accurate positioning in the X-Y plane using a movable gantry. This allows us to collect translational data. Meanwhile rotational data is possible through a servomechanism that cycles through different receiver angles.

While functional, this apparatus still needed to be motorized which led us to version 2: motorized angle tilt turret (MATT), shown in Fig. 9·4a. MATT functions with two mechanical servos for translational motion and a micro-controller responsible for rotating the custom turret on which the receiver is mounted. We show a close up of the turret in the same figure.

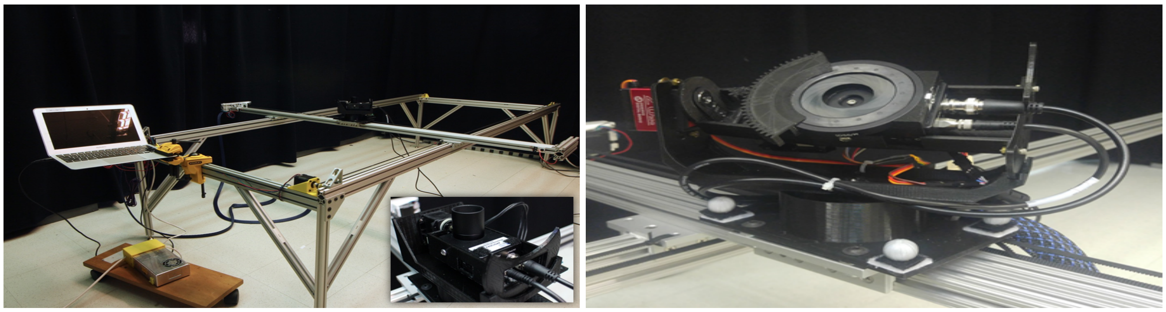

(a) (b)

Figure 9·4: Data Collection Apparatus Versions 2 and 3: (a) MATT with a Close-up of the Turret; (b) PATT.

The final and finest version of the system is achieved by switching out the MATT turret for a different custom turret that can change its Pan, Aperture and Tilt Turret (PATT) (see Fig. 9·4b). It is also able to move autonomously along the x and y coordinates for translational data collection. To change the aperture we use 1) a circular mechanical iris (Thorlabs #ID50/M), in Fig. 9·5a, and 2) a partially oval mechanical iris (Thorlabs #ID75Z), in Fig. 9·5b. The turret and the x-y translational unit are each controlled by a micro-controller interfaced to a central control station. The control station is programmed to move the turret position and velocity based on the sequencing defined for our experiments. Our closed loop data collection system employs a motion capture system (OptiTrack, 2021) to provide ground truth locations and avoid errors in the translational positions that the turret is instructed to move to. This helps provide accuracy to our measurements.

9.2 Reconciling Experimental Data and Mathematical Simulations

In this section we show how our analysis and simulations aligned with the data measured in the lab. We start by quantifying the error between simulations and measurements, then we discuss how noise varied in both settings then we end with visuals that show the closeness of both sets.

(a) (b)

Figure 9·5: Different Aperture Iris: (a) Circular; (b) Non-Uniformly Circular.

9.2.1 Error Quantification

Using the experimental setup described above, we transmit 15 different sine waves and measure the RSS for a total of 144 locations, 2 different static FOVs (wide and narrow) and 4 different elevation angles, $\theta_{elev} = \{45°, 60°, 75°, 90°\}$. We also measure the noise variance in the lab and accordingly are able to evaluate the received SNRs (Abdalla et al., 2018). We then calculate the error in optical power received from the measured data as opposed to the theoretical simulated optical power at wide vs. narrow FOV for an untilted device (see Fig. 9·6a and 9·6b respectively). At this point in our work we had used a point source model to represent the rectangular luminaires nevertheless the measured results conform well with the model simulation. This allowed us to trust our model.

9.2.2 Theoretical Versus Empirical Noise

Any VLC system has noise contributed by thermal and shot origins, some may be thermal-noise-dominated and others shot-noise-dominated (Ramirez-Iniguez et al., 2008). Our system is considered to be shot-noise-dominated, for example, the thermal noise caused by our receiver is around $1.26\mu V$ rms (ThorLabs Inc, 2013) while shot noise is 7.18 mV rms at a FOV$= 20°$.

In the noise formula provided in eq. (2.7), by changing the FOV χ, we are able to

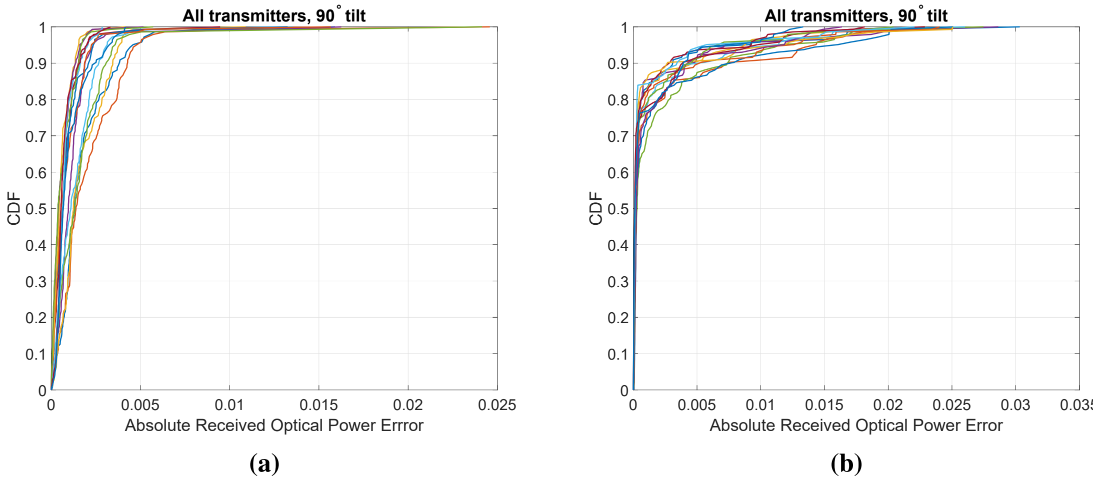

Figure 9·6: Comparisons Between Theoretical and Measured Data (a) Absolute Error in Optical Power (Wide FOV); (b) Absolute Error in Optical Power (Narrow FOV).

count how many transmitters (elements more specifically) are included within the FOV to calculate the total electrical amplitude received at the detector that contributes to shot noise. As an example, in Fig.3·1b we can see that if the receiver is in the center of the room and receives its signal from the center transmitter (T_{x8}) at 20° FOV then there are 9 sources contributing to the incident noise (T_{x8} included). To calculate the noise we sum the elements from within these 9 transmitters that appear in the receiver scope.

Fig. 9·7a shows the maximum SNR calculated using theoretical noise vs. noise measured in the lab in the context of the DFOV receiver which we discussed in Section 3.3. The receiver is set in the middle of the lighting array, its elevation angle is varied from $20° - 60°$ and we optimize the SNR through FOV control. The figure also reveals that the noise model provides a reasonable approximation of the lab environment. However, it has been our experience, that minimizing noise in the lab instrumentation requires careful attention to detail. The development of practical VLC systems are expected to show robustness in these practical considerations. The figure also shows that for the two theoretical curves, allowing the FOV to be a continuous set provides smoother results than when it is restricted

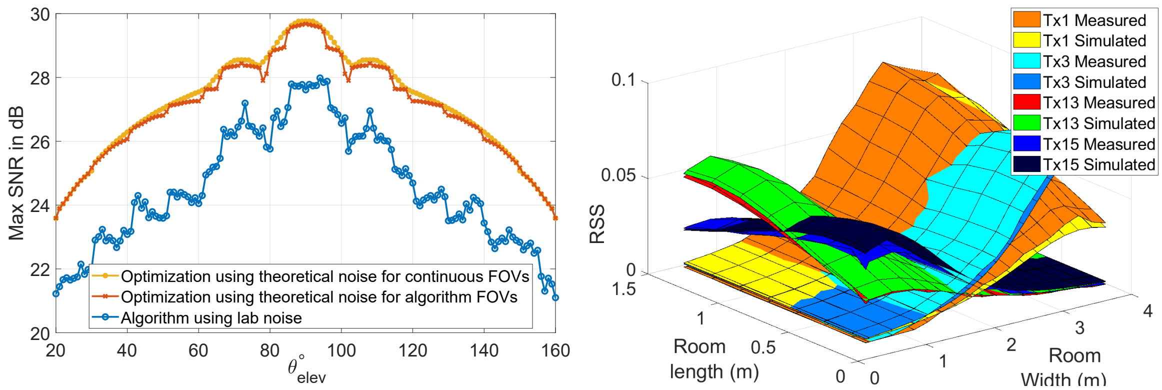

(a) **(b)**

Figure 9·7: Theory vs. Data: (a) Comparison of Lab Noise vs. Calculated Theoretical Noise; (b) Comparison of Data From Four Transmitters in the Lab with Theortical Simulations.

to discrete non smooth FOVs given to the receiver such as the case in Algorithm 1. The smoothness also depends on the FOV step chosen as discussed in Section 3.3.

9.2.3 Data Measurements

We show a comparison of a subset of our collected data with simulated data for four transmitters from our configuration in Fig. 3·1b, namely transmitters 1, 3, 13, 15. To accommodate the CREE luminaires' limited frequency response, we simulate according to the empirical constant measured at each frequency (different $C_T C_R$ values per frequency). The comparison is plotted in Fig. 9·7b. This is plotted for a flat receiver facing the lights. The peaks occur when the receiver is aligned underneath a light. Meanwhile in Fig. 9·8 we plot all cells data along with the simulated data offering a plan view perspective on the strongest RSS within the space.

9.3 Experiments Run

To discuss our experimental results we first categorize each experiment relative to the theoretical analysis discussed throughout this dissertation.

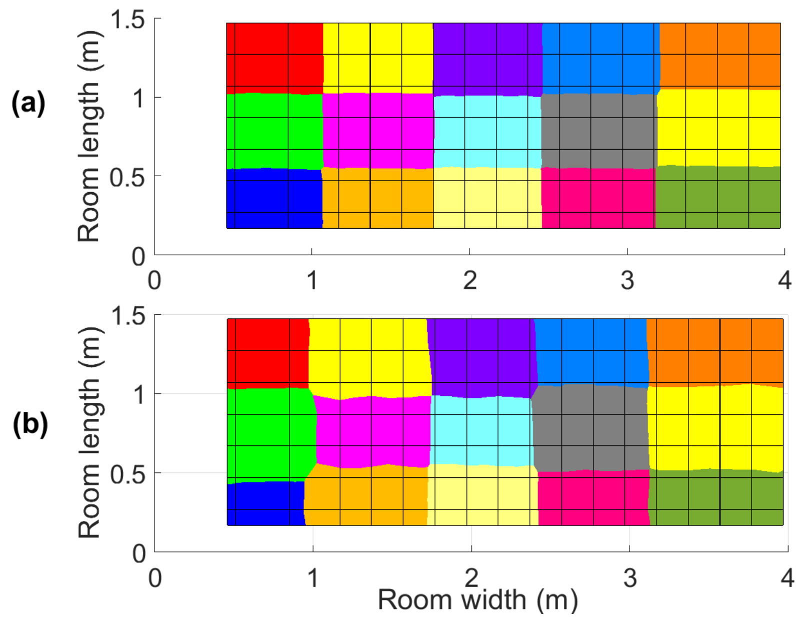

Figure 9·8: Cellular RSS Lab vs. Theory.

9.3.1 Impact of Receiver FOV and Orientation

The experiments in this section validate our analysis regarding the effects of variable device tilts and FOV on the signal quality and overall user experience. We use version 1 of the data collection system (Fig. 9·3). The APD is positioned on a servo so we dynamically alter its elevation angle between the following set of fixed values $\{45^\circ, 60^\circ, 75^\circ, 90^\circ\}$ to achieve different tilts. To vary FOV statically we experience 1) FOV $= 90^\circ$ when the receiver is bare, 2) FOV $= 20.89^\circ$ when an empty lens tube (not containing a lens) of internal diameter measured to be 25.64 mm with a length of 33.5 mm is mounted onto the receiver. The allows us to explore wide vs. narrow FOV effects.

To fully analyze the system and validate our model, we measure RSS at many points in our grid. The receiver's height is fixed at 0.63 m from the floor. We then carry out extensive measurements for a grid 8 points along the y-axis and 18 points along the x-axis for all angle tilts and both FOVs mentioned above. Translational and rotational data are collected by stepping the receiver through positions in the lighting field by incrementing X

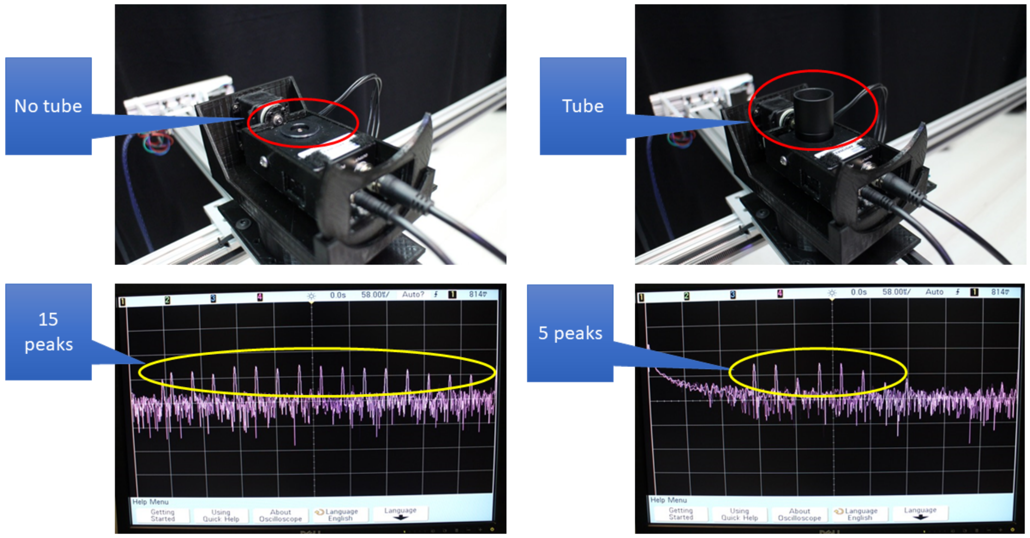

Figure 9·9: Effect of FOV on Signal Reception.

and Y coordinates. At each coordinate, the PD is rotated to collect RSS at elevation angles of $\{45°, 60°, 75°, 90°\}$, where 90° represents the receiver pointing directly upward. In Fig. 9·9 we show how FOV affects the reception of the 15 transmitted signals, when FOV $= 90°$ (no lens tube) the receiver detects all 15 signals as is apparent on the oscilloscope, however, once the tube is mounted the receiver is only able to detect 5 signals and the rest are no longer in its LOS. Confirming the receiver scope vs. system resource reuse discussed in Section 3.6.

Fig. 9·10 plots the 15 received signals from the transmitters in the lab when a narrow FOV is employed (bottom) vs. a wide FOV (top). Considering OOK modulated signals and a BER threshold of 10^{-3} (formula provided in the analysis in Section 3.1). The figure shows the effect narrow FOV has in improving the SNR, as well as the much weaker signal provided by a wide FOV (top figure). The wide FOV only creates high enough SNR to pass the BER threshold when the receiver is under the lights.

Lastly, we plot the SNR received from each transmitter in the middle section (transmitters 4 - 12) at narrow (7.1°) vs. wide (40°) FOV in Fig. 9·11, while the receiver is untilted. Here we use PATT for more dynamic FOV control. For each case, a smaller FOV realizes a

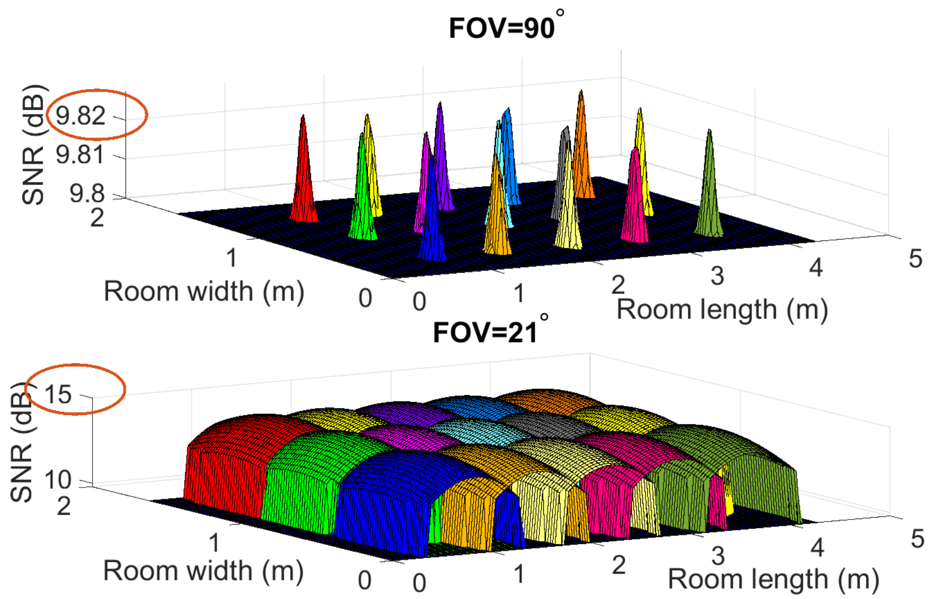

Figure 9·10: SNR Experienced with/without Empty Lens Tube.

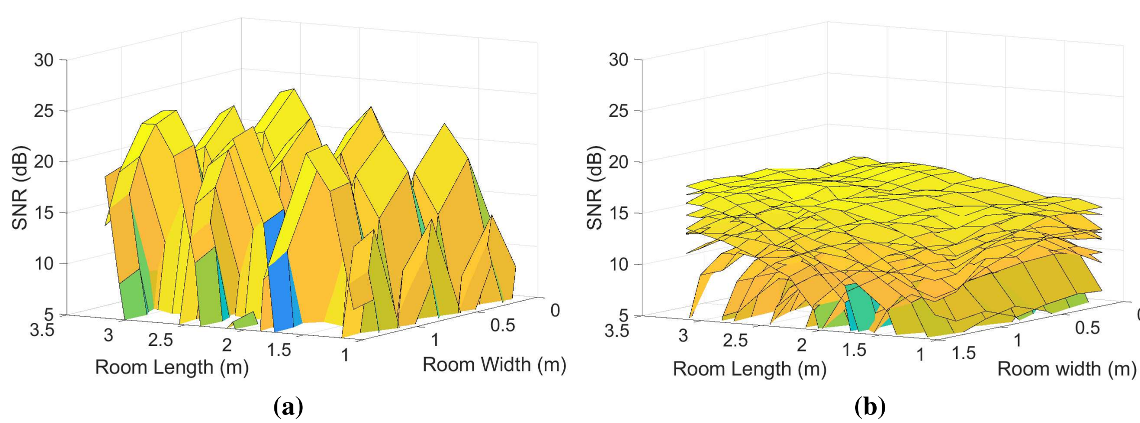

Figure 9·11: All Lab Transmitters Measured Data: (a) Narrow FOV; (b) Wide FOV.

more concentrated signal, with fewer noise sources, but also creates more coverage holes. The wide FOV scenario shows signal continuity while sacrificing the SNR in comparison to the narrow FOV scenario. As mentioned earlier, the CREE luminaires have a frequency dependent signal attenuation that disadvantages higher frequencies. Due to the range of test frequencies used to isolate individual luminaires, there is a pattern of signal strength attributed to this frequency selection that is apparent in Fig. 9·11 but is only an artifact of the limits of the luminaires used in the testbed.

9.3.2 Variable FOV

The experiments mentioned here show the results of the dynamic FOV receiver. The observed range of receiver locations for data collection is shown by the black rectangle in the center of Fig.3·1b. The turret and platform (PATT) are sequenced to collect data in the marked grid by ranging over 12 points in the x-axis and 7 points in the y-axis. At each coordinate 9 different FOVs are evaluated $\{7.1°, 12.3°, 17.4°, 26.6°, 36.9°, 47.6°, 57.4°, 67.2°, 72.3°\}$, each at 2 elevation angles $\{90°, 120°\}$. In this data set, we fix the receiver azimuth angle to zero.

With this setup, we devise 4 experimental runs: 1) Measuring RSS from one transmitter for different FOVs for an untilted circular aperture receiver. 2) Measuring RSS from one transmitter for different FOVs for a circular aperture receiver with $\theta_{elev} = 120°$. 3) Measuring RSS from all transmitters for a fixed FOV for an untilted circular aperture receiver. 4) Measuring RSS from one transmitter for different FOVs for an untilted non-circular aperture receiver. Single transmitter results are provided for the central transmitter, Tx8.

Circular Iris First we show results for a circular FOV by using the circular shaped iris in Fig. 9·5a:

1. *FOV effect:* Fig. 9·12 shows each SNR value received from Tx8 under 9 FOVs ranging from 7.1° to 72.3°. The effect of variable FOV on the receiver SNR is demonstrated

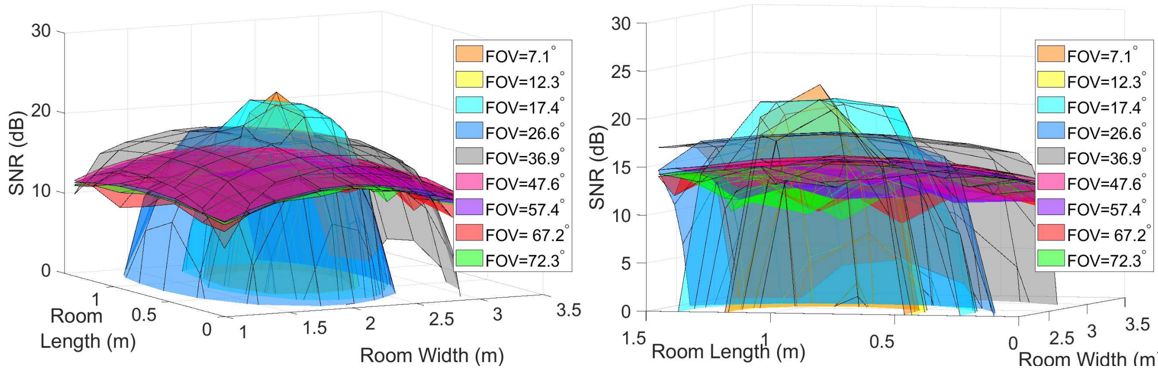

(a) (b)

Figure 9·12: Variable FOV Effect on Tx8 SNR for an Untilted Receiver: (a) Showing all the Grid Data; (b) Showing a Cross-Section underneath the center of the transmitter.

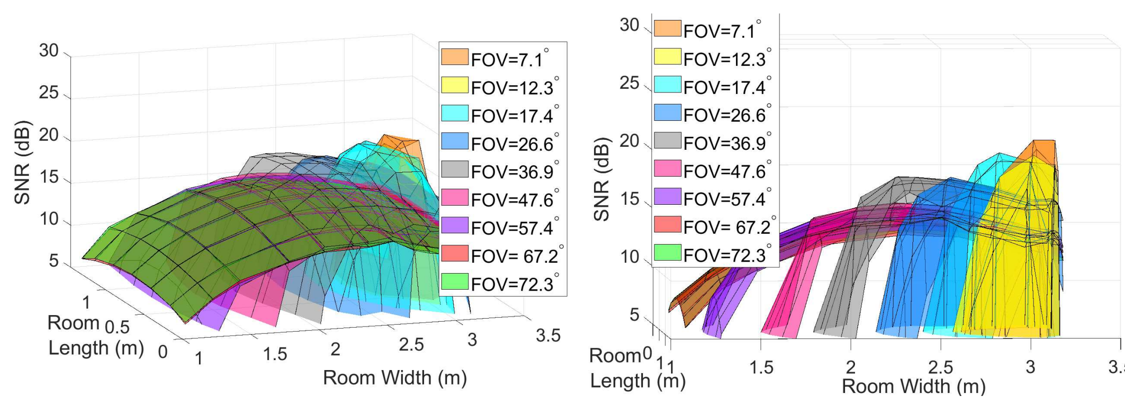

(a) (b)

Figure 9·13: Variable FOV Effect on Tx8 SNR for a Receiver with $\theta_{elev} = 120°$: (a) Showing all the Grid Data; (b) Showing a Different Perspective that Vividly Shows SNR Ordering per FOV.

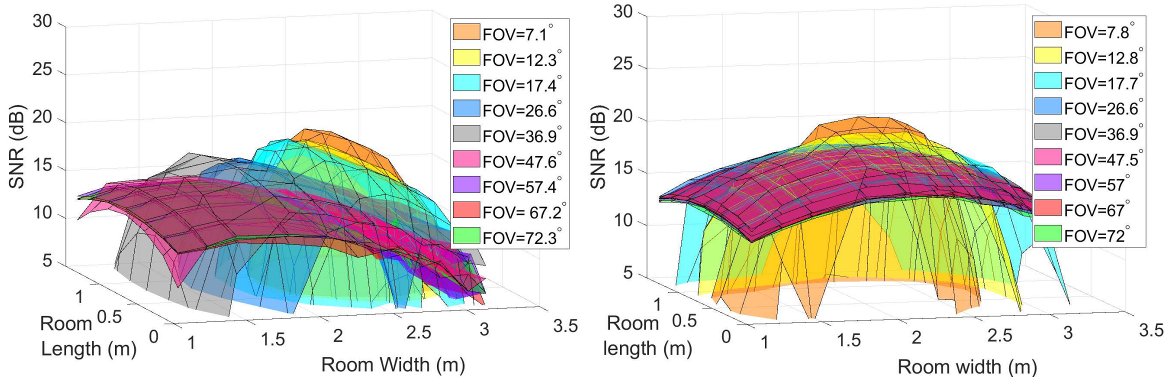

(a) **(b)**

Figure 9·14: Lab Transmitters Measured Data: (a) Variable FOV Effect on Tx11 SNR for a Receiver with $\theta_{elev} = 120°$ Using a Circular Aperture; (b) Tx8 SNR Using Oval Aperture on an Untilted Receiver.

where Fig. 9·12a shows all the measured data within the grid and then we focus on the middle cross-section under the lights in Fig. 9·12b to clearly show the ordering of FOV with SNR. It is observed that the smaller FOVs have higher SNR but quickly fall out of coverage when the receiver and the light are unaligned. This vividly illustrates the SNR-coverage trade-off. The wider FOVs show poorer SNR performance but better continuity, i.e, less coverage holes. When employing a variable FOV receiver, this trade-off guides the optimization for each receiver position and orientation.

2. *Orientation Effect:*

Meanwhile, Fig. 9·13 shows the impact of receiver tilt on the received signal from transmitter 8 at $\theta_{elev} = 120°$ using the circular aperture iris. This plot shows why orientation has an important role in determining the optimal FOV for the given receiver location, position, and velocity. A comparison between Fig. 9·12a and Fig. 9·13a shows you that the device tilt, caused the optimal SNR value received from Tx8 to move from under it (where the receiver is situated). It is better for the tilted receiver underneath Tx8 to connect to Tx11 for a stronger connection[2]. This is why we show the SNR obtained from Tx11

[2]This result also agrees with the optimization shown in Fig. 3·6b.

when the receiver is under Tx8 with the same 120° elevation. This plot confirms that the SNR received from Tx11 is higher although the receiver is under Tx8. An example like this shows how directionality and the effect of orientation breaks the expectations of what is the norm in an omni-directional medium.

Using Different FOV Shape: The results above consider a receiver with circular FOV which is consistent with the industrial design of optical components such as lenses, lens tubes, and irises. However, PDs are often rectangular, as are the arrays of luminaires deployed for lighting. This suggests that alternative geometries in FOV are worth testing and could potentially be able to support maximizing performance in an adaptive receiver design in that it could better match the receiver scope to the transmitter layout. For example, a different aperture shape might realize a different coverage region and a different set of coverage holes. We offer a sample test of a different FOV shape where we explore the impact of using a non-uniformly circular aperture (Thorlabs #ID75Z), which is oval in smaller FOVs and then conforms to the circular FOV at larger FOVs. It is not a complete investigation of possible FOV shapes but a step in that direction. Fig. 9·14b shows SNR for the partially oval aperture at different FOVs when the receiver is flat and positioned under Tx8. It is observed that at the minimum FOV, while the circular iris in Fig. 9·12a shows only one signal, the non-uniform iris shows two. With FOV growth, this aperture adds more signals faster than the circular iris while still allowing less noise to enter than the wide FOV aperture but more than the circular aperture noise. This behavior is potentially valuable in a scenario where diversity is needed at a lower noise floor than what the circular wide FOV provides. This result motivates us to explore the interaction among diversity, interference, the shapes of the receiver, aperture, and lighting array in future works.

9.3.3 Resource Reuse vs. Scope

We continue the discussion of the system resource reuse-scope trade-off and confirm its effect through experimental data using the DFOV receiver setup. The figures we discuss here are measured at two extreme FOVs $\chi_{min} = 7.1^\circ$ and $\chi_{max} = 47.6^\circ$.[3] Fig. 9·15a shows the signals received at the two extreme FOVs. The SNR-FOV trade-off is shown here; the small FOV indicates a peak SNR underneath the transmitter but yields low signal everywhere else. In contrast, the wider FOV provides higher scope almost everywhere in the room but at the cost of lower SNR. Fig. 9·15b illustrates the impact of tilting the receiver by $\theta_{elev} = 120$ under the same conditions. These indicate how a narrow FOV is more susceptible to changes in device orientation.

Both figures enhance the Reuse-Scope trade-off because it draws attention to the static FOV design that does not allow FOV fluidity. If the receiver is stuck in narrow FOV mode, it experiences the high SNR and high reuse scenario but accompanied by the drawbacks of coverage holes, high susceptibility to orientation and blockage effects. Not to mention a longer time to scan for transmitters within any space. Choosing to stick to a wide FOV may support reliability, scope and occlusion issues but at the price of reduced signal quality and reduced system resource reuse efficiency. This supports the argument for using a DFOV receiver.

9.4 Implementation of RF/VLC Asymmetric Link with Handover

In this implementation we were able to establish a hybrid RF/VLC system (as shown in Fig. 9·16) that forms a connection between an APD and a VLC luminaire by enforcing the downlink data to be transmitted from the VLC Tx to the Rx while maintaining WiFi as our uplink. As seen in the figure the VLC AP transmits signals through the light using a USRP

[3]Note: We previously defined χ_{min} as the lowest FOV needed for an untilted receiver centered under a light to cover it at a given receiver height and χ_{max} as the maximum FOV required to cover all transmitters under the same circumstances.

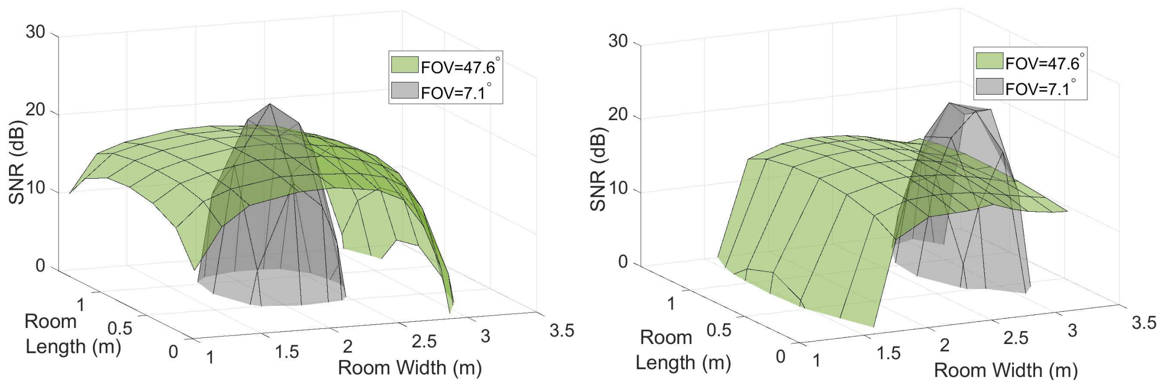

(a) (b)

Figure 9·15: FOV-Tilt-SNR Trifecta: (a) SNR vs. FOV; (b) Tilting Effects on SNR.

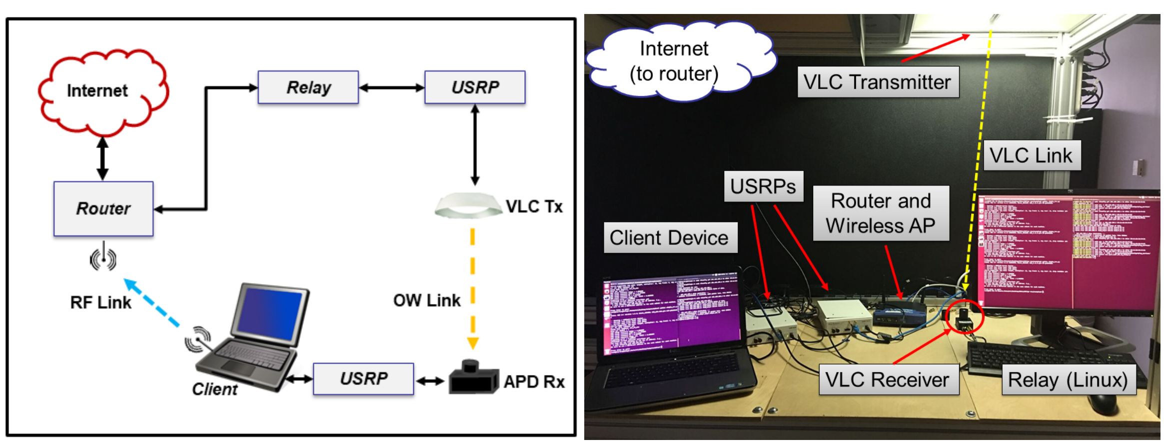

(a) (b)

Figure 9·16: RF/VLC Asymmetric Routing Link: (a) Schematic Illustration; (b) Our Lab Setup.

and the client device receives the signal through another USRP connected to our receiver (APD). Another link implementation is available in (Shao et al., 2014; Li et al., 2018).

To convince the system to reroute the downlink traffic to our OWC link and maintain the uplink on WiFi, we need to setup a static routing table at the router, disable IP packet forwarding and specify to the router that the relay path goes through the "virtual" VLC link. The client PC also needs to recognize the packets it requests and enter its system through the virtual link. Pinging each connection helps in checking that these routes are configured correctly. An example providing IP addresses is available in (Rahaim, 2015, Fig 9.3).

After the connection is established we implement a code on the client laptop to measure RSS, if it is below a predefined threshold, we switch the downlink back to WiFi otherwise maintain the VLC connection. In our experiment we run data streaming websites such as youTube. When we artificially block the VLC link, the code allows the system to switch to WiFi successfully. We were also able to implement a code on the linux client device to measure the VLC downlink RSS, successfully triggering a switch to the WiFi downlink in case of low signal levels as well.

9.5 Chapter Conclusions

In this chapter, we focus on confirming many of the theoretical results we reached through simulations. Most importantly, we validate our system models through experimentation with a prototype system. We also establish the effect FOV and orientation have on a practical VLC system. Our results lead us to many important trade-offs such as Scope-Reuse and Scope-SNR. We provide experimental results for the DFOV receiver and show that it plays a role in diversity, interference and user experience. We also propose the usage of different FOV shapes for different lighting/APD combinations. Finally, we successfully implement a hybrid VLC/RF link that is able to support RSS-based handovers.

Chapter 10

Conclusions and Summary of Future Work

10.1 Summary of the work

Directional technologies are vital towards solving the problem of spectrum crunch. In this work we argue for using VLC technology indoors to enhance user throughput and system fairness as well as sum throughput. VLC has many benefits most importantly are its non-interfering property with RF as well as its confinement within walls for added security and easier deployment in local networks. This ease of use helps also in creating dense network deployments capable of pushing the limit of what indoor RF traditional systems can achieve solo. Chapter 3 focuses on enhancing the VLC single link capability by employing the directionality properties to the user's advantage. This is done by re-imagining how the receiver can function whether by adapting its field of view to achieve a stronger signal and cut out noise or to control its orientation to point to a desired transmitter. This chapter reveals important results related to system resource reuse, coverage perspectives and interference mitigation using the proposed receivers which motivated more analysis. The concept of dense deployment brings along with it the concern of higher interference due to higher overlap between cells. This is addressed in Chapter 4 where we discuss causes of interference in directional OWC systems, possible interference management techniques and key aspects that differentiate interference in the optical medium as opposed to the RF medium.

Enhancement in indoor systems through employing VLC is guaranteed for systems that are designed properly taking into consideration both the communication aspect as well as the illumination aspect. This is why we turn to this issue in Chapter 5. The results from this chapter motivate future systems to aim at fulfilling both goals in the design phase and not later on to avoid the pitfalls of reduced performance for better illuminance experience or vice versa. Chapter 6 employs the techniques from Chapter 5 to a system that studies the effects of optimizing both receiver FOV as well as user association while balancing the VLC AP load. It captures the effect of receiver parameters on the system as well as system architecture changes. The results obtained from this chapter show how promising the receivers we proposed are in a VLC multi-user setup.

Chapter 7 serves as the final chapter looking into the VLC-only aspect of our work. The focus here is the VLC network outage probability. We first tie system outage to handover time and user velocity in a novel probabilistic model. Second for a multi-user setting employing SDFOV receivers, we obtain a closed form for the user outage which helps in future system design. While Chapter 8 discusses the hybrid RF/VLC setup, first for two different algorithms that target lifting the VLC system from outage through utilizing an indoor RF AP. A scenario very plausible in indoor settings that can include several luminares and a single RF AP. Second, we derive a hybrid outage formula for a typical individual user rate employing an SDFOV receiver which is very useful in determining how well the hybrid system can help as opposed to the single VLC or RF only.

Finally, we end with Chapter 9 which confirms our work through experimentation and detailed explanation of our lab setup and experiments design. We show pivotal results here that confirm the accuracy of our models and allow us to simulate more results with confidence in the system capability.

10.2 Future Work and Broader Applications

In this dissertation we focus on employing dynamic FOV receivers to enhance system communication performance in typical indoor illumination scenarios. While there are many applications in which a dynamic FOV has utility we discuss two here: vehicular communications and light-based positioning. For positioning, a wide FOV is advantageous in finding more light sources to accurately position a device, but also causes increased noise which results in higher root mean square (RMS) error in the localization. This trade-off is described in (Zhuang et al., 2018). In vehicular communications, wide FOV gives wider receiver scope (Masini et al., 2018). An enlarged scope can include more interfering sources. A narrow FOV on the other hand becomes challenged in terms of sustaining alignment between vehicles. Setting a fixed narrow FOV also proves non-beneficial as the optimal FOV will change with the proximity of the transmitter/receiver pair.

Steerable DFOV receivers add the advantages of protecting the communication quality under orientation effects and dealing with alignment challenges. This can be very beneficial in relay systems where an SDFOV receiver can be used to relay messages to devices that lack line of sight communication.

10.3 Conclusion

In conclusion, hybrid VLC/RF systems can provide much needed aggregate rates in future indoor systems. There still is much work that needs to be done to enhance these promising systems. Adaptive design with dynamic control over many parameters would help in allowing for more seamless connectivity. There still needs to be work to address queuing in the hybrid network and accurately model the vertical handover delays caused by various system designs and protocols. Realistic models that can explore the device behavior while a user is still/in motion remain premature specially since new devices and new apps change the norm. Systems that have the ability to predict the user needs based on his traffic in a reliable and robust way are yet to be uncovered but what is clear is that directional communications generally and VLC specifically can play a key role alongside RF to help reach the performance needed for future 6G networks. Can imagination picture what the future of this invention is to be?

Appendix A

Appendix

A.1 Outage Upper Bound

$$
\begin{aligned}
&P_{outage} < P\left(t_{HO} > \frac{g(m)}{v_u}\right) \\
&\overset{(a)}{=} P\left(t_{HO} > \frac{g(m)}{v_u} \middle| l(m) \leq \frac{L}{2}\right) P\left(l(m) \leq \frac{L}{2}\right) \\
&+ P\left(t_{HO} > \frac{g(m)}{v_u} \middle| l(m) > \frac{L}{2}\right) P\left(l(m) > \frac{L}{2}\right) \\
&\overset{(b)}{=} 2P\left(t_{HO} > \frac{g(m)}{v_u} \middle| l(m) \leq \frac{L}{2}\right) P\left(l(m) \leq \frac{L}{2}\right) \\
&= 2P\left(g(m) < t_{HO}v_u \middle| l(m) \leq \frac{L}{2}\right) P\left(l(m) \leq \frac{L}{2}\right) \\
&\overset{(c)}{=} 2P\left(l(m) < \frac{L}{2} - \sqrt{(R - t_{HO}v_u)^2 - \frac{S^2}{4}} \middle| l(m) \leq \frac{L}{2}\right) P\left(l(m) \leq \frac{L}{2}\right) \\
&= 2P\left(\left\{l(m) < \frac{L}{2} - \sqrt{(R - t_{HO}v_u)^2 - \frac{S^2}{4}}\right\} \bigcap \left\{l(m) \leq \frac{L}{2}\right\}\right) \\
&= 2P\left(l(m) < \frac{L}{2} - \sqrt{(R - t_{HO}v_u)^2 - \frac{S^2}{4}}\right) \\
&= 2F_{l(m)}\left(\frac{L}{2} - \sqrt{(R - t_{HO}v_u)^2 - \frac{S^2}{4}}\right) = \frac{\frac{L}{2} - \sqrt{(R - t_{HO}v_u)^2 - \frac{S^2}{4}}}{L/2} \\
&= 1 - \sqrt{\frac{(R - t_{HO}v_u)^2 - \frac{S^2}{4}}{R^2 - \frac{S^2}{4}}}
\end{aligned} \tag{A.1}
$$

where (a) follows from the total law of probability and (b) follows from the symmetry of the arc and (c) follows from the geometric relation between $l(m)$ and $g(m)$.

A.2 SDFOV Closed Form Outage Probability

$$
\begin{aligned}
P_{outage-SDFOV} &= P\left(\frac{B_{VLC}}{2N_{VLC}}\log_2(1+SINR) < T_{out}\right) \\
&\overset{(a)}{=} P\left(\frac{B_{VLC}}{2N_{VLC}}\log_2(1+SNR) < T_{out}\right) \\
&= P\left(SNR < 2^{\frac{2N_{VLC}T_{out}}{B_{VLC}}} - 1\right) \\
&= \mathbb{E}_{N_{VLC}}\left[P\left(H_{DC} < \sqrt{\frac{\sigma_n^2}{P_t^2R_r^2}(2^{\frac{2nT_{out}}{B_{VLC}}}-1)}|N_{VLC}=n\right)\right] \\
&= \mathbb{E}_{N_{VLC}}\left[P\left(\frac{(m+1)AV^m\cos(\psi)}{2\pi d^{2+m}} < \sqrt{\frac{\sigma_n^2}{P_t^2R_r^2}(2^{\frac{2nT_{out}}{B_{VLC}}}-1)}|N_{VLC}=n\right)\right] \\
&\overset{(b)}{=} \mathbb{E}_{N_{VLC}}\left[P\left(d > \left(\frac{(m+1)AV^m}{2\pi}\sqrt{\frac{P_t^2R_r^2}{\sigma_n^2(2^{\frac{2nT_{out}}{B_{VLC}}}-1)}}\right)^{\frac{1}{m+2}}|N_{VLC}=n\right)\right] \\
&\overset{(c)}{=} \mathbb{E}_{N_{VLC}}\left[P\left(r_v > \sqrt{\left(\frac{(m+1)AV^m}{2\pi}\sqrt{\frac{P_t^2R_r^2}{\sigma_n^2(2^{\frac{2nT_{out}}{B_{VLC}}}-1)}}\right)^{\frac{2}{m+2}} - V^2}|N_{VLC}=n\right)\right] \\
&= \mathbb{E}_{N_{VLC}}\left[1 - F_{r_v|N_{VLC}}\left(\sqrt{\left(\frac{(m+1)AV^m}{2\pi}\sqrt{\frac{P_t^2R_r^2}{\sigma_n^2(2^{\frac{2nT_{out}}{B_{VLC}}}-1)}}\right)^{\frac{2}{m+2}} - V^2}\right)\right] \qquad \text{(A.2)}
\end{aligned}
$$

where (a) follows from the ability of the SDFOV receiver to isolate signals due to its steerability and acquisition capabilities, (b) $\cos(\psi) = 1$ in the tracking receiver and (c) follows from the relation between d and r_v such that $d^2 = r_v^2 + V^2$.

We derive the PDF of r_v as:

$$f_{r_v}(x) = \begin{cases} \frac{2\pi x}{W^2} & 0 < x \le W - x_c \\ \frac{x}{W^2}[2\pi - 4\cos^{-1}(\frac{W-x_c}{x})] & W - x_c < x \le \sqrt{2(W-x_c)^2} \\ \frac{x}{W^2}[\frac{3\pi}{2} - 2\cos^{-1}(\frac{W-x_c}{x})] & \sqrt{2(W-x_c)^2} < x \le x_c \\ \frac{x}{W^2}[\frac{3\pi}{2} - 2\cos^{-1}(\frac{W-x_c}{x}) - 4\cos^{-1}(\frac{xc}{x})] & x_c < x \le \sqrt{x_c^2 + (W-x_c)^2} \\ \frac{x}{W^2}[\frac{\pi}{2} - 2\cos^{-1}(\frac{x_c}{x})] & x > \sqrt{x_c^2 + (W-x_c)^2} \end{cases}$$

As for the derivation of the CDF of r_v:

Using the identity $C(q) \triangleq x^2 \cos^{-1}(\frac{q}{x}) - qx\sqrt{1 - (\frac{q}{x})^2}$

$$F_{r_v}(x) = \begin{cases} \frac{\pi x^2}{W^2} & 0 < x \le W - x_c \\ \frac{1}{W^2}[\pi x^2 - 2C(W-x_c)] & W - x_c < x \le \sqrt{2(W-x_c)^2} \\ \frac{1}{W^2}[\frac{3\pi x^2}{4} - C(W-x_c)] + (\frac{W-x_c}{W})^2 & \sqrt{2(W-x_c)^2} < x \le x_c \\ \frac{1}{W^2}[\frac{3\pi x^2}{4} - C(W-x_c) - 2C(x_c)] + (\frac{W-x_c}{W})^2 & x_c < x \le \sqrt{x_c^2 + (W-x_c)^2} \\ \frac{1}{W^2}[\frac{\pi x^2}{4} - C(x_c)] + (\frac{W-x_c}{W})^2 + \frac{2x_c(W-x_c)}{W^2} & x > \sqrt{x_c^2 + (W-x_c)^2} \end{cases} \tag{A.3}$$

A.3 RF-Only Outage Probability

$$
\begin{aligned}
P_{outage-RF} &= P\left(\frac{B_{RF}}{N_{RF}}\log_2(1+SNR) < T_{out}\right) \\
&= P\left(SNR < 2^{\frac{N_{RF}T_{out}}{B_{RF}}} - 1\right) \\
&= \sum_{n=1}^{\infty} P\left(\frac{|h_{RF}|^2 P_{RF}}{GN_oB_{RF}} < 2^{\frac{2nT_{out}}{B_{RF}}} - 1 | N_{RF} = n\right) P(N_{RF} = n) \\
&\overset{(a)}{=} \mathbb{E}_{d_{RF}}\left[\mathbb{E}_{N_{RF}}\left[P\left(|h_{RF}|^2 < n_o d^{\gamma_{nak}} | N_{RF} = n, d_{RF} = d\right)\right]\right] \\
&= \mathbb{E}_{N_{RF}}\left[\mathbb{E}_{d_{RF}}\left[F_{|h_{RF}|^2|N_{RF}=n,d_{RF}=d}(n_o(d^2)^{\frac{\gamma_{nak}}{2}})\right]\right] \\
&\overset{(b)}{=} \mathbb{E}_{N_{RF}}\left[\int\limits_{V^2}^{r_{RF}^2+V^2} \frac{1}{\Gamma(m_{nak})}\Gamma(m_{nak}, m_{nak}n_o x^{\frac{\gamma_{nak}}{2}})p(x)dx\right] \\
&\overset{(c)}{=} \mathbb{E}_{N_{RF}}\left[\int\limits_{V^2}^{r_{RF}^2+V^2} \frac{1}{r_{RF}^2\Gamma(m_{nak})}\Gamma(m_{nak}, m_{nak}n_o x^{\frac{\gamma_{nak}}{2}})dx\right] \\
&= \mathbb{E}_{N_{RF}}\left[\frac{1}{r_{RF}^2\Gamma(m_{nak})}\left(x\Gamma(m_{nak}, m_{nak}n_o x^{\frac{\gamma_{nak}}{2}}) - \frac{\Gamma(m_{nak}+\frac{2}{\gamma_{nak}}, m_{nak}n_o x^{\frac{\gamma_{nak}}{2}})}{(m_{nak}n_o)^{\frac{2}{\gamma_{nak}}}}\right)_{V^2}^{V^2+r_{RF}^2}\right]
\end{aligned}
\tag{A.4}
$$

where (a) comes from defining $n_o \triangleq \frac{16\pi^2 B_{RF}N_o}{\lambda_c^2 P_{RF}}(2^{\frac{nT_{out}}{B_{RF}}} - 1)$, (b) follows along from knowing the PDF of d^2 which is uniform $p(d^2) = \frac{1}{r_{RF}^2}$ and (c) comes from defining $x = d^2$.

A.4 RF/VLC Hybrid Outage Probability

$$
\begin{aligned}
&P_{Outage-Hybrid} \overset{(a)}{=} P(V_o \cap RF_o|A1)P(A1) + P(V_o|A2)P(A2) \\
&\overset{(b)}{=} P(V_o|A1)P(RF_o|V_o,A1)P(A1) + P(V_o|A2)P(A2) \\
&\overset{(c)}{=} \left[\sum_{n'=1}^{\infty} P(V_o|A1,N_t=n')P(N_t=n') \sum_{n''=1}^{\infty} P(RF_o|V_o,A1,N_{RF}=n'')P(N_{RF}=n'')\right] P(A1) \\
&+ \sum_{n=1}^{\infty} P(V_o|A2,N_{VLC}=n)P(N_{VLC}=n)P(A2) \\
&\overset{(d)}{\approx} \left[\sum_{n'=1}^{\infty} P(V_o|A1,N_t=n')P(N_t=n') \sum_{n''=1}^{\infty} P(RF_o|A1,N_{RF}=n'')P(N_{RF}=n'')\right] P(A1) \\
&+ \sum_{n=1}^{\infty} P(V_o|A2,N_{VLC}=n)P(N_{VLC}=n)P(A2)
\end{aligned} \tag{A.5}
$$

where (a) comes from total probability by partitioning the space, (b) can be achieved by using the lemma $P(A \cap B) = P(A)P(B|A)$, (c) comes from conditioning on the variable in the rate (N_{VLC} for V_o and N_{RF} for RF_o) and finally the approximation (d) is due to assuming that the RF users will be uniform over the area a_1. Uniformity is only true if all the users in a_1 transfer to RF which depends on the realization of the random variable N_t. This is true for some (not all) realizations of N_t. Another implication of non-uniformity, based on some N_t realizations, is that N_t does not split into two Poisson random variables. However we adopt the Poisson approximation for both of these random variables (N_{RF} and N_{VLC}).

Next we derive the CDF of the VLC radius r_v for event $A1$ as well as $A2$, both CDFs depend on the radius of the RF AP. Define $r_{\text{diff}} = \sqrt{(x_{VLC} - x_{RF})^2 + (y_{VLC} - y_{RF})^2}$ as the distance between the two AP centers, where the VLC AP is centered at (x_{VLC}, y_{VLC}) while the RF AP is centered at (x_{RF}, y_{RF}). Define $D^2 \triangleq \frac{1}{r_{\text{diff}}^2}(4r_v^2 r_{\text{diff}}^2 - (r_v^2 - r_{RF}^2 + r_{\text{diff}}^2)^2)$, $C(q) \triangleq x^2 \cos^{-1}(\frac{q}{x}) - qx\sqrt{1-(\frac{q}{x})^2}$ and $x_h \triangleq \sqrt{x_c^2 + (r_{RF} - x_c)^2}$.

First we derive the CDF of r_v given event $A1$, for the r_{RF} cases of interest which allow

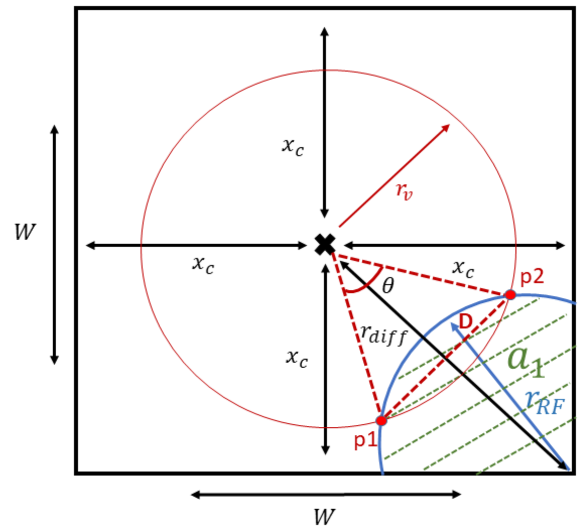

Figure A·1: Hybrid Setup Geometry for event $A1$.

RF connections to be contained within the space:

The following functions are used for both Cases 1 and 2:

$$F_{1,2}(x) \triangleq \int \frac{x}{a_1}\cos^{-1}(1-\frac{D^2}{2x^2})dx$$
$$F_{1,4}(x) \triangleq \frac{1}{a_1}[x^2\cos^{-1}(\frac{x_c}{r_{\text{diff}}}) - C(x_c)]$$

Case 1: $0 < r_{RF} \leq r_{\text{diff}} - x_c$.

$$F_{r_v|A1}(x) = \begin{cases} F_{1,2}(x) & x_c < x \leq x_h \\ F_{1,4}(x) - F_{1,4}(x_h) + F_{1,2}(x_h) & x_h < x \leq r_{\text{diff}} \end{cases} \quad \text{(A.6)}$$

Case 2: $r_{\text{diff}} - x_c < r_{RF} \leq x_c$.

$$F_{r_v|A1}(x) = \begin{cases} F_{1,2}(x) & |r_{\text{diff}} - r_{RF}| < x \leq x_h \\ F_{1,4}(x) - F_{1,4}(x_h) + F_{1,2}(x_h) & x_h < x \leq r_{\text{diff}} \end{cases} \quad \text{(A.7)}$$

Case 3: $x_c < r_{RF} \le r_{\text{diff}}$. Define the following functions:

$$
\begin{aligned}
F_{1,2}(x) &\triangleq \int \frac{x}{a_1} \cos^{-1}(1 - \frac{D^2}{2x^2}) dx \\
F_{1,3}(x) &\triangleq \int \frac{x}{a_1} [\cos^{-1}(1 - \frac{D^2}{2x^2}) - 4\cos^{-1}(\frac{x_c}{x})] dx \\
F_{1,4}(x) &\triangleq \frac{1}{a_1} [x^2 \cos^{-1}(\frac{x_c}{r_{\text{diff}}}) - C(x_c)]
\end{aligned}
$$

$$
F_{r_v|A1}(x) = \begin{cases} F_{1,2}(x) & r_{\text{diff}} - r_{RF} < x \le x_c \\ F_{1,3}(x) + F_{1,2}(x_c) & x_c < x \le x_h \\ F_{1,4}(x) - F_{1,4}(x_h) + F_{1,3}(x_h) + F_{1,2}(x_c) & x_h < x \le r_{\text{diff}} \end{cases} \tag{A.8}
$$

Case 4: $r_{\text{diff}} < r_{RF} \le 2$. We use:

$$
\begin{aligned}
F_{1,1}(x) &\triangleq \frac{\pi x^2}{a_1} \\
F_{1,2}(x) &\triangleq \int \frac{x}{a_1} [2\pi - \cos^{-1}(1 - \frac{D^2}{2x^2})] dx \\
F_{1,3}(x) &\triangleq \int \frac{x}{a_1} [2\pi - \cos^{-1}(1 - \frac{D^2}{2x^2}) - 4\cos^{-1}(\frac{x_c}{x})] dx \\
F_{1,4}(x) &\triangleq \frac{1}{a_1} [x^2 \cos^{-1}(\frac{x_c}{r_{\text{diff}}}) - C(x_c)]
\end{aligned}
$$

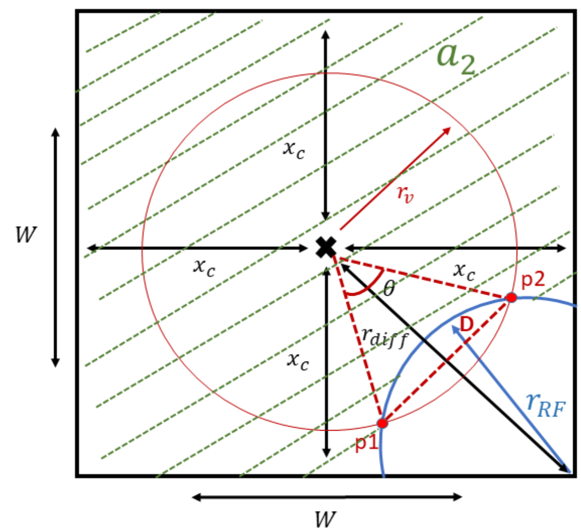

Figure A·2: Hybrid Setup Geometry for event $A2$.

$$F_{r_v|A1}(x) = \begin{cases} F_{1,1}(x) & 0 < x \leq r_{RF} - r_{\text{diff}} \\ F_{1,2}(x) + F_{1,1}(r_{RF} - r_{\text{diff}}) & r_{RF} - r_{\text{diff}} < x \leq x_c \\ F_{1,3}(x) + F_{1,2}(x_c) + F_{1,1}(r_{RF} - r_{\text{diff}}) & x_c < x \leq x_h \\ F_{1,4}(x) - F_{1,4}(x_h) + F_{1,3}(x_h) + F_{1,2}(x_c) + F_{1,1}(r_{RF} - r_{\text{diff}}) & x_h < x \leq r_{\text{diff}} \end{cases} \tag{A.9}$$

Second, we derive the conditional CDF of r_v for event $A2$:

Case 1: $0 < r_{RF} \leq r_{\text{diff}} - x_c$. Define the following functions:

$$F_{2,1}(x) \triangleq \frac{\pi x^2}{a_2}$$

$$F_{2,3}(x) \triangleq \int \frac{x}{a_2}[\cos^{-1}(1 - \frac{D^2}{2x^2}) - 4\cos^{-1}(\frac{x_c}{x})]dx$$

$$F_{2,4}(x) \triangleq \frac{3}{a_2}[x^2 \cos^{-1}(\frac{x_c}{r_{\text{diff}}}) - C(x_c)]$$

$$F_{r_v|A2}(x) = \begin{cases} F_{2,1}(x) & 0 < x \le x_c \\ F_{2,3}(x) + F_{2,1}(x_c) & x_c < x \le x_h \\ F_{2,4}(x) - F_{2,4}(x_h) + F_{2,3}(x_h) + F_{2,1}(x_c) & x_h < x \le r_{\text{diff}} \end{cases} \tag{A.10}$$

Case 2: $r_{\text{diff}} - x_c < r_{RF} \le x_c$. We define the following functions:

$$\begin{aligned} F_{2,1}(x) &\triangleq \frac{\pi x^2}{a_2} \\ F_{2,2}(x) &\triangleq \int \frac{x}{a_2}[2\pi - \cos^{-1}(1 - \frac{D^2}{2x^2})]dx \\ F_{2,3}(x) &\triangleq \int \frac{x}{a_2}[2\pi - \cos^{-1}(1 - \frac{D^2}{2x^2}) - 8\cos^{-1}(\frac{x_c}{x})]dx \\ F_{2,4}(x) &\triangleq \frac{3}{a_2}[x^2 \cos^{-1}(\frac{x_c}{r_{\text{diff}}}) - C(x_c)] \end{aligned}$$

$$F_{r_v|A2}(x) = \begin{cases} F_{2,1}(x) & 0 < x \le |r_{\text{diff}} - r_{RF}| \\ F_{2,2}(x) + F_{2,1}(|r_{\text{diff}} - r_{RF}|) & |r_{\text{diff}} - r_{RF}| < x \le x_c \\ F_{2,3}(x) + F_{2,2}(x_c) + F_{2,1}(|r_{\text{diff}} - r_{RF}|) & x_c < x \le x_h \\ F_{2,4}(x) - F_{2,4}(x_h) + F_{2,3}(x_h) + F_{2,2}(x_c) + F_{2,1}(|r_{\text{diff}} - r_{RF}|) & x_h < x \le r_{\text{diff}} \end{cases} \tag{A.11}$$

Case 3: $x_c < r_{RF} \leq r_{\text{diff}}$. The functions needed are:

$$
\begin{aligned}
F_{2,1}(x) &\triangleq \frac{\pi x^2}{a_2} \\
F_{2,2}(x) &\triangleq \int \frac{x}{a_2}[2\pi - \cos^{-1}(1-\frac{D^2}{2x^2})]dx \\
F_{2,3}(x) &\triangleq \int \frac{x}{a_2}[2\pi - \cos^{-1}(1-\frac{D^2}{2x^2}) - 4\cos^{-1}(\frac{x_c}{x})]dx \\
F_{2,4}(x) &\triangleq \frac{3}{a_2}[x^2\cos^{-1}(\frac{x_c}{r_{\text{diff}}}) - C(x_c)]
\end{aligned}
$$

$$
F_{r_v|A2}(x) = \begin{cases} F_{2,1}(x) & 0 < x \leq r_{\text{diff}} - r_{RF} \\ F_{2,2}(x) + F_{2,1}(r_{\text{diff}} - r_{RF}) & r_{\text{diff}} - r_{RF} < x \leq x_c \\ F_{2,3}(x) + F_{2,2}(x_c) + F_{2,1}(r_{\text{diff}} - r_{RF}) & x_c < x \leq x_h \\ F_{2,4}(x) - F_{2,4}(x_h) + F_{2,3}(x_h) + F_{2,2}(x_c) + F_{2,1}(r_{\text{diff}} - r_{RF}) & x_h < x \leq r_{\text{diff}} \end{cases} \tag{A.12}
$$

Case 4: $r_{\text{diff}} < r_{RF} \leq 2$. We define the following functions:

$$
\begin{aligned}
F_{2,2}(x) &\triangleq \int \frac{x}{a_2}[\cos^{-1}(1-\frac{D^2}{2x^2})]dx \\
F_{2,3}(x) &\triangleq \int \frac{x}{a_2}[\cos^{-1}(1-\frac{D^2}{2x^2}) - 4\cos^{-1}(\frac{x_c}{x})]dx \\
F_{2,4}(x) &\triangleq \frac{3}{a_2}[x^2\cos^{-1}(\frac{x_c}{r_{\text{diff}}}) - C(x_c)]
\end{aligned}
$$

$$F_{r_v|A2}(x) = \begin{cases} F_{2,2}(x) & r_{RF} - r_{\text{diff}} < x \leq x_c \\ F_{2,3}(x) + F_{2,2}(x_c) & x_c < x \leq x_h \\ F_{2,4}(x) - F_{2,4}(x_h) + F_{2,3}(x_h) + F_{2,2}(x_c) & x_h < x \leq r_{\text{diff}} \end{cases} \tag{A.13}$$

References

Abdalla, I., Rahaim, M. B., and Little, T. D. C. (2018). Impact of receiver FOV and orientation on dense optical networks. In *Proceedings of the 2018 IEEE Global Communications Conference (GLOBECOM)*, pages 1–6.

Abdalla, I., Rahaim, M. B., and Little, T. D. C. (2019a). Dynamic FOV tracking receiver for dense optical wireless networks. In *Proceedings of the 2019 IEEE Global Communications Conference (GLOBECOM)*, pages 1–6.

Abdalla, I., Rahaim, M. B., and Little, T. D. C. (2019b). Dynamic FOV visible light communications receiver for dense optical networks. *IET Communications*, 13(7):822–830.

Abdalla, I., Rahaim, M. B., and Little, T. D. C. (2019c). Investigation of outage probability and AP placement for mobile users in indoor VLC system design. In *Proceedings of the 2019 IEEE Wireless Communications and Networking Conference (WCNC)*, pages 1–6.

Abdalla, I., Rahaim, M. B., and Little, T. D. C. (2020a). Illuminance constrained emission pattern optimization in indoor VLC networks. In *Proceedings of the 2020 IEEE Global Communications Conference Workshops (GC Wkshps)*, pages 1–7.

Abdalla, I., Rahaim, M. B., and Little, T. D. C. (2020b). Interference in multi-user optical wireless communications systems. *Philosophical Transactions of the Royal Society A*, 378(2169):20190190.

Abdalla, I., Rahaim, M. B., and Little, T. D. C. (2020c). Interference mitigation through user association and receiver field of view optimization in a multi-user indoor hybrid RF/VLC illuminance-constrained network. *IEEE Access*, 8:228779–228797.

Abdalla, I., Rahaim, M. B., and Little, T. D. C. (2020d). On the importance of dynamic FOV receivers for dense indoor optical wireless networks. In *Proceedings of the 2020 IEEE International Conference on Communications (ICC)*, pages 1–6.

Adiono, T. and Fuada, S. (2017). Optical interference noise filtering over visible light communication system utilizing analog high-pass filter circuit. In *Proceedings of the 2017 International Symposium on Nonlinear Theory and Its Applications*, pages 616–619.

Adnan-Qidan, A., Morales Céspedes, M., and García Armada, A. (2019). User-centric blind interference alignment design for visible light communications. *IEEE Access*, 7:21220–21234.

Alouini, M. . and Goldsmith, A. (1997). Area spectral efficiency of cellular mobile radio systems. In *1997 IEEE 47th Vehicular Technology Conference. Technology in Motion*, volume 2, pages 652–656.

Ayyash, M., Elgala, H., Khreishah, A., Jungnickel, V., Little, T. D. C., Shao, S., Rahaim, M., Schulz, D., Hilt, J., and Freund, R. (2016). Coexistence of WiFi and LiFi toward 5G: concepts, opportunities, and challenges. *IEEE Communications Magazine*, 54(2):64–71.

Bababekova, Y., Rosenfield, M., Hue, J. E., and Huang, R. R. (2011). Font size and viewing distance of handheld smart phones. *Optometry and Vision Science*, 88(7):795–797.

Bai, R., Tian, H., Fan, B., and Liang, S. (2015). Coordinated transmission based interference mitigation in VLC network. In *2015 IEEE 82nd Vehicular Technology Conference (VTC2015-Fall)*, pages 1–5.

Bao, X., Yu, G., Dai, J., and Zhu, X. (2015). Li-Fi: Light fidelity-a survey. *Wireless Networks*, 21(6):1879–1889.

Bas, C. L., Sahuguede, S., Julien-Vergonjanne, A., Behlouli, A., Combeau, P., and Aveneau, L. (2015). Impact of receiver orientation and position on visible light communication link performance. In *2015 4th International Workshop on Optical Wireless Communications (IWOW)*, pages 1–5.

Bell, A. G. (1880). The photophone. *Science*, 1(11):130–134.

Bertsimas, D. and Tsitsiklis, J. N. (1997). *Introduction to linear optimization*, volume 6. Athena Scientific Belmont, MA.

Biagi, M., Vegni, A. M., Pergoloni, S., Butala, P. M., and Little, T. D. C. (2015). Trace-orthogonal PPM-space time block coding under rate constraints for visible light communication. *Journal of Lightwave Technology*, 33(2):481–494.

Butala, P. M., Elgala, H., Little, T. D. C., and Zarkesh-Ha, P. (2014). Multi-wavelength visible light communication system design. In *2014 IEEE Globecom Workshops (GC Wkshps)*, pages 530–535.

Cadambe, V. R. and Jafar, S. A. (2008). Interference alignment and spatial degrees of freedom for the K user interference channel. In *2008 IEEE International Conference on Communications*, pages 971–975.

Calvanese Strinati, E., Barbarossa, S., Gonzalez-Jimenez, J. L., Ktenas, D., Cassiau, N., Maret, L., and Dehos, C. (2019). 6G: The next frontier: From holographic messaging to artificial intelligence using subterahertz and visible light communication. *IEEE Vehicular Technology Magazine*, 14(3):42–50.

Carruthers, J. B. and Kahn, J. M. (1998). Angle diversity for nondirected wireless infrared communication. In *ICC '98. 1998 IEEE International Conference on Communications. Conference Record. Affiliated with SUPERCOMM'98 (Cat. No.98CH36220)*, volume 3, pages 1665–1670.

Cebula III, S. L., Ahmad, A., Graham, J. M., Hinds, C. V., Wahsheh, L. A., Williams, A. T., and DeLoatch, S. J. (2011). Empirical channel model for 2.4 GHz IEEE 802.11 WLAN. In *Proceedings of the International Conference on Wireless Networks (ICWN)*, pages 1–5. Citeseer.

Chang, C., Su, Y., Kurokawa, U., and Choi, B. I. (2012). Interference rejection using filter-based sensor array in VLC systems. *IEEE Sensors Journal*, 12(5):1025–1032.

Chau, J. C., Morales, C., and Little, T. D. (2016). Using spatial light modulators in MIMO visible light communication receivers to dynamically control the optical channel. In *Proceedings of the 2016 International Conference on Embedded Wireless Systems and Networks*, EWSN '16, pages 347–352, USA. Junction Publishing.

Chen, C., Serafimovski, N., and Haas, H. (2013a). Fractional frequency reuse in optical wireless cellular networks. In *2013 IEEE 24th Annual International Symposium on Personal, Indoor, and Mobile Radio Communications (PIMRC)*, pages 3594–3598.

Chen, C., Tsonev, D., and Haas, H. (2013b). Joint transmission in indoor visible light communication downlink cellular networks. In *2013 IEEE Globecom Workshops (GC Wkshps)*, pages 1127–1132.

Chen, C., Zhong, W., Yang, H., and Du, P. (2018). On the performance of MIMO-NOMA-based visible light communication systems. *IEEE Photonics Technology Letters*, 30(4):307–310.

Chen, C., Zhong, W., Yang, H., Du, P., and Yang, Y. (2019). Flexible-rate SIC-Free NOMA for downlink VLC based on constellation partitioning coding. *IEEE Wireless Communications Letters*, 8(2):568–571.

Chen, C., Zhong, W.-D., Yang, H., Zhang, S., and Du, P. (2018). Reduction of SINR fluctuation in indoor multi-cell VLC systems using optimized angle diversity receiver. *Journal of Lightwave Technology*, 36(17):3603–3610.

Chen, Z., Serafimovski, N., and Haas, H. (2014a). Angle diversity for an indoor cellular visible light communication system. In *2014 IEEE 79th Vehicular Technology Conference (VTC Spring)*, pages 1–5.

Chen, Z., Tsonev, D., and Haas, H. (2014b). Improving SINR in indoor cellular visible light communication networks. In *2014 IEEE International Conference on Communications (ICC)*, pages 3383–3388.

Cincotta, S., He, C., Neild, A., and Armstrong, J. (2018). High angular resolution visible light positioning using a quadrant photodiode angular diversity aperture receiver (QADA). *Optics Express*, 26(7):9230–9242.

Cisco (2020). Cisco visual networking index: global mobile data traffic forecast update, 2018–2023. `https://www.cisco.com/c/en/us/solutions/collateral/executive-perspectives/annual-internet-report/white-paper-c11-741490.html`. Accessed: 2020-12-30.

Cisco (2021). Global 2021 forecast highlights. `https://www.cisco.com/c/dam/m/en_us/solutions/service-provider/vni-forecast-highlights/pdf/Global_2021_Forecast_Highlights.pdf`. Accessed: 2020-12-30.

Cui, K., Quan, J., and Xu, Z. (2013). Performance of indoor optical femtocell by visible light communication. *Optics Communications*, 298-299:59 – 66.

Dehghani Soltani, M., Purwita, A. A., Tavakkolnia, I., Haas, H., and Safari, M. (2019). Impact of device orientation on error performance of LiFi systems. *IEEE Access*, 7:41690–41701.

Dehghani Soltani, M., Wu, X., Safari, M., and Haas, H. (2016). Access point selection in Li-Fi cellular networks with arbitrary receiver orientation. In *2016 IEEE 27th Annual International Symposium on Personal, Indoor, and Mobile Radio Communications (PIMRC)*, pages 1–6.

Elgala, H., Mesleh, R., and Haas, H. (2011). Indoor optical wireless communication: potential and state-of-the-art. *IEEE Communications Magazine*, 49(9):56–62.

Emmelmann, M. (2005). Influence of velocity on the handover delay associated with a radio-signal-measurement-based handover decision. In *VTC-2005-Fall. 2005 IEEE 62nd Vehicular Technology Conference, 2005.*, volume 4, pages 2282–2286.

Eroğlu, Y. S., Yapıcı, Y., and Güvenç, İ. (2019). Impact of random receiver orientation on visible light communications channel. *IEEE Transactions on Communications*, 67(2):1313–1325.

Ettus Research (2020). Ettus research - the leader in software defined radio (SDR). `https://www.ettus.com/`. Accessed: 2017-09-30.

Fryar, C. D., Kruszan-Moran, D., Gu, Q., and Ogden, C. L. (2018). Mean body weight, weight, waist circumference, and body mass index among adults: United states, 1999–2000 through 2015–2016. `https://stacks.cdc.gov/view/cdc/61430`. Accessed: 2019-07-1.

Ghimire, B. and Haas, H. (2012). Self-organising interference coordination in optical wireless networks. *EURASIP Journal on Wireless Communications and Networking*, 2012(1):131.

GNU Radio (2020). GNU radio - the free & open source radio ecosystem. `https://gnuradio.org/`. Accessed: 2016-09-30.

Guan, X., Yang, Q., and Chan, C. (2017). Joint detection of visible light communication signals under non-orthogonal multiple access. *IEEE Photonics Technology Letters*, 29(4):377–380.

Guo, W., Wang, S., and Chu, X. (2013). Capacity expression and power allocation for arbitrary modulation and coding rates. In *2013 IEEE Wireless Communications and Networking Conference (WCNC)*, pages 3294–3299. IEEE.

Hammouda, M., Vegni, A. M., Haas, H., and Peissig, J. (2018). Resource allocation and interference management in OFDMA-based VLC networks. *Physical Communication*, 31:169 – 180.

Hong, Y., Chen, J., Wang, Z., and Yu, C. (2013). Performance of a precoding MIMO system for decentralized multiuser indoor visible light communications. *IEEE Photonics Journal*, 5(4):7800211–7800211.

In Hwan Park, Kim, Y. H., and Kim, J. Y. (2012). Interference mitigation scheme of visible light communication systems for aircraft wireless applications. In *2012 IEEE International Conference on Consumer Electronics (ICCE)*, pages 355–356.

Islam, S. M. R., Avazov, N., Dobre, O. A., and Kwak, K. (2017). Power-domain non-orthogonal multiple access (NOMA) in 5G systems: Potentials and challenges. *IEEE Communications Surveys Tutorials*, 19(2):721–742.

Jafar, S. A. (2012). Blind interference alignment. *IEEE Journal of Selected Topics in Signal Processing*, 6(3):216–227.

Jian-Hui Liu, Q. L. and Zhang, X.-Y. (2014). Cellular coverage optimization for indoor visible light communication and illumination networks. *Journal of Communications*, 9(11):891–898.

Jung, S.-Y., Kwon, D.-H., Yang, S.-H., and Han, S.-K. (2016). Inter-cell interference mitigation in multi-cellular visible light communications. *Optics Express*, 24(8):8512–8526.

Kahn, J. M. and Barry, J. R. (1997). Wireless infrared communications. *Proceedings of the IEEE*, 85(2):265–298.

Karunatilaka, D., Zafar, F., Kalavally, V., and Parthiban, R. (2015). LED based indoor visible light communications: State of the art. *IEEE Communications Surveys Tutorials*, 17(3):1649–1678.

Kashef, M., Abdallah, M., Qaraqe, K., Haas, H., and Uysal, M. (2015). Coordinated interference management for visible light communication systems. *Journal of Optical Communications and Networking*, 7(11):1098–1108.

Kashef, M., Ismail, M., Abdallah, M., Qaraqe, K. A., and Serpedin, E. (2016). Energy efficient resource allocation for mixed RF/VLC heterogeneous wireless networks. *IEEE Journal on Selected Areas in Communications*, 34(4):883–893.

Kim, H., Kim, D., Yang, S., Son, Y., and Han, S. (2012). Mitigation of inter-cell interference utilizing carrier allocation in visible light communication system. *IEEE Communications Letters*, 16(4):526–529.

Kizilirmak, R. C., Rowell, C. R., and Uysal, M. (2015). Non-orthogonal multiple access (NOMA) for indoor visible light communications. In *2015 4th International Workshop on Optical Wireless Communications (IWOW)*, pages 98–101.

Komine, T. and Nakagawa, M. (2004). Fundamental analysis for visible-light communication system using LED lights. *IEEE Transactions on Consumer Electronics*, 50(1):100–107.

Li, B., Wang, J., Zhang, R., Shen, H., Zhao, C., and Hanzo, L. (2015a). Multiuser MISO transceiver design for indoor downlink visible light communication under per-LED optical power constraints. *IEEE Photonics Journal*, 7(4):1–15.

Li, L., Zhang, Y., Fan, B., and Tian, H. (2016). Mobility-aware load balancing scheme in hybrid VLC-LTE networks. *IEEE Communications Letters*, 20(11):2276–2279.

Li, X., Jin, F., Zhang, R., Wang, J., Xu, Z., and Hanzo, L. (2016). Users first: User-centric cluster formation for interference-mitigation in visible-light networks. *IEEE Transactions on Wireless Communications*, 15(1):39–53.

Li, X., Zhang, R., and Hanzo, L. (2015b). Cooperative load balancing in hybrid visible light communications and WiFi. *IEEE Transactions on Communications*, 63(4):1319–1329.

Li, X., Zhang, R., and Hanzo, L. (2015). Cooperative load balancing in hybrid visible light communications and WiFi. *IEEE Transactions on Communications*, 63(4):1319–1329.

Li, Z., Shao, S., Khreishah, A., Ayyash, M., Abdalla, I., Elgala, H., Rahaim, M., and Little, T. D. C. (2018). Design and implementation of a hybrid RF-VLC system with bandwidth aggregation. In *2018 14th International Wireless Communications & Mobile Computing Conference (IWCMC)*, pages 194–200. IEEE.

Lian, J. and Brandt-Pearce, M. (2017). Multiuser MIMO indoor visible light communication system using spatial multiplexing. *Journal of Lightwave Technology*, 35(23):5024–5033.

Little, T. D. C., Rahaim, M. B., Abdalla, I., Lam, E. W., Mcallister, R., and Vegni, A. M. (2018). A multi-cell lighting testbed for VLC and VLP. In *2018 Global LIFI Congress (GLC)*, pages 1–6.

Liu, Y. F., Yeh, C. H., Chow, C. W., Liu, Y., Liu, Y. L., and Tsang, H. K. (2012). Demonstration of bi-directional LED visible light communication using TDD traffic with mitigation of reflection interference. *Optics Express*, 20(21):23019–23024.

Ma, H., Lampe, L., and Hranilovic, S. (2013). Robust MMSE linear precoding for visible light communication broadcasting systems. In *2013 IEEE Globecom Workshops (GC Wkshps)*, pages 1081–1086.

Ma, H., Mostafa, A., Lampe, L., and Hranilovic, S. (2018). Coordinated beamforming for downlink visible light communication networks. *IEEE Transactions on Communications*, 66(8):3571–3582.

Marsh, G. W. and Kahn, J. M. (1997). Channel reuse strategies for indoor infrared wireless communications. *IEEE Transactions on Communications*, 45(10):1280–1290.

Marshoud, H., Kapinas, V. M., Karagiannidis, G. K., and Muhaidat, S. (2016). Non-orthogonal multiple access for visible light communications. *IEEE Photonics Technology Letters*, 28(1):51–54.

Marshoud, H., Muhaidat, S., Sofotasios, P. C., Hussain, S., Imran, M. A., and Sharif, B. S. (2018). Optical non-orthogonal multiple access for visible light communication. *IEEE Wireless Communications*, 25(2):82–88.

Marshoud, H., Sofotasios, P. C., Muhaidat, S., Karagiannidis, G. K., and Sharif, B. S. (2017). On the performance of visible light communication systems with non-orthogonal multiple access. *IEEE Transactions on Wireless Communications*, 16(10):6350–6364.

Marzetta, T. L., Larsson, E. G., Yang, H., and Ngo, H. Q. (2016). *Fundamentals of Massive MIMO, Preface*. Cambridge University Press.

Masini, B. M., Bazzi, A., and Zanella, A. (2018). Vehicular visible light networks for urban mobile crowd sensing. *Sensors*, 18(4):1177.

Mondal, R. K., Chowdhury, M. Z., Saha, N., and Jang, Y. M. (2012). Interference-aware optical resource allocation in visible light communication. In *2012 International Conference on ICT Convergence (ICTC)*, pages 155–158.

Ntogari, G., Kamalakis, T., and Sphicopoulos, T. (2009). Performance analysis of space time block coding techniques for indoor optical wireless systems. *IEEE Journal on Selected Areas in Communications*, 27(9):1545–1552.

Obeed, M., Salhab, A. M., Zummo, S. A., and Alouini, M.-S. (2018). Joint optimization of power allocation and load balancing for hybrid VLC/RF networks. *Journal of Optical Communications and Networking*, 10(5):553–562.

O'Brien, D. C. (2019). Beamsteering for ultra-high data-rate optical wireless communications. In *Broadband Access Communication Technologies XIII*, volume 10945, page 109450J. International Society for Optics and Photonics.

OptiTrack (2021). Optitrack - motion capture systems. `https://optitrack.com/`. Accessed: 2017-04-30.

Pew Research Center (2019). Smartphone ownership in advanced economies higher than in emerging. `https://www.pewresearch.org/global/2019/02/05/smartphone-ownership-is-growing-rapidly-around-the-world-but-not-always-equally/pg_global-technology-use-2018_2019-02-05_0-01/`. Accessed: 2020-12-30.

Pham, T. V., Le Minh, H., Ghassemlooy, Z., Hayashi, T., and Pham, A. T. (2015). Sum-rate maximization of multi-user MIMO visible light communications. In *2015 IEEE International Conference on Communication Workshop (ICCW)*, pages 1344–1349.

Pham, T. V., Le-Minh, H., and Pham, A. T. (2017). Multi-user visible light communication broadcast channels with zero-forcing precoding. *IEEE Transactions on Communications*, 65(6):2509–2521.

Philips (2014). Philips office lighting. `http://images.philips.com/is/content/PhilipsConsumer/PDFDownloads/Global/ODLI20150723_001-UPD-en_AA-Lighting-for-BREEAM-in-offices.pdf`. Accessed: 2019-09-30.

Prince, G. B. and Little, T. D. C. (2010). On the performance gains of cooperative transmission concepts in intensity modulated direct detection visible light communication networks. In *2010 6th International Conference on Wireless and Mobile Communications*, pages 297–302.

Rae, M. S. (2000). *The IESNA Lighting Handbook–Reference and Application, Illuminating Society of North America*. IESNA Publications Department, New York.

Rahaim, M. (2015). Heterogeneous integration of optical wireless communications within next generation networks. `https://open.bu.edu/handle/2144/13681`. PhD dissertation, Boston University.

Rahaim, M., Abdalla, I., Ayyash, M., Elgala, H., Khreishah, A., and Little, T. D. C. (2019). Welcome to the crowd: Design decisions for coexisting radio and optical wireless deployments. *IEEE Network*, 33(5):174–182.

Rahaim, M. and Little, T. D. C. (2013). SINR analysis and cell zooming with constant illumination for indoor VLC networks. In *2013 2nd International Workshop on Optical Wireless Communications (IWOW)*, pages 20–24.

Rahaim, M. and Little, T. D. C. (2015). Optical interference analysis in visible light communication networks. In *2015 IEEE International Conference on Communication Workshop (ICCW)*, pages 1410–1415.

Rahaim, M. and Little, T. D. C. (2016). Bounding SINR with the constraints of an optical wireless channel. In *2016 IEEE International Conference on Communications Workshops (ICC)*, pages 417–422.

Rahaim, M. and Little, T. D. C. (2017). Interference in IM/DD optical wireless communication networks. *IEEE/OSA Journal of Optical Communications and Networking*, 9(9):D51–D63.

Rahaim, M. B., Borogovac, T., and Carruthers, J. B. (2010). Candles: Communication and lighting emulation software. In *Proceedings of the Fifth ACM International Workshop on Wireless Network Testbeds, Experimental Evaluation and Characterization*, WiNTECH '10, pages 9–14, New York, NY, USA. ACM.

Rahaim, M. B. and Little, T. D. C. (2015). Toward practical integration of dual-use VLC within 5G networks. *IEEE Wireless Communications*, 22(4):97–103.

Rahaim, M. B., Morrison, J., and Little, T. D. C. (2017). Beam control for indoor FSO and dynamic dual-use VLC lighting systems. *Journal of Communications and Information Networks*, 2(4):11–27.

Rahaim, M. B., Vegni, A. M., and Little, T. D. C. (2011). A hybrid radio frequency and broadcast visible light communication system. In *2011 IEEE GLOBECOM Workshops (GC Wkshps)*, pages 792–796.

Raj, R., Jaiswal, S., and Dixit, A. (2019). Optimization of LED semi-angle in multipath indoor visible light communication links. In *2019 IEEE International Conference on Advanced Networks and Telecommunications Systems (ANTS)*, pages 1–6.

Ramirez-Iniguez, R., Idrus, S., and Sun, Z. (2008). *Optical Wireless Communications*. New York: Auerbach Publications.

Rappaport, T. S. et al. (1996). *Wireless communications: principles and practice*, volume 2. Prentice hall PTR New Jersey.

Richman, E. E. (2015). Requirements for lighting levels. http://www.lumitronlighting.com/lighting_nowledge/LUX%20LEVEL_usace_Requirements%20for%20Lighting%20Levels.pdf,. Pacific Northwest National Laboratory. Accessed: 2019-05-30.

Ryoo, H., Kwon, D., Yang, S., and Han, S. (2016). Differential optical detection in VLC for inter-cell interference reduced flexible cell planning. *IEEE Photonics Technology Letters*, 28(23):2728–2731.

S. O'Dea (2020). Global smartphone shipments forecast 2010-2023. https://www.statista.com/statistics/263441/global-smartphone-shipments-forecast/#statisticContainer. Accessed: 2020-12-30.

Saad, W., Bennis, M., and Chen, M. (2020). A vision of 6G wireless systems: Applications, trends, technologies, and open research problems. *IEEE Network*, 34(3):134–142.

Sarris, J. and Nix, A. R. (2007). Ricean K-factor measurements in a home and an office environment in the 60 GHz band. In *2007 16th IST Mobile and Wireless Communications Summit*, pages 1–5. IEEE.

Shao, S., Khreishah, A., Rahaim, M. B., Elgala, H., Ayyash, M., Little, T. D. C., and Wu, J. (2014). An indoor hybrid WiFi-VLC internet access system. In *2014 IEEE 11th International Conference on Mobile Ad Hoc and Sensor Systems*, pages 569–574. IEEE.

Shashikant, Saini, R., and Gupta, A. (2017). Comparative analysis of coverage aspects for various LEDs placement schemes in indoor VLC system. In *2017 2nd International Conference for Convergence in Technology (I2CT)*, pages 487–491.

Shi, J., Wang, Y., Huang, X., Tao, L., and Chi, N. (2015). Enhanced performance using stbc aided coding for LED-based multiple input single output visible light communication network. *Microwave and Optical Technology Letters*, 57(12):2943–2946.

Simon, M. K. and Alouini, M.-S. (2005). *Digital communication over fading channels*, volume 95. John Wiley & Sons.

Stefan, I. and Haas, H. (2013). Analysis of optimal placement of LED arrays for visible light communication. In *2013 IEEE 77th Vehicular Technology Conference (VTC Spring)*, pages 1–5.

Strinati, E. C., Barbarossa, S., Gonzalez-Jimenez, J. L., Ktenas, D., Cassiau, N., Maret, L., and Dehos, C. (2019). 6G: The next frontier: From holographic messaging to artificial intelligence using subterahertz and visible light communication. *IEEE Vehicular Technology Magazine*, 14(3):42–50.

Tariq, F., Khandaker, M. R., Wong, K.-K., Imran, M. A., Bennis, M., and Debbah, M. (2020). A speculative study on 6G. *IEEE Wireless Communications*, 27(4):118–125.

Tarokh, V., Jafarkhani, H., and Calderbank, A. R. (1999). Space-time block coding for wireless communications: performance results. *IEEE Journal on Selected Areas in Communications*, 17(3):451–460.

ThorLabs Inc (2013). Thorlabs apd110x/120x operation manual 2013. https://www.thorlabs.com/drawings/89ac670f41e9e49c-064F6EAA-06CC-A669-59290195870DFE39/APD120A2-Manual.pdf. Accessed: 2017-08-01.

Valagiannopoulos, C., Tsiftsis, T. A., and Kovanis, V. (2019). Metasurface-enabled interference suppression at visible-light communications. *arXiv preprint arXiv:1904.08858*.

Vavoulas, A., Sandalidis, H. G., Tsiftsis, T. A., and Vaiopoulos, N. (2015). Coverage aspects of indoor VLC networks. *Journal of Lightwave Technology*, 33(23):4915–4921.

Vegni, A. M. and Biagi, M. (2019). Optimal LED placement in indoor VLC networks. *Optics Express*, 27(6):8504–8519.

Vegni, A. M. and Little, T. D. C. (2012). Handover in VLC systems with cooperating mobile devices. In *2012 International Conference on Computing, Networking and Communications (ICNC)*, pages 126–130.

Wang, Q., Wang, Z., and Dai, L. (2015). Multiuser MIMO-OFDM for visible light communications. *IEEE Photonics Journal*, 7(6):1–11.

Wang, Y., Wu, X., and Haas, H. (2017). Load balancing game with shadowing effect for indoor hybrid LiFi/RF networks. *IEEE Transactions on Wireless Communications*, 16(4):2366–2378.

Wang, Z., Yu, C., Zhong, W.-D., Chen, J., and Chen, W. (2012). Performance of a novel LED lamp arrangement to reduce SNR fluctuation for multi-user visible light communication systems. *Optics Express*, 20(4):4564–4573.

Wang, Z.-Y., Yu, H.-Y., and Wang, D.-M. (2018). Energy efficient transceiver design for NOMA VLC downlinks with finite-alphabet inputs. *Applied Sciences*, 8(10).

Wikipedia (2020a). Human head. https://en.wikipedia.org/wiki/Human_head. Accessed: 2019-07-1.

Wikipedia (2020b). Law of cosines. https://en.wikipedia.org/wiki/Law_of_cosines. Accessed: 2018-09-1.

Wu, D., Ghassemlooy, Z., Le Minh, H., Rajbhandari, S., Khalighi, M. A., and Tang, X. (2012). Optimisation of lambertian order for indoor non-directed optical wireless communication. In *2012 1st IEEE International Conference on Communications in China Workshops (ICCC)*, pages 43–48.

Wu, D., Ghassemlooy, Z., Zhong, W.-D., Khalighi, M.-A., Minh, H. L., Chen, C., Zvanovec, S., and Boucouvalas, A. C. (2016). Effect of optimal Lambertian order for cellular indoor optical wireless communication and positioning systems. *Optical Engineering*, 55(6):1 – 8.

Wu, L., Zhang, Z., Dang, J., and Liu, H. (2017). Blind interference alignment for multiuser MISO indoor visible light communications. *IEEE Communications Letters*, 21(5):1039–1042.

Wu, X. and Haas, H. (2017). Access point assignment in hybrid LiFi and WiFi networks in consideration of LiFi channel blockage. In *2017 IEEE 18th international workshop on signal processing advances in wireless communications (SPAWC)*, pages 1–5. IEEE.

Wu, X. and Haas, H. (2019). Handover skipping for LiFi. *IEEE Access*, 7:38369–38378.

Wu, Y., Yang, A., Feng, L., Zuo, L., and nan Sun, Y. (2012). Modulation based cells distribution for visible light communication. *Optics Express*, 20(22):24196–24208.

Yang, Z., Xu, W., and Li, Y. (2017). Fair non-orthogonal multiple access for visible light communication downlinks. *IEEE Wireless Communications Letters*, 6(1):66–69.

Yin, L., Islim, M. S., and Haas, H. (2017). LiFi: transforming fibre into wireless. In *Broadband Access Communication Technologies XI*, volume 10128, page 1012802. International Society for Optics and Photonics.

Yin, L., Popoola, W. O., Wu, X., and Haas, H. (2016). Performance evaluation of non-orthogonal multiple access in visible light communication. *IEEE Transactions on Communications*, 64(12):5162–5175.

Yin, L., Wu, X., and Haas, H. (2015). On the performance of non-orthogonal multiple access in visible light communication. In *2015 IEEE 26th Annual International Symposium on Personal, Indoor, and Mobile Radio Communications (PIMRC)*, pages 1354–1359.

Yu, Z., Baxley, R. J., and Zhou, G. T. (2013). Multi-user MISO broadcasting for indoor visible light communication. In *2013 IEEE International Conference on Acoustics, Speech and Signal Processing*, pages 4849–4853.

Zabini, F., Bazzi, A., Masini, B. M., and Verdone, R. (2017). Optimal performance versus fairness tradeoff for resource allocation in wireless systems. *IEEE Transactions on Wireless Communications*, 16(4):2587–2600.

Zhang, R., Cui, Y., Claussen, H., Haas, H., and Hanzo, L. (2018). Anticipatory association for indoor visible light communications: Light, follow me! *IEEE Transactions on Wireless Communications*, 17(4):2499–2510.

Zhang, X., Gao, Q., Gong, C., and Xu, Z. (2016). User grouping and power allocation for NOMA visible light communication multi-cell networks. *IEEE communications letters*, 21(4):777–780.

Zhou, K., Gong, C., and Xu, Z. (2017). Color planning and intercell interference coordination for multicolor visible light communication networks. *Journal of Lightwave Technology*, 35(22):4980–4993.

Zhuang, Y., Hua, L., Qi, L., Yang, J., Cao, P., Cao, Y., Wu, Y., Thompson, J., and Haas, H. (2018). A survey of positioning systems using visible LED lights. *IEEE Communications Surveys & Tutorials*, 20(3):1963–1988.

Zumtobel Lighting GmbH (2018). The lighting handbook. `https://www.zumtobel.com/PDB/teaser/EN/lichthandbuch.pdf`. Accessed: 2020-04-30.

CURRICULUM VITAE

[redacted]

[redacted]

[redacted]

[redacted]

[redacted]